



저작자표시-비영리-변경금지 2.0 대한민국

이용자는 아래의 조건을 따르는 경우에 한하여 자유롭게

- 이 저작물을 복제, 배포, 전송, 전시, 공연 및 방송할 수 있습니다.

다음과 같은 조건을 따라야 합니다:



저작자표시. 귀하는 원저작자를 표시하여야 합니다.



비영리. 귀하는 이 저작물을 영리 목적으로 이용할 수 없습니다.



변경금지. 귀하는 이 저작물을 개작, 변형 또는 가공할 수 없습니다.

- 귀하는, 이 저작물의 재이용이나 배포의 경우, 이 저작물에 적용된 이용허락조건을 명확하게 나타내어야 합니다.
- 저작권자로부터 별도의 허가를 받으면 이러한 조건들은 적용되지 않습니다.

저작권법에 따른 이용자의 권리는 위의 내용에 의하여 영향을 받지 않습니다.

이것은 [이용허락규약\(Legal Code\)](#)을 이해하기 쉽게 요약한 것입니다.

[Disclaimer](#)

공 학 박 사 학 위 논 문

**Design and Analysis of CDI Techniques for
High Energy Efficiency and Energy Recovery**

고 에너지 효율 및 에너지 회수를 위한
축전식 탈염기술의 설계 및 분석

2016년 2월

서울대학교 대학원

화학생명공학부

강 전 일

**Design and Analysis of CDI Techniques for
High Energy Efficiency and Energy Recovery**

by

Junil Kang

under the supervision of

Professor Jeyong Yoon, Ph. D.

A dissertation submitted in partial fulfillment of the requirements for
the Degree of
Doctor of Philosophy

FEBRUARY 2016

SCHOOL OF CHEMICAL AND BIOLOGICAL ENGINEERING
SEOUL NATIONAL UNIVERSITY

**Design and Analysis of CDI Techniques for High Energy
Efficiency and Energy Recovery**

고 에너지 효율 및 에너지 회수를 위한
축전식 탈염기술의 설계 및 분석

지도교수 윤 제 용

이 논문을 공학박사 학위논문으로 제출함

2015년 12월

서울대학교 대학원

공과대학 화학생물공학부

강 전 일

강전일의 공학박사 학위논문을 인준함

2016년 1월

위 원 장	<u>성 영 은 (인)</u>
부 위 원 장	<u>윤 제 용 (인)</u>
위 원	<u>하 정 익 (인)</u>
위 원	<u>탁 용 석 (인)</u>
위 원	<u>강 경 석 (인)</u>

Abstract

Water and energy scarcity by industrialization and population growth has emerged as global crisis to humanity, which cause the demand for efficient desalination technique with low-energy cost. Compared to conventional desalination processes such as reverse osmosis (RO) and distillation, capacitive deionization (CDI), an electrochemical desalination technology using electrical double layer on the electrode, has come into spotlight in terms of environment-friendly and low-energetic process. Since the desalination performance and energy efficiency of CDI process are determined by operation techniques such as constant current operation and energy recovery, design and analysis for these techniques are needed for enhancing energy efficiency. Therefore, in this dissertation, design and analysis of CDI techniques for high energy efficiency and energy recovery was implemented by focusing on the evaluation of energy consumption according to operational modes and energy recovery system. Firstly, salt adsorption capacity (deionization capacity) and energy consumption of two CDI operational modes (CV and CC) were comparatively investigated. As major results, CV mode resulted in faster salt adsorption while CC mode showed much lower energy consumption than CV mode by 26 ~ 30% due to the overall lower cell voltage used in CC mode than in CV mode. Secondly, the successful construction of an energy recovery system in an actual MCDI cell with a

buck-boost converter was implemented; the buck-boost converter facilitated the delivery of the energy stored in the MCDI cell into a supercapacitor. The salt adsorption capacity was found to play an important role in the energy recovery and constant current charging was found to be more favorable for energy recovery than constant voltage charging. Lastly, energy recovery ratio in MCDI depending on electrode properties was investigated using constant current operation. Almost the whole carbon electrodes showed energy recovery ratios of 0.5 ~ 0.75 and we found out that not only salt adsorption capacity but also salt adsorption rate play an important role in energy recovery performance. In conclusion, this dissertation focused on design and analysis of operating techniques, CC operation and energy recovery process with investigating energy efficiency and energy recovery according to operating condition. We expect that this dissertation will provide a comprehensive guide for the construction and operation of high energy-efficiency CDI process.

Keywords: Desalination; capacitive deionization; energy efficiency; constant current operation; energy recovery; electrode properties

Student number: 2010-30802

Tables of Contents

1. Introduction	1
1.1. Backgrounds.....	1
1.2. Objectives	4
2. Literature review	6
2.1. The history of CDI	6
2.2. CDI operation and evaluation	11
2.3. MCDI (Membrane-assisted CDI)	17
2.4. Energy recovery in CDI	23
2.5. State of the art CDI system	27
3. Comparison of salt adsorption capacity and energy consumption between constant voltage and constant current operation in capacitive deionization.....	33
3.1. Introduction.....	33
3.2. Materials and Methods.....	37

3.3. Results and Discussion.....	43
3.4. Summary	63
4. Direct energy recovery system for capacitive deionization	64
4.1. Introduction.....	64
4.2. Materials and Methods.....	69
4.3. Results and Discussion.....	79
4.4. Summary	104
5. Influential electrode properties on energy recovery performance in capacitive deionization.....	105
5.1. Introduction.....	105
5.2. Materials and Methods.....	108
5.3. Results and Discussion.....	113
5.4. Summary	139
6. Conclusions	140

List of Figures

Figure 2-1. Capacitive deionization (CDI).....	7
Figure 2-2. Timeline of CDI development.	10
Figure 2-3. Operational process for CDI.....	12
Figure 2-4. Operational conditions for CDI; flow types (top) and operational types (bottom).	14
Figure 2-5. Ion distribution and movement of MCDI during the charging and discharging process.	18
Figure 2-6. The schematic of Membrane assisted CDI (MCDI) (Biesheuvel and Van der Wal 2010).	19
Figure 2-7. The concentration transient of effluent: solid line; MCDI, dashed line; CDI (Kim and Choi 2010b).....	21
Figure 2-8. The SEM images of carbon electrode (a) coated with ion-exchange resin (Kim and Choi 2010a) and (b) fabricated with ion-exchange resin as a binder (Kim and Choi 2010a; Liu et al. 2014).	22
Figure 2-9. (a) Comparison for energy consumption between CDI and RO, (b) theoretical energy consumption with different energy recovery ratio.....	25
Figure 2-10. The methodologies for energy recovery in CDI process	26
Figure 2-11. Flow-CDI (FCDI); (a) schematic and (b) variation in the NaCl concentration in the effluent stream (HeeáCho et al. 2013).	28
Figure 2-12. Hybrid CDI (HCDI); (a) schematic and (b) comparison of specific capacity (Lee et al. 2014).....	30

Figure 2-13. Inverted CDI (i-CDI); (a) schematic and (b) enhanced stability by the i-CDI system (Gao et al. 2015).	32
Figure 3-1. Control of the effluent concentration of freshwater and concentrate in MCDI-CC-RCD mode, using as control variable: (a) current, (c) water flow rate (Zhao et al. 2012).	36
Figure 3-2. Schematic of flow mode capacitive deionization process used in this study. The capacitive deionization module comprised (1) current collectors (graphite), (2) electrodes (activated carbon sheet), and a (3) spacer (polymer).	39
Figure 3-3. Two criteria for accurate comparison of CV and CC operation; identical consumed charge and ion removal during the desalination step.	42
Figure 3-4. Comparison of constant voltage (CV) and constant current (CC) modes in capacitive deionization. Shown are conductivity (a), current (b), and cell voltage (c) graphs from CV mode. (cell voltage = 1.2 V, charging & discharging time = 10 min respectively, flow rate = 10 mL/min) and conductivity (d), current (e), and cell voltage (f) from CC mode (current density = 2.5 mA/cm ² for charging and -2.5 mA/cm ² for discharging, flow rate = 10 mL/min).	44
Figure 3-5. Comparison of constant voltage (CV) and constant current (CC) modes in membrane-assisted capacitive deionization. Shown are conductivity (a), current (b), and cell voltage (c) graphs from CV mode. (cell voltage = 1.2 V, charging & discharging time = 10 min respectively, flow rate = 10 mL/min)	

and conductivity (d), current (e), and cell voltage (f) from CC mode (current density = 2.5 mA/cm² for charging and -2.5 mA/cm² for discharging, flow rate = 10 mL/min).48

Figure 3-6. The representative salt adsorption capacity curve in (a) constant voltage (CV) and (b) constant current (CC) operation during charging step. The salt adsorption capacity from (a) constant voltage (CV) mode (cell voltage = 1.2 V, charging and discharging time = 10 min respectively, flow rate = 10 mL/min) and (b) constant current (CC) mode (current density = 2.5 mA/cm² for charging and -2.5 mA/cm² for discharging, flow rate = 10 mL/min) during capacitive deionization. The inserted figure displays the effluent conductivity during charging time (from Figure 3-4a & d). The shaded areas in the inserts represent the salt adsorption capacity.52

Figure 3-7. The salt adsorption capacity curve (a) and salt adsorption rate (b) of constant voltage (CV, 1.2V) and constant current (CC) operation with various constant current densities (1.5 ~ 3.5 mA/cm²).....54

Figure 3-8. (a) Energy consumption and charge efficiency, (b) voltage profiles depending on charging currents (1, 1.5, 2.5, 5 mA/cm²) with CC operation in MCDI.58

Figure 3-9. Comparison of energy consumption and charge efficiency in CDI constant voltage (CV) and constant current (CC) mode with various constant current densities (1.5, 2, 2.5, 3.0, 3.5 mA/cm²). Two criteria of identical electrical charge consumed (a and c) and identical amount of ion removal (b &

d) were employed. The arrows indicate the increasing current in CC operation.59

Figure 3-10. Comparison of energy consumption in MCDI constant voltage (CV) and constant current (CC) mode with various constant current densities (1, 1.5, 2.5, 5 mA/cm²). Two criteria of identical electrical charge consumed (a and c) and identical amount of ion removal (b & d) were employed. The arrows indicate the increasing current in CC operation.60

Figure 3-11. Integration of CV and CC operation. The (a) concentration, (b) voltage, (c) salt adsorption capacity profiles were obtained by integrated CDI operations with CC (1.5 mA/cm² to 1.2 V) and CV (1.2 V). The energy consumption (d) of integrated operation was compared to that of CV and CC operation, respectively.....62

Figure 4-1. Prediction of energy recovery of CDI process using constant current charging and discharging. Energy recovery ratio can be calculated by the ratio of recovered energy during the discharging step to consumed energy during the charging step (Długołęcki and van der Wal 2013).....67

Figure 4-2. The schematic of proposed circuit of energy recovery system in CDI with a buck-boost converter (Pernia et al. 2014).....68

Figure 4-3. The schematic of an actual membrane capacitive deionization (MCDI) cell for energy recovery that is connected with a supercapacitor via a buck-boost converter. The MCDI cell is composed of electrodes, ion exchange membranes and a spacer. The electrical energy consumed during the desalination step is partially transferred to the supercapacitor.71

Figure 4-4. Schematic of the buck-boost converter operation during delivery of the energy stored in the CDI cell into the supercapacitor. The buck-boost converter is operated by a) an automatic switching depending on the current intensity at an inductor (L), and it generates b) specific current profiles in the CDI cell and the supercapacitor. The ratio of the duration of stage #1 over the whole duration in one cycle (stage #1 and stage #2) is presented as the converter duty (D), and the average current through the CDI cell is expressed as the reference current (I_{ref})..... 75

Figure 4-5. The calculation of energy recovery ratio. The energy recovery is obtained from the ratio of energy consumed for desalination (ion adsorption) to energy recovered (stored into the supercapacitor) by the buck-boost converter..... 78

Figure 4-6. Representative voltage and conductivity profile in one cycle during MCDI operation with energy recovery. Shown are the potential (a) and conductivity (b) from constant voltage (CV) charging (1.2 V, 10 min, and 10 mM) and the potential (c) and conductivity (d) from constant current (CC) charging (1.5 mA/cm² and 10 mM). The energy recovery process was performed with a reference current of 5 mA of the buck-boost converter and capacitance of 5 F of the supercapacitor. The voltage profiles of the CDI cell and the supercapacitor are depicted as the blue solid line and red solid line, respectively..... 80

Figure 4-7. The actual current profile applied to the MCDI cell during the

discharging step. The discharging current is obtained from the experimental data set of I_{ref} (=5 mA), V_{MCDI} , $V_{supercapacitor}$	83
Figure 4-8. Three-dimensional representation of the energy recovery ratio in the MCDI with two charging modes. Constant voltage (CV) charging (a) was conducted with various charging voltages and times for a NaCl concentration of 10 mM. Similarly, constant current (CC) charging (b) was conducted with various charging currents and concentrations of feed water. The discharging step was performed with reference current of 5 mA of the buck-boost converter and capacitance of 5 F of the supercapacitor.....	85
Figure 4-9. The relationship between the energy recovery ratio and the salt adsorption capacity in MCDI with two charging modes. Shown are the constant voltage (CV, 0.3 ~ 1.2 V at 10 mM) charging (a) and the constant current (CC, 1 ~ 4 mA/cm ² at 5 ~ 100 mM) charging (b). The arrow indicates the direction of increasing charging time in CV mode and charging current in CC mode.....	90
Figure 4-10. The salt adsorption capacity with CV charging as a function of a) charging time at 1.2 V and b) charging voltage for 10 min and with CC charging as a function of c) charging current at 10 mM and d) concentration of feed water at 1.5 mA/cm ²	91
Figure 4-11. The mean power of charged MCDI cell during the discharging step as a function of the salt adsorption capacity in case of a) CV charging and b) CC charging.....	94

Figure 4-12. Solution resistance as a function of charging current with various concentration of feed water (5~100 mM).....	96
Figure 4-13. Three-dimensional representation of the energy recovery ratio with various reference currents of the buck-boost converter and capacitances of the supercapacitor. The charging step was performed with constant current operation at 1.5 mA/cm ² and a NaCl concentration of 10 mM. The average salt adsorption capacity was 19 mg/g.....	100
Figure 4-14. Calculation of energy loss during converter operation (energy recovery step). (a) voltage profiles of supercapacitor#1 (energy donor) and supercapacitor#2 (energy receptor), (b) energy loss of converter as a function of charging potentials and reference currents.....	102
Figure 4-15. Comparison of energy recovery ratio with considering energy loss of converter (30% in this study) and without considering energy loss of converter. This data is based on the energy recovery ratio with CV charging depicted in Figure 4-9a.....	103
Figure 5-1. Definition of energy recovery ratio in CDI with constant current operation.....	112
Figure 5-2. The meso- and macropore distributions of carbon materials derived from BJH equation; (a) MSP-20, (b) MDC, (c) CA.....	115
Figure 5-3. Galvanostatic charge/discharge voltage profiles of MSP-20.....	118
Figure 5-4. Galvanostatic charge/discharge voltage profiles of P-60	119
Figure 5-5. Galvanostatic charge/discharge voltage profiles of SX-PLUS.....	120

Figure 5-6. Galvanostatic charge/discharge voltage profiles of S-51HF 121

Figure 5-7. Galvanostatic charge/discharge voltage profiles of MDC 122

Figure 5-8. Galvanostatic charge/discharge voltage profiles of Carbon aerogel 123

Figure 5-9. Retention of specific capacitance as a function of scan rate (0.5 mA/cm² ~ 20 mA/cm²) with various carbon composite electrodes..... 125

Figure 5-10. (a) The representative voltage profiles and (b) salt adsorption capacities (mg/g) of CC mode in MCDI operation with various carbon electrodes. (current density = 1 mA/cm² for charging and -1 mA/cm² for discharging, flow rate = 10 mL/min, NaCl concentration = 10 mM)..... 129

Figure 5-11. Salt adsorption capacities (mg/cm³) of CC mode in MCDI operation with various carbon electrodes. (current density = 1 mA/cm² for charging and -1 mA/cm² for discharging, flow rate = 10 mL/min, NaCl concentration = 10 mM)..... 130

Figure 5-12. The energy consumed during the charging step (E_c) and energy recovered during the discharging step (E_r) with various carbon materials. Inserted table shows the energy recovery ratio calculated from E_r/E_c as presented in Figure 5-2. CC operation in desalination test was performed with 1/-1 mA/cm² of charging/discharging current density up to 1.2 V of cut-off voltage and 10 mM NaCl solution. The symbols are located between $E_r=0.5E_c$ and $E_r=0.75E_c$, indicating the energy recovery ratios of carbon materials ranged from 50% to 75%. 133

Figure 5-13. Correlation between the salt adsorption capacity and energy

recovery ratio. Salt adsorption capacity was obtained from Figure 5-11b and regression line was plotted with MSP-20, P-60, SX PLUS and S-51HF. The red star indicates the energy recovery ratio of converter system in Figure 4-9. 135

Figure 5-14. Correlation between the average salt adsorption rate and mean power. The average salt adsorption rate was calculated by dividing the salt adsorption capacity by the duration of charging step (mg/g/s) and mean power was obtained by dividing the energy recovered during the discharging step by the duration of discharging step and the mass of electrodes (mW/g)..... 137

Figure 5-15. The normalized energy recovery as a function of different charging-discharging current density (± 1 , ± 2 , ± 4 mA/cm²). All of desalination test were identically performed with 1.2 V of Cut-off voltage and 10 mM NaCl solution..... 138

1. Introduction

1.1. Backgrounds

With greater water scarcity caused by worldwide industrialization and population growth, demand for available water resources have come into spotlights as a main task for humanity (Jury and Vaux 2007; Shannon et al. 2008). Considering that 98% of Earth's water resources exist as seawater or brackish water (Anderson et al. 2010; Elimelech and Phillip 2011), desalination can be a major strategic technical approach to address this problem. Thus far, thermal distillation and membrane separation are utilized as the most common desalination processes (Shannon et al. 2008). However, these desalination processes have a considerable disadvantage in terms of high energy consumption for securing high pressure and temperature although they show high salt removal and have been successfully commercialized. Recently, capacitive deionization (CDI) emerged as an alternative and complement to conventional desalination processes (Porada et al. 2013b). This state-of-the-art desalination approach is based on the electrical double layer induced by a cell voltage difference between two porous carbon electrodes, which is derived from the principle of electric double layer capacitor (EDLC) (Zhang and Zhao 2009). CDI has many advantages with environmental and energetic aspects because chemical treatment is not required and a low electrical voltage is applied for the operation

(Farmer et al. 1996; Porada et al. 2013b; Welgemoed and Schutte 2005).

Low energy consumption for the operation is one of powerful strengths in CDI compared to the conventional processes in the way that high energy efficiency, indicating low energy required for deionization, is the key requirement for desalination (Elimelech and Phillip 2011; Zhao et al. 2013a). High energy efficiency directly related with CDI performance is the major interest in many CDI research groups. For this reasoning, there have been numerous studies reporting the improvement of energy efficiency and CDI performance through the electrode materials such as carbon aerogel, mesoporous carbon, fiber, graphene, carbon nanotube, MOF(metal organic framework)-derived carbon (Gabelich et al. 2002; Li et al. 2010; Porada et al. 2013a; Tsouris et al. 2011; Wang et al. 2012; Wang et al. 2011; Yang et al. 2014), operating conditions such as cell voltage, flow rate, concentration (Porada et al. 2013b; Zhao et al. 2013b).

In particular, operating techniques such as constant current operation, energy recovery (Alkuran et al. 2008; Długolecki and van der Wal 2013; Zhao et al. 2012) are major factors to affect the desalination performance and energy efficiency of CDI process. Constant current (CC) operation which is introduces to produce constant concentration in desalinated water compared to conventional constant voltage (CV) operation (Kang et al. 2014; Zhao et al. 2012) is directly connected with energy consumption of CDI. In addition, the energy recovery is the substantial advantageous operating technique of CDI versus other

desalination processes because the partial recovery of consumed energy for desalination is easily feasible due to capacitive nature (Demirer et al. 2013; García-Quismondo et al. 2013a). In this respect, design and analysis for these operating techniques are necessarily required for enhancing energy efficiency of CDI process. However, most of previous studies about CC operation have been report the production of constant desalinated stream and the effect of operating condition without the accurate evaluation of energy efficiency. Moreover, the energy recovery of CDI have been limited to only suggest the conceptual model without realization of energy recovery system. Therefore, further studies are required for design and analysis for CDI techniques including CC operation and energy recovery to achieve high energy efficiency.

1.2. Objectives

In this dissertation, design and analysis of CDI techniques for high energy efficiency and energy recovery was implemented by focusing on the evaluation of energy consumption according to operational modes and energy recovery system. To accomplish the intended goal of this dissertation, three parts of studies were implemented as follows:

Firstly, the energy consumption according to operational modes in CDI was evaluated by comparison of CV and CC operation in terms of salt adsorption capacity (Desalination performance), energy consumption and charge efficiency. The salt adsorption capacity was analyzed based on its conductivity profile with capacity and rate. For the accurate comparison, two criteria (identical electrical charge consumed and identical amount of ion removal during desalination process) are considered.

Secondly, the energy recovery system in CDI process was realized and the influential parameters affecting energy recovery ratio were investigated. For this, the direct energy recovery system in an actual MCDI cell was constructed by introducing a buck-boost converter, electronic power conversion device. The energy recovery was implemented with storage of recovered energy into a supercapacitor. Also, the energy recovery ratio was investigated under various operational conditions (CV charging with various voltages and times, CC

charging with various currents and concentrations of feed water, discharging with various reference currents of the buck-boost converter, and capacitances of the supercapacitor).

Lastly, the relationship between electrode characteristics and energy recovery performance was investigated by using various carbon materials with different properties. Electrochemical properties were checked by galvanostatic charge/discharge and desalination test using CC operation was implemented. The ratio of consumed energy during desalination step and released energy during regeneration step was defined as energy recovery ratio. To determine the effect on energy recovery performance, influential factors (electrode characteristics) were considered as capacity (salt adsorption capacity) and rate (salt adsorption rate), and the salt adsorption rate was correlated with mean power during energy recovery process.

2. Literature review

2.1. The history of CDI

Capacitive deionization (CDI) is an electrochemically controlled desalination technology using an electrical double layer based on non-faradaic process, as shown in Figure 2-1. Its principle is similar with that of supercapacitor, electric energy storage media, in regard to collecting ions in electrolyte by electrical double layer formed on the electrode surface. However, in case of CDI, electrolyte (feed water) flows between two electrodes where cell voltage is applied through the charging and discharging step (Anderson et al. 2010).

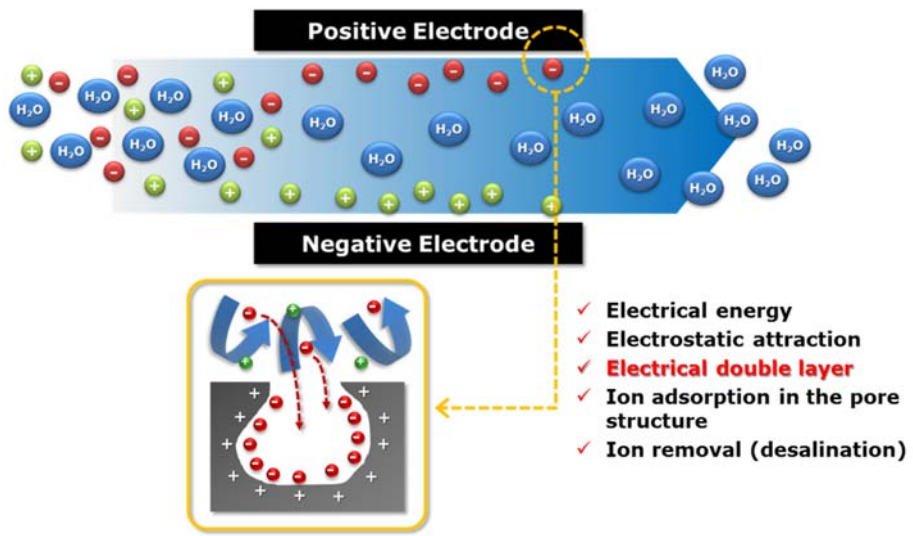


Figure 2-1. Capacitive deionization (CDI).

Figure 2-2 shows the historical schematic of CDI development. From 1960 when the technical concept of CDI had been firstly introduced (Blair and Murphy 1960) to the present, numerous studies have been examined in the theoretical, systematic and material aspects. In the early stages (1960~1990), the principle of ion removal from feed water was investigated based on electro-sorption occurred at electrode's surfaces. Although the principle of ion removal had been reported as the result of ion exchange process between salts and functional group on electrode's surfaces (Evans and Hamilton 1966; Murphy and Caudle 1967), this null hypothesis have been changed into the formation of electrical double layer as the principle of CDI which is now widely accepted (Johnson and Newman 1971; Soffer and Folman 1972). After that, in 2000s, the development of materials and fabrication technologies contributed to the application of various carbon materials such as an activated carbon, carbon aerogel, carbon nanotube, mesoporous carbon, graphene to the CDI electrode for enhancing desalination performances (Farmer et al. 1996; Li et al. 2010; Zhang et al. 2006; Zou et al. 2008). The relationship between electrode properties and desalination performance was also investigated in this period. In addition, many operating techniques was developed to enhance desalination performances and efficiency such as constant current (CC) operation which can produce fixed concentration of desalinated water (Zhao et al. 2012), membrane-assisted CDI (MCDI) which dramatically raise desalination performances using ion-exchange membrane (Biesheuvel and Van der Wal 2010; Kim and Choi 2010b), hybrid-CDI (HCDI)

which is derived from battery system for gaining large capacity (Lee et al. 2014), flow-CDI (FCDI) which uses not immobilized electrodes but flowable carbon slurry as electrodes (HeeáCho et al. 2013), inverted-CDI (i-CDI) which inverts the sequence of charging and discharging step with the modified surface charge of electrodes (Gao et al. 2014; Gao et al. 2015).

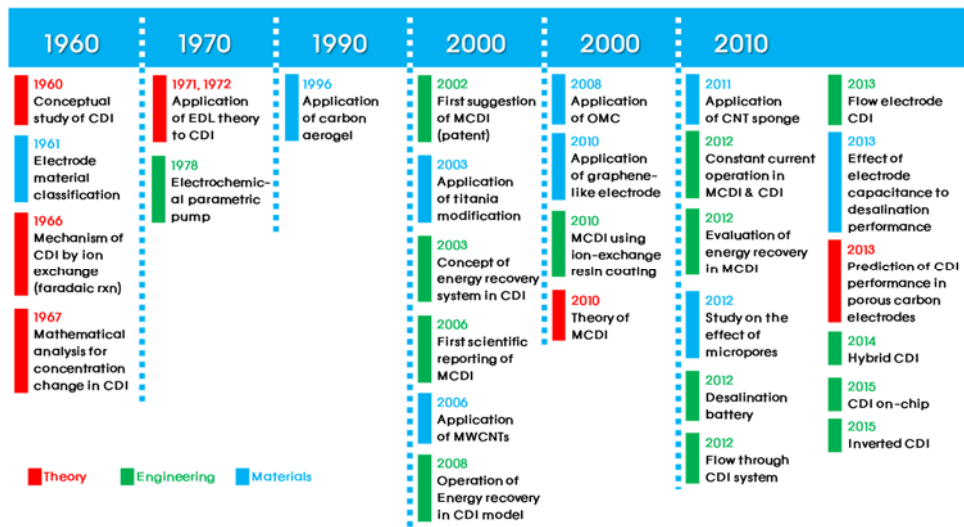


Figure 2-2. Timeline of CDI development.

2.2. CDI operation and evaluation

In this chapter, the methods for CDI operation and evaluation of CDI performance implemented in this study will be addressed. The sequence of CDI operation consist of charging and discharging steps as shown in Figure 2-3. Salts in feed water are removed through ion adsorption into pores of carbon electrodes by applying electrical energy, called charging (desalination) step. After charging step, by applying reverse electrical energy or short-circuiting, adsorbed ions are released to the flow channel and electrodes are regenerated, called discharging (regeneration) step. The regeneration step is essential to provide adsorption site required for the next desalination step. Discontinuous production of desalinated water is one of characteristics in CDI operation because ion removal ceases during the regeneration step. Considering ion removal by the formation of electrical double layer as the principle of CDI, desalination should be occurred without faradaic reaction. Therefore, the cell voltage between two electrodes is below 1.23 V (vs. NHE as water splitting reaction) (Farmer et al. 1996; Porada et al. 2012; Welgemoed and Schutte 2005). Compared to the conventional electrochemical desalination method, electrodialysis (ED), the energy consumption of CDI is lower than ED due to operation with low cell voltage (Porada et al. 2012).

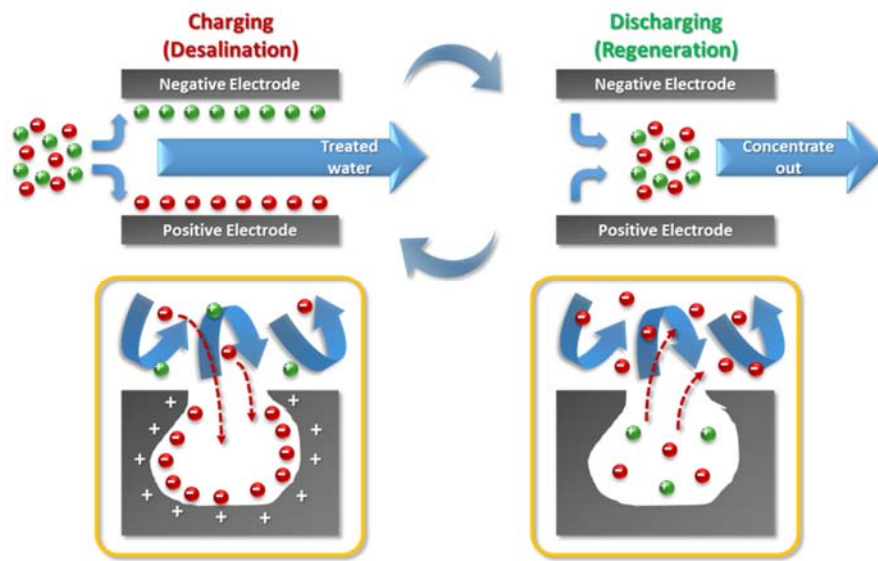


Figure 2-3. Operational process for CDI.

The CDI performance is dependent on operational conditions such as flow type (Farmer et al. 1997; Lee et al. 2009), flow channel (Suss et al. 2012; 이주영 et al. 2010), module design (손덕영 et al. 2010), the operational mode for applying electrical energy (Jande and Kim 2013; Kang et al. 2014; Zhao et al. 2012), the concentration of feed water (Porada et al. 2013a; Zhao et al. 2013b). The type of flow channel is representatively classified into the batch and flow system. In case of the batch system which have been frequently used in academic fields, it is difficult to maintain a constant concentration of feed stream. The flow system, therefore, is more suitable for actual process or commercialization than the batch system (Porada et al. 2013b). The flow type is depicted in Figure 2-4 (top). The operational mode for applying electrical energy is classified into constant voltage (CV) and constant current (CC) operation. CV operation is beneficial to easily adjust cell voltages and desalination times. While, CC operation is favorable for manufacturing targeted constant concentration of desalinated water and low energy consumption, as shown in Figure 2-4 (bottom). The concentration of feed water also have a strong influence on the CDI performance because the charge capacity in electrical double layer is charged with the electrolyte concentration (Bard and Faulkner 2001; Kim and Yoon 2013). However, the aimed concentration is generally in the range of 5 to 50 mM due to the limitation of adsorption site in carbon electrode pores (Zhao et al. 2013b).

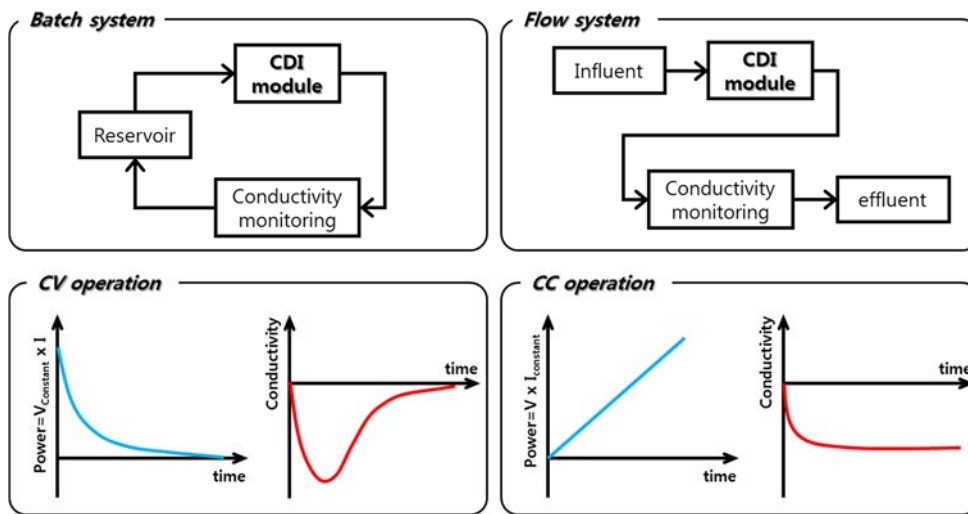


Figure 2-4. Operational conditions for CDI; flow types (top) and operational types (bottom).

To evaluate and compare results of various CDI operations, some operational indexes representing CDI performances and energy efficiency are required, which are salt adsorption capacity, average salt adsorption rate, energy consumption and charge efficiency (Porada et al. 2013b; Suss et al. 2015).

The performance of CDI operation is determined by the salt adsorption capacity (SAC) which shows the amount of salts removed during the desalination step and the average salt adsorption rate (ASAR) which shows the salt removal rate. The SAC is calculated by total amount of salt removed during the desalination step divided by total weights of electrodes and represented in mg/g_{electrode} (Equation 1).

$$\text{Salt adsorption capacity (mg/g)} = \frac{\int (C_{\text{in}} - C_{\text{out}}) \times \Phi \times dt}{M_{\text{electrode}}} \quad (2-1)$$

(C_{in}; inlet concentration, C_{out}; outlet concentration, Φ; flow rate, M_{electrode}; Electrode weight)

In addition, the SAC measured at equilibrium state (without the change in feed concentration) is represented as maximum SAC (mSAC). While the SAC can be changed depending on operational conditions, the mSAC is the characteristic of carbon material independent of operational conditions because it indicates the maximum amount of salts available for specific carbon material. The ASAR is calculated by the SAC divided by the duration of desalination step and represented in mg/g_{electrode}/sec or mg/g_{electrode}/min. Unlike the mSAC determined by only carbon

materials, the ASAR is highly suitable index to synthetically evaluate the CDI performance including carbon material and operational conditions.

The energy efficiency is determined by energy consumptions required for removing specific amount of salts. This index can be calculated by total electrical energy consumed during the desalination step divided by total salts removed and represented in kJ/mol or kT per ion removed ([kT per ion removed] = [kJ/mol] / # of Avogadro) (Equation 2).

$$\text{Energy consumption (kJ/mol)} = \frac{\int V \times I \times dt}{2 \times \int (C_{in} - C_{out}) \times \Phi \times dt} \quad (2-2)$$

(V; voltage, I; current)

The charge efficiency is calculated by the amount of charge converted from removed salts divided by total electrical charge during the desalination step and directly indicates the efficiency of energy utilization (Equation 3).

$$\text{Charge efficiency} = \frac{F \times \int (C_{in} - C_{out}) \times \Phi \times dt}{\int I \times dt} \quad (2-3)$$

Although the ideal capacitor system should show unity of charge efficiency, general CDI process reveals the charge efficiency below unity due to co-ion repulsion (Avraham et al. 2009; Avraham et al. 2010; Zhao et al. 2009).

2.3. MCDI (Membrane-assisted CDI)

In this study, experiments were conducted with MCDI system, the combination of conventional CDI system and ion-exchange membrane to achieve high desalination performance.

When electrical potential is applied to the electrode, co-ions (same charge with the applied potential) and counter-ions (opposite charge with applied potential) are simultaneously distributed near the electrode surface. The electrical double layer induced by applying potential not only attracts counter-ions, but also repels co-ions from the electrode surface to bulk phase, which is called co-ion expulsion effect. This co-ion expulsion effect results in the decrease of energy efficiency in CDI process (Avraham et al. 2009). To prevent co-ion expulsion and increase the energy efficiency of CDI, the ion-exchange membrane was firstly introduced by Lee et al. in Korea Electric Power Research Institute (KEPRI) (Lee et al. 2006), called membrane-assisted CDI (MCDI). As shown in Figure 2-5, co-ion expulsion effect is decreased by restriction of co-ion's movement, which results in higher desalination performance. In addition, the efficiency of regeneration process is enhanced because the reverse potential can be applied without concerning re-adsorption of released ions (Biesheuvel and Van der Wal 2010). MCDI is innovative operating system to obtain remarkable enhancement in desalination performances using CDI module installed with ion-exchange membrane; cation and anion exchange membrane were equipped to

negative and positive charged electrode, respectively (Figure 2-6).

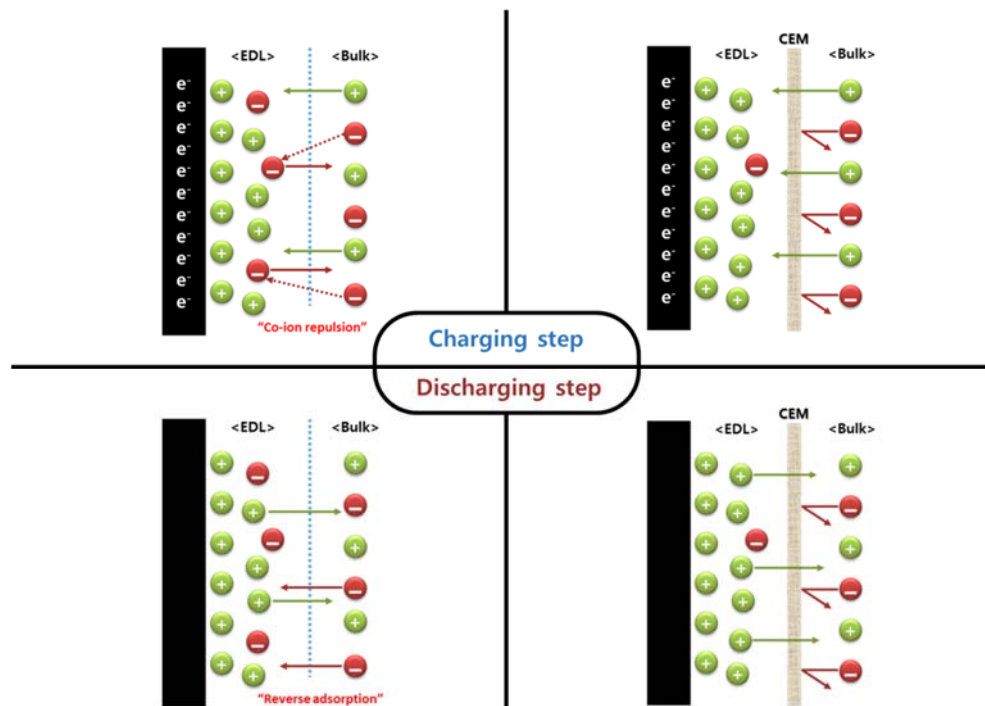


Figure 2-5. Ion distribution and movement of MCDI during the charging and discharging process.

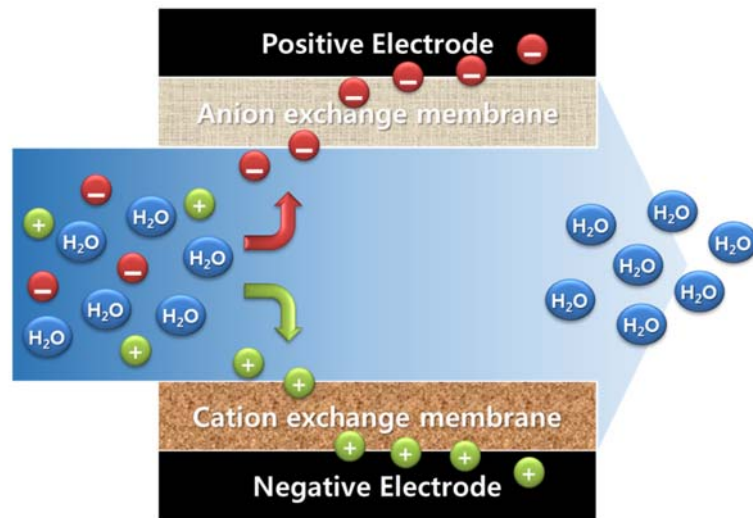


Figure 2-6. The schematic of Membrane assisted CDI (MCDI) (Biesheuvel and Van der Wal 2010).

By introducing MCDI, the desalination performance and CDI efficiency are dramatically improved as shown in Figure 2-7 (Kim and Choi 2010b). Moreover, it was reported in further studies that ion-exchange resin was directly coated on the electrode surface (Kim and Choi 2010a; Kim and Choi 2010c) or utilized as a binder for electrode fabrication (Liu et al. 2014) to not only decrease interfacial resistance between electrodes and membranes but also substitute expensive ion-exchange membrane as shown in Figure 2-8.

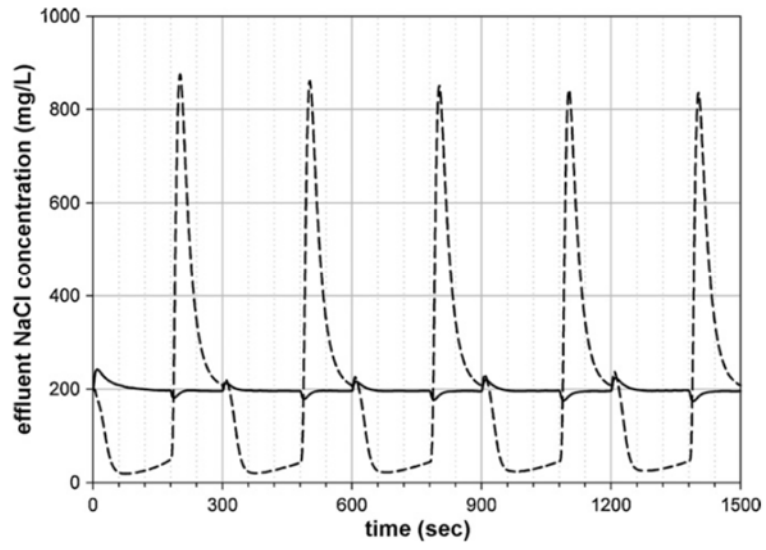
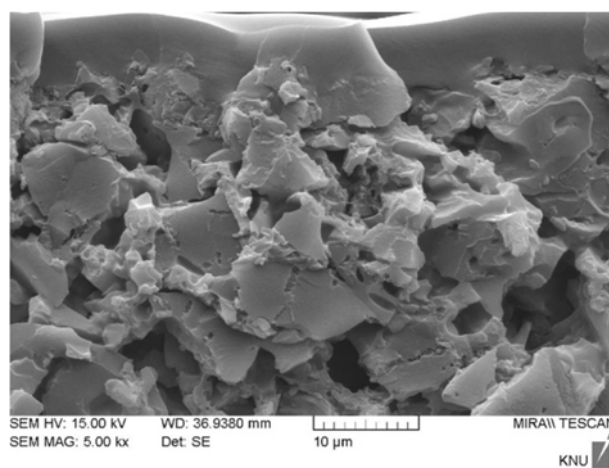
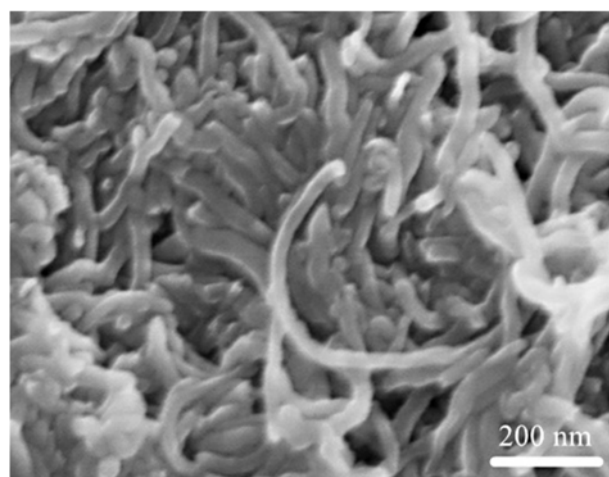


Figure 2-7. The concentration transient of effluent: solid line; MCDI, dashed line; CDI (Kim and Choi 2010b).



(a)



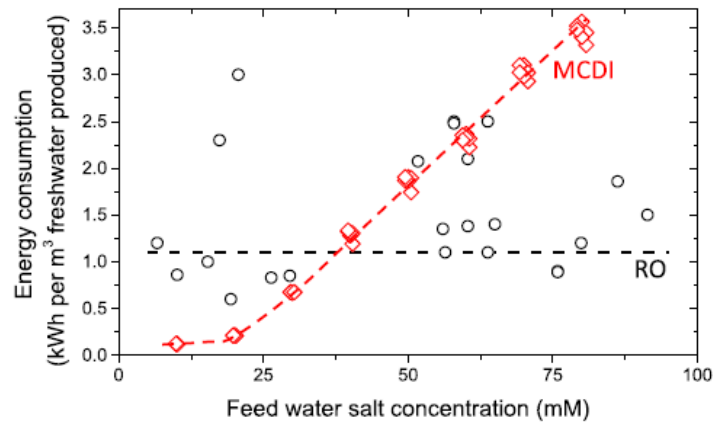
(b)

Figure 2-8. The SEM images of carbon electrode (a) coated with ion-exchange resin (Kim and Choi 2010a) and (b) fabricated with ion-exchange resin as a binder (Kim and Choi 2010a; Liu et al. 2014).

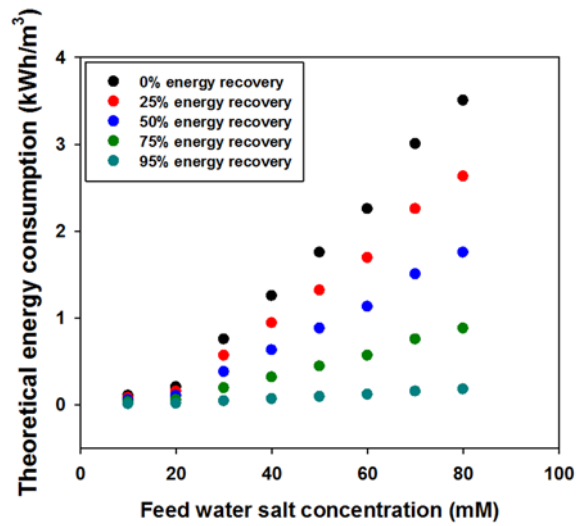
2.4. Energy recovery in CDI

Energy recovery in CDI is the energy-saving technique for storage or reuse of electrical energy generated by ion release from electrodes during the regeneration step. It was suggested based on similarity of the principle between CDI and capacitors. Due to the limitation of carbon electrode capacity, CDI is suitable desalination technology for low feed concentration such as brackish water. In other words, at high feed concentration, RO is superior process than CDI as shown in Figure 2-9a. The energy consumption of CDI is determined by cell voltage and charge capacity and is proportional to the concentration of feed water. To secure the competitiveness of CDI compared to the conventional process such as RO, the energy consumption of CDI should be below 1 kWh/m³ of energy consumption for RO aimed to seawater desalination and it is feasible on condition that 75% of consumed energy is recovered (Figure 2-9b) (Anderson et al. 2010; Shannon et al. 2008). If the brackish water would be targeted, it is expected that the efficiency and competitiveness of CDI is superior to RO process. Lately, the prediction of energy recovery ratio using CC operation was reported by Długolecki and van der Wal (Długolecki and van der Wal 2013) and conceptual energy recovery system using converter (electric device for power conversion) was proposed by Alkuran et al. and Pernia et al. (Alkuran et al. 2008; Pernia et al. 2012). The methodologies for energy recovery is classified into two categories; storage of recovered energy into supercapacitor and energy transfer

from primary CDI module to secondary CDI module (Figure 2-10). The former, firstly suggested by Shiue et al., is conducted by connection between CDI cell and supercapacitor through DC/DC converter and enables recovered energy to be utilized for various purposes (Shiue et al. 2003). The latter is conducted by connection of two CDI modules using alternating charge-discharge in parallel CDI modules and enables direct utilization of recovered energy for charging process. Considering that energy recovery is necessarily required for large-scale CDI process, the energy recovery with alternating charge-discharge in parallel CDI is suitable method rather than storage of recovered energy into supercapacitor because the cost and stacking volume for supercapacitors to deal with large-scale energy is very high.



(a)



(b)

Figure 2-9. (a) Comparison for energy consumption between CDI and RO, (b) theoretical energy consumption with different energy recovery ratio.

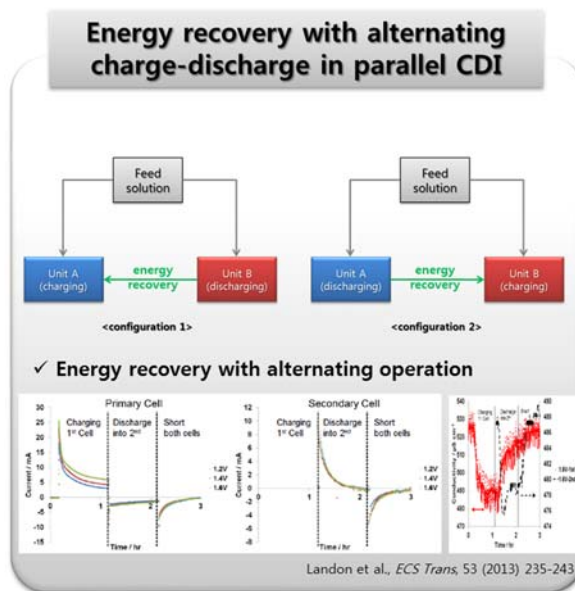
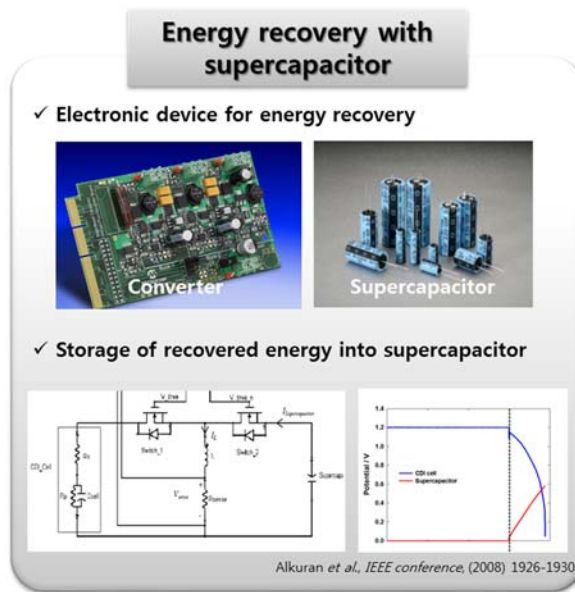


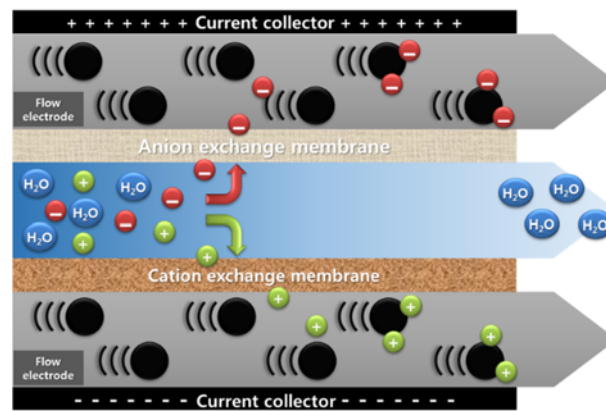
Figure 2-10. The methodologies for energy recovery in CDI process

2.5. State of the art CDI system

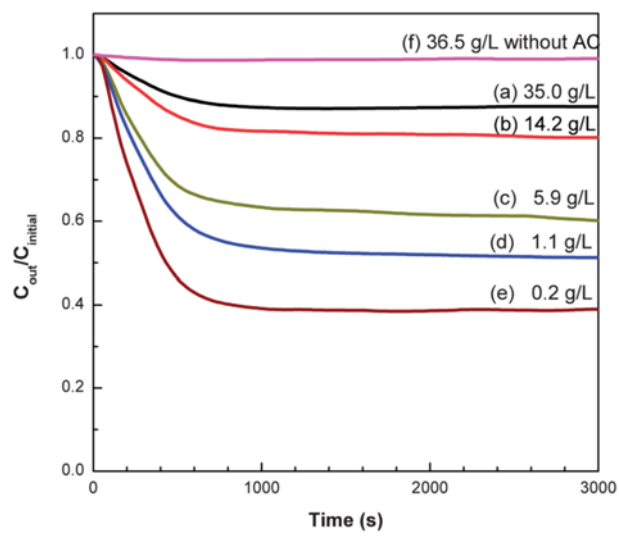
The enhancement of desalination performance and energy efficiency has been a perennial problem to many researchers in the CDI field. Numerous studies reporting the increasing performance and efficiency is established on modified electrode materials and operating system. In this chapter, some state of the art CDI system which innovatively enhance the performance and efficiency will be introduced; those are flow-CDI (FCDI), hybrid CDI (HCDI), inverted CDI (i-CDI).

Flow-CDI (FCDI), firstly reported by Kim et al. in Korea Institute of Energy Research, is advanced CDI process using slurry electrodes which are forms of activated carbon particles dispersed in electrolyte as shown in Figure 2-11 (HeeáCho et al. 2013). Compared to conventional immobilized carbon sheet electrodes, this novel process can provide infinite desalination capacity because flowable carbon particles holding salts are continuously replaced by new ones. Therefore, it is the most powerful advantage of FCDI that FCDI is applicable to desalination process for high-concentration saline water such as seawater desalination which conventional CDI cannot be applied. In addition, in case of treating positive flow electrodes (which adsorb anions) and negative electrodes (which adsorb cations) in same reservoir, it enables continuous production of desalinated water because electrodes are automatically regenerated by electro-neutrality. This means that a separated regeneration step is not required in FCDI

(Jeon et al. 2014).



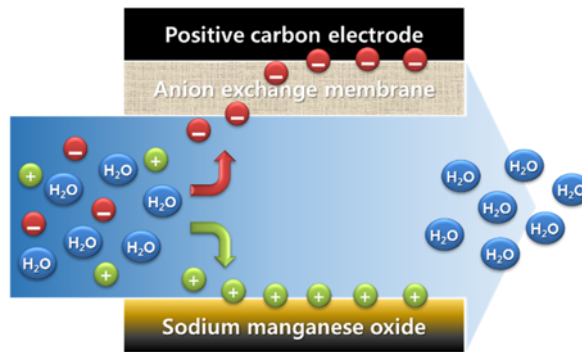
(a)



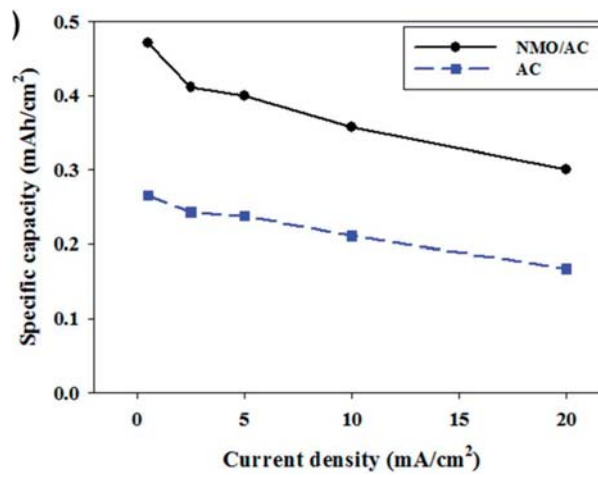
(b)

Figure 2-11. Flow-CDI (FCDI); (a) schematic and (b) variation in the NaCl concentration in the effluent stream (HeeáCho et al. 2013).

Hybrid-CDI (HCDI), firstly reported by Yoon et al. in Seoul National University, is desalination process with very high-capacity derived from sodium manganese oxide ($\text{Na}_4\text{Mn}_9\text{O}_{18}$)(Lee et al. 2014) as shown in Figure 2-12a. Sodium manganese oxide electrode, widely used as positive electrode materials, has very high-capacity compared to carbon electrode due to its faradaic intercalation of sodium ions. While general CDI process is operated with symmetrical system composed of two identical carbon electrodes, HCDI utilizes asymmetrical system composed of sodium manganese oxide and carbon electrode. This advanced system is beneficial to provide high desalination capacity more than two times that of general CDI (the most highest capacity numerous studies have ever been reported, see Figure 2-12b) (Suss et al. 2015), rapid desalination rate and high stability for long periods.



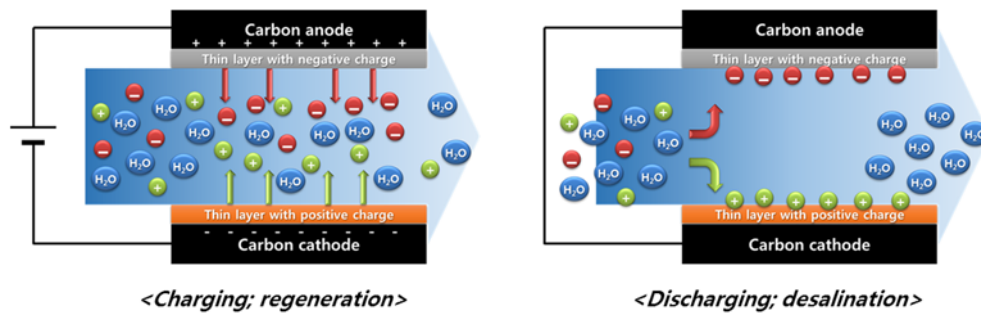
(a)



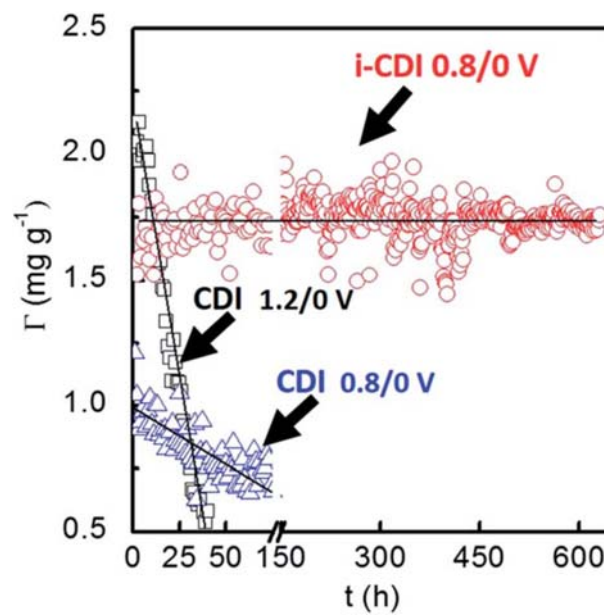
(b)

Figure 2-12. Hybrid CDI (HCDI); (a) schematic and (b) comparison of specific capacity (Lee et al. 2014).

Inverted CDI (i-CDI), firstly reported by James et al in Kentucky University, is highly stable desalination process for long-term operation using modified surface charge of electrodes. As shown in Figure 2-13a, the electrode regeneration by ion desorption is unusually conducted during the charging step and desalination is occurred during the discharging step, which resulted from the modified point of zero charge (PZC) in electrodes (Gao et al. 2014; Gao et al. 2015). The name “i-CDI” is originated by inversed sequences of desalination and regeneration in conventional CDI. Because the desalination (salts adsorption) is implemented during the discharging step without applying electrical energy, the energy efficiency is quite high and the carbon electrode oxidation, main cause of performance degradation in CDI, does not occur (Gao et al. 2014). It was reported that the performance degradation was not observed for long-term operation (600 hours) and this improved stability was superior to conventional CDI over 530% (Figure 2-13b).



(a)



(b)

Figure 2-13. Inverted CDI (i-CDI); (a) schematic and (b) enhanced stability by the i-CDI system (Gao et al. 2015).

3. Comparison of salt adsorption capacity and energy consumption between constant voltage and constant current operation in capacitive deionization

3.1. Introduction

Critical water shortages have come into the spotlight as a result of increasing water demands caused by worldwide industrialization and population growth (Jury and Vaux Jr 2007; Shannon et al. 2008). Many investigators have pursued technical solutions to address such shortages. A major strategic technical approach to water shortage is desalination because 98% of Earth's water resources are either salt or brackish (Anderson et al. 2010; Elimelech and Phillip 2011; Greenlee et al. 2009). Thus far, thermal distillation and membrane separation are the most common desalination processes. Although these processes can achieve high salt removal with excellent stability, they have several major disadvantages including high energy consumption, high maintenance costs, and equipment fouling problems. To overcome such problems, innovative desalination technologies are required.

Capacitive deionization (CDI) is an electrochemically controlled desalination technology which removes ions from salt water by electro-sorption via a two-

step, non-faradaic process occurring in the electrical double layer region. During the CDI process, ions in the feed water flowing through a spacer between the cathode and the anode are removed by electrostatic attraction, referred to as the charging (purification) step. Subsequently, when the applied electrical energy is stopped, the adsorbed ions are released from the electrodes, referred to as the discharging (regeneration) step. CDI is reported to have many environmental and energy consumption advantages over thermal distillation desalination and membrane separation desalination methods because CDI does not require chemical treatment to regenerate membranes nor high pressure for water recovery (Farmer et al. 1996; Gabelich et al. 2002; Li et al. 2010; Nadakatti et al. 2011; Xu et al. 2008)

Electrode properties and operating conditions are the two main factors affecting CDI performance. CDI-based desalination performance is widely reported to be affected by various physicochemical electrode properties such as materials, electrical conductivity, specific surface area, pore structure, and wettability (Farmer et al. 1996; Gabelich et al. 2002; Jung et al. 2007; Li et al. 2010; Lim et al. 2009; Nadakatti et al. 2011; Park et al. 2011; Porada et al. 2012; Wang et al. 2011; Welgemoed and Schutte 2005; Yoram 2008). In addition, CDI performance is also affected by operating conditions such as cell voltage, flow rate, concentration, and operational mode as reported in the previous studies (Porada et al. 2013b; Zhao et al. 2012; Zhao et al. 2013b). In particular, the type

of operational mode is important operating condition because it is directly related to electrical energy consumption or charge efficiency of CDI process. CDI operational modes generally consist of constant voltage (CV) and constant current (CC) modes. Compared to CC mode studies, reports on CV mode are more common in both the academic and commercial fields (Anderson et al. 2010; Welgemoed and Schutte 2005; Yoram 2008), presumably because there is difficulty in controlling voltage levels in CC mode. Several studies recently reported the operational technique and energy consumption of CC mode in membrane assisted CDI (MCDI) with emphasizing the strength of CC mode which can produce constant concentration in desalinated water, as shown in Figure 3-1 (Jande and Kim 2013; Porada et al. 2013b; van Limpt and van der Wal 2014; Zhao et al. 2012; Zhao et al. 2013a; Zhao et al. 2013b). However, no study was done on direct comparison of salt adsorption capacity and energy consumption between CV and CC mode in CDI. Therefore, this study intends to evaluate comparatively salt adsorption capacity and energy consumption in addition to charge efficiency of two operational modes (CV and CC mode) in CDI operation as identical electrical charge consumed or identical amount of ion removal are considered.

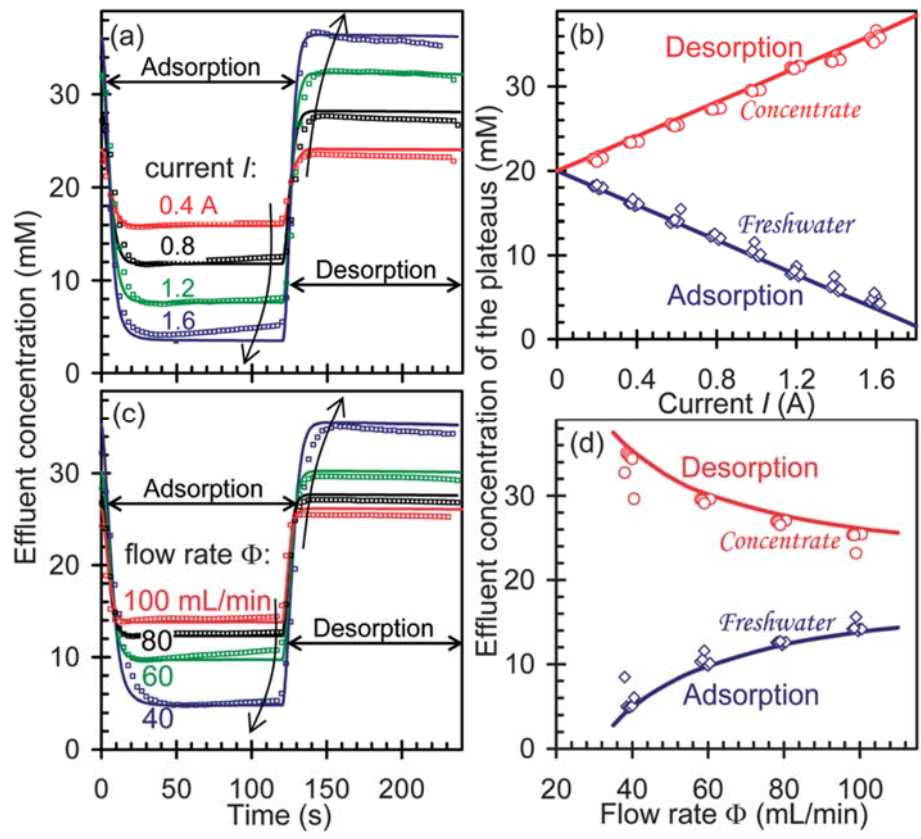


Figure 3-1. Control of the effluent concentration of freshwater and concentrate in MCDI-CC-RCD mode, using as control variable: (a) current, (c) water flow rate (Zhao et al. 2012).

3.2. Materials and Methods

Experimental deionization setup

Figure 3-2 shows a schematic of the flow mode CDI system employed in this study. The CDI unit cell comprised graphite current collectors, carbon sheet electrodes (thickness $\sim 300\ \mu\text{m}$, electrode weight $\sim 42.6\pm 2.1\ \text{mg}$), and a polymer spacer (nylon filter, thickness $\sim 180\ \mu\text{m}$). The carbon sheet electrodes were fabricated by compressing a mixture of 86 wt% activated carbon powder (MSP20, Kansai Coke and Chemicals, Amagasaki, Japan), 7 wt% carbon black (Super P, Timcal, Bodio, Switzerland), and 7 wt% polytetrafluoroethylene (PTFE, Sigma-Aldrich, St. Louis, MO, USA). The MSP20 carbon for electrode material was selected due to its high electrical conductivity and capacitance (Kim and Yoon 2013; Porada et al. 2013a). A feed solution of 10 mM NaCl was supplied to the CDI cell by using a peristaltic pump (Gilson, Middleton, WI, USA) at a flow rate of 10 mL/min. Electrical energy was applied to the CDI cell by using an automatic battery cycler (WBCS3000, WonaTech, Korea), which was also used to measure cell voltage and current. The CDI operation process comprises cyclic charging (purification) and discharging (regeneration) steps. During CV operation, 1.2 V (charging) and 0 V (discharging) were applied to the CDI module for 10 min each. A constant cell voltage of 1.2 V was used as an application of more than 1.2 V may cause undesirable reactions such as water splitting. In contrast, during CC charging period, various constant current

densities with a range of 1.5 to 3.5 mA/cm² (electrode area = 3.14 cm²) was applied to the CDI unit until cell voltage reached 1.2 V. During CC discharging step, the reversal current was applied until the cell voltage fell to zero. The conductivity of the effluent from the CDI unit cell was measured by using a conductivity meter (3573-10C, HORIBA, Kyoto, Japan). Conductivity measures were converted to actual concentration by using a calibration curve. Within that curve, a 10 mM NaCl solution corresponded to a 1.2 mS/cm solution conductivity. All experiments were conducted at 25°C and repeated three times for reproducibility.

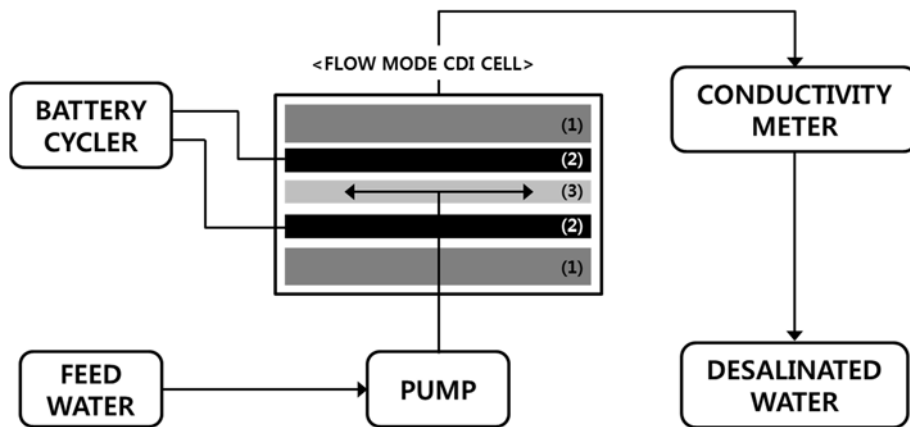


Figure 3-2. Schematic of flow mode capacitive deionization process used in this study. The capacitive deionization module comprised (1) current collectors (graphite), (2) electrodes (activated carbon sheet), and a (3) spacer (polymer).

Calculation of salt adsorption capacity, energy consumption, and charge efficiency

The salt adsorption capacity (mg/g) indicating the amount of salt removed was calculated by integrating salt concentration over time during the charging time, multiplying by flow rate and molecular weight of NaCl in the feed solution, and dividing by both electrode weight, that is:

$$\text{Salt adsorption capacity (mg/g)} = \frac{M_w \times \int (C_i - C_o) \Phi dt}{M_e} \quad (3-1)$$

where M_w is the molecular weight of NaCl (58.443 mg/mmol); C_i and C_o are the influent and effluent concentrations (mM), respectively, during charging; Φ is the flow rate (mL/min), and M_e is the total weight of both electrodes (g).

Energy consumption (kJ/mol) is presented as the ratio of the applied electrical energy to the removed amount of ions. The amount of applied electrical energy in CV (or CC) mode was obtained by integrating cell voltage (or current) over time during charging, and then multiplying by the current (or cell voltage) applied. Energy consumption is thus determined by:

$$\text{Energy consumption (kJ/mol)} = \frac{\int V_c I dt}{2 \times \int (C_i - C_o) \Phi dt} \quad (3-2)$$

, where V_c is cell voltage (V); I is current (A). The factor of 2 is applied to include both positive and negative ions in the salt solution.

Charge efficiency (faradaic efficiency) is the ratio of the removed amount of ions multiplied by Faraday's constant (F , C/mol) to the total charge transferred to the CDI cell, that is:

$$\text{Charge efficiency} = \frac{F \times \int (C_i - C_o) \Phi dt}{\int I dt} \quad (3-3)$$

Charging time (10 min) was established before the start of CV mode, but while in CC mode, charging time was dependent upon the duration required for cell voltage to increase to 1.2 V. Thus, results from the two operational modes with different charging time were adjusted to have the identical electrical charge consumed criterion needed to precisely compare the energy consumption and charge efficiency of the two operational modes. Additionally, analysis based on attaining identical amount of ion removal in the two operational modes was considered (Figure 3-3). For CV operation, 1.2 V was fixed to obtained large capacity with avoiding faradaic reaction such as water splitting. All experimental results are presented as if they were collected from third charging-discharging cycle which showed steady-state.

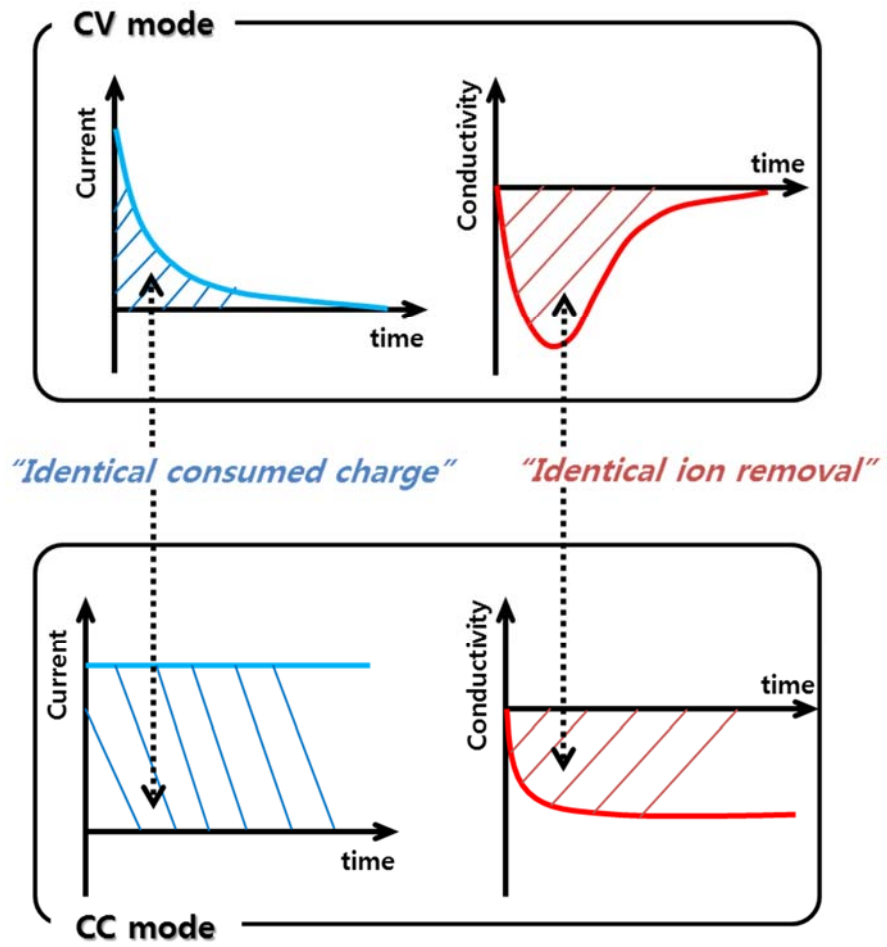


Figure 3-3. Two criteria for accurate comparison of CV and CC operation; identical consumed charge and ion removal during the desalination step.

3.3. Results and Discussion

Constant voltage and constant current modes in CDI operation

Figure 3-4 presents representative conductivity, current, and voltage results of CDI operation in CV and CC modes with 2.5 mA/cm^2 of current density. In CV mode, a constant voltage ($V_c = 1.2 \text{ V}$, Figure 3-4c) was applied for 600 s to the CDI unit. The associated conductivity and current profiles for one cycle are presented in Figure 3-4a and 3-4b, respectively. After application of a constant 1.2 V during 600 s of charging, the voltage was zero for 600 s of discharging (Figure 3-4c).

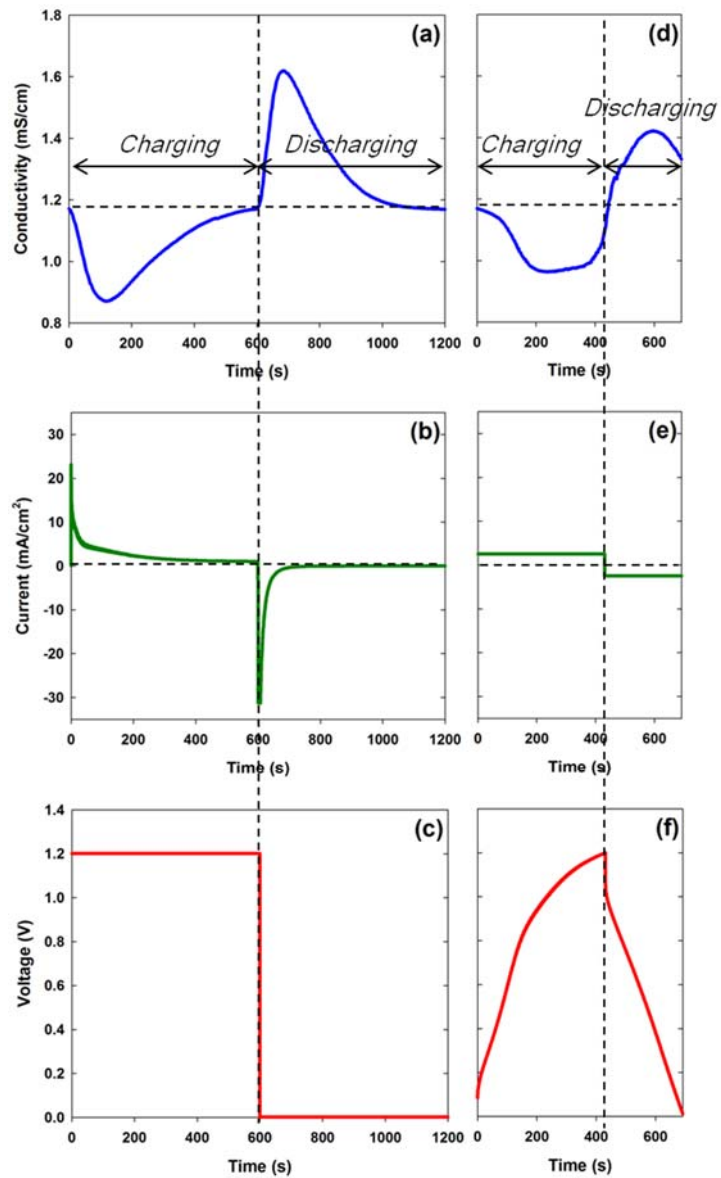


Figure 3-4. Comparison of constant voltage (CV) and constant current (CC) modes in capacitive deionization. Shown are conductivity (a), current (b), and cell voltage (c) graphs from CV mode. (cell voltage = 1.2 V, charging &

discharging time = 10 min respectively, flow rate = 10 mL/min) and conductivity (d), current (e), and cell voltage (f) from CC mode (current density = 2.5 mA/cm² for charging and -2.5 mA/cm² for discharging, flow rate = 10 mL/min).

During CV operation, as a result of ion adsorption to the electrode of the CDI cell, effluent conductivity rapidly decreased to a minimum (~ 0.9 mS/cm at ~ 150 s) from the initial conductivity (1.2 mS/cm; Figure 2a). Subsequently, effluent conductivity gradually increased to the initial conductivity as the ion adsorption capability of the electrode was gradually being exhausted during continuous ion adsorption. During discharging, a rapid increase in conductivity was observed, possibly as a result of the abrupt release of ions as they were desorbed from CDI cell's electrode. Afterwards, there was a gradual decrease in conductivity until the conductivity level of the influent solution was attained. The electrical current in charging step dramatically increased at initiation of charging and then gradually decreased to zero at the end of charging (Figure 3-4b). The current pattern during discharging was similar to that during charging step, but opposite in sign.

During CC mode, a constant current (2.5 mA/cm²) was applied until the CDI cell voltage reaches to 1.2V, whereas for discharging, a reversal current (-2.5 mA/cm²) was applied until the CDI cell voltage reaches to zero (Figure 3-4e). Corresponding conductivity and voltage profiles are displayed in Figure 3-4d & f, respectively. In CC mode, cell voltage gradually increased to the prescribed upper voltage limit (1.2 V) from zero during charging and then decreased to zero during discharging (Figure 3-4f). Note that an instantaneous rise in cell voltage from zero to 0.2 V occurred at the initiation of charging. Similarly, a 0.2 V drop

(1.2 V to 1.0 V) occurred at the beginning of discharging. This 0.2 V change is the result of an ohmic drop caused by the CDI cell's electrolyte resistance.

Two major differences were observed in the conductivity profiles (i.e., the ion removal profile) of CV and CC modes. First, in CV mode, the time to reach the minimum conductivity level was shorter than that in CC mode (~100 s for CV mode and ~200 s for CC mode). Second, in CC mode compared with CV mode, the low conductivity level in the desalinated stream was broadly maintained over a longer period (approximately 200 ~ 350 s). Those results indicate that CC mode may be advantageous as it can produce a more constant ion concentration in the desalinated stream (Zhao et al. 2012). These tendency of differences between CV and CC modes are identically observed in MCDI as shown in Figure 3-5

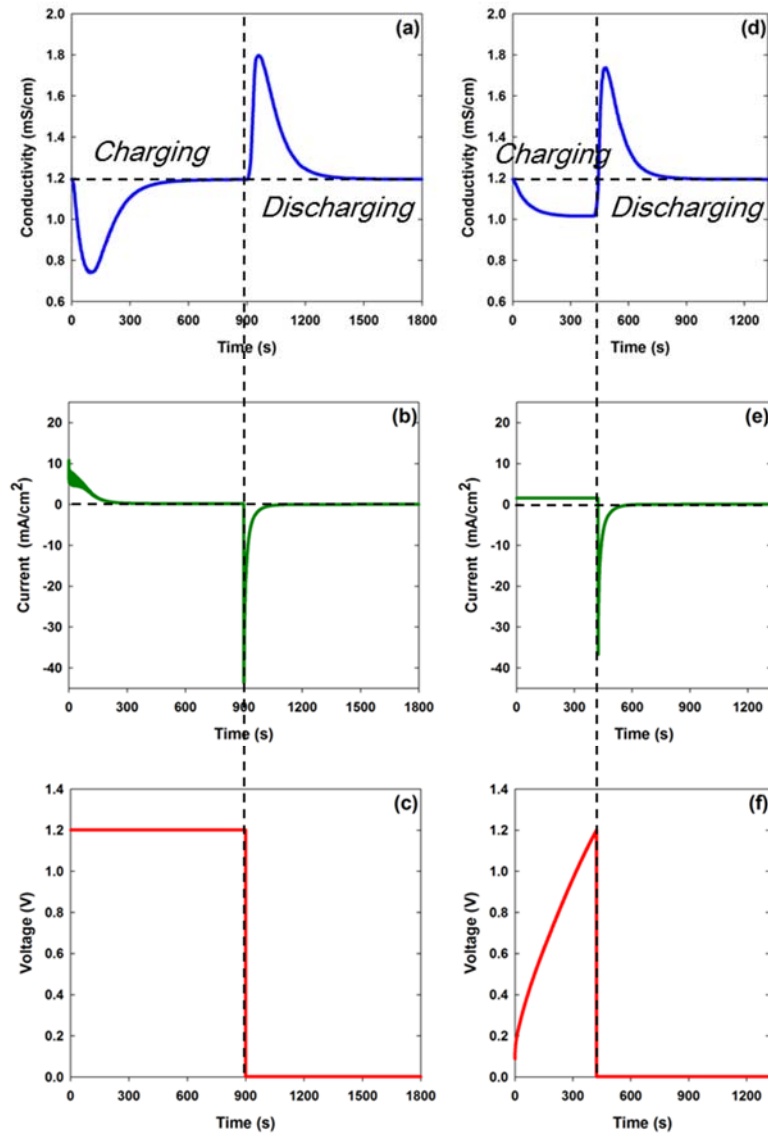


Figure 3-5. Comparison of constant voltage (CV) and constant current (CC) modes in membrane-assisted capacitive deionization. Shown are conductivity (a), current (b), and cell voltage (c) graphs from CV mode. (cell voltage = 1.2 V, charging & discharging time = 10 min respectively, flow rate = 10 mL/min) and

conductivity (d), current (e), and cell voltage (f) from CC mode (current density = 2.5 mA/cm² for charging and -2.5 mA/cm² for discharging, flow rate = 10 mL/min).

Salt adsorption capacity

Figure 3-6 presents the representative salt adsorption capacity from CV and CC modes with 2.5 mA/cm^2 of current density (Figure 3-4a & b, respectively). The salt adsorption capacity was derived by applying equation (1) to the effluent conductivity data obtained during the charging step. In CV mode (Figure 3-4a), the salt adsorption curve was convex and its primary differential value indicating the rate of change in salt adsorption capacity with time approached zero, which means the salt adsorption capacity without further increase. This behavior indicates that ion removal was fastest at the beginning of charging (after a short lag period) and then gradually slowed. In contrast, in CC mode (Figure 3-4b), there was a longer lag period than CV mode and the salt adsorption curve approached that of a straight line. The curves primary differential value remained steady, which indicates approximately constant ion removal rate during CC charging. Similar observations were made at the conditions of other current densities ($1.5 \text{ mA/cm}^2 \sim 3.5 \text{ mA/cm}^2$), refer to Figure 3-7. Figure 3-7 shows the salt adsorption capacity and salt adsorption rate of CV and CC modes with various constant current densities ($1.5 \sim 3.5 \text{ mA/cm}^2$). As shown in Figure 3-7, the salt adsorption capacity in CV and CC modes is fundamentally different. For example, during charging period, the salt adsorption capacity curve of CV mode is convex, while that of CC mode appeared to be linear after initial significant lag period. This difference is more vividly displayed by salt adsorption rate in

Figure 3-7b. In CV mode, the ion removal rate rapidly increased at the very beginning, and gradually decreased passing its maximum, and eventually became zero at the end of charging. On the other hand, in CC mode, that appeared to be steady for a considerable period of time after sluggish increasing at the beginning (1.5, 2.0, 2.5 mA/cm², Figure 3-7b). Note that the steady ion removals were not observed at the conditions of the higher current density (3.0, 3.5 mA/cm²). This is because the maximum allowable voltage (1.2V) was quickly reached before the region of steady ion removal rate.

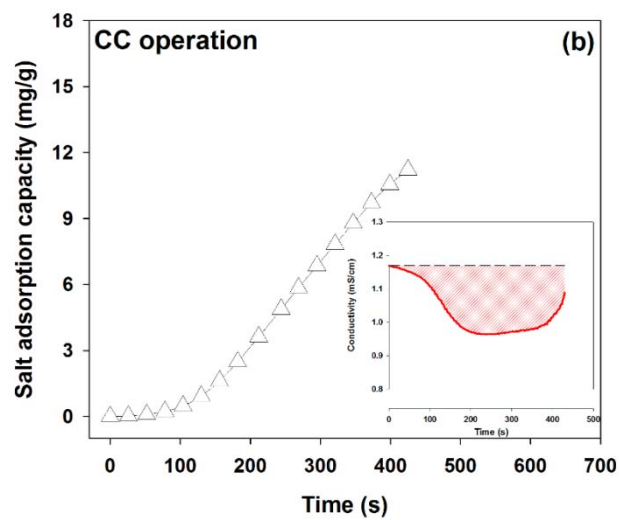
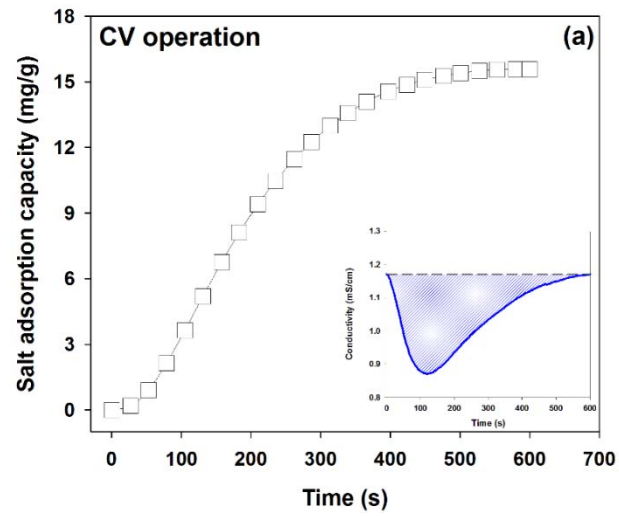


Figure 3-6. The representative salt adsorption capacity curve in (a) constant voltage (CV) and (b) constant current (CC) operation during charging step. The salt adsorption capacity from (a) constant voltage (CV) mode (cell voltage = 1.2 V, charging and discharging time = 10 min respectively, flow rate = 10 mL/min)

and (b) constant current (CC) mode (current density = 2.5 mA/cm^2 for charging and -2.5 mA/cm^2 for discharging, flow rate = 10 mL/min) during capacitive deionization. The inserted figure displays the effluent conductivity during charging time (from Figure 3-4a & d). The shaded areas in the inserts represent the salt adsorption capacity.

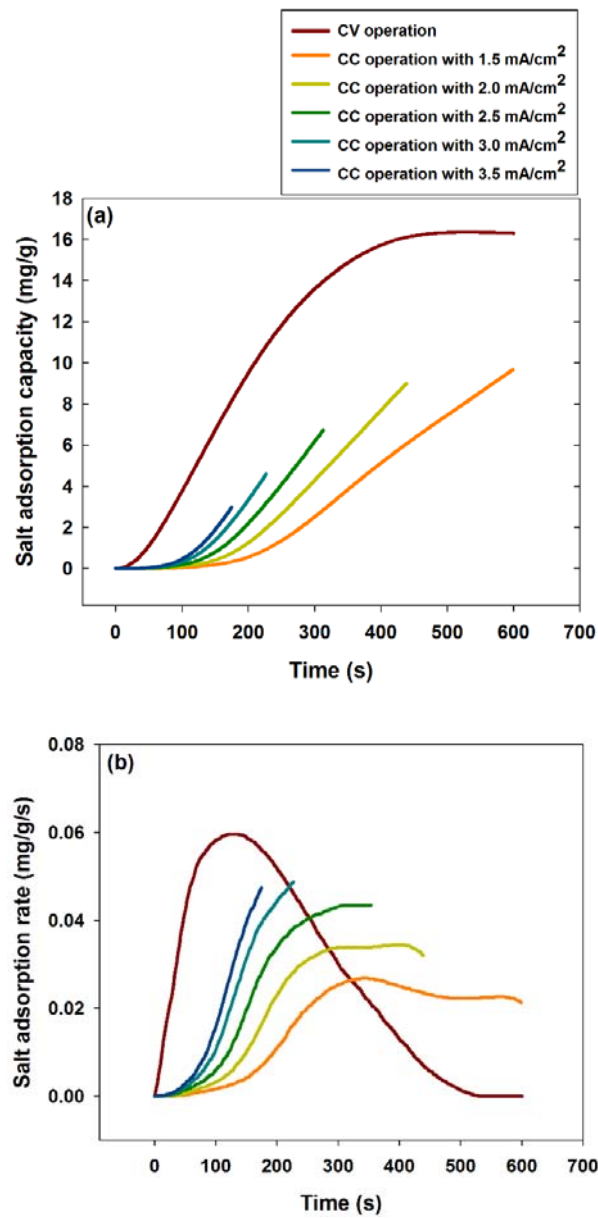


Figure 3-7. The salt adsorption capacity curve (a) and salt adsorption rate (b) of constant voltage (CV, 1.2V) and constant current (CC) operation with various constant current densities (1.5 ~ 3.5 mA/cm²).

The different ion adsorption characteristics in the two CDI operational modes are the result of differences in cell voltage between the two modes. For CV mode, large amounts of ions are rapidly adsorbed due to the strong initial electrostatic force ($V_c \sim 1.2$ V) applied at the beginning of the charging step. Subsequently, ion adsorption decreased gradually due to the gradual exhaustion of ion adsorption capacity of the electrodes. However, in CC mode, a fixed current level results in a gradual increase in cell voltage from zero to the limiting voltage (1.2 V; see Figure 3-4f). This constant current results in a linear increase in ion adsorption, following an initial lag time at the beginning of the charging step. The lag time in CC mode was induced by the low initial cell voltage. Application of voltage to the CDI electrodes simultaneously generates counter-ion adsorption and co-ion expulsion. The ratio of counter-ion adsorption to co-ion expulsion increases with an increase in cell voltage (Porada et al. 2013b). Therefore, the ion removal rate at the beginning of charging step in CC mode is slow because co-ion expulsion and counter-ion adsorption rates are equivalent, thus producing the initial lag time. With similar logic, the short lag time in CV mode is the result of high initial adsorption rate and a low initial expulsion rate.

Energy consumption and charge efficiency

Figure 3-8a shows the energy consumption and charge efficiency depending on charging current with typical CC operation. It was observed that with increasing charging current, energy consumption is increased and charge efficiency is decreased due to conduction loss. In addition, high charging current could not provide the sufficient charging time (Figure 3-8b) for desalination step and this caused the high energy consumption and low charge efficiency.

Figure 3-9 shows the energy consumption and charge efficiency in CV and CC modes under two comparison conditions: identical electrical charge consumed and identical amounts of ion removal. As shown in Figure 3-9, energy consumption in CC mode with various constant current densities was reduced by about 26 ~ 30% compared to CV mode at two criteria for comparison (Figure 3-8a & b). The lower energy consumption in CC mode is due to the lower overall cell voltage in CC mode than in CV mode, suggesting that CC mode is superior to CV mode in terms of energy consumption. In MCDI, this preferable energy consumption of CC mode was also observed as shown in Figure 3-10. On the other hand, the charge efficiencies of the two modes of operation were notably similar (Figure 3-9c & d). These charge efficiency are similar to those reported in the previous studies (Kim and Choi 2010b; Zhao et al. 2012). However, because our CDI process operated at a low voltage (<1.2 V) with no faradaic reaction, our charge efficiency is lower than expected. Current leakage due to

CDI cell design characteristics or to secondary reactions such as localized oxidation of the electrode surface (electrode degradation) and pH change, may have contributed to this lower than expected level of charge efficiency (Bouhadana et al. 2011). Compared to results of CDI, the charge efficiencies of MCDI as shown in Figure 3-10 was over 90% at high salt adsorption capacity and charge. This can be explained by the prevention of side effect in MCDI using ion exchange membrane.

Although the results indicate that CC mode is more energy-efficient than CV mode, CC mode is not absolutely favorable in all CDI processes because the CV operation can result in faster desalination than CC operation under a given operation time due to the use of a high cell voltage. That is., CV operation is advantageous in case of seeking for a high desalination rate (kinetic point of view). On the other hand, CC operation is more energy efficient than CV operation due to the use of low cell voltage. CC operation, in other words, is advantageous in case of seeking for low energy consumption (thermodynamic point of view). In these respect, we can achieve optimal salt adsorption capacity and energy consumption in a CDI facility by selecting or integrating appropriate CV and CC operations to meet the required CDI process.

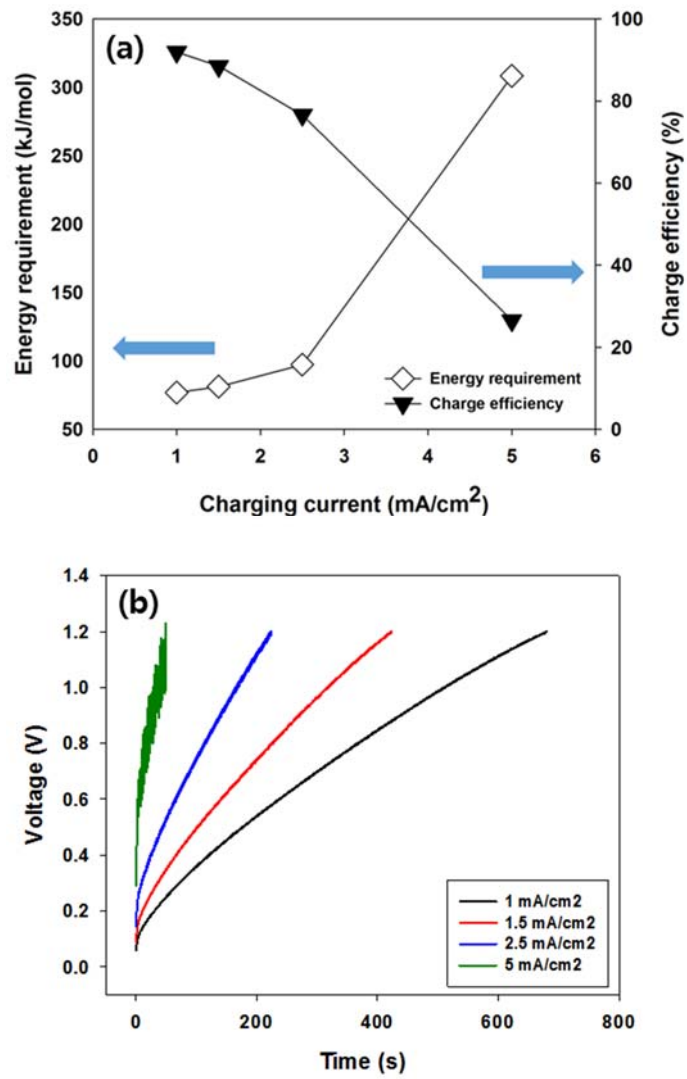


Figure 3-8. (a) Energy consumption and charge efficiency, (b) voltage profiles depending on charging currents (1, 1.5, 2.5, 5 mA/cm²) with CC operation in MCDI.

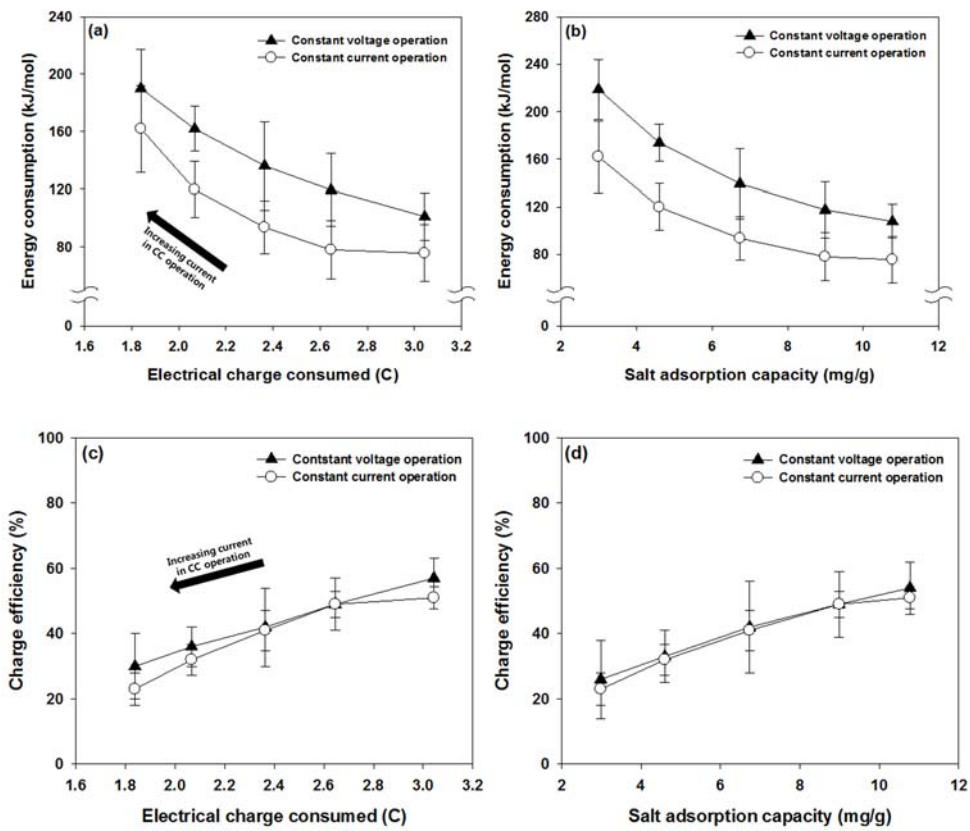


Figure 3-9. Comparison of energy consumption and charge efficiency in CDI constant voltage (CV) and constant current (CC) mode with various constant current densities (1.5, 2, 2.5, 3.0, 3.5 mA/cm²). Two criteria of identical electrical charge consumed (a and c) and identical amount of ion removal (b & d) were employed. The arrows indicate the increasing current in CC operation.

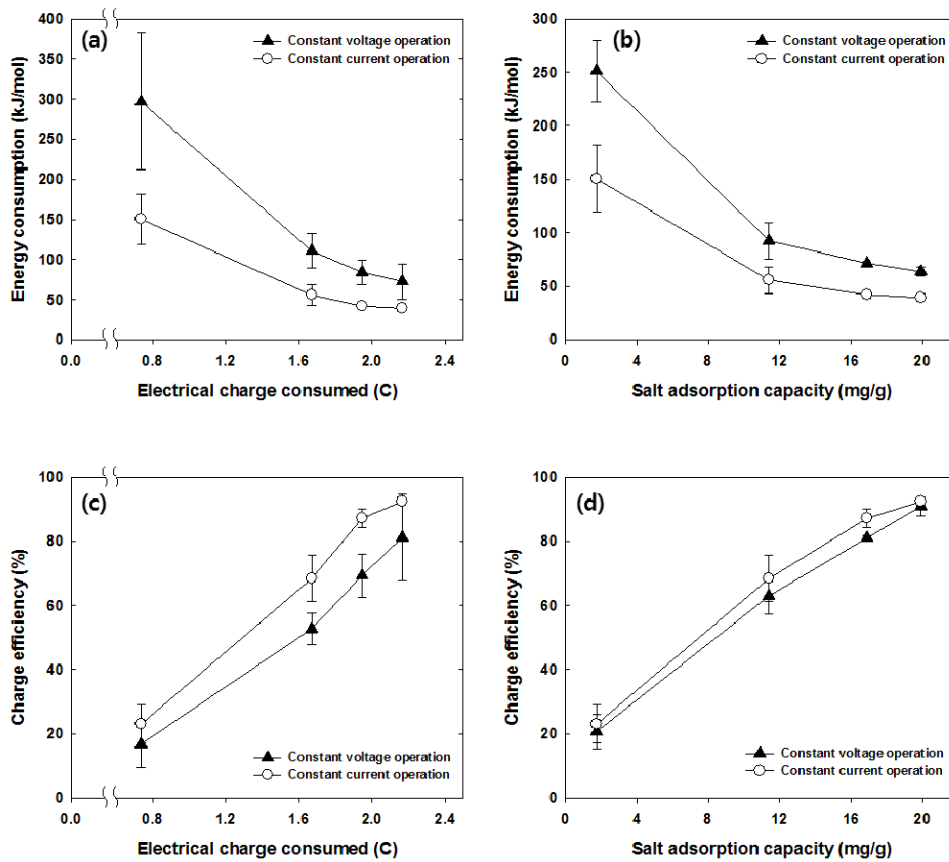


Figure 3-10. Comparison of energy consumption in MCDI constant voltage (CV) and constant current (CC) mode with various constant current densities (1, 1.5, 2.5, 5 mA/cm²). Two criteria of identical electrical charge consumed (a and c) and identical amount of ion removal (b & d) were employed. The arrows indicate the increasing current in CC operation.

Figure 3-11 shows desalination performance and energy consumptions of integrated CDI operation with CV and CC. To investigate integrated operation, desalination process was designed to operate with CC operation until cell voltage reached to 1.2 V, and followed by CV operation for 10 min. The concentration and voltage profiles (Figure 3-11a and 11b) reflected the characteristics of each operation (CC and CV) as discussed in Figure 3-5. In desalination performance (Figure 3-11c), the integrated operation with CV and CC showed similar salt adsorption capacity with single CV operation (~20 mg/g) and higher salt adsorption capacity than single CC operation (~12 mg/g). This suggests that integrated operation can compensate insufficient desalination capacity of single CC operation. Moreover, in Figure 3-11d, energy consumption of integrated operation was lower than single CV operation in spite of similar salt adsorption capacity, indicating good energy efficiency of integrated operation.

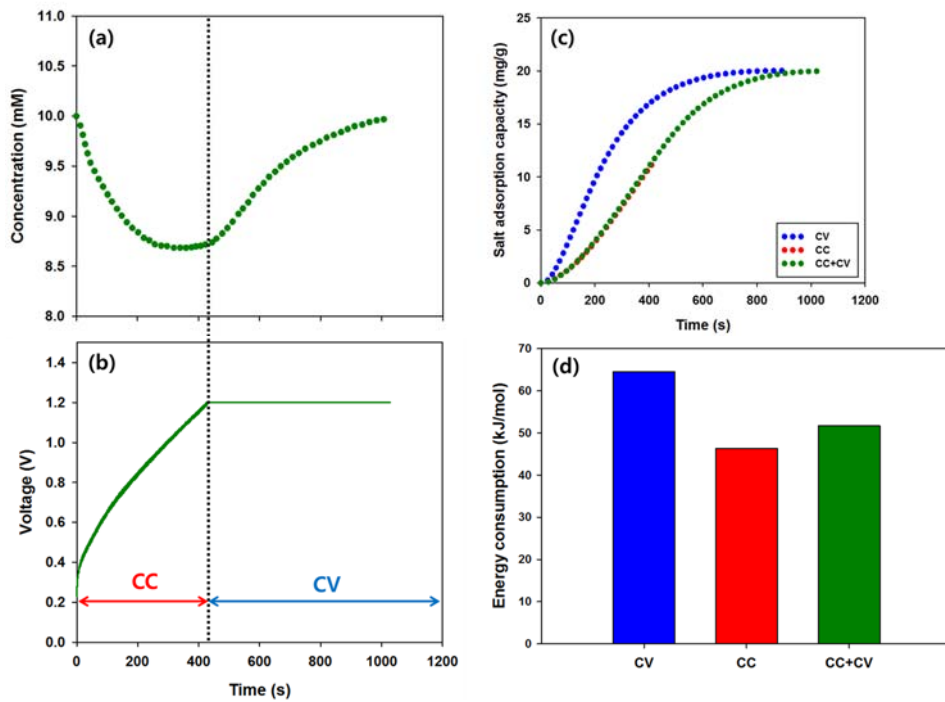


Figure 3-11. Integration of CV and CC operation. The (a) concentration, (b) voltage, (c) salt adsorption capacity profiles were obtained by integrated CDI operations with CC (1.5 mA/cm^2 to 1.2 V) and CV (1.2 V). The energy consumption (d) of integrated operation was compared to that of CV and CC operation, respectively.

3.4. Summary

The salt adsorption capacity and energy consumption in two operational modes (CV and CC) in a CDI desalination cell were compared on the bases of identical amount of ion removal and electrical charge consumed criteria. The higher overall cell voltage of CV mode results in faster salt adsorption under a given charging time than CC mode. Nevertheless, CC mode consumed approximately 26 ~ 30% less energy than that consumed in CV mode in both criteria, but there were similar charge efficiencies in CC and CV modes. Our results suggest that, in practice, optimal salt adsorption capacity and energy consumption in a CDI facility can be achieved by combining or selecting appropriate CV and CC modes.

4. Direct energy recovery system for capacitive deionization

4.1. Introduction

With greater water scarcity caused by worldwide industrialization and population growth, desalination has become a crucial strategy to address water scarcity; desalination involves the use of a water treatment technology that produces fresh water from sea or brackish water (Anderson et al. 2010; Elimelech and Phillip 2011; Greenlee et al. 2009; Jury and Vaux 2007; Shannon et al. 2008). Capacitive deionization (CDI) is the state-of-the-art desalination approach that is based on the use of the electrical double layer induced by a cell voltage difference between two electrodes (Farmer et al. 1997; Jia and Zou 2012; Oh et al. 2006; Ryoo and Seo 2003).

CDI has many advantages in terms of environmental aspects and energy efficiency because chemical treatment for regeneration is not required and a low electrical voltage is applied for the desalination process (Porada et al. 2013b; Suss et al. 2015; Welgemoed and Schutte 2005). Furthermore, the energy consumed during the desalination step can be partially recovered by ion release during the regeneration step due to the capacitive nature of CDI (Anderson et al. 2010; Demirer et al. 2013; García-Quismondo et al. 2013a; García-Quismondo

et al. 2013b; Zhao et al. 2013a). Recovered energy can be utilized to charge another CDI cell operating in a purification step or captured in an energy storage medium such as a supercapacitor for another use, which enhances the energy efficiency of CDI. Because the energy efficiency is an important parameter in today's desalination technology, the energy recovery in CDI is a substantial advantage versus other desalination technologies. In addition, the energy recovery system combined with CDI technology will facilitate its application to desalinate a high concentration brine such as seawater, which is not generally recommended because of the high energy consumption (Anderson et al. 2010).

Following the first study on the conceptual energy recovery in CDI reported in 2003 (Shiue et al. 2003), Długolecki and van der Wal estimated the potential of energy recovery in membrane-assisted CDI (MCDI) without the actual energy recovery by calculating the consumed and recoverable energy from the voltage profiles under constant current operation as shown in Figure 4-1 (Długolecki and van der Wal 2013). However, this approach has a limitation in that the energy from the charged MCDI cell was not actually recovered. Alternatively, Alkuran et al. and Pernía et al. introduced a buck-boost converter in the energy recovery system of the modeled CDI cell (composed of a resistor and a capacitor), and the extent of energy recovery was reported (Alkuran and Orabi 2008; Alkuran et al. 2008; Pernía et al. 2014; Pernía et al. 2012; Pernía et al. 2014). Figure 4-2 illustrates the proposed circuit of recovery system in CDI combined with a buck-

boost converter. A buck-boost converter is an electronic device used to control the energy transfer between the CDI cell and the supercapacitor. These studies had a limitation in that the modeled CDI cell cannot describe the actual desalination behavior of the CDI.

Therefore, this study intended to construct the direct energy recovery system in an actual MCDI cell with a buck-boost converter and to investigate the energy recovery ratio (recovered energy / consumed energy) under various operational conditions (Kang et al. 2014; Kim and Yoon 2013; Porada et al. 2013a; Zhao et al. 2012; Zhao et al. 2013b) (constant voltage (CV) charging with various voltages and times, constant current (CC) charging with various currents and concentrations of feed water, discharging with various reference currents of the buck-boost converter, and capacitances of the supercapacitor) to determine the influential parameters affecting energy recovery in the MCDI cell.

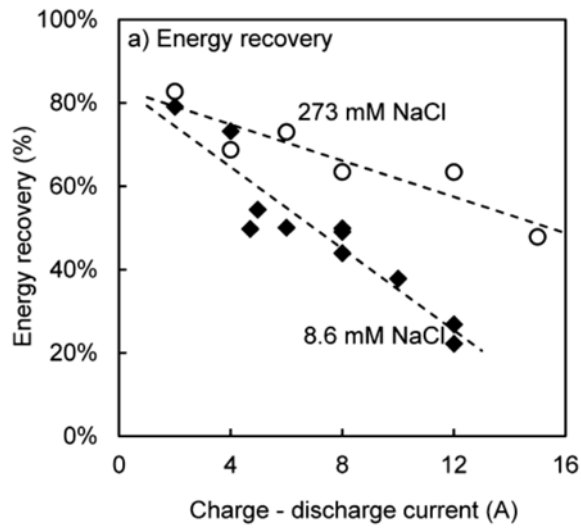
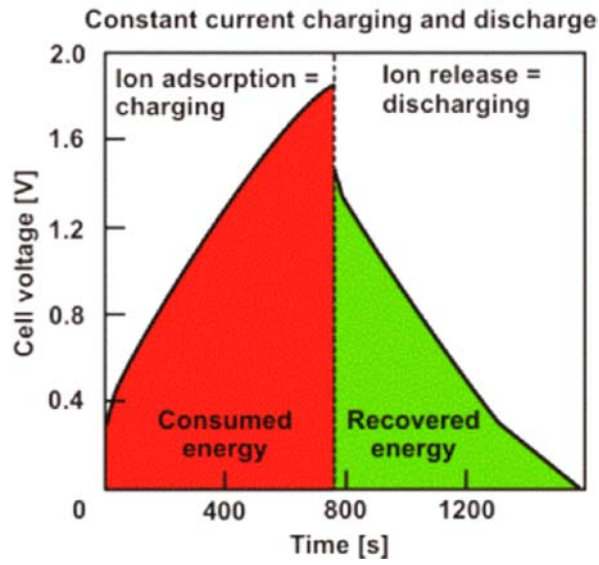


Figure 4-1. Prediction of energy recovery of CDI process using constant current charging and discharging. Energy recovery ratio can be calculated by the ratio of recovered energy during the discharging step to consumed energy during the charging step (Długolecki and van der Wal 2013).

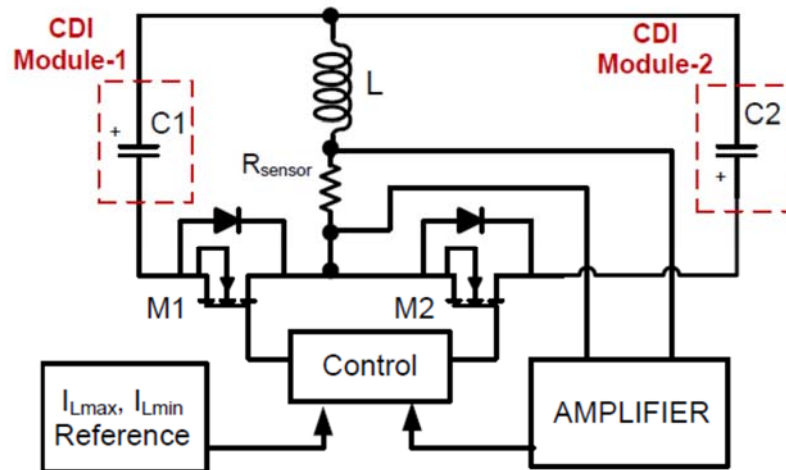


Figure 4-2. The schematic of proposed circuit of energy recovery system in CDI with a buck-boost converter (Pernia et al. 2014)

4.2. Materials and Methods

Electrode preparation

The carbon sheet electrodes for the CDI cell were fabricated from a mixture of activated carbon powder (MSP20, Kansai Coke and Chemicals, Amagasaki, Japan) (Kim and Yoon 2013; Porada et al. 2013a), carbon black (Super P, Timcal), and polytetrafluoroethylene (PTFE, Sigma-Aldrich, USA) with a weight ratio of 86:7:7. The mixture was kneaded with a few ml of ethanol for uniformity and then made into a sheet form using a roll press machine (electrode thickness of $\sim 300 \mu\text{m}$). The pressed mixture in sheet form was dried in a vacuum oven at $120 \text{ }^\circ\text{C}$ for 12 h and then cut for use for desalination and energy recovery processes after drying.

Construction of a real MCDI cell with a buck-boost converter

Figure 4-3 shows a schematic of the actual MCDI cell for energy recovery that is connected with a supercapacitor via a buck-boost converter. The MCDI cell is composed of a graphite current collector, anion- and cation-exchange membranes (Selemion, AGC ENGINEERING CO. LTD, Japan), carbon sheet electrodes (area $\sim 3 \text{ cm}^2$), and a polymer spacer (nylon sheet, thickness $\sim 200 \text{ }\mu\text{m}$). Note that the buck-boost converter is composed of an inductor and an electronic switch for controlling the energy transfer between the MCDI cell and the supercapacitor.

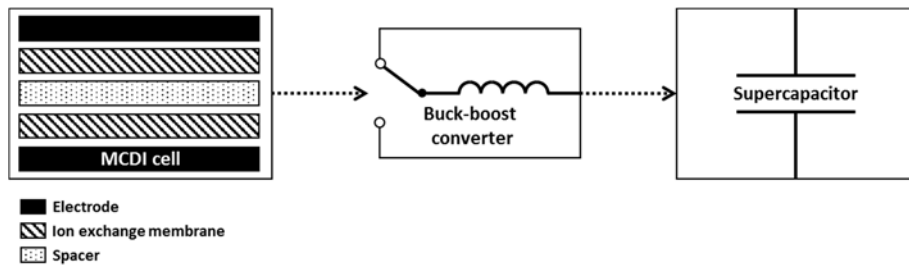


Figure 4-3. The schematic of an actual membrane capacitive deionization (MCDI) cell for energy recovery that is connected with a supercapacitor via a buck-boost converter. The MCDI cell is composed of electrodes, ion exchange membranes and a spacer. The electrical energy consumed during the desalination step is partially transferred to the supercapacitor.

MCDI operation with energy recovery is divided into the desalination (charging) step and the energy recovery (discharging) step. The desalination step in a real MCDI cell was performed in single-pass mode in this study (Porada et al. 2013b). A NaCl feed solution was supplied to the MCDI cell with a peristaltic pump at a flow rate of 2 mL/min. The conductivity of the effluent from the MCDI cell was measured using a flow-type conductivity meter (3573-10C, HORIBA, Japan) and then converted to the actual concentration. Two charging modes, CV and CC charging, were employed for desalination using a cycler (WBCS3000, WonaTech, Korea).

For CV charging, a constant voltage (0.3, 0.6, 0.9, and 1.2 V) was applied to the MCDI cell for the predetermined charging time (1, 3, 6, and 10 min) with a fixed concentration of NaCl (10 mM). For CC charging, constant current (1, 1.5, 2.5, and 4 mA/cm²) was applied until the cell voltage reached 1.2 V with several levels of NaCl concentration (5, 10, 50, and 100 mM). The voltage and current of the MCDI cell during the charging step were recorded by a cycler. Following the completion of charging, the discharging step was conducted to transfer energy from the MCDI cell to the supercapacitor using the buck-boost converter controlled by a digital signal processor (TMS320C28346, Texas Instrument, USA). Note that zero or reverse voltage are applied during the discharging step in a typical MCDI process without an energy recovery system.

Figure 4-4 shows the schematic for how the buck-boost converter is operated to deliver the energy stored in the CDI cell into the supercapacitor. The energy flow is dominated by the voltage difference between the input voltage (CDI cell) and the output voltage (supercapacitor). A buck-boost converter is required to construct an energy recovery system in the CDI process. Without a buck-boost converter, the energy transfer is terminated if the voltage is equal on both sides with remaining residual energy in the CDI cell. In addition, the energy transfer through the direct connection has the possibility to damage the cell by generating unexpected massive current flow. As shown in Figure 4-4a, the electrical current flows from the CDI cell to the inductor as the switch toward the CDI cell is closed (stage #1). Next, the CDI cell is discharged until the inductor current reaches the maximum value. As the switch toward the CDI cell is opened and the switch toward the supercapacitor is closed (stage #2), the current starts to charge the supercapacitor until the inductor current reaches zero. Figure 4-4b shows the specific current profiles of the CDI cell and the supercapacitor corresponding to stage #1 and stage #2. These numerous cyclic operations continue until the CDI cell is completely discharged. Please refer to a previous study for the details regarding the operation of the buck-boost converter (Pernía et al. 2012). The ratio of the duration of stage #1 over the entire duration in one cycle (stage #1 and stage #2) is presented as the converter duty (D), and the average current through the CDI cell is expressed as the reference current (I_{ref}), which is the operating parameter controlling the energy transfer rate during the discharging

step. The reference current and the capacitance of supercapacitor were adjusted over the values of 5, 25, 50, and 100 mA and 2.5, 5, 10, and 20 F, respectively.

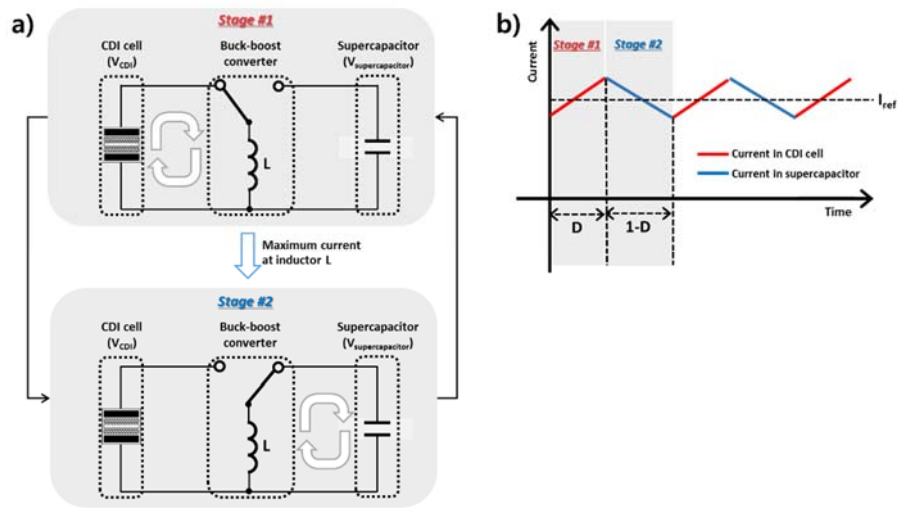


Figure 4-4. Schematic of the buck-boost converter operation during delivery of the energy stored in the CDI cell into the supercapacitor. The buck-boost converter is operated by a) an automatic switching depending on the current intensity at an inductor (L), and it generates b) specific current profiles in the CDI cell and the supercapacitor. The ratio of the duration of stage #1 over the whole duration in one cycle (stage #1 and stage #2) is presented as the converter duty (D), and the average current through the CDI cell is expressed as the reference current (I_{ref}).

Energy recovery ratio and salt adsorption capacity

The energy recovery ratio is defined as the amount of energy recovered in the supercapacitor during the discharging step divided by the consumed energy during the charging step. The consumed energy can be calculated by integrating the power of the MCDI cell over the charging time, and the recovered energy can be calculated as the square of the voltage increase of the supercapacitor multiplied by half of the capacitance, as expressed in Equation 4-1.

$$\text{Energy recovery ratio} = \frac{0.5 C_s \Delta V^2}{\int V_c I dt} \quad (4-1)$$

, where C_s is the capacitance of the supercapacitor (F); ΔV is the voltage increase (V) in the supercapacitor from 0 V; V_c is the cell voltage (V); I is the current (A). Figure 4-5 shows how the energy recovery ratio was obtained in this study.

In Equation 4-1, the current (I) in the denominator reflects the ion adsorption rate during the charging step, and the voltage increase in supercapacitor (ΔV) in the numerator reflects the amount of electrons delivered from the MCDI cell during the discharging step. This equation implies that the energy recovery ratio is closely related to the ion removal performance. Accordingly, the salt

adsorption capacity was investigated under various operational conditions affecting the energy recovery ratio. As expressed in Equation 4-2, the salt adsorption capacity (mg/g) was calculated by integrating the concentration difference over time, multiplied by the flow rate and molecular weight of NaCl over two electrode weights.

$$\text{Salt adsorption capacity (mg/g)} = \frac{M_w \int (C_i - C_o) \Phi dt}{M_e} \quad (4-2)$$

, where M_w is the molecular weight of NaCl (58.443 mg/mmol); C_i and C_o are the influent and effluent concentrations (mM), respectively, during charging; Φ is the flow rate (mL/min); and M_e is the total weight of both electrodes (g).

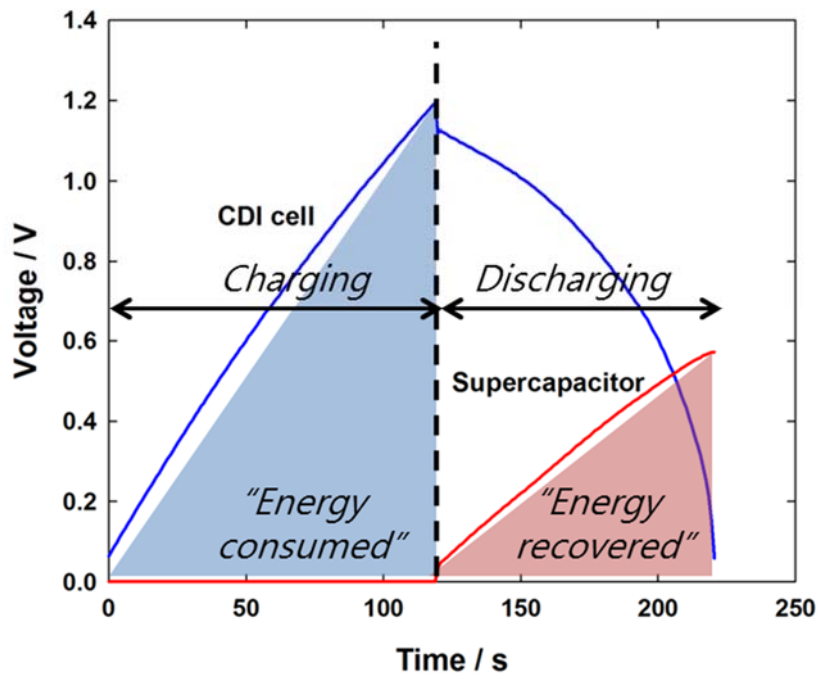


Figure 4-5. The calculation of energy recovery ratio. The energy recovery is obtained from the ratio of energy consumed for desalination (ion adsorption) to energy recovered (stored into the supercapacitor) by the buck-boost converter.

4.3. Results and Discussion

MCDI operation with energy recovery process

Figure 4-6 shows the representative voltage and conductivity profiles during the charging (desalination) and discharging (energy recovery) steps with two charging modes: CV (Figures 4-6a and b) and CC (Figures 4-6c and d) charging. Figure 3a shows the constant voltage (1.2 V) during the CV charging step, and its corresponding conductivity was rapidly decreased to a minimum and then gradually increased to the initial value (~ 1.2 mS/cm, Figure 4-6b), while Figure 4-6c shows the linear increase in voltage from zero to 1.2 V (a pre-set voltage) during the CC charging step, which is the capacitive characteristic of the MCDI cell (Zhao et al. 2012). The corresponding conductivity in CC charging was widely maintained with a constant value (Figure 4-6d). Note the instantaneous cell voltage increase of approximately 0.1 V at the beginning of charging, which indicates the ohmic resistance of the MCDI cell (Xu et al. 2007). This characteristic of conductivity according to charging modes is consistent with previous studies (Kang et al. 2014; Zhao et al. 2012).

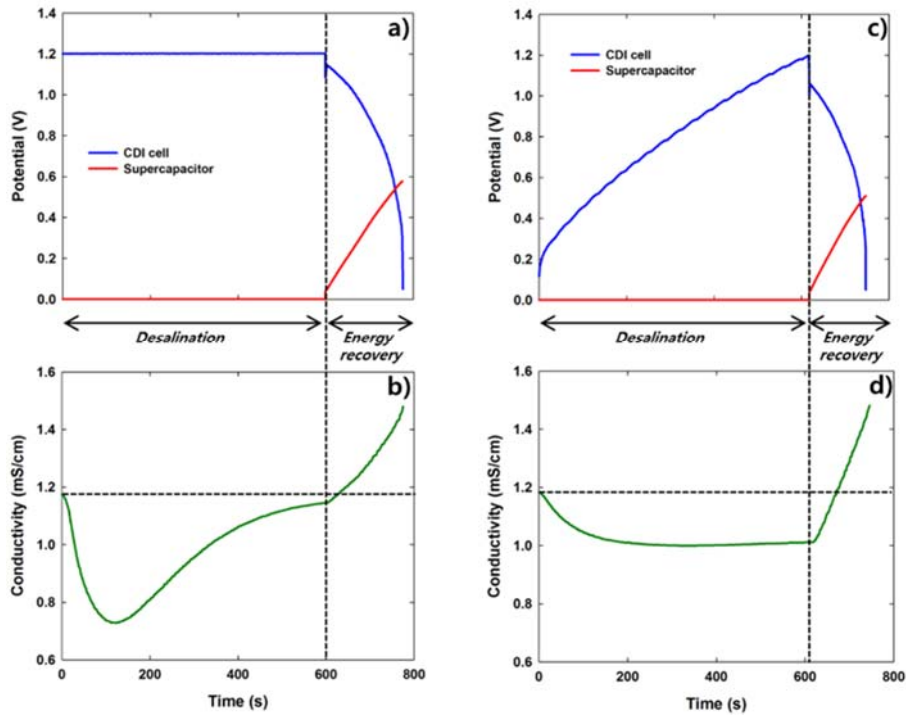


Figure 4-6. Representative voltage and conductivity profile in one cycle during MCDI operation with energy recovery. Shown are the potential (a) and conductivity (b) from constant voltage (CV) charging (1.2 V, 10 min, and 10 mM) and the potential (c) and conductivity (d) from constant current (CC) charging (1.5 mA/cm² and 10 mM). The energy recovery process was performed with a reference current of 5 mA of the buck-boost converter and capacitance of 5 F of the supercapacitor. The voltage profiles of the CDI cell and the supercapacitor are depicted as the blue solid line and red solid line, respectively.

During the discharging step, two important observations can be made in Figure 4-6. The first observation is that the voltage profile of the MCDI cell (expressed as V_{CDI} in Figure 4-4) decreases to zero (Figures 4-6a and c), regardless of CV or CC charging, indicating the energy release as a result of ion desorption from the electrodes. Simultaneously, the voltage increase in the supercapacitor (expressed as $V_{\text{supercapacitor}}$ in Figure 4-4) from zero indicates the actual energy transfer from the MCDI cell to the supercapacitor. The energy consumed during the charging step to desalt the feed water is released by ion desorption from the electrodes during the discharging step and is partially transferred into the supercapacitor via the buck-boost converter. The second observation is that the conductivity increases in an approximately linear manner during the discharging step (corresponding to the voltage decrease in the MCDI cell) as a result of desorption and release of ions from electrodes to the flow channel, as shown in Figures 4-6b and d. This linearly increasing conductivity profile during the discharging step is a distinctive phenomenon in the MCDI system with a buck-boost converter in contrast with that without a buck-boost converter (Zhao et al. 2012). This observation can be explained by the specific current profile with time applied to the MCDI cell, which is determined by multiplying the converter duty (D) by the reference current (I_{ref}) of the buck-boost converter. Figure 4-7 shows the actual current profile applied to the MCDI cell during the discharging step. In energy recovery process using buck-boost converter, actual current applied to the MCDI cell is determined by multiplying converter duty (D) with

reference current (I_{ref}) of the buck-boost converter, the relationship between input / output voltage (MCDI cell / supercapacitor voltage in this study) and converter duty is defined as follows:

$$\frac{V_{supercapacitor}}{V_{MCDI}} = \frac{D}{1 - D} \quad (4-3)$$

$$D = \frac{V_{supercapacitor}}{V_{supercapacitor} + V_{MCDI}} \quad (4-4)$$

, where V_{MCDI} is voltage in MCDI cell (V); $V_{supercapacitor}$ is voltage in supercapacitor (V); D is converter duty with dimensionless value varied from zero to unity. While buck-boost converter was operated by tuning the reference current, I_{ref} (A), actual current in the MCDI cell is applied with $I_{ref} \times D$ as shown in Figure 4-7. The linearly increasing current with time flows through the MCDI cell and causes a linearly increasing conductivity, which is characteristic of the MCDI system with a buck-boost converter.

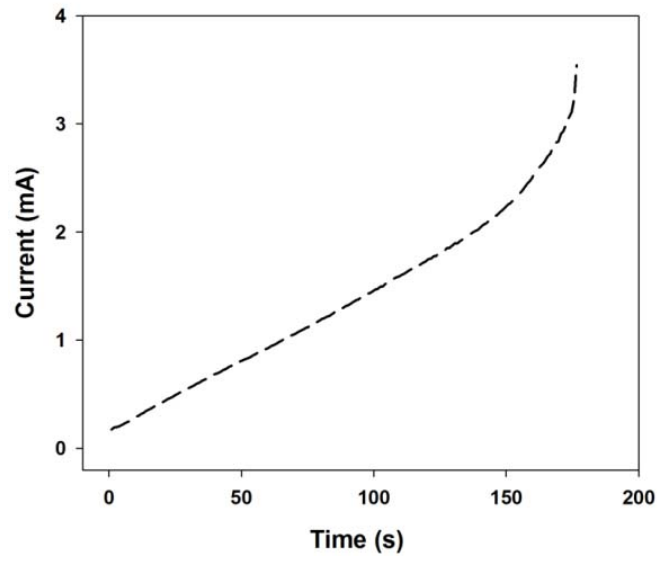
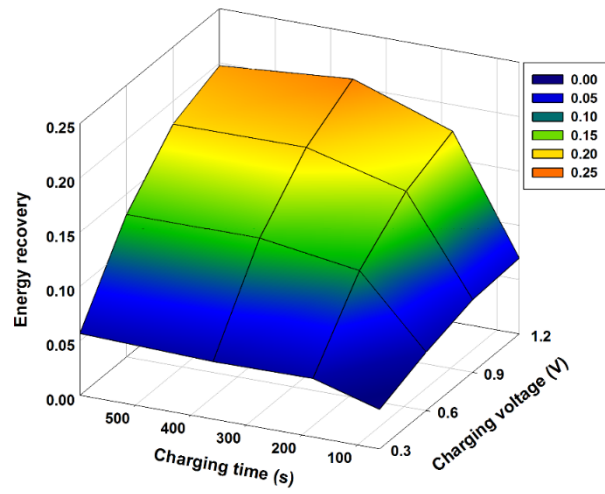


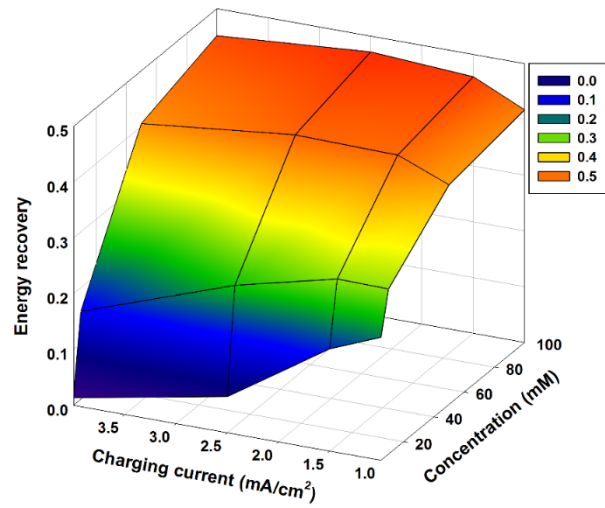
Figure 4-7. The actual current profile applied to the MCDI cell during the discharging step. The discharging current is obtained from the experimental data set of I_{ref} ($=5$ mA), V_{MCDI} , $V_{supercapcitor}$.

Energy recovery in MCDI with CV and CC charging

Figure 4-8 shows the energy recovery ratio (calculated by Equation 4-1) in MCDI operation as a function of the charging time and the voltage in CV mode (Figure 4-8a) and as a function of the charging current and the concentration in CC mode (Figure 4-8b). Note that a reference current of 5 mA of the buck-boost converter and a capacitance of 5 F of the supercapacitor were employed during the discharging step. As shown in Figure 4-8a, in CV charging mode, the higher energy recovery ratio was achieved with the longer charging time and higher voltage. The energy recovery ratio was approximately 0.2 at a charging voltage of 1.2 V and charging time of 10 min. The energy recovery ratio of 0.2 means that 20% out of the total energy consumed for desalting the feed water is recovered. The energy recovery ratio was approximately 0.036 (3.6%) at a charging voltage of 0.3 V and a charging time of 1 min. In CV charging mode, the change in the energy recovery ratio became more sensitive at the region of the longer charging time (0.06 ~ 0.20 of energy recovery ratio for 10 min vs. 0.06 ~ 0.07 of energy recovery ratio for 1 min with varying charging voltages) and the region of the higher charging voltages (0.07 ~ 0.20 of energy recovery ratio at 1.2 V vs. 0.04 ~ 0.06 of energy recovery ratio at 0.3 V with varying charging times).



(a)



(b)

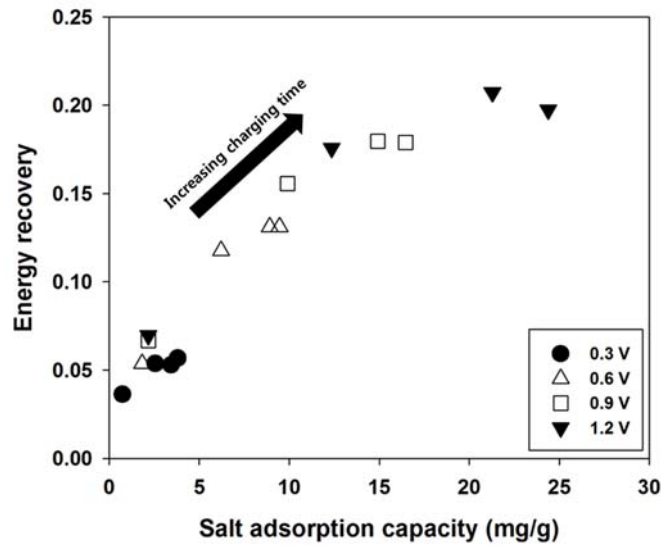
Figure 4-8. Three-dimensional representation of the energy recovery ratio in the MCDI with two charging modes. Constant voltage (CV) charging (a) was conducted with various charging voltages and times for a NaCl concentration of

10 mM. Similarly, constant current (CC) charging (b) was conducted with various charging currents and concentrations of feed water. The discharging step was performed with reference current of 5 mA of the buck-boost converter and capacitance of 5 F of the supercapacitor.

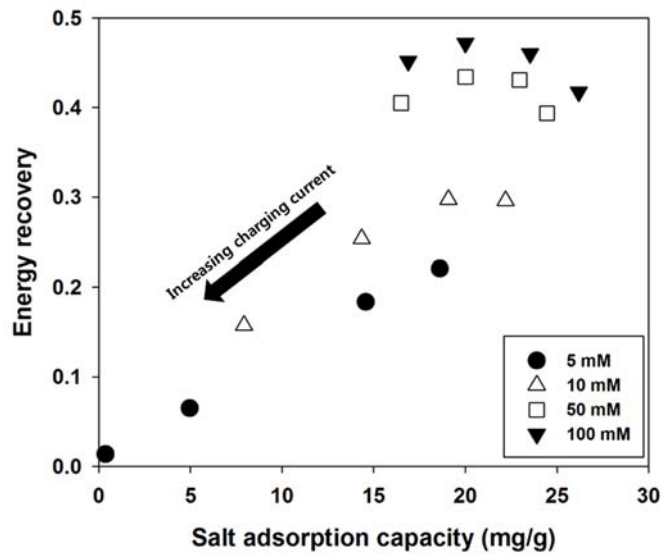
For CC charging, as shown in Figure 4-8b, the higher energy recovery ratio was achieved with the lower charging current and the higher concentration of the feed water. The change in the energy recovery ratio appears to be more sensitive to charging current at low concentration, (for the region of 1 ~ 4 mA/cm² of charging current, 0.01 ~ 0.22 of energy recovery ratio at 5 mM vs. 0.41 ~ 0.47 of energy recovery ratio at 100 mM), while it is similarly sensitive to the solution concentration at all conditions of charging currents.

Figure 4-9 shows the relationship between the energy recovery ratio and the salt adsorption capacity (calculated by Equation 4-2) at CV charging (a) and CC charging (b), with all of the experimental observations in this study considered. From Figure 4-9, two noticeable observations can be made. First, as shown in Figures 4-9a and b, a positive relationship can be found between the energy recovery ratio and the salt adsorption capacity, although it is not exactly linear. This observation indicates that the salt adsorption capacity can be one of the indicating parameters for evaluating the extent of the energy recovery ratio. This observation is further supported by the positive relationship between the salt adsorption capacity with charging time and charging voltage in CV mode and that between the salt adsorption capacity with the solution concentration and the reciprocal of charging current in CC mode (see Figure 4-10), which were similarly observed in the energy recovery ratio in Figure 4-8a and b. Figure 4-10S shows the salt adsorption capacity with CV and CC charging under various

operational condition. In CV charging, the salt adsorption capacity was increased with increasing charging time (Figure 4-10a) and increasing charging voltage (Figure 4-10b). In CC charging, the salt adsorption capacity was increased with decreasing charging current (Figure 4-10c) and increasing concentration of feed water (Figure 4-10d).



(a)



(b)

Figure 4-9. The relationship between the energy recovery ratio and the salt adsorption capacity in MCDI with two charging modes. Shown are the constant voltage (CV, 0.3 ~ 1.2 V at 10 mM) charging (a) and the constant current (CC, 1 ~ 4 mA/cm² at 5 ~ 100 mM) charging (b). The arrow indicates the direction of increasing charging time in CV mode and charging current in CC mode.

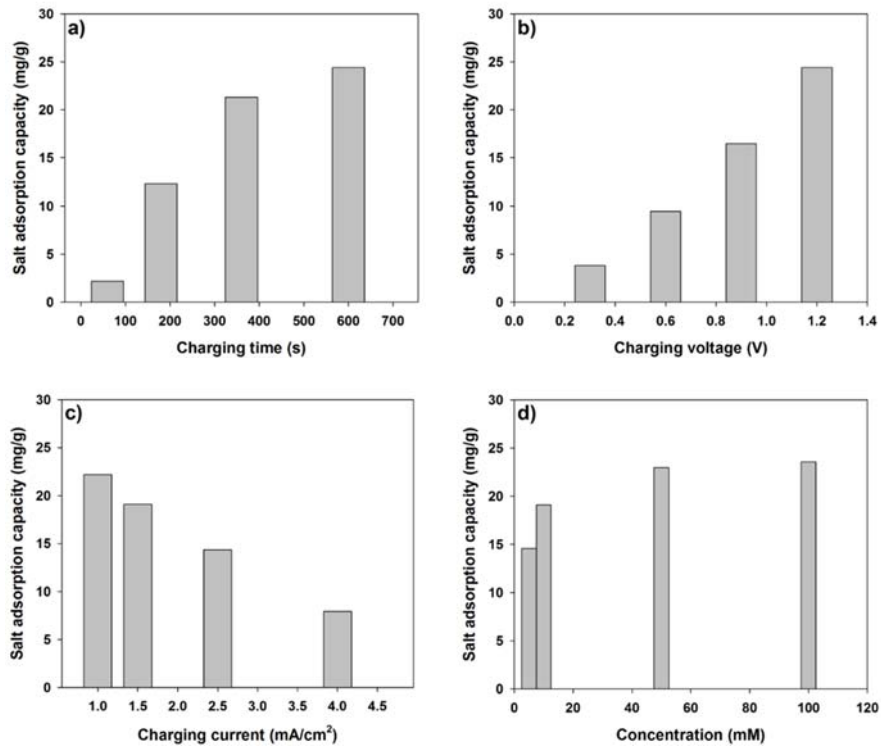
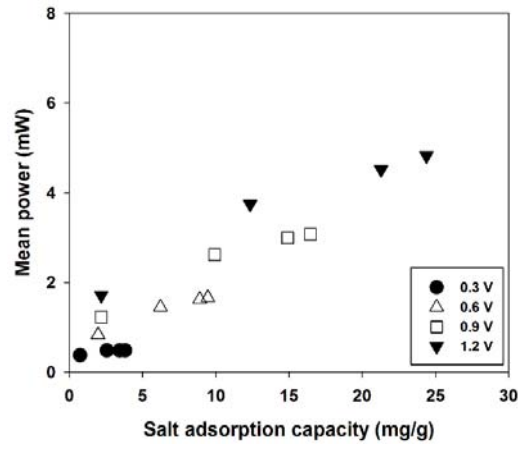


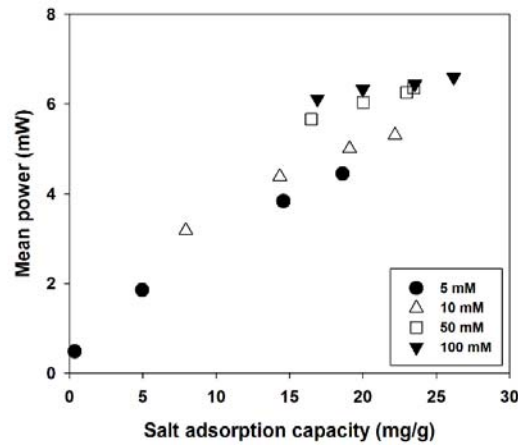
Figure 4-10. The salt adsorption capacity with CV charging as a function of a) charging time at 1.2 V and b) charging voltage for 10 min and with CC charging as a function of c) charging current at 10 mM and d) concentration of feed water at 1.5 mA/cm².

In this study, the energy recovery ratio is defined as the amount of energy recovered during the discharging step over the amount of energy consumed during the charging step (Equation 4-1). The salt adsorption capacity (indicating the ion removal performance during the charging step) is closely related to the amount of consumed energy because the ion removal performance is proportional to the amount of charge applied to the electrodes. This means that the amount of consumed energy is directly converted into the salt adsorption capacity under conditions of good charge efficiency. As a result, the positive relationship between the energy recovery ratio and the salt adsorption capacity indicates that the high salt adsorption capacity can also lead to an increase in the recovered energy under identical discharging conditions. In the mathematical expression of Equation 4-1, a larger increase in the numerator versus the increase in the denominator is required to realize the positive relationship between the energy recovery and the salt adsorption capacity, i.e., the state of a highly charged MCDI cell (which reflects the high salt adsorption capacity) is more favorable for energy transfer to the supercapacitor. This observation can be further explained by the power of the charged MCDI cell, which represents the energy transfer capability of the charged state as shown in Figure 4-11. The mean power of the charged MCDI cell can be obtained from the energy recovered in the supercapacitor divided by the discharging time. In Figure 4-11, a positive relationship was found between the mean power of the charged MCDI cell and the high salt adsorption capacity, providing an explanation for the

positive relationship between the energy recovery ratio and salt adsorption capacity.



(a)



(b)

Figure 4-11. The mean power of charged MCDI cell during the discharging step as a function of the salt adsorption capacity in case of a) CV charging and b) CC charging.

In Figure 4-9, in CC mode, it is interesting to observe that the sudden rise of the energy recovery ratio at high solution concentrations (50 ~ 100 mM) is off the linear relationship between the salt adsorption capacity and the energy recovery ratio. This phenomenon can be explained by solution resistance depicted in Figure 4-12 resulting from the concentration of feed water. The solution resistance was obtained from initial voltage increase divided by the charging current according to ohm's law ($V=iR$). In high concentration conditions exceeding 50 mM, the solution resistance was approximately $24 \Omega \cdot \text{cm}^2$, which is much less than $80 \Omega \cdot \text{cm}^2$ in low concentration conditions below 10 mM, thereby facilitating energy transfer from the charged MCDI cell to the supercapacitor.

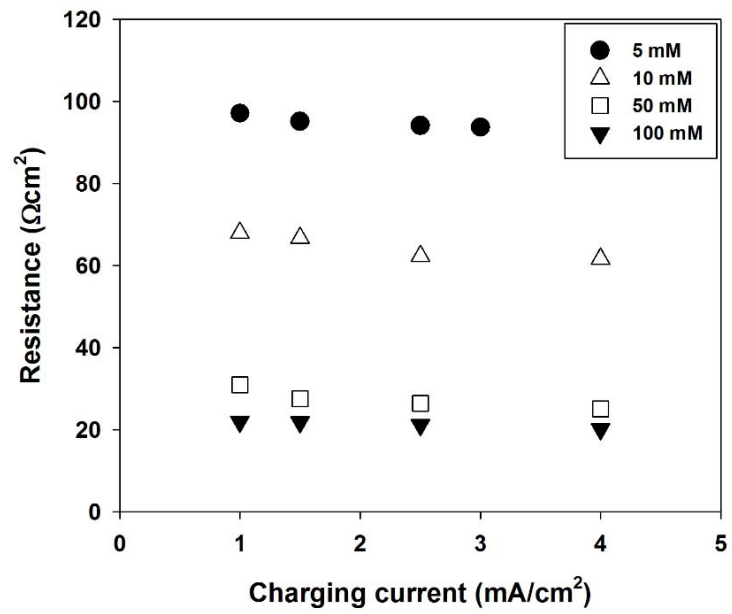


Figure 4-12. Solution resistance as a function of charging current with various concentration of feed water (5~100 mM).

In addition, the energy recovery in CC charging is much more favorable than CV charging. For example, the energy recovery at CC charging (Δ , Figure 4-9b) is approximately 0.3 at the solution concentration of 10 mM and salt adsorption capacity of approximately 20 mg/g, which is 50% higher compared to that at CV charging with 1.2 V at identical conditions (\blacktriangledown , Figure 4-9a); that is, the energy recovery ratio curve in CC charging was greater than that in CV charging with the salt adsorption capacity. This observation is consistent with the previous study that reported that CC charging consumed less energy to obtain the same salt adsorption capacity than CV charging due to the overall lower cell voltage (Kang et al. 2014). This lower energy consumption in CC charging indicates a high energy recovery ratio compared with CV charging for the same salt adsorption capacity.

Energy recovery with operational conditions in the buck-boost converter

Figure 4-13 shows the energy recovery ratio in the MCDI with the reference current of the buck-boost converter and the capacitance of the supercapacitor, i.e., the operational conditions of the buck-boost converter during the discharging step. Note that charging was made at the identical charging current (~ 1.5 mA/cm²) and concentration (~ 10 mM) to make the energy consumed during the charging step equal. As shown in Figure 4-13, a higher energy recovery ratio was achieved with a lower reference current and a higher capacitance of the supercapacitor. In addition, the energy recovery was more sensitively affected by the reference current rather than the capacitance of the supercapacitor. The effect of the reference current in the energy recovery ratio can be explained by the conduction loss, which indicates that the loss of electrical energy resulting from the current flow through the conductive materials is proportional to the square of the electric current (Mulligan et al. 2005). Accordingly, the lower reference current resulted in a higher energy recovery ratio due to lower conduction loss, indicating that a slow rate of energy transfer is favorable to attain a higher energy recovery ratio.

The capacitance of the supercapacitor did not appear to have a significant effect on the energy recovery ratio in comparison with the reference current, as shown in Figure 4-13. However, the capacitance of the supercapacitor plays an important role in determining the speed of energy recovery due to their voltage

rating (Alkuran et al. 2008). For example, with 5 mA of the reference current, the recovery time in the case of employing 2.5 F of the supercapacitor was 106 s, whereas that in the case of employing 20 F of the supercapacitor was 373 s. This result indicates that the low capacitance of the supercapacitor can contribute to faster energy recovery.

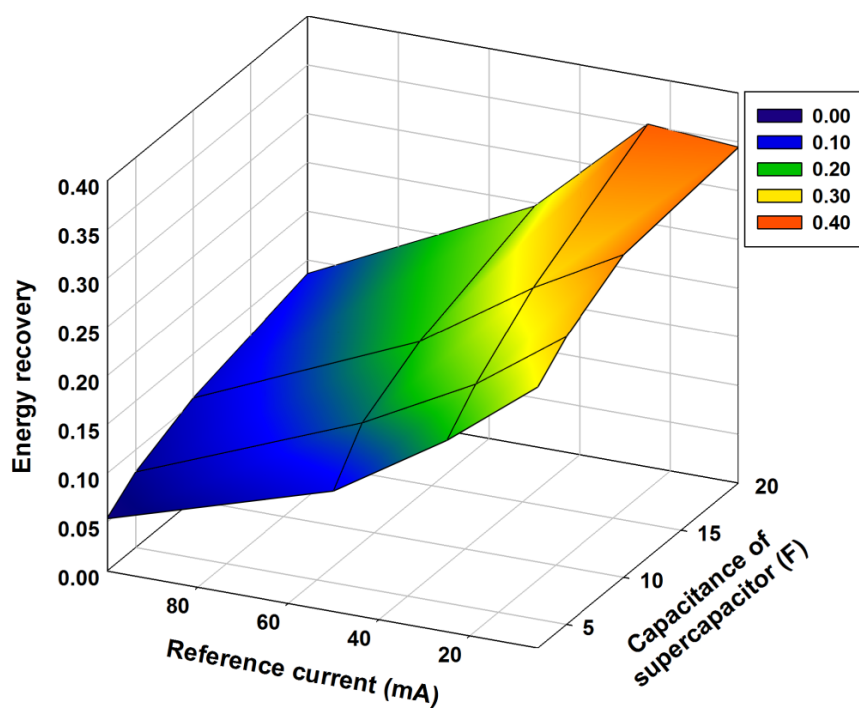


Figure 4-13. Three-dimensional representation of the energy recovery ratio with various reference currents of the buck-boost converter and capacitances of the supercapacitor. The charging step was performed with constant current operation at 1.5 mA/cm^2 and a NaCl concentration of 10 mM. The average salt adsorption capacity was 19 mg/g.

Energy loss during converter operation (energy recovery step)

Figure 4-14 shows the energy loss of converter during energy recovery step. To calculate the energy loss of converter, two energy storage medium (supercapacitor in this study) were connected through the converter and energy was transferred from supercapacitor#1 to supercapacitor#2 as shown in Figure 4-14a. The energy loss of converter was calculated from the ratio of energy released from supercapacitor#1 and energy stored into supercapacitor#2.

Figure 4-14a and 14b shows the energy loss of converter as a function of charging potentials and reference currents. It was observed that energy loss was increased with decreasing charging potentials and increasing reference current. The reference current is especially main factor to govern the energy loss of converter. The average energy loss was about 30 % as shown in Figure 4-14b and it was assumed that this energy loss resulted in low energy recovery ratio (20~30% in this study). In addition, energy loss in supercapacitor and leakage current of external circuit might be also reduce the energy recovery ratio. It is assumed that these energy loss in converter is mainly dominated by low-energy scale of CDI cell in this study. If the energy scale has increased, the efficiency of converter will approach over 99% and the energy recovery ratio will be increased as shown in Figure 4-15. In this respect, the optimization of converter is necessarily required to enhance energy recovery ratio.

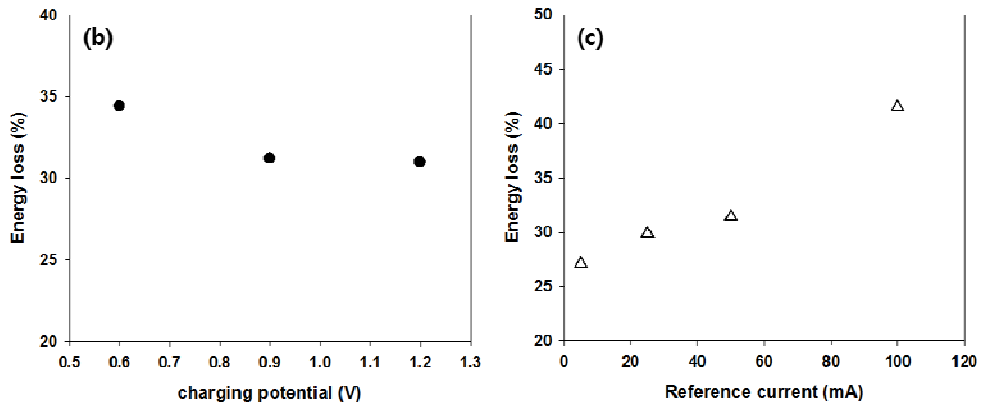
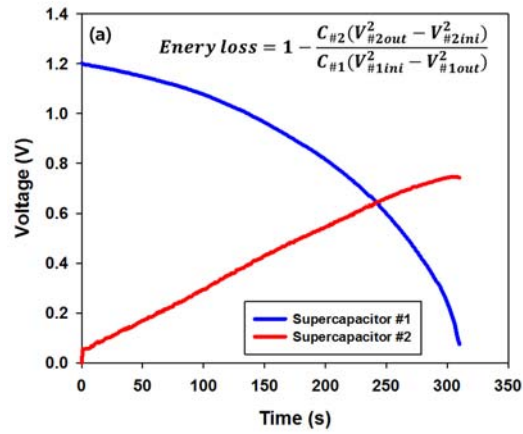


Figure 4-14. Calculation of energy loss during converter operation (energy recovery step). (a) voltage profiles of supercapacitor#1 (energy donor) and supercapacitor#2 (energy receptor), (b) energy loss of converter as a function of charging potentials and reference currents.

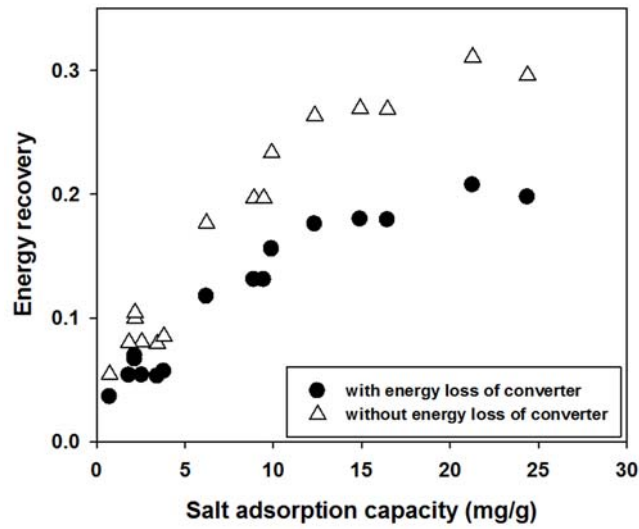


Figure 4-15. Comparison of energy recovery ratio with considering energy loss of converter (30% in this study) and without considering energy loss of converter. This data is based on the energy recovery ratio with CV charging depicted in Figure 4-9a.

4.4. Summary

This study reports the successful construction of an energy recovery system in an actual MCDI cell with a buck-boost converter; the buck-boost converter facilitated the delivery of the energy stored in the CDI cell into a supercapacitor. The energy recovery ratio was investigated under various operational conditions to determine the influential parameters affecting energy recovery in the MCDI cell. For charging conditions, the energy recovery was increased with the longer charging time and higher charging voltage in the case of CV mode and with the lower charging current and the higher concentration in the case of CC mode. From these results, the salt adsorption capacity was found to play an important role in the energy recovery and constant current charging was found to be more favourable for energy recovery than constant voltage charging. For discharging conditions with the buck-boost converter operation, the energy recovery was more sensitively affected by the reference current rather than the capacitance of the supercapacitor. The smaller reference current mainly resulted in a higher energy recovery ratio in contrast with the capacitance of the supercapacitor. In summary, to achieve the high energy recovery system, the development of an electrode with a high salt adsorption capacity and a cell design with low cell resistance will be required with a well-optimized buck-boost converter to facilitate a high energy recovery ratio.

5. Influential electrode properties on energy recovery performance in capacitive deionization

5.1. Introduction

With demands for efficient desalination technology against the industrialization and population growth (Jury and Vaux 2007; Shannon et al. 2008), many desalination technologies have been proposed to cope with this increasing requirements such as thermal distillation (Freshwater 1951), reverse osmosis (RO) (Greenlee et al. 2009), membrane distillation (MD) (Lawson and Lloyd 1997), electrodialysis (ED) (Strathmann 2010) and capacitive deionization (CDI) (Porada et al. 2013b). Among those, Capacitive deionization (CDI), an electrochemical desalination technology using electrical double layer on the electrode surface, has come into spotlight in terms of environment-friendly and low-energetic process (Anderson et al. 2010; Farmer et al. 1996; Welgemoed and Schutte 2005).

One of important strengths in CDI is an easily feasible energy recovery; partial energy consumed to operate the system can be recovered (Anderson et al. 2010). The principle of CDI is based on electrical double layer capacitor (EDLC), indicating that it is possible to harness some energy consumed for the desalination (where capacitor is charged) during the regeneration step (where

capacitor is discharged). The recovered energy can be either stored as electricity in electronic storage media (Alkuran and Orabi 2008; Alkuran et al. 2008; Pernía et al. 2014; Pernía et al. 2012) or directly utilized for the next purification step (Landon et al. 2013). The energy recovery technique enables the energy efficiency of CDI to be improved and the importance of energy recovery deserves attention in this regard.

In previous literature, Długolecki and van der Wal have reported energy recovery ratio under different currents and salt concentrations using constant current (CC) operation (Długolecki and van der Wal 2013). From the voltage profiles, the ratio of released energy during the discharging step to consumed energy during the charging step was defined as energy recovery ratio. This approach was also employed in other studies (Demirer et al. 2013; García-Quismondo et al. 2013a; Zhao et al. 2013a). However, so far, no study have been reported that provide the effect of electrode properties on energy recovery performance whereas the effect of operating conditions was exclusively reported. The approach to electrode properties on energy recovery performance must be inevitable because the carbon materials for CDI electrodes play an important role in desalination capacity and rate (Kim and Yoon 2013; Kim and Yoon 2015; Porada et al. 2013a; Suss et al. 2015; Yang et al. 2014)

Therefore, this study aimed to investigate the relationship between electrode properties and energy recovery performance by using various carbon materials

with different properties. To determine the effect on energy recovery performance, influential factors (electrode properties) were considered as capacity (salt adsorption capacity) and rate (salt adsorption rate).

5.2. Materials and Methods

Materials and electrode preparation

Six carbons were utilized as follows; MSP-20 (Kansai Coke and Chemicals) (Kang et al. 2012; Kim and Yoon 2013), P-60 (Kuraray), SX PLUS and S-51HF (Norit) (Kim and Yoon 2013), Metal-organic framework derived carbons, (MDC, Carbon Nanomaterials Design Laboratory in Seoul National University) (Yang et al. 2014), Carbon aerogel (CA, Enen). Among these carbons, MDC was fabricated by a template-free and solvent evaporation method during carbonizing a metal-organic framework while others were commercially purchased. Nitrogen adsorption/desorption measurement (at 77 K) was implemented using a Micromeritics ASAP2010 and specific surface area (SSA) was determined according to the Brunauer–Emmett–Teller (BET) equation. In addition, pore distributions were analyzed by Barrett-Joyner-Halenda (BJH) equation to investigate pore structure of various carbon powders.

The carbon sheet electrodes were fabricated from a mixture of activated carbon powder, carbon black (Super P, Timcal), and polytetrafluoroethylene (PTFE, Sigma-Aldrich, USA) with a weight ratio of 86:7:7. This mixture was kneaded with a few ml of ethanol for uniformity and then made into a sheet form using a roll press machine (electrode thickness of ~ 300 μm). The pressed dough in sheet form was dried in a vacuum oven at 120 °C for 12 h and then cut for use for

desalination and energy recovery processes after drying.

Electrochemical characterization

The electrochemical properties of carbon composite electrodes were investigated by using galvanostatic charge/discharge tests. An electrochemical cell was assembled with graphite current collectors (diameter~ 18 mm), cellulose nitrate filter (thickness~ 110 μm , Advanced Microdevices, India) as a spacer. Galvanostatic charge/discharge tests were implemented in a two-electrode system with 1 M of NaCl as an electrolyte using automatic battery cycler (WBCS3000, WonaTech, Korea). Voltage profiles were recorded with various current densities (0.5, 2.5, 5, 10, 20 mA/cm^2) in the potential range of 0.0 ~ 0.4 V. From voltage profiles, the specific capacitance was calculated as follows (Khomenko et al. 2005; Yang et al. 2014);

$$C = 2i\Delta t/m\Delta V \quad (5-1)$$

, where C is the specific capacitance (F/g); i is the current (A); Δt is the duration of charging step (s); ΔV is the potential difference (0.4 V in this study); m is the mass of an electrode (g).

To analyze the rate response characteristic of carbon materials, retention was obtained by the ratio of specific capacitance at current density of $x \text{ mA}/\text{cm}^2$ (C_x) to the specific capacitance at current density of $0.5 \text{ mA}/\text{cm}^2$ ($C_{0.5}$).

Deionization test and performance evaluation

For deionization test, The custom-made MCDI cell composed of a graphite current collector, anion- and cation-exchange membranes (Selemion, AGC ENGINEERING CO. LTD, Japan), carbon sheet electrodes (area $\sim 3 \text{ cm}^2$), and a polymer spacer (nylon sheet, thickness $\sim 200 \text{ }\mu\text{m}$) was utilized. The deionization test was performed under constant current operation (Kang et al. 2014; Zhao et al. 2012) with 10 mM of NaCl concentration and 2 ml/min of flow rate. The constant current density during the charging step was controlled by WBCS3000 and tuned in the range of $1 \sim 4 \text{ mA/cm}^2$ with cut-off voltage of 1.2 V. The discharging step was conducted by reverse current with opposite value to the charging step. The conductivity of effluents was measured by using a conductivity meter (3573-10C, HORIBA, Japan) and the measured conductivity were converted to actual concentration by a calibration curve. Within that curve, a 10 mM NaCl solution corresponded to a 1.2 mS/cm of solution conductivity.

The energy recovery performance using constant current charge and discharge was evaluated by the ratio of the amount of energy consumed during the charging step to the energy recovered during the discharging step as shown in Figure 5-1 (Długolecki and van der Wal 2013; García-Quismondo et al. 2013a; Zhao et al. 2013a). Note that energy recovery ratio in this chapter is different from that in chapter 4; the ratio of consumed energy during the charging step to the stored energy in the supercapacitor. The salt adsorption capacity and salt

adsorption rate was calculated to evaluate the desalination performance according to carbon materials. The salt adsorption capacity derived from the area below effluent conductivity during the charging step was calculated by the mass of removed NaCl divided by the mass of both electrodes (mg/g) (Kang et al. 2014; Kim and Yoon 2013). The average salt adsorption rate was calculated by dividing the salt adsorption capacity by the duration of charging step (mg/g/s) (Zhao et al. 2013b). In addition, the mean power was obtained by dividing the energy recovered during the discharging step by the duration of discharging step and the mass of electrodes (mW/g).

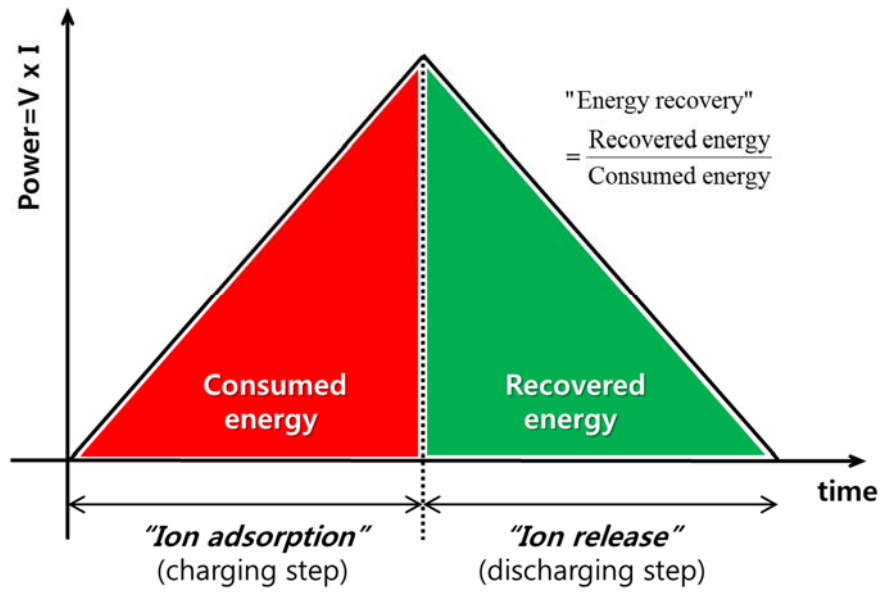


Figure 5-1. Definition of energy recovery ratio in CDI with constant current operation

5.3. Results and Discussion

Characterization of carbon composite electrode

The Physical properties of various carbon electrodes used in this study are presented in Table 5-1. The BET surface area ranged from 534 to 1578 m²/g, where MSP-20 and S-51HF respectively showed the lowest and highest area. The various BET surface area was closely connected with the development of micropore structures (< 2 nm) with considering that the micropore ratio in S-51HF was 0.65 and that of MSP-20 was 0.72. In table 5-1, one notable thing could be observed that MDC had quite high BET surface area (1537 m²/g) in spite of its low micropore ratio (0.31). To understand this trend, it is required to check the meso- (2 ~ 50 nm) and macropore (> 50 nm) distribution of carbon materials

Figure 5-2 shows the meso- and macropore distributions of carbon materials derived from BJH equation. Almost the whole pores of MSP-20 were developed with micro structure, which caused high BET surface area. However, in case of MDC, the pore sizes were distributed ranging from micro-, meso- and macro structures and small mesopores below 10 nm were especially developed. Although the micropore ratio was low, the development of low meso-structures lead to high BET surface area. This explanation could be confirmed by the pore distribution of CA. The relatively well-developed large meso- and macro-

structure resulted in low BET surface area as shown in table 5-1.

Table 5-1. Characterization of activated carbons

	MSP-20	P-60	SX PLUS	S-51HF	MDC	Aerogel
BET surface area (m ² /g)	1578	1062	673	434	1537	534
Micropore area (m ² /g) ^a	1133	740	434	132	479	118
Ratio ^b	0.72	0.70	0.65	0.30	0.31	0.22
Mesopore area (m ² /g) ^c	445	232	239	302	1058	416

^a calculated from *t*-plot analysis

^b Micropore area / BET surface area

^c BET surface area – micropore area

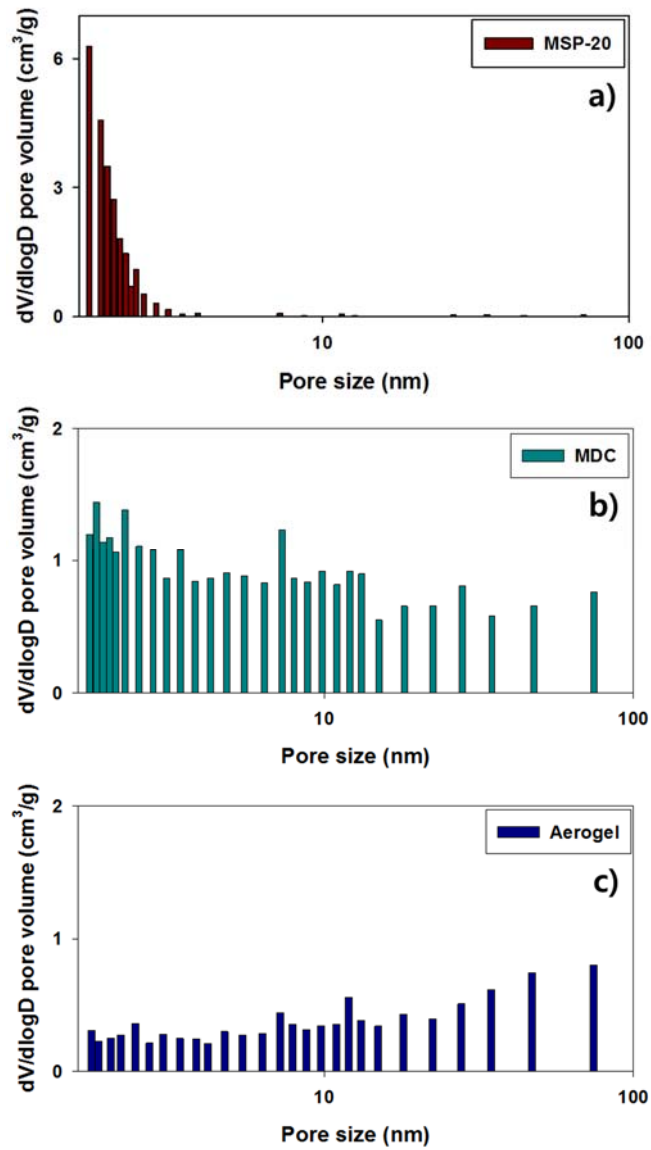


Figure 5-2. The meso- and macropore distributions of carbon materials derived from BJH equation; (a) MSP-20, (b) MDC, (c) CA.

Figure 5-3 ~ 5-8 respectively show the voltage profiles of MSP-20, P-60, SX PLUS, S-51HF, MDC, CA obtained from galvanostatic charge/discharge tests under different constant current densities. As shown in each voltage profile, typical capacitive behavior was observed at the lowest current density (0.5 mA/cm²) and the specific capacity was decreased with increasing current densities due to ohmic resistance (Bard and Faulkner 2001). This deformation of voltage profiles is related with the rate response characteristic of carbon materials, which means that the carbon material with fast rate response show little or no deformation of voltage profiles. Previous studies reported that rate response of carbon materials is influenced by their pore structure (Porada et al. 2013a; Yang et al. 2014). Considering the pore distributions in Figure 5-2, the rate responses were coincident with previous studies. For example, MDC and CA showed relative little deformation of voltage profiles because they mainly had not micropore but meso- and macropore compared to other materials with primary micropore structure.

In table 5-2, specific capacitances of carbon materials calculated from voltage profiles using equation 5-1 were presented. The specific capacitances were ranged from 120 to 38 F/g and the increase in specific capacitance corresponded to the increase of micropore shown in table 5-1. This is why the micropore is mainly available for ion adsorption site to motivate capacitance (Zhang and Zhao 2009). Figure 5-9 shows the retention obtained by the ratio of specific

capacitance at current density of $x \text{ mA/cm}^2$ (C_x) to the specific capacitance at current density of 0.5 mA/cm^2 ($C_{0.5}$). The retention of specific capacitance also indicates the rate response characteristic of materials like the deformation of voltage profiles in galvanostatic charge/discharge tests. As shown in Figure 5-9, MDC and aerogel had high retention of specific capacitance of 0.97 and 0.99, indicating that meso- and macropore structure is advantageous for excellent rate response. These results suggested that the ions in electrolyte could be rapidly transported into the pore structures of the electrode with the development of meso- and macropores (Yang et al. 2014).

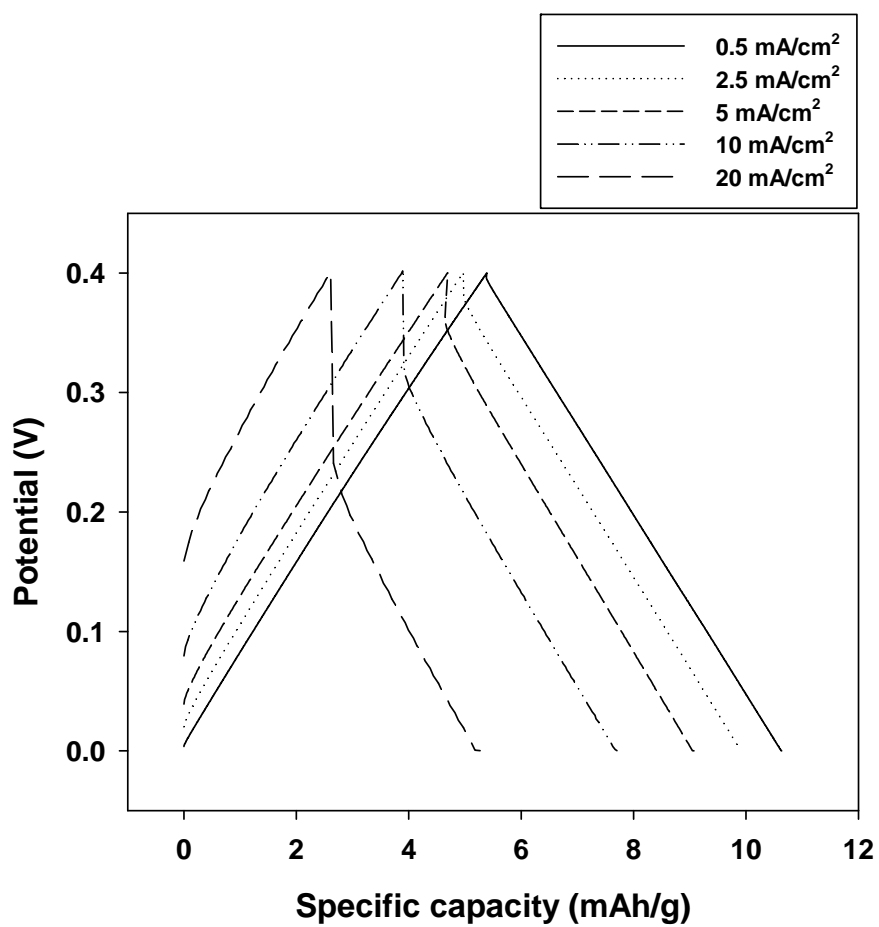


Figure 5-3. Galvanostatic charge/discharge voltage profiles of MSP-20

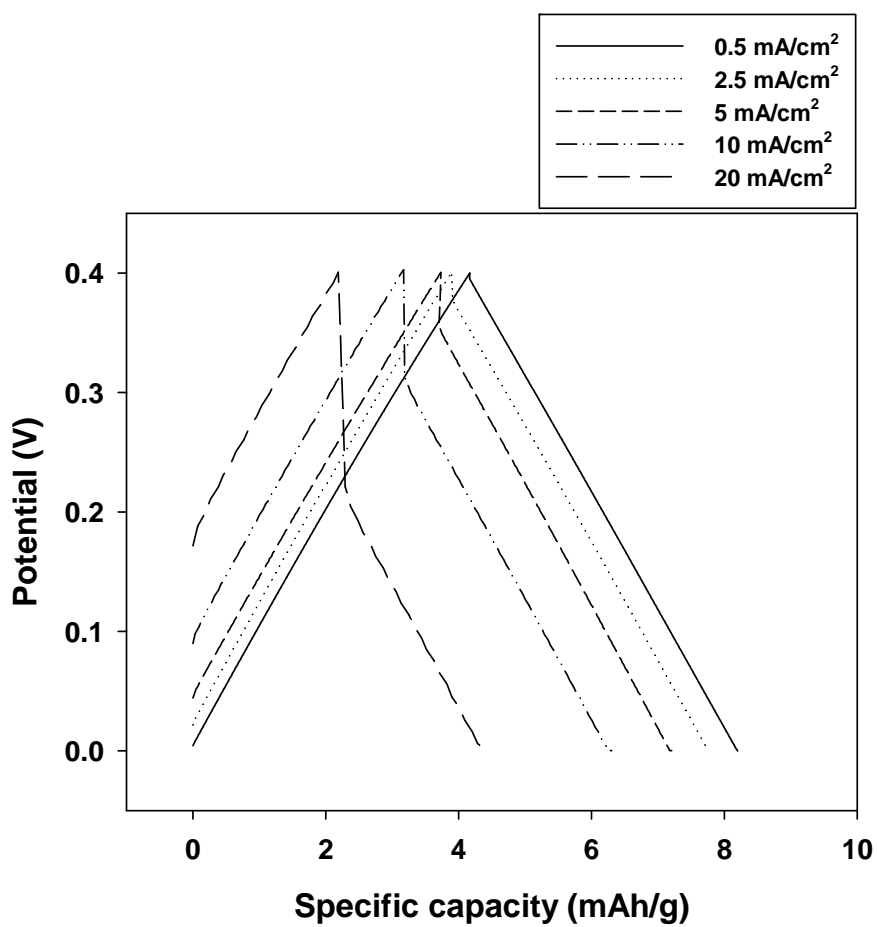


Figure 5-4. Galvanostatic charge/discharge voltage profiles of P-60

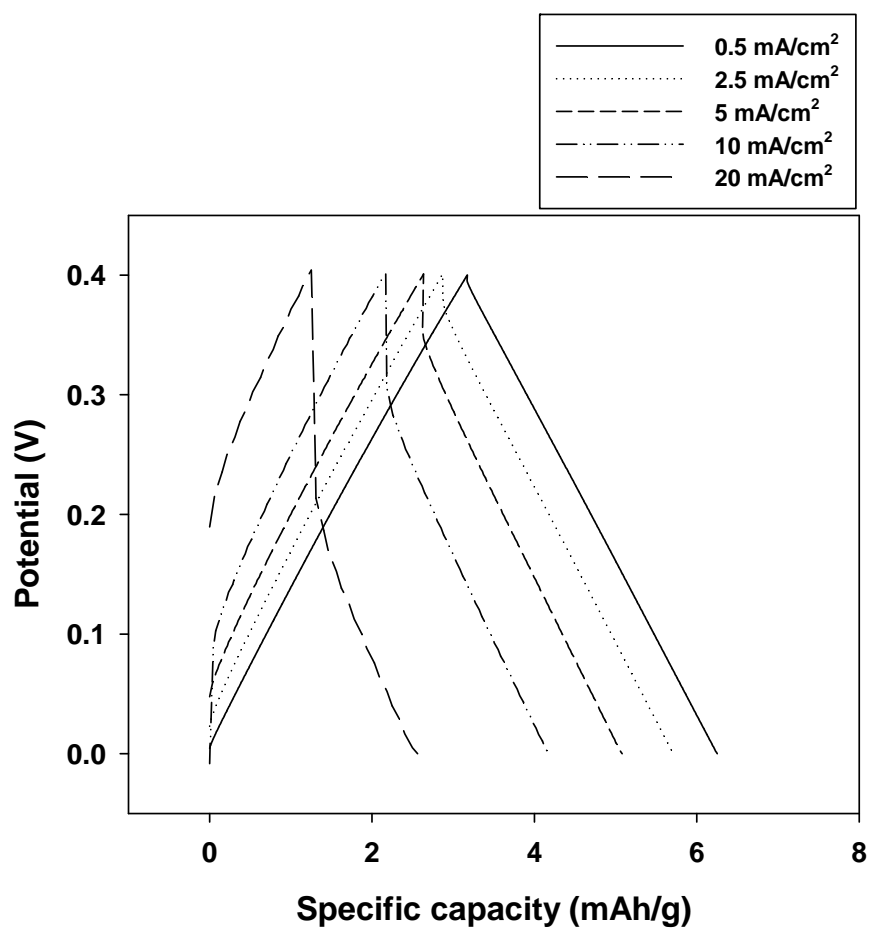


Figure 5-5. Galvanostatic charge/discharge voltage profiles of SX-PLUS

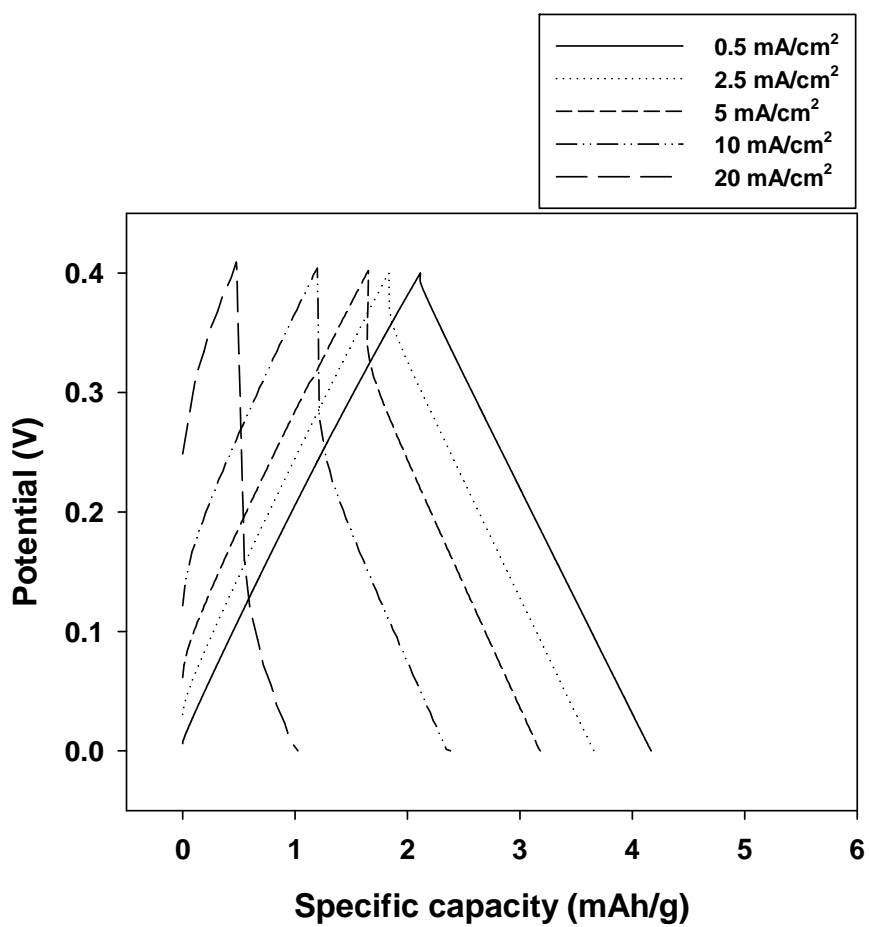


Figure 5-6. Galvanostatic charge/discharge voltage profiles of S-51HF

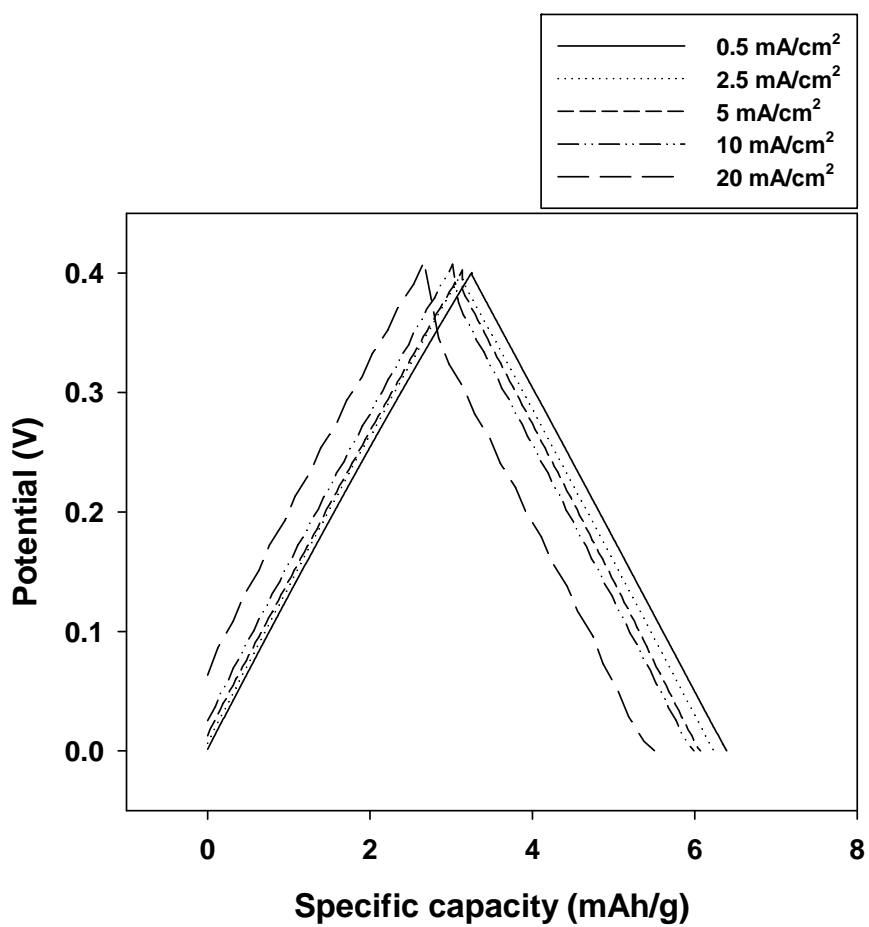


Figure 5-7. Galvanostatic charge/discharge voltage profiles of MDC

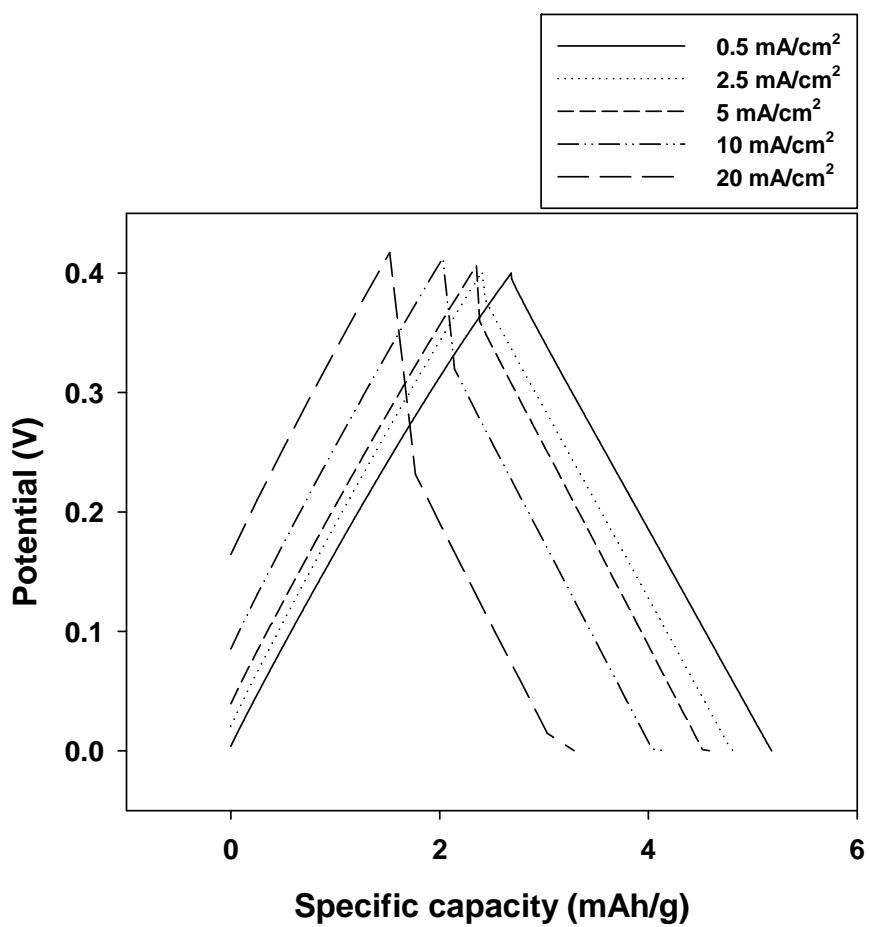


Figure 5-8. Galvanostatic charge/discharge voltage profiles of Carbon aerogel

Table 5-2. Specific capacitance of various carbon composite electrodes derived from galvanostatic charge/discharge voltage profile.

	MSP-20	P-60	SX PLUS	S-51HF	MDC	Aerogel
Capacitance (F/g)	120	73	56	38	57	46
Retention (%)	93	95	76	60	97	99

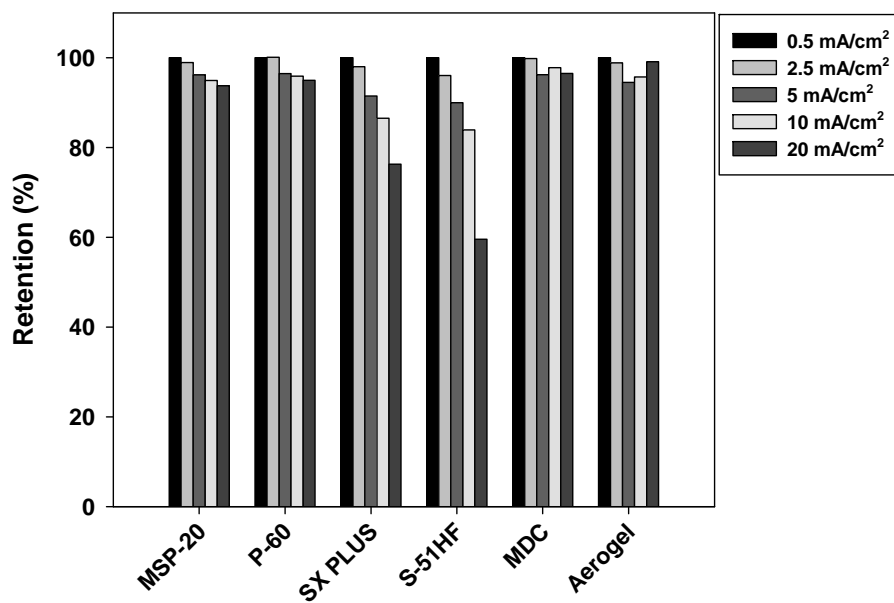


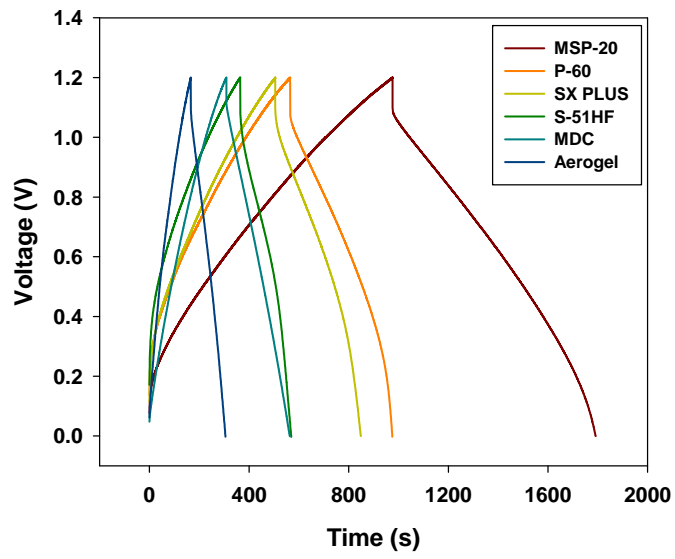
Figure 5-9. Retention of specific capacitance as a function of scan rate (0.5 mA/cm² ~ 20 mA/cm²) with various carbon composite electrodes.

Desalination performance with CC operation

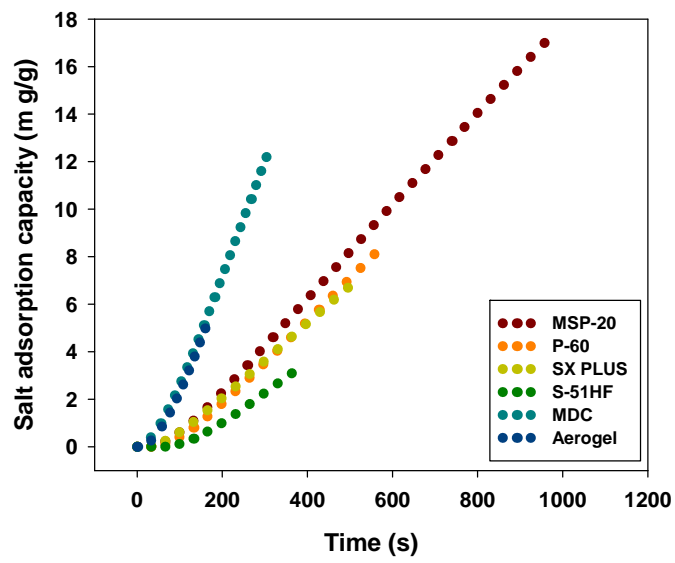
Figure 5-10 shows the representative voltage profiles and salt adsorption capacities of CC mode in MCDI operation. A constant current (1 mA/cm^2) as applied until the CDI cell voltage reaches to 1.2V, whereas for discharging step, a reverse current (-1 mA/cm^2) was applied until the CDI cell voltage reaches to zero. The linear increasing/decreasing voltage during the charging/discharging step, which is characteristic of CC operation (Jande and Kim 2013; Kang et al. 2014; Zhao et al. 2012). An instantaneous rise of cell voltage about 0.1 V occurred at the beginning of charging (also drop at the beginning of discharging) is the result of an ohmic drop caused by the MCDI cell's electrolyte resistance. As shown in Figure 5-10a, various voltage profiles according to carbon materials are observed due to their different capacity and rate response affecting on desalination performances.

In Figure 5-10b, salt adsorption capacities as a function of time are presented according to carbon materials. Note that these salt adsorption capacities are measured under not only equilibrium state but also dynamic state (Biesheuvel and Bazant 2010; Biesheuvel et al. 2009; Zhao et al. 2009). The highest and lowest salt adsorption capacity were 17 mg/g with MSP-20 and 3 mg/g with S-51HF, respectively. These value is directly related with specific capacitance presented in table 5-2 because the salt adsorption capacity can be converted to about 70% of electrode capacitance (Kim and Yoon 2013). However, the MDC

showed the second highest salt adsorption capacity (13 mg/g) in spite of low capacitance, which is due to low electrode density, i.e., low mass of electrodes. In addition, desalination rate capability is qualitatively analyzed by the slope of salt adsorption curve. From Figure 5-10b, the carbon materials can be intuitively split into two groups; MDC, CA with fast desalination rate capability and MSP-20, P-60, SX PLUS, S-51HF with slow desalination rate capability. This classification according to rate capability is due to the development of large meso- and macropores, which trend is partly confirmed by the results in Figure 5-9. In addition, note that these results were based on salt adsorption capacity per electrode weight (mg/g). If the salt adsorption capacity per electrode volume (mg/cm^3) is considered, electrodes with low density such as MDC and aerogel show poor desalination performance compared other materials (Figure 5-11). In large-scale CDI process, electrode volume is important due to module design and MDC might not be suitable for large-scale process in spite of its fast rate capability.



(a)



(b)

Figure 5-10. (a) The representative voltage profiles and (b) salt adsorption capacities (mg/g) of CC mode in MCDI operation with various carbon electrodes. (current density = 1 mA/cm² for charging and -1 mA/cm² for discharging, flow rate = 10 mL/min, NaCl concentration = 10 mM).

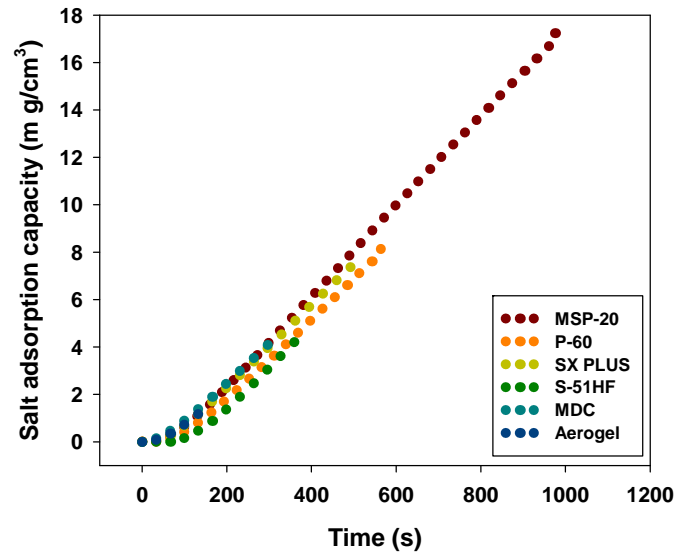


Figure 5-11. Salt adsorption capacities (mg/cm^3) of CC mode in MCDI operation with various carbon electrodes. (current density = $1 \text{ mA}/\text{cm}^2$ for charging and $-1 \text{ mA}/\text{cm}^2$ for discharging, flow rate = $10 \text{ mL}/\text{min}$, NaCl concentration = 10 mM).

Energy recovery performance depending on electrode properties

To analyze the energy recovery performance, energy consumed during the charging step and energy recovered during the discharging step was calculated from the voltage profile shown in Figure 5-10a and all the values of carbon materials are plotted in Figure 5-12.

Figure 5-12 shows the energy consumed during the charging step (E_c) and energy recovered during the discharging step (E_r) with various carbon materials under identical CDI operating conditions. As can be seen, it was observed E_c and E_r was increased with increasing salt adsorption capacity depicted in Figure 5-11b. MSP-20 showed the highest E_c and E_r with the highest salt adsorption capacity, whereas S-51HF showed the lowest E_c and E_r with the lowest salt adsorption capacity. The slope of depicted line in Figure 5-12 refers to proportional constant, indicating energy recovery ratio. For example, the line with proportional constant of unity means that all of the energy consumed during the charging step are perfectly recovered during the discharging step. Interestingly, the noticeable observation can be made in Figure 5-12; almost the whole data points of carbon materials are located between $E_r=0.5E_c$ and $E_r=0.75E_c$, indicating the energy recovery ratios of carbon materials ranged from 50% to 75%. This phenomenon can be explained by the high resistance of low electrolyte. The targeting concentration of CDI process with typical carbon sheet electrodes is low concentration due to the their limitation in adsorption site

(HeeáCho et al. 2013; Lee et al. 2014). However, this low concentration revealing high electrical resistance resulted in energy loss during the charging step. The previous study reported that the resistance over the MCDI cell is mainly dominated by the spacer which act as an flow channel of feed water with low concentration (Dykstra et al. 2016). The inserted table presents the calculated value of energy recovery ratio, showing that different energy recovery ratios according to carbon materials under the same operating conditions. To analyze this result, we investigated the relationship of energy recovery ratio, salt adsorption capacity and salt adsorption rate.

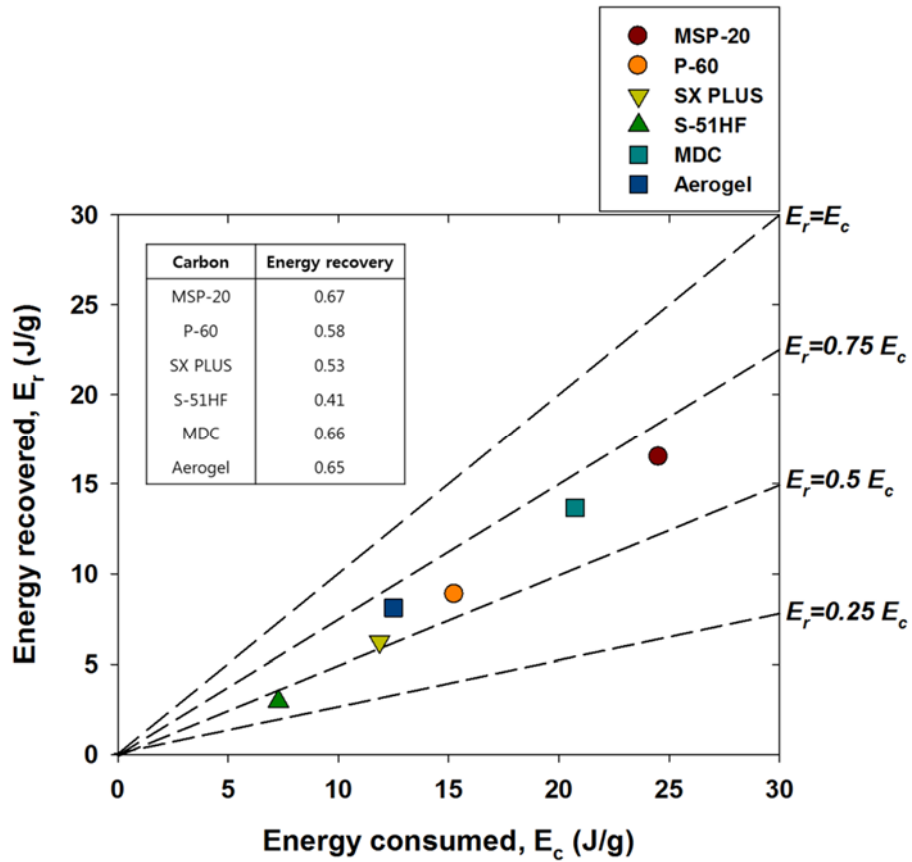


Figure 5-12. The energy consumed during the charging step (E_c) and energy recovered during the discharging step (E_r) with various carbon materials. Inserted table shows the energy recovery ratio calculated from E_r/E_c as presented in Figure 5-2. CC operation in desalination test was performed with 1/-1 mA/cm² of charging/discharging current density up to 1.2 V of cut-off voltage and 10 mM NaCl solution. The symbols are located between $E_r=0.5E_c$ and $E_r=0.75E_c$, indicating the energy recovery ratios of carbon materials ranged from 50% to 75%.

Figure 5-13 shows the correlation between the salt adsorption capacity and energy recovery ratio. As can be seen in Figure 5-13, we can infer the linear correlation between salt adsorption capacity and energy recovery ratio with data points of MSP-20, P-60, SX PLUS and S-51HF. This correlation unambiguously proves that the capacity of carbon electrode (which is excellent agreement with salt adsorption capacity) plays an important role in energy recovery performance. This result is strongly coincident with previous experimental results in part 4, especially Figure 4-9. In part 4, salt adsorption capacities were varied with operating conditions and it was suggested that a highly charged MCDI cell (which reflects the high salt adsorption capacity) is more favorable for energy recovery.

However, in Figure 5-13, it is required to take notice of exceptional data points with MDC and CA. These two carbon materials deviated from the correlation between salt adsorption capacity and energy recovery ratio; higher energy recovery ratios of MDC (0.66) and CA (0.65) compared to P-60 (0.58) and SX PLUS (0.53) in spite of similar salt adsorption capacities, respectively. This can be explained by fast rate response characteristics of MDC and CA which has the development of meso- and macropores.

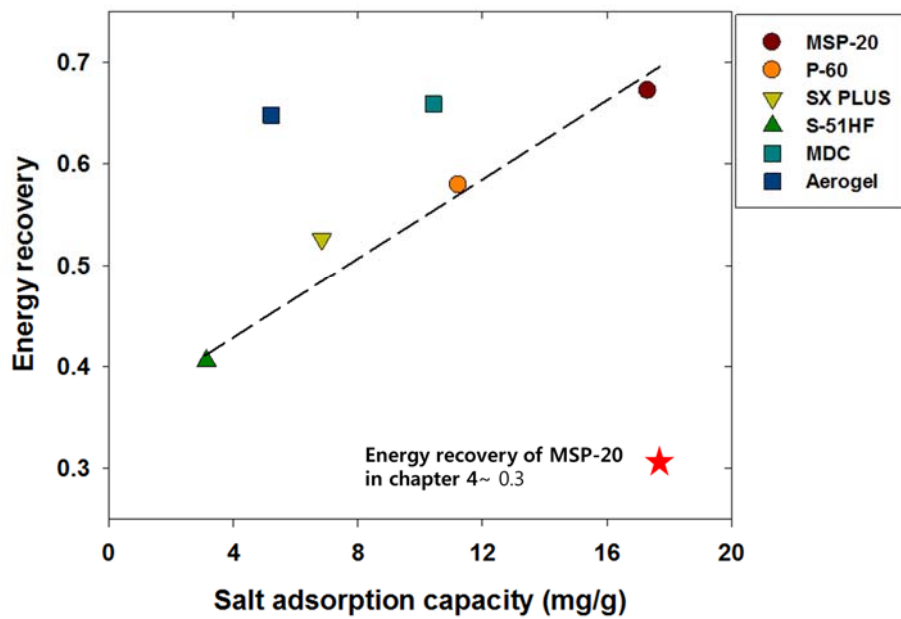


Figure 5-13. Correlation between the salt adsorption capacity and energy recovery ratio. Salt adsorption capacity was obtained from Figure 5-11b and regression line was plotted with MSP-20, P-60, SX PLUS and S-51HF. The red star indicates the energy recovery ratio of converter system in Figure 4-9.

Figure 5-14 shows the correlation between the average salt adsorption rate and mean power. As shown in Figure 5-14, the group with MDC and CA and the other group with MSP-20, P-60, SX PLUS and S-51HF are distinctively classified, which clearly explains the reason why MDC and CA showed high energy recovery ratio. Considering that the energy recovery (or energy extraction) of CDI is induced by the release of ions away from electrode pores, pore structures necessarily affect the energy recovery performance. High mean powers of MDC and CA caused by fast ion transport into/from electrode pores support the hypothesis because mean power strongly reflects energy recovery rate. This observation suggests that high salt adsorption rate, *i.e.*, fast rate response are also important electrode properties as an influential factor on energy recover performance as well as salt adsorption capacity.

After establishing the salt adsorption capacity and salt adsorption rate as influential factors on energy recovery performance, degradation of energy recovery ratio by varying charging current density was investigated. Figure 5-15 shows the normalized energy recovery as a function of different charging-discharging current density. It was observed that MDC with high salt adsorption capacity and rate showed the least degradation in energy recovery performance and our discussions are strongly underpinned by this result.

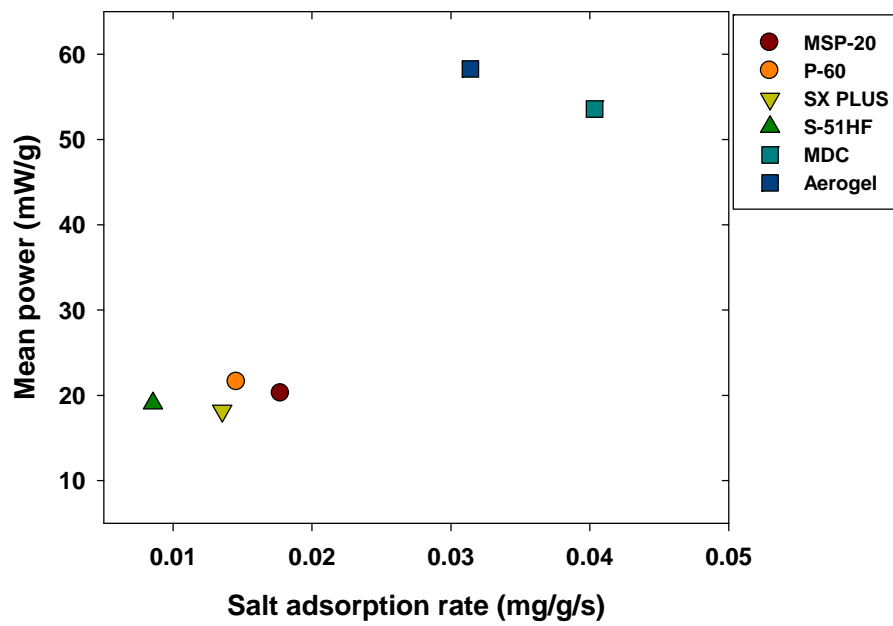


Figure 5-14. Correlation between the average salt adsorption rate and mean power. The average salt adsorption rate was calculated by dividing the salt adsorption capacity by the duration of charging step (mg/g/s) and mean power was obtained by dividing the energy recovered during the discharging step by the duration of discharging step and the mass of electrodes (mW/g).

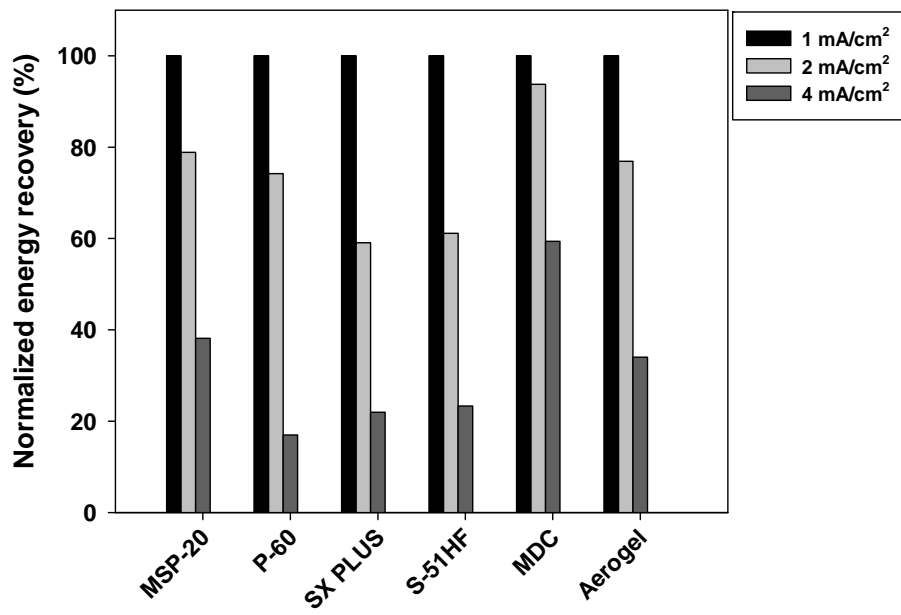


Figure 5-15. The normalized energy recovery as a function of different charging-discharging current density (± 1 , ± 2 , ± 4 mA/cm²). All of desalination test were identically performed with 1.2 V of Cut-off voltage and 10 mM NaCl solution.

5.4. Summary

In this study, energy recovery ratio in MCDI depending on electrode properties was investigated using constant current operation. Almost the whole carbon electrodes showed energy recovery ratios of 0.5 ~ 0.75 due to high electrical resistance of low electrolyte. In particular, we found out that not only salt adsorption capacity but also salt adsorption rate play an important role in energy recovery performance. Our findings were confirmed by the least degradation of energy recovery performance in case of using carbon electrode with excellent salt adsorption capacity and rate. We expect that this study can provide important considerations to design and fabricate carbon materials and electrodes which are applied energy recovery system in MCDI.

6. Conclusions

In this dissertation, design and analysis of CDI techniques for high energy efficiency and energy recovery was implemented by focusing on the evaluation of energy consumption according to operational modes and energy recovery system. In the first part, the salt adsorption capacity and energy consumption in two operational modes (CV and CC) in a CDI desalination cell were compared on the bases of identical amount of ion removal and electrical charge consumed criteria. The higher overall cell voltage of CV mode results in faster salt adsorption under a given charging time than CC mode. Nevertheless, CC mode consumed less energy than that consumed in CV mode in both criteria, but there were similar charge efficiencies in CC and CV modes. In the second part, the energy recovery system in an actual MCDI cell with a buck-boost converter was constructed and the energy recovery ratio was investigated under various operational conditions to determine the influential parameters affecting energy recovery in the MCDI cell. As major results, the salt adsorption capacity was found to play an important role in the energy recovery and constant current charging was found to be more favourable for energy recovery than constant voltage charging. In addition, for discharging conditions with the buck-boost converter operation, the energy recovery was more sensitively affected by the reference current rather than the capacitance of the supercapacitor. The smaller reference current mainly resulted in a higher energy recovery ratio in contrast

with the capacitance of the supercapacitor. We suggested that the development of an electrode with a high salt adsorption capacity and a cell design with low cell resistance will be required with a well-optimized buck-boost converter to facilitate a high energy recovery ratio. Lastly, energy recovery ratio in MCDI depending on electrode properties was investigated using constant current operation. Almost the whole carbon electrodes showed partial loss of energy recovery ratios due to high electrical resistance of low electrolyte. In particular, we found out that not only salt adsorption capacity but also salt adsorption rate play an important role in energy recovery performance. Our findings were confirmed by the least degradation of energy recovery performance in case of using carbon electrode with excellent salt adsorption capacity and rate. In conclusion, this dissertation focused on design and analysis of operating techniques, CC operation and energy recovery process with investigating energy efficiency and energy recovery according to operating condition. We expect that this dissertation will provide a comprehensive guide for the construction and operation of high energy-efficiency CDI process.

References

- Alkuran M, Orabi M. Utilization of a buck boost converter and the method of segmented capacitors in a CDI water purification system; 2008. IEEE. p 470-474.
- Alkuran M, Orabi M, Scheinberg N. Highly efficient Capacitive De-Ionization (CDI) water purification system using a buck-boost converter; 2008. IEEE. p 1926-1930.
- Anderson MA, Cudero AL, Palma J. 2010. Capacitive deionization as an electrochemical means of saving energy and delivering clean water. Comparison to present desalination practices: Will it compete? *Electrochimica Acta* 55(12):3845-3856.
- Avraham E, Bouhadana Y, Soffer A, Aurbach D. 2009. Limitation of charge efficiency in capacitive deionization I. on the behavior of single activated carbon. *Journal of the Electrochemical Society* 156(6):P95-P99.
- Avraham E, Noked M, Bouhadana Y, Soffer A, Aurbach D. 2010. Limitations of charge efficiency in capacitive deionization processes III: The behavior of surface oxidized activated carbon electrodes. *Electrochimica Acta* 56(1):441-447.
- Bard AJ, Faulkner LR. 2001. *Electrochemical methods: fundamentals and applications*, 2nd. Hoboken: Wiley and Sons.
- Biesheuvel P, Bazant M. 2010. Nonlinear dynamics of capacitive charging and

- desalination by porous electrodes. *Physical review E* 81(3):031502.
- Biesheuvel P, Van der Wal A. 2010. Membrane capacitive deionization. *Journal of Membrane Science* 346(2):256-262.
- Biesheuvel P, Van Limpt B, Van der Wal A. 2009. Dynamic adsorption/desorption process model for capacitive deionization. *The Journal of Physical Chemistry C* 113(14):5636-5640.
- Blair JW, Murphy GW. 1960. Electrochemical demineralization of water with porous electrodes of large surface area: University of Oklahoma.
- Bouhadana Y, Ben-Tzion M, Soffer A, Aurbach D. 2011. A control system for operating and investigating reactors: the demonstration of parasitic reactions in the water desalination by capacitive de-ionization. *Desalination* 268(1):253-261.
- Demirer ON, Naylor RM, Rios Perez CA, Wilkes E, Hidrovo C. 2013. Energetic performance optimization of a capacitive deionization system operating with transient cycles and brackish water. *Desalination* 314:130-138.
- Długolecki P, van der Wal A. 2013. Energy recovery in membrane capacitive deionization. *Environmental science & technology* 47(9):4904-4910.
- Dykstra J, Zhao R, Biesheuvel P, van der Wal A. 2016. Resistance identification and rational process design in Capacitive Deionization. *Water research* 88:358-370.
- Elimelech M, Phillip WA. 2011. The future of seawater desalination: energy, technology, and the environment. *Science* 333(6043):712-717.
- Evans S, Hamilton W. 1966. The mechanism of demineralization at carbon

electrodes. *Journal of The Electrochemical Society* 113(12):1314-1319.

Farmer JC, Bahowick SM, Harrar JE, Fix DV, Martinelli RE, Vu AK, Carroll KL. 1997. Electrosorption of chromium ions on carbon aerogel electrodes as a means of remediating ground water. *Energy & fuels* 11(2):337-347.

Farmer JC, Fix DV, Mack GV, Pekala RW, Poco JF. 1996. Capacitive deionization of NaCl and NaNO₃ solutions with carbon aerogel electrodes. *Journal of the Electrochemical Society* 143(1):159-169.

Freshwater D. 1951. Thermal economy in distillation. *Trans. Inst. Chem. Eng* 29:149-160.

Gabelich CJ, Tran TD, Suffet IM. 2002. Electrosorption of inorganic salts from aqueous solution using carbon aerogels. *Environmental science & technology* 36(13):3010-3019.

Gao X, Omosebi A, Landon J, Liu K. 2014. Dependence of the capacitive deionization performance on potential of zero charge shifting of carbon xerogel electrodes during long-term operation. *Journal of The Electrochemical Society* 161(12):E159-E166.

Gao X, Omosebi A, Landon J, Liu K. 2015. Surface charge enhanced carbon electrodes for stable and efficient capacitive deionization using inverted adsorption–desorption behavior. *Energy & Environmental Science* 8(3):897-909.

García-Quismondo E, Gómez R, Vaquero F, Cudero AL, Palma J, Anderson M. 2013a. New testing procedures of a capacitive deionization reactor. *Physical Chemistry Chemical Physics* 15(20):7648-7656.

- García-Quismondo E, Santos C, Lado J, Palma Js, Anderson MA. 2013b. Optimizing the energy efficiency of capacitive deionization reactors working under real-world conditions. *Environmental science & technology* 47(20):11866-11872.
- Greenlee LF, Lawler DF, Freeman BD, Marrot B, Moulin P. 2009. Reverse osmosis desalination: water sources, technology, and today's challenges. *Water research* 43(9):2317-2348.
- HeeáCho C, HeeáHan M, KookáKim D. 2013. Desalination via a new membrane capacitive deionization process utilizing flow-electrodes. *Energy & Environmental Science* 6(5):1471-1475.
- Jande Y, Kim W. 2013. Desalination using capacitive deionization at constant current. *Desalination* 329:29-34.
- Jeon S-i, Yeo J-g, Yang S, Choi J, Kim DK. 2014. Ion storage and energy recovery of a flow-electrode capacitive deionization process. *Journal of Materials Chemistry A* 2(18):6378-6383.
- Jia B, Zou L. 2012. Graphene nanosheets reduced by a multi-step process as high-performance electrode material for capacitive deionisation. *Carbon* 50(6):2315-2321.
- Johnson A, Newman J. 1971. Desalting by means of porous carbon electrodes. *Journal of the Electrochemical Society* 118(3):510-517.
- Jung H-H, Hwang S-W, Hyun S-H, Lee K-H, Kim G-T. 2007. Capacitive deionization characteristics of nanostructured carbon aerogel electrodes

synthesized via ambient drying. *Desalination* 216(1):377-385.

Jury WA, Vaux HJ. 2007. The emerging global water crisis: managing scarcity and conflict between water users. *Advances in Agronomy* 95:1-76.

Jury WA, Vaux Jr HJ. 2007. The emerging global water crisis: managing scarcity and conflict between water users. *Advances in Agronomy* 95:1-76.

Kang J, Kim T, Jo K, Yoon J. 2014. Comparison of salt adsorption capacity and energy consumption between constant current and constant voltage operation in capacitive deionization. *Desalination* 352:52-57.

Kang J, Kim T, Tak Y, Lee J-H, Yoon J. 2012. Cyclic voltammetry for monitoring bacterial attachment and biofilm formation. *Journal of Industrial and Engineering Chemistry* 18(2):800-807.

Khomenko V, Frackowiak E, Beguin F. 2005. Determination of the specific capacitance of conducting polymer/nanotubes composite electrodes using different cell configurations. *Electrochimica Acta* 50(12):2499-2506.

Kim J-S, Choi J-H. 2010a. Fabrication and characterization of a carbon electrode coated with cation-exchange polymer for the membrane capacitive deionization applications. *Journal of membrane science* 355(1):85-90.

Kim T, Yoon J. 2013. Relationship between capacitance of activated carbon composite electrodes measured at a low electrolyte concentration and their desalination performance in capacitive deionization. *Journal of Electroanalytical Chemistry* 704:169-174.

Kim T, Yoon J. 2015. CDI ragone plot as a functional tool to evaluate

desalination performance in capacitive deionization. *RSC Advances* 5(2):1456-1461.

Kim Y-J, Choi J-H. 2010b. Enhanced desalination efficiency in capacitive deionization with an ion-selective membrane. *Separation and Purification Technology* 71(1):70-75.

Kim Y-J, Choi J-H. 2010c. Improvement of desalination efficiency in capacitive deionization using a carbon electrode coated with an ion-exchange polymer. *Water research* 44(3):990-996.

Landon J, Gao X, Neathery JK, Liu K. 2013. Energy Recovery in Parallel Capacitive Deionization Operations. *ECS Transactions* 53(30):235-243.

Lawson KW, Lloyd DR. 1997. Membrane distillation. *Journal of membrane Science* 124(1):1-25.

Lee J-B, Park K-K, Eum H-M, Lee C-W. 2006. Desalination of a thermal power plant wastewater by membrane capacitive deionization. *Desalination* 196(1):125-134.

Lee J-B, Park K-K, Yoon S-W, Park P-Y, Park K-I, Lee C-W. 2009. Desalination performance of a carbon-based composite electrode. *Desalination* 237(1):155-161.

Lee J, Kim S, Kim C, Yoon J. 2014. Hybrid capacitive deionization to enhance the desalination performance of capacitive techniques. *Energy & Environmental Science* 7(11):3683-3689.

Li H, Zou L, Pan L, Sun Z. 2010. Novel graphene-like electrodes for capacitive

- deionization. *Environmental science & technology* 44(22):8692-8697.
- Lim J-A, Park N-S, Park J-S, Choi J-H. 2009. Fabrication and characterization of a porous carbon electrode for desalination of brackish water. *Desalination* 238(1):37-42.
- Liu Y, Pan L, Xu X, Lu T, Sun Z, Chua DH. 2014. Enhanced desalination efficiency in modified membrane capacitive deionization by introducing ion-exchange polymers in carbon nanotubes electrodes. *Electrochimica Acta* 130:619-624.
- Mulligan MD, Broach B, Lee TH. 2005. A constant-frequency method for improving light-load efficiency in synchronous buck converters. *Power Electronics Letters, IEEE* 3(1):24-29.
- Murphy G, Caudle D. 1967. Mathematical theory of electrochemical demineralization in flowing systems. *Electrochimica Acta* 12(12):1655-1664.
- Nadakatti S, Tendulkar M, Kadam M. 2011. Use of mesoporous conductive carbon black to enhance performance of activated carbon electrodes in capacitive deionization technology. *Desalination* 268(1):182-188.
- Oh H-J, Lee J-H, Ahn H-J, Jeong Y, Kim Y-J, Chi C-S. 2006. Nanoporous activated carbon cloth for capacitive deionization of aqueous solution. *Thin Solid Films* 515(1):220-225.
- Park B-H, Kim Y-J, Park J-S, Choi J. 2011. Capacitive deionization using a carbon electrode prepared with water-soluble poly (vinyl alcohol) binder. *Journal of Industrial and Engineering Chemistry* 17(4):717-722.

- Pernía AM, J Alvarez-González F, Díaz J, Villegas PJ, Nuño F. 2014. Optimum peak current hysteresis control for energy recovering converter in CDI desalination. *Energies* 7(6):3823-3839.
- Pernía AM, Normiella JG, Martín-Ramos JA, Díaz J, Martínez JA. 2012. Up-Down Converter for Energy Recovery in a CDI Desalination System. *Power Electronics, IEEE Transactions on* 27(7):3257-3265.
- Pernia A, Alvarez-Gonzalez FJ, Prieto M, Villegas P, Nuno F. 2014. New control strategy of an up-down converter for energy recovery in a CDI desalination System.
- Porada S, Borchardt L, Oschatz M, Bryjak M, Atchison J, Keesman K, Kaskel S, Biesheuvel P, Presser V. 2013a. Direct prediction of the desalination performance of porous carbon electrodes for capacitive deionization. *Energy & Environmental Science* 6(12):3700-3712.
- Porada S, Weinstein L, Dash R, Van Der Wal A, Bryjak M, Gogotsi Y, Biesheuvel P. 2012. Water desalination using capacitive deionization with microporous carbon electrodes. *ACS applied materials & interfaces* 4(3):1194-1199.
- Porada S, Zhao R, Van Der Wal A, Presser V, Biesheuvel P. 2013b. Review on the science and technology of water desalination by capacitive deionization. *Progress in Materials Science* 58(8):1388-1442.
- Ryoo M-W, Seo G. 2003. Improvement in capacitive deionization function of activated carbon cloth by titania modification. *Water Research* 37(7):1527-1534.

Shannon MA, Bohn PW, Elimelech M, Georgiadis JG, Mariñas BJ, Mayes AM. 2008. Science and technology for water purification in the coming decades. *Nature* 452(7185):301-310.

Shiue L-R, Sun A, Shiue C-C, Hsieh F-C, Hsieh Y-H, Jou J-J. 2003. Deionizers with energy recovery. Google Patents.

Soffer A, Folman M. 1972. The electrical double layer of high surface porous carbon electrode. *Journal of Electroanalytical Chemistry and Interfacial Electrochemistry* 38(1):25-43.

Strathmann H. 2010. Electrodialysis, a mature technology with a multitude of new applications. *Desalination* 264(3):268-288.

Suss M, Porada S, Sun X, Biesheuvel P, Yoon J, Presser V. 2015. Water desalination via capacitive deionization: what is it and what can we expect from it? *Energy & Environmental Science*.

Suss ME, Baumann TF, Bourcier WL, Spadaccini CM, Rose KA, Santiago JG, Stadermann M. 2012. Capacitive desalination with flow-through electrodes. *Energy & Environmental Science* 5(11):9511-9519.

Tsouris C, Mayes R, Kiggans J, Sharma K, Yiacoumi S, DePaoli D, Dai S. 2011. Mesoporous carbon for capacitive deionization of saline water. *Environmental science & technology* 45(23):10243-10249.

van Limpt B, van der Wal A. 2014. Water and chemical savings in cooling towers by using membrane capacitive deionization. *Desalination*.

Wang G, Dong Q, Ling Z, Pan C, Yu C, Qiu J. 2012. Hierarchical activated

carbon nanofiber webs with tuned structure fabricated by electrospinning for capacitive deionization. *Journal of Materials Chemistry* 22(41):21819-21823.

Wang L, Wang M, Huang Z-H, Cui T, Gui X, Kang F, Wang K, Wu D. 2011. Capacitive deionization of NaCl solutions using carbon nanotube sponge electrodes. *Journal of Materials Chemistry* 21(45):18295-18299.

Welgemoed T, Schutte C. 2005. Capacitive deionization technology™: an alternative desalination solution. *Desalination* 183(1):327-340.

Xu B, Wu F, Chen S, Zhang C, Cao G, Yang Y. 2007. Activated carbon fiber cloths as electrodes for high performance electric double layer capacitors. *Electrochimica Acta* 52(13):4595-4598.

Xu P, Drewes JE, Heil D, Wang G. 2008. Treatment of brackish produced water using carbon aerogel-based capacitive deionization technology. *Water research* 42(10):2605-2617.

Yang SJ, Kim T, Lee K, Kim YS, Yoon J, Park CR. 2014. Solvent evaporation mediated preparation of hierarchically porous metal organic framework-derived carbon with controllable and accessible large-scale porosity. *Carbon* 71:294-302.

Yoram O. 2008. Capacitive deionization (CDI) for desalination and water treatment-past, present and future. *Desalination* 228:10-29.

Zhang D, Shi L, Fang J, Dai K, Li X. 2006. Preparation and desalination performance of multiwall carbon nanotubes. *Materials Chemistry and Physics* 97(2):415-419.

Zhang LL, Zhao X. 2009. Carbon-based materials as supercapacitor electrodes.

Chemical Society Reviews 38(9):2520-2531.

Zhao R, Biesheuvel P, Miedema H, Bruning H, Van der Wal A. 2009. Charge efficiency: a functional tool to probe the double-layer structure inside of porous electrodes and application in the modeling of capacitive deionization. *The Journal of Physical Chemistry Letters* 1(1):205-210.

Zhao R, Biesheuvel P, Van der Wal A. 2012. Energy consumption and constant current operation in membrane capacitive deionization. *Energy & Environmental Science* 5(11):9520-9527.

Zhao R, Porada S, Biesheuvel P, Van der Wal A. 2013a. Energy consumption in membrane capacitive deionization for different water recoveries and flow rates, and comparison with reverse osmosis. *Desalination* 330:35-41.

Zhao R, Satpradit O, Rijnaarts H, Biesheuvel P, van der Wal A. 2013b. Optimization of salt adsorption rate in membrane capacitive deionization. *Water research* 47(5):1941-1952.

Zou L, Li L, Song H, Morris G. 2008. Using mesoporous carbon electrodes for brackish water desalination. *Water research* 42(8):2340-2348.

손덕영, 최윤호, 박대욱, 정충효. 2010. 수치모사를 이용한 CDI Unit Cell 내부의 유로성능 평가. *한국전산유체공학회지* 15(1):31-36.

이주영, 서석준, 박정우, 문승현. 2010. 축전식 탈염 시스템을 위한 셀 구조에 관한 연구. *Korean Chem. Eng. Res.(화학공학)* 48(6):791-794.

국문초록

축전식 탈염 (Capacitive Deionization, CDI) 기술은 전극표면에 형성되는 전기이중층을 이용하여 수내 이온을 제거하는 담수화 기술로서 역삼투막법과 증류법과 같은 기존 담수화 공정에 비하여 친환경적이고 낮은 에너지를 이용하는 새로운 담수화 기술로서 각광받고 있다. CDI 공정은 정전류 운전과 에너지 회수와 같은 운전 기술에 의해 공정 및 에너지 효율이 결정되므로 이러한 운전기술에 대한 적절한 설계 및 분석이 요구된다. 따라서 본 논문에서는 고 에너지 효율 및 에너지 회수를 위한 CDI의 운전기술의 설계 및 분석을 위해 전기인가방식에 따른 에너지 효율을 분석하고 운전조건과 전극 특성에 따른 에너지 회수 성능을 조사하고자 하였다. 우선 정전류 운전과 정전위 운전의 탈염 용량과 에너지 소비량을 인가 전하와 탈염량이 동일한 조건에서 비교 분석한 결과 탈염 용량 측면에서 평균 인가 전위가 높은 정전위 운전이 더 높은 탈염용량을 나타내는 반면, 정전류 운전은 약 26 ~ 30% 낮은 에너지 소비량을 나타내는 것을 확인하였다. 다음으로, 실제 에너지 회수 시스템을 구현하기 위해 전력 변환 장치인 buck-boost 컨버터를 MCDI와 결합한 회수 시스템을 구축하였으며 이를 이용하여 슈퍼캐패시터에 회수에너지를 저장하였다. 또한 CDI셀의 탈염용량이 에너지 회수율에

매우 중요한 영향을 미친다는 것을 알 수 있었으며 정전류 운전에서 높은 에너지 회수율을 달성됨을 밝혔다. 마지막으로, 에너지 회수 성능에 영향을 미치는 전극 특성을 조사하고자 다양한 기공구조를 가지는 재료를 이용해 전극을 제조하고 에너지 회수 성능을 평가한 결과, 일반적인 CDI공정에서 50 ~ 75%의 에너지 회수율이 나타남과 전극의 탈염용량과 탈염속도 특성이 에너지 회수 성능에 미치는 영향을 규명하였다. 결론적으로, 본 논문에서는 운전 방식에 따른 에너지 소비량을 비교하고 소비된 에너지를 회수하는 시스템 및 운전조건을 조사함으로써 고 에너지 효율 및 에너지 회수를 위한 CDI 운전기술의 설계 및 분석이 이루어졌다. 이러한 결과를 통하여 에너지 회수 시스템의 구축 및 운전에 요구되는 종합적인 지식을 제공할 수 있을 것으로 기대된다.

주요어: 담수화, 축전식 탈염기술, 에너지 효율성, 정전류 운전, 에너지 회수, 전극 특성

학 번: 2010-30802



저작자표시-비영리-변경금지 2.0 대한민국

이용자는 아래의 조건을 따르는 경우에 한하여 자유롭게

- 이 저작물을 복제, 배포, 전송, 전시, 공연 및 방송할 수 있습니다.

다음과 같은 조건을 따라야 합니다:



저작자표시. 귀하는 원저작자를 표시하여야 합니다.



비영리. 귀하는 이 저작물을 영리 목적으로 이용할 수 없습니다.



변경금지. 귀하는 이 저작물을 개작, 변형 또는 가공할 수 없습니다.

- 귀하는, 이 저작물의 재이용이나 배포의 경우, 이 저작물에 적용된 이용허락조건을 명확하게 나타내어야 합니다.
- 저작권자로부터 별도의 허가를 받으면 이러한 조건들은 적용되지 않습니다.

저작권법에 따른 이용자의 권리는 위의 내용에 의하여 영향을 받지 않습니다.

이것은 [이용허락규약\(Legal Code\)](#)을 이해하기 쉽게 요약한 것입니다.

[Disclaimer](#)

공 학 박 사 학 위 논 문

**Design and Analysis of CDI Techniques for
High Energy Efficiency and Energy Recovery**

고 에너지 효율 및 에너지 회수를 위한
축전식 탈염기술의 설계 및 분석

2016년 2월

서울대학교 대학원

화학생명공학부

강 전 일

**Design and Analysis of CDI Techniques for
High Energy Efficiency and Energy Recovery**

by

Junil Kang

under the supervision of

Professor Jeyong Yoon, Ph. D.

A dissertation submitted in partial fulfillment of the requirements for
the Degree of
Doctor of Philosophy

FABRARY 2016

SCHOOL OF CHEMICAL AND BIOLOGICAL ENGINEERING
SEOUL NATIONAL UNIVERSITY

**Design and Analysis of CDI Techniques for High Energy
Efficiency and Energy Recovery**

고 에너지 효율 및 에너지 회수를 위한
축전식 탈염기술의 설계 및 분석

지도교수 윤 제 용

이 논문을 공학박사 학위논문으로 제출함

2015년 12월

서울대학교 대학원

공과대학 화학생물공학부

강 전 일

강전일의 공학박사 학위논문을 인준함

2016년 1월

위 원 장	<u>성 영 은 (인)</u>
부 위 원 장	<u>윤 제 용 (인)</u>
위 원	<u>하 정 익 (인)</u>
위 원	<u>곽 용 석 (인)</u>
위 원	<u>강 경 석 (인)</u>

Abstract

Water and energy scarcity by industrialization and population growth has emerged as global crisis to humanity, which cause the demand for efficient desalination technique with low-energy cost. Compared to conventional desalination processes such as reverse osmosis (RO) and distillation, capacitive deionization (CDI), an electrochemical desalination technology using electrical double layer on the electrode, has come into spotlight in terms of environment-friendly and low-energetic process. Since the desalination performance and energy efficiency of CDI process are determined by operation techniques such as constant current operation and energy recovery, design and analysis for these techniques are needed for enhancing energy efficiency. Therefore, in this dissertation, design and analysis of CDI techniques for high energy efficiency and energy recovery was implemented by focusing on the evaluation of energy consumption according to operational modes and energy recovery system. Firstly, salt adsorption capacity (deionization capacity) and energy consumption of two CDI operational modes (CV and CC) were comparatively investigated. As major results, CV mode resulted in faster salt adsorption while CC mode showed much lower energy consumption than CV mode by 26 ~ 30% due to the overall lower cell voltage used in CC mode than in CV mode. Secondly, the successful construction of an energy recovery system in an actual MCDI cell with a

buck-boost converter was implemented; the buck-boost converter facilitated the delivery of the energy stored in the MCDI cell into a supercapacitor. The salt adsorption capacity was found to play an important role in the energy recovery and constant current charging was found to be more favorable for energy recovery than constant voltage charging. Lastly, energy recovery ratio in MCDI depending on electrode properties was investigated using constant current operation. Almost the whole carbon electrodes showed energy recovery ratios of 0.5 ~ 0.75 and we found out that not only salt adsorption capacity but also salt adsorption rate play an important role in energy recovery performance. In conclusion, this dissertation focused on design and analysis of operating techniques, CC operation and energy recovery process with investigating energy efficiency and energy recovery according to operating condition. We expect that this dissertation will provide a comprehensive guide for the construction and operation of high energy-efficiency CDI process.

Keywords: Desalination; capacitive deionization; energy efficiency; constant current operation; energy recovery; electrode properties

Student number: 2010-30802

Tables of Contents

1. Introduction	1
1.1. Backgrounds.....	1
1.2. Objectives	4
2. Literature review	6
2.1. The history of CDI	6
2.2. CDI operation and evaluation	11
2.3. MCDI (Membrane-assisted CDI)	17
2.4. Energy recovery in CDI	23
2.5. State of the art CDI system	27
3. Comparison of salt adsorption capacity and energy consumption between constant voltage and constant current operation in capacitive deionization.....	33
3.1. Introduction.....	33
3.2. Materials and Methods.....	37

3.3. Results and Discussion.....	43
3.4. Summary	63
4. Direct energy recovery system for capacitive deionization	64
4.1. Introduction.....	64
4.2. Materials and Methods.....	69
4.3. Results and Discussion.....	79
4.4. Summary	104
5. Influential electrode properties on energy recovery performance in capacitive deionization.....	105
5.1. Introduction.....	105
5.2. Materials and Methods.....	108
5.3. Results and Discussion.....	113
5.4. Summary	139
6. Conclusions	140

List of Figures

Figure 2-1. Capacitive deionization (CDI).....	7
Figure 2-2. Timeline of CDI development.	10
Figure 2-3. Operational process for CDI.....	12
Figure 2-4. Operational conditions for CDI; flow types (top) and operational types (bottom).	14
Figure 2-5. Ion distribution and movement of MCDI during the charging and discharging process.	18
Figure 2-6. The schematic of Membrane assisted CDI (MCDI) (Biesheuvel and Van der Wal 2010).	19
Figure 2-7. The concentration transient of effluent: solid line; MCDI, dashed line; CDI (Kim and Choi 2010b).....	21
Figure 2-8. The SEM images of carbon electrode (a) coated with ion-exchange resin (Kim and Choi 2010a) and (b) fabricated with ion-exchange resin as a binder (Kim and Choi 2010a; Liu et al. 2014).	22
Figure 2-9. (a) Comparison for energy consumption between CDI and RO, (b) theoretical energy consumption with different energy recovery ratio.....	25
Figure 2-10. The methodologies for energy recovery in CDI process	26
Figure 2-11. Flow-CDI (FCDI); (a) schematic and (b) variation in the NaCl concentration in the effluent stream (HeeáCho et al. 2013).	28
Figure 2-12. Hybrid CDI (HCDI); (a) schematic and (b) comparison of specific capacity (Lee et al. 2014).....	30

Figure 2-13. Inverted CDI (i-CDI); (a) schematic and (b) enhanced stability by the i-CDI system (Gao et al. 2015).	32
Figure 3-1. Control of the effluent concentration of freshwater and concentrate in MCDI-CC-RCD mode, using as control variable: (a) current, (c) water flow rate (Zhao et al. 2012).	36
Figure 3-2. Schematic of flow mode capacitive deionization process used in this study. The capacitive deionization module comprised (1) current collectors (graphite), (2) electrodes (activated carbon sheet), and a (3) spacer (polymer).	39
Figure 3-3. Two criteria for accurate comparison of CV and CC operation; identical consumed charge and ion removal during the desalination step.	42
Figure 3-4. Comparison of constant voltage (CV) and constant current (CC) modes in capacitive deionization. Shown are conductivity (a), current (b), and cell voltage (c) graphs from CV mode. (cell voltage = 1.2 V, charging & discharging time = 10 min respectively, flow rate = 10 mL/min) and conductivity (d), current (e), and cell voltage (f) from CC mode (current density = 2.5 mA/cm ² for charging and -2.5 mA/cm ² for discharging, flow rate = 10 mL/min).	44
Figure 3-5. Comparison of constant voltage (CV) and constant current (CC) modes in membrane-assisted capacitive deionization. Shown are conductivity (a), current (b), and cell voltage (c) graphs from CV mode. (cell voltage = 1.2 V, charging & discharging time = 10 min respectively, flow rate = 10 mL/min)	

and conductivity (d), current (e), and cell voltage (f) from CC mode (current density = 2.5 mA/cm² for charging and -2.5 mA/cm² for discharging, flow rate = 10 mL/min).48

Figure 3-6. The representative salt adsorption capacity curve in (a) constant voltage (CV) and (b) constant current (CC) operation during charging step. The salt adsorption capacity from (a) constant voltage (CV) mode (cell voltage = 1.2 V, charging and discharging time = 10 min respectively, flow rate = 10 mL/min) and (b) constant current (CC) mode (current density = 2.5 mA/cm² for charging and -2.5 mA/cm² for discharging, flow rate = 10 mL/min) during capacitive deionization. The inserted figure displays the effluent conductivity during charging time (from Figure 3-4a & d). The shaded areas in the inserts represent the salt adsorption capacity.52

Figure 3-7. The salt adsorption capacity curve (a) and salt adsorption rate (b) of constant voltage (CV, 1.2V) and constant current (CC) operation with various constant current densities (1.5 ~ 3.5 mA/cm²).....54

Figure 3-8. (a) Energy consumption and charge efficiency, (b) voltage profiles depending on charging currents (1, 1.5, 2.5, 5 mA/cm²) with CC operation in MCDI.58

Figure 3-9. Comparison of energy consumption and charge efficiency in CDI constant voltage (CV) and constant current (CC) mode with various constant current densities (1.5, 2, 2.5, 3.0, 3.5 mA/cm²). Two criteria of identical electrical charge consumed (a and c) and identical amount of ion removal (b &

d) were employed. The arrows indicate the increasing current in CC operation.59

Figure 3-10. Comparison of energy consumption in MCDI constant voltage (CV) and constant current (CC) mode with various constant current densities (1, 1.5, 2.5, 5 mA/cm²). Two criteria of identical electrical charge consumed (a and c) and identical amount of ion removal (b & d) were employed. The arrows indicate the increasing current in CC operation.60

Figure 3-11. Integration of CV and CC operation. The (a) concentration, (b) voltage, (c) salt adsorption capacity profiles were obtained by integrated CDI operations with CC (1.5 mA/cm² to 1.2 V) and CV (1.2 V). The energy consumption (d) of integrated operation was compared to that of CV and CC operation, respectively.....62

Figure 4-1. Prediction of energy recovery of CDI process using constant current charging and discharging. Energy recovery ratio can be calculated by the ratio of recovered energy during the discharging step to consumed energy during the charging step (Długołęcki and van der Wal 2013).....67

Figure 4-2. The schematic of proposed circuit of energy recovery system in CDI with a buck-boost converter (Pernia et al. 2014).....68

Figure 4-3. The schematic of an actual membrane capacitive deionization (MCDI) cell for energy recovery that is connected with a supercapacitor via a buck-boost converter. The MCDI cell is composed of electrodes, ion exchange membranes and a spacer. The electrical energy consumed during the desalination step is partially transferred to the supercapacitor.71

Figure 4-4. Schematic of the buck-boost converter operation during delivery of the energy stored in the CDI cell into the supercapacitor. The buck-boost converter is operated by a) an automatic switching depending on the current intensity at an inductor (L), and it generates b) specific current profiles in the CDI cell and the supercapacitor. The ratio of the duration of stage #1 over the whole duration in one cycle (stage #1 and stage #2) is presented as the converter duty (D), and the average current through the CDI cell is expressed as the reference current (I_{ref})..... 75

Figure 4-5. The calculation of energy recovery ratio. The energy recovery is obtained from the ratio of energy consumed for desalination (ion adsorption) to energy recovered (stored into the supercapacitor) by the buck-boost converter..... 78

Figure 4-6. Representative voltage and conductivity profile in one cycle during MCDI operation with energy recovery. Shown are the potential (a) and conductivity (b) from constant voltage (CV) charging (1.2 V, 10 min, and 10 mM) and the potential (c) and conductivity (d) from constant current (CC) charging (1.5 mA/cm² and 10 mM). The energy recovery process was performed with a reference current of 5 mA of the buck-boost converter and capacitance of 5 F of the supercapacitor. The voltage profiles of the CDI cell and the supercapacitor are depicted as the blue solid line and red solid line, respectively..... 80

Figure 4-7. The actual current profile applied to the MCDI cell during the

discharging step. The discharging current is obtained from the experimental data set of I_{ref} (=5 mA), V_{MCDI} , $V_{supercapacitor}$ 83

Figure 4-8. Three-dimensional representation of the energy recovery ratio in the MCDI with two charging modes. Constant voltage (CV) charging (a) was conducted with various charging voltages and times for a NaCl concentration of 10 mM. Similarly, constant current (CC) charging (b) was conducted with various charging currents and concentrations of feed water. The discharging step was performed with reference current of 5 mA of the buck-boost converter and capacitance of 5 F of the supercapacitor. 85

Figure 4-9. The relationship between the energy recovery ratio and the salt adsorption capacity in MCDI with two charging modes. Shown are the constant voltage (CV, 0.3 ~ 1.2 V at 10 mM) charging (a) and the constant current (CC, 1 ~ 4 mA/cm² at 5 ~ 100 mM) charging (b). The arrow indicates the direction of increasing charging time in CV mode and charging current in CC mode. 90

Figure 4-10. The salt adsorption capacity with CV charging as a function of a) charging time at 1.2 V and b) charging voltage for 10 min and with CC charging as a function of c) charging current at 10 mM and d) concentration of feed water at 1.5 mA/cm². 91

Figure 4-11. The mean power of charged MCDI cell during the discharging step as a function of the salt adsorption capacity in case of a) CV charging and b) CC charging. 94

Figure 4-12. Solution resistance as a function of charging current with various concentration of feed water (5~100 mM).....	96
Figure 4-13. Three-dimensional representation of the energy recovery ratio with various reference currents of the buck-boost converter and capacitances of the supercapacitor. The charging step was performed with constant current operation at 1.5 mA/cm ² and a NaCl concentration of 10 mM. The average salt adsorption capacity was 19 mg/g.....	100
Figure 4-14. Calculation of energy loss during converter operation (energy recovery step). (a) voltage profiles of supercapacitor#1 (energy donor) and supercapacitor#2 (energy receptor), (b) energy loss of converter as a function of charging potentials and reference currents.....	102
Figure 4-15. Comparison of energy recovery ratio with considering energy loss of converter (30% in this study) and without considering energy loss of converter. This data is based on the energy recovery ratio with CV charging depicted in Figure 4-9a.....	103
Figure 5-1. Definition of energy recovery ratio in CDI with constant current operation.....	112
Figure 5-2. The meso- and macropore distributions of carbon materials derived from BJH equation; (a) MSP-20, (b) MDC, (c) CA.....	115
Figure 5-3. Galvanostatic charge/discharge voltage profiles of MSP-20.....	118
Figure 5-4. Galvanostatic charge/discharge voltage profiles of P-60	119
Figure 5-5. Galvanostatic charge/discharge voltage profiles of SX-PLUS.....	120

Figure 5-6. Galvanostatic charge/discharge voltage profiles of S-51HF 121

Figure 5-7. Galvanostatic charge/discharge voltage profiles of MDC 122

Figure 5-8. Galvanostatic charge/discharge voltage profiles of Carbon aerogel 123

Figure 5-9. Retention of specific capacitance as a function of scan rate (0.5 mA/cm² ~ 20 mA/cm²) with various carbon composite electrodes..... 125

Figure 5-10. (a) The representative voltage profiles and (b) salt adsorption capacities (mg/g) of CC mode in MCDI operation with various carbon electrodes. (current density = 1 mA/cm² for charging and -1 mA/cm² for discharging, flow rate = 10 mL/min, NaCl concentration = 10 mM)..... 129

Figure 5-11. Salt adsorption capacities (mg/cm³) of CC mode in MCDI operation with various carbon electrodes. (current density = 1 mA/cm² for charging and -1 mA/cm² for discharging, flow rate = 10 mL/min, NaCl concentration = 10 mM)..... 130

Figure 5-12. The energy consumed during the charging step (E_c) and energy recovered during the discharging step (E_r) with various carbon materials. Inserted table shows the energy recovery ratio calculated from E_r/E_c as presented in Figure 5-2. CC operation in desalination test was performed with 1/-1 mA/cm² of charging/discharging current density up to 1.2 V of cut-off voltage and 10 mM NaCl solution. The symbols are located between $E_r=0.5E_c$ and $E_r=0.75E_c$, indicating the energy recovery ratios of carbon materials ranged from 50% to 75%. 133

Figure 5-13. Correlation between the salt adsorption capacity and energy

recovery ratio. Salt adsorption capacity was obtained from Figure 5-11b and regression line was plotted with MSP-20, P-60, SX PLUS and S-51HF. The red star indicates the energy recovery ratio of converter system in Figure 4-9. 135

Figure 5-14. Correlation between the average salt adsorption rate and mean power. The average salt adsorption rate was calculated by dividing the salt adsorption capacity by the duration of charging step (mg/g/s) and mean power was obtained by dividing the energy recovered during the discharging step by the duration of discharging step and the mass of electrodes (mW/g)..... 137

Figure 5-15. The normalized energy recovery as a function of different charging-discharging current density (± 1 , ± 2 , ± 4 mA/cm²). All of desalination test were identically performed with 1.2 V of Cut-off voltage and 10 mM NaCl solution..... 138

1. Introduction

1.1. Backgrounds

With greater water scarcity caused by worldwide industrialization and population growth, demand for available water resources have come into spotlights as a main task for humanity (Jury and Vaux 2007; Shannon et al. 2008). Considering that 98% of Earth's water resources exist as seawater or brackish water (Anderson et al. 2010; Elimelech and Phillip 2011), desalination can be a major strategic technical approach to address this problem. Thus far, thermal distillation and membrane separation are utilized as the most common desalination processes (Shannon et al. 2008). However, these desalination processes have a considerable disadvantage in terms of high energy consumption for securing high pressure and temperature although they show high salt removal and have been successfully commercialized. Recently, capacitive deionization (CDI) emerged as an alternative and complement to conventional desalination processes (Porada et al. 2013b). This state-of-the-art desalination approach is based on the electrical double layer induced by a cell voltage difference between two porous carbon electrodes, which is derived from the principle of electric double layer capacitor (EDLC) (Zhang and Zhao 2009). CDI has many advantages with environmental and energetic aspects because chemical treatment is not required and a low electrical voltage is applied for the operation

(Farmer et al. 1996; Porada et al. 2013b; Welgemoed and Schutte 2005).

Low energy consumption for the operation is one of powerful strengths in CDI compared to the conventional processes in the way that high energy efficiency, indicating low energy required for deionization, is the key requirement for desalination (Elimelech and Phillip 2011; Zhao et al. 2013a). High energy efficiency directly related with CDI performance is the major interest in many CDI research groups. For this reasoning, there have been numerous studies reporting the improvement of energy efficiency and CDI performance through the electrode materials such as carbon aerogel, mesoporous carbon, fiber, graphene, carbon nanotube, MOF(metal organic framework)-derived carbon (Gabelich et al. 2002; Li et al. 2010; Porada et al. 2013a; Tsouris et al. 2011; Wang et al. 2012; Wang et al. 2011; Yang et al. 2014), operating conditions such as cell voltage, flow rate, concentration (Porada et al. 2013b; Zhao et al. 2013b).

In particular, operating techniques such as constant current operation, energy recovery (Alkuran et al. 2008; Długolecki and van der Wal 2013; Zhao et al. 2012) are major factors to affect the desalination performance and energy efficiency of CDI process. Constant current (CC) operation which is introduces to produce constant concentration in desalinated water compared to conventional constant voltage (CV) operation (Kang et al. 2014; Zhao et al. 2012) is directly connected with energy consumption of CDI. In addition, the energy recovery is the substantial advantageous operating technique of CDI versus other

desalination processes because the partial recovery of consumed energy for desalination is easily feasible due to capacitive nature (Demirer et al. 2013; García-Quismondo et al. 2013a). In this respect, design and analysis for these operating techniques are necessarily required for enhancing energy efficiency of CDI process. However, most of previous studies about CC operation have been report the production of constant desalinated stream and the effect of operating condition without the accurate evaluation of energy efficiency. Moreover, the energy recovery of CDI have been limited to only suggest the conceptual model without realization of energy recovery system. Therefore, further studies are required for design and analysis for CDI techniques including CC operation and energy recovery to achieve high energy efficiency.

1.2. Objectives

In this dissertation, design and analysis of CDI techniques for high energy efficiency and energy recovery was implemented by focusing on the evaluation of energy consumption according to operational modes and energy recovery system. To accomplish the intended goal of this dissertation, three parts of studies were implemented as follows:

Firstly, the energy consumption according to operational modes in CDI was evaluated by comparison of CV and CC operation in terms of salt adsorption capacity (Desalination performance), energy consumption and charge efficiency. The salt adsorption capacity was analyzed based on its conductivity profile with capacity and rate. For the accurate comparison, two criteria (identical electrical charge consumed and identical amount of ion removal during desalination process) are considered.

Secondly, the energy recovery system in CDI process was realized and the influential parameters affecting energy recovery ratio were investigated. For this, the direct energy recovery system in an actual MCDI cell was constructed by introducing a buck-boost converter, electronic power conversion device. The energy recovery was implemented with storage of recovered energy into a supercapacitor. Also, the energy recovery ratio was investigated under various operational conditions (CV charging with various voltages and times, CC

charging with various currents and concentrations of feed water, discharging with various reference currents of the buck-boost converter, and capacitances of the supercapacitor).

Lastly, the relationship between electrode characteristics and energy recovery performance was investigated by using various carbon materials with different properties. Electrochemical properties were checked by galvanostatic charge/discharge and desalination test using CC operation was implemented. The ratio of consumed energy during desalination step and released energy during regeneration step was defined as energy recovery ratio. To determine the effect on energy recovery performance, influential factors (electrode characteristics) were considered as capacity (salt adsorption capacity) and rate (salt adsorption rate), and the salt adsorption rate was correlated with mean power during energy recovery process.

2. Literature review

2.1. The history of CDI

Capacitive deionization (CDI) is an electrochemically controlled desalination technology using an electrical double layer based on non-faradaic process, as shown in Figure 2-1. Its principle is similar with that of supercapacitor, electric energy storage media, in regard to collecting ions in electrolyte by electrical double layer formed on the electrode surface. However, in case of CDI, electrolyte (feed water) flows between two electrodes where cell voltage is applied through the charging and discharging step (Anderson et al. 2010).

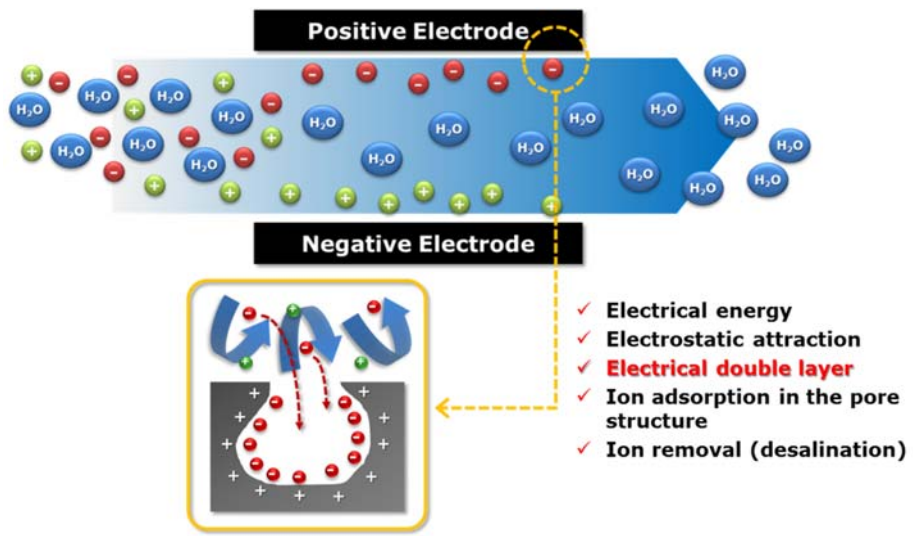


Figure 2-1. Capacitive deionization (CDI).

Figure 2-2 shows the historical schematic of CDI development. From 1960 when the technical concept of CDI had been firstly introduced (Blair and Murphy 1960) to the present, numerous studies have been examined in the theoretical, systematic and material aspects. In the early stages (1960~1990), the principle of ion removal from feed water was investigated based on electro-sorption occurred at electrode's surfaces. Although the principle of ion removal had been reported as the result of ion exchange process between salts and functional group on electrode's surfaces (Evans and Hamilton 1966; Murphy and Caudle 1967), this null hypothesis have been changed into the formation of electrical double layer as the principle of CDI which is now widely accepted (Johnson and Newman 1971; Soffer and Folman 1972). After that, in 2000s, the development of materials and fabrication technologies contributed to the application of various carbon materials such as an activated carbon, carbon aerogel, carbon nanotube, mesoporous carbon, graphene to the CDI electrode for enhancing desalination performances (Farmer et al. 1996; Li et al. 2010; Zhang et al. 2006; Zou et al. 2008). The relationship between electrode properties and desalination performance was also investigated in this period. In addition, many operating techniques was developed to enhance desalination performances and efficiency such as constant current (CC) operation which can produce fixed concentration of desalinated water (Zhao et al. 2012), membrane-assisted CDI (MCDI) which dramatically raise desalination performances using ion-exchange membrane (Biesheuvel and Van der Wal 2010; Kim and Choi 2010b), hybrid-CDI (HCDI)

which is derived from battery system for gaining large capacity (Lee et al. 2014), flow-CDI (FCDI) which uses not immobilized electrodes but flowable carbon slurry as electrodes (HeeáCho et al. 2013), inverted-CDI (i-CDI) which inverts the sequence of charging and discharging step with the modified surface charge of electrodes (Gao et al. 2014; Gao et al. 2015).

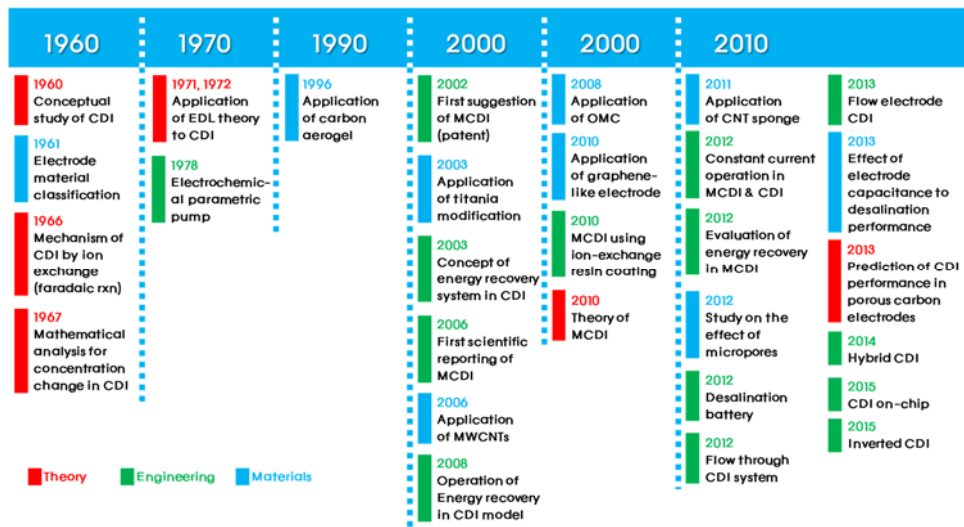


Figure 2-2. Timeline of CDI development.

2.2. CDI operation and evaluation

In this chapter, the methods for CDI operation and evaluation of CDI performance implemented in this study will be addressed. The sequence of CDI operation consist of charging and discharging steps as shown in Figure 2-3. Salts in feed water are removed through ion adsorption into pores of carbon electrodes by applying electrical energy, called charging (desalination) step. After charging step, by applying reverse electrical energy or short-circuiting, adsorbed ions are released to the flow channel and electrodes are regenerated, called discharging (regeneration) step. The regeneration step is essential to provide adsorption site required for the next desalination step. Discontinuous production of desalinated water is one of characteristics in CDI operation because ion removal ceases during the regeneration step. Considering ion removal by the formation of electrical double layer as the principle of CDI, desalination should be occurred without faradaic reaction. Therefore, the cell voltage between two electrodes is below 1.23 V (vs. NHE as water splitting reaction) (Farmer et al. 1996; Porada et al. 2012; Welgemoed and Schutte 2005). Compared to the conventional electrochemical desalination method, electrodialysis (ED), the energy consumption of CDI is lower than ED due to operation with low cell voltage (Porada et al. 2012).

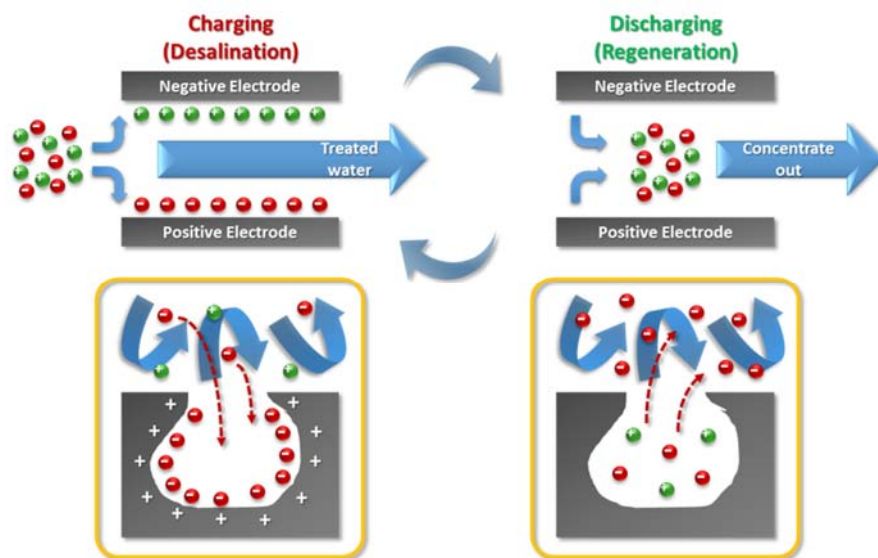


Figure 2-3. Operational process for CDI.

The CDI performance is dependent on operational conditions such as flow type (Farmer et al. 1997; Lee et al. 2009), flow channel (Suss et al. 2012; 이주영 et al. 2010), module design (손덕영 et al. 2010), the operational mode for applying electrical energy (Jande and Kim 2013; Kang et al. 2014; Zhao et al. 2012), the concentration of feed water (Porada et al. 2013a; Zhao et al. 2013b). The type of flow channel is representatively classified into the batch and flow system. In case of the batch system which have been frequently used in academic fields, it is difficult to maintain a constant concentration of feed stream. The flow system, therefore, is more suitable for actual process or commercialization than the batch system (Porada et al. 2013b). The flow type is depicted in Figure 2-4 (top). The operational mode for applying electrical energy is classified into constant voltage (CV) and constant current (CC) operation. CV operation is beneficial to easily adjust cell voltages and desalination times. While, CC operation is favorable for manufacturing targeted constant concentration of desalinated water and low energy consumption, as shown in Figure 2-4 (bottom). The concentration of feed water also have a strong influence on the CDI performance because the charge capacity in electrical double layer is charged with the electrolyte concentration (Bard and Faulkner 2001; Kim and Yoon 2013). However, the aimed concentration is generally in the range of 5 to 50 mM due to the limitation of adsorption site in carbon electrode pores (Zhao et al. 2013b).

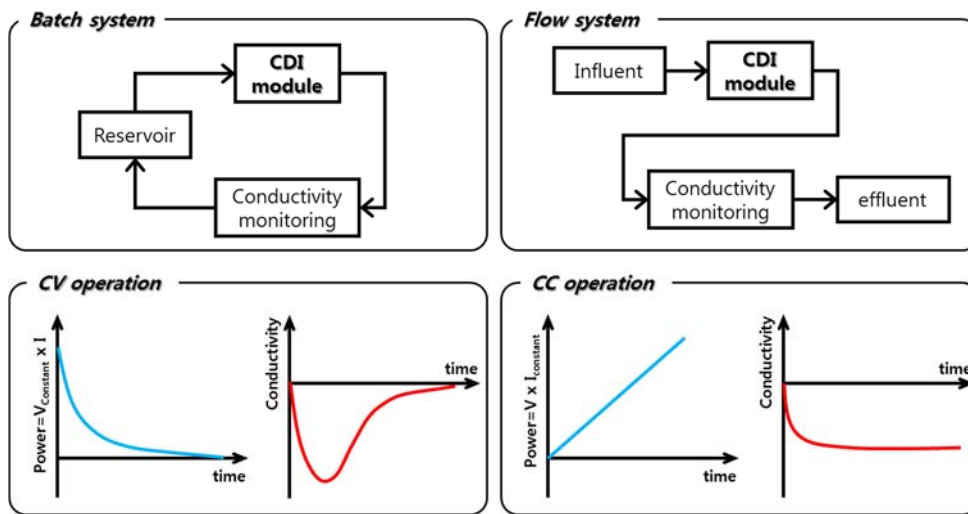


Figure 2-4. Operational conditions for CDI; flow types (top) and operational types (bottom).

To evaluate and compare results of various CDI operations, some operational indexes representing CDI performances and energy efficiency are required, which are salt adsorption capacity, average salt adsorption rate, energy consumption and charge efficiency (Porada et al. 2013b; Suss et al. 2015).

The performance of CDI operation is determined by the salt adsorption capacity (SAC) which shows the amount of salts removed during the desalination step and the average salt adsorption rate (ASAR) which shows the salt removal rate. The SAC is calculated by total amount of salt removed during the desalination step divided by total weights of electrodes and represented in mg/g_{electrode} (Equation 1).

$$\text{Salt adsorption capacity (mg/g)} = \frac{\int (C_{\text{in}} - C_{\text{out}}) \times \Phi \times dt}{M_{\text{electrode}}} \quad (2-1)$$

(C_{in}; inlet concentration, C_{out}; outlet concentration, Φ; flow rate, M_{electrode}; Electrode weight)

In addition, the SAC measured at equilibrium state (without the change in feed concentration) is represented as maximum SAC (mSAC). While the SAC can be changed depending on operational conditions, the mSAC is the characteristic of carbon material independent of operational conditions because it indicates the maximum amount of salts available for specific carbon material. The ASAR is calculated by the SAC divided by the duration of desalination step and represented in mg/g_{electrode}/sec or mg/g_{electrode}/min. Unlike the mSAC determined by only carbon

materials, the ASAR is highly suitable index to synthetically evaluate the CDI performance including carbon material and operational conditions.

The energy efficiency is determined by energy consumptions required for removing specific amount of salts. This index can be calculated by total electrical energy consumed during the desalination step divided by total salts removed and represented in kJ/mol or kT per ion removed ($[\text{kT per ion removed}] = [\text{kJ/mol}] / \#$ of Avogadro) (Equation 2).

$$\text{Energy consumption (kJ/mol)} = \frac{\int V \times I \times dt}{2 \times \int (C_{\text{in}} - C_{\text{out}}) \times \Phi \times dt} \quad (2-2)$$

(V; voltage, I; current)

The charge efficiency is calculated by the amount of charge converted from removed salts divided by total electrical charge during the desalination step and directly indicates the efficiency of energy utilization (Equation 3).

$$\text{Charge efficiency} = \frac{F \times \int (C_{\text{in}} - C_{\text{out}}) \times \Phi \times dt}{\int I \times dt} \quad (2-3)$$

Although the ideal capacitor system should show unity of charge efficiency, general CDI process reveals the charge efficiency below unity due to co-ion repulsion (Avraham et al. 2009; Avraham et al. 2010; Zhao et al. 2009).

2.3. MCDI (Membrane-assisted CDI)

In this study, experiments were conducted with MCDI system, the combination of conventional CDI system and ion-exchange membrane to achieve high desalination performance.

When electrical potential is applied to the electrode, co-ions (same charge with the applied potential) and counter-ions (opposite charge with applied potential) are simultaneously distributed near the electrode surface. The electrical double layer induced by applying potential not only attracts counter-ions, but also repels co-ions from the electrode surface to bulk phase, which is called co-ion expulsion effect. This co-ion expulsion effect results in the decrease of energy efficiency in CDI process (Avraham et al. 2009). To prevent co-ion expulsion and increase the energy efficiency of CDI, the ion-exchange membrane was firstly introduced by Lee et al. in Korea Electric Power Research Institute (KEPRI) (Lee et al. 2006), called membrane-assisted CDI (MCDI). As shown in Figure 2-5, co-ion expulsion effect is decreased by restriction of co-ion's movement, which results in higher desalination performance. In addition, the efficiency of regeneration process is enhanced because the reverse potential can be applied without concerning re-adsorption of released ions (Biesheuvel and Van der Wal 2010). MCDI is innovative operating system to obtain remarkable enhancement in desalination performances using CDI module installed with ion-exchange membrane; cation and anion exchange membrane were equipped to

negative and positive charged electrode, respectively (Figure 2-6).

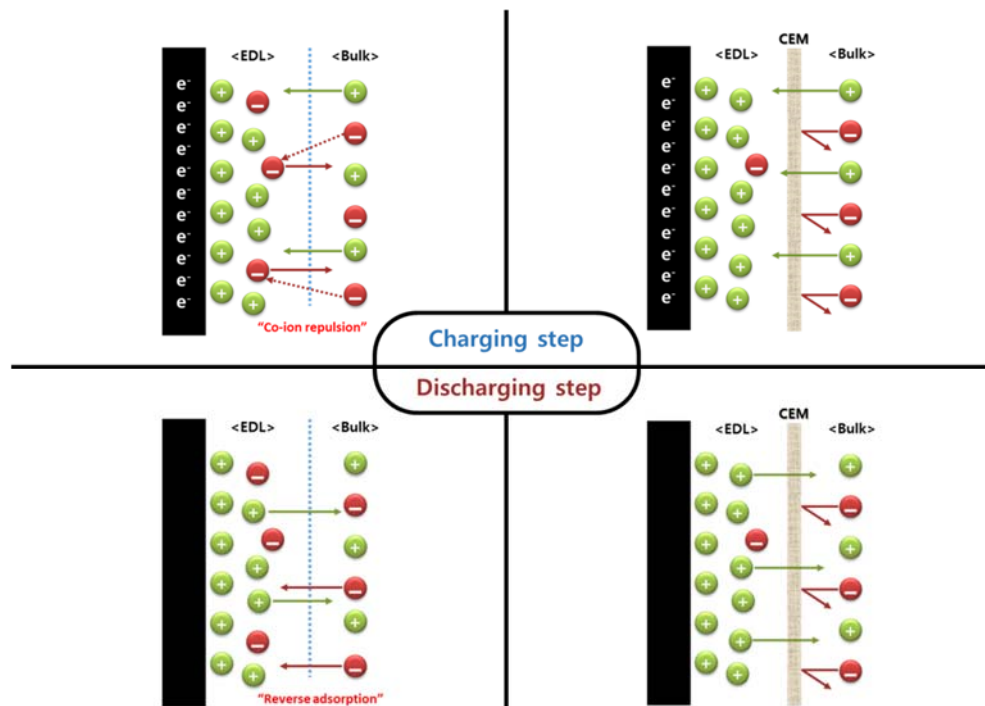


Figure 2-5. Ion distribution and movement of MCDI during the charging and discharging process.

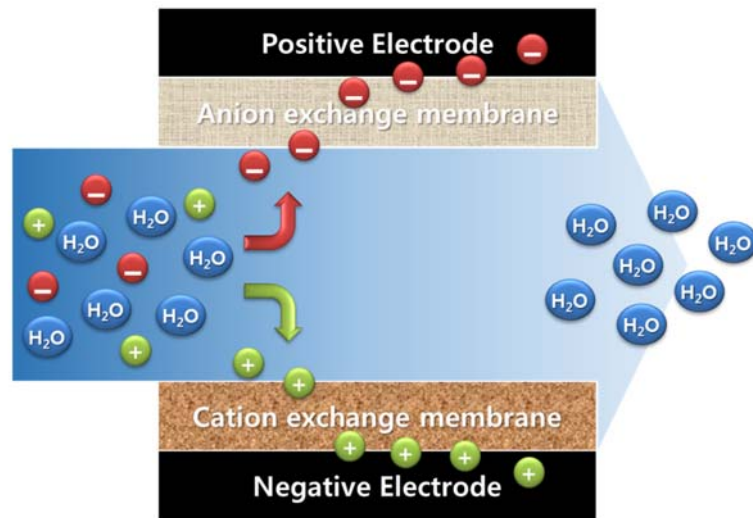


Figure 2-6. The schematic of Membrane assisted CDI (MCDI) (Biesheuvel and Van der Wal 2010).

By introducing MCDI, the desalination performance and CDI efficiency are dramatically improved as shown in Figure 2-7 (Kim and Choi 2010b). Moreover, it was reported in further studies that ion-exchange resin was directly coated on the electrode surface (Kim and Choi 2010a; Kim and Choi 2010c) or utilized as a binder for electrode fabrication (Liu et al. 2014) to not only decrease interfacial resistance between electrodes and membranes but also substitute expensive ion-exchange membrane as shown in Figure 2-8.

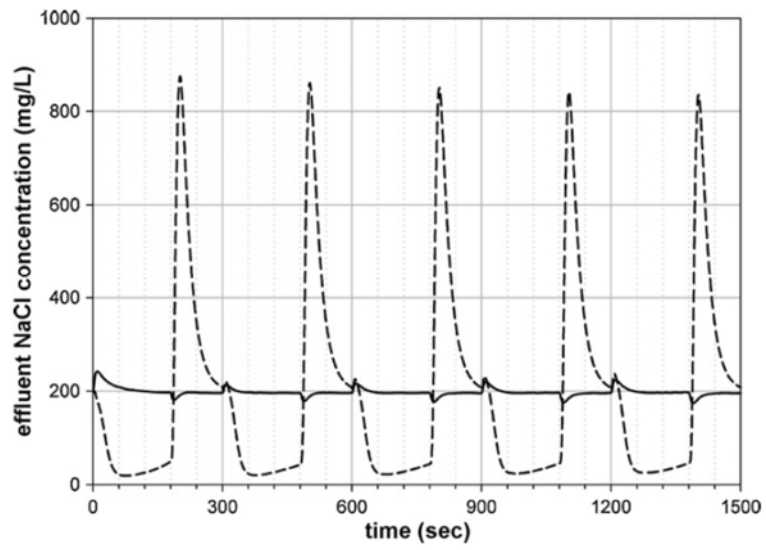
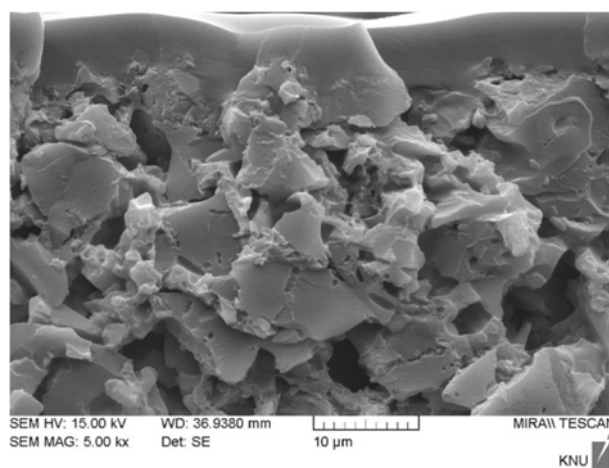
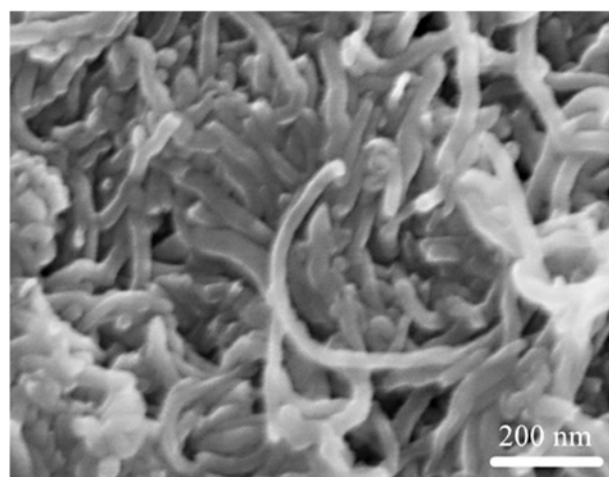


Figure 2-7. The concentration transient of effluent: solid line; MCDI, dashed line; CDI (Kim and Choi 2010b).



(a)



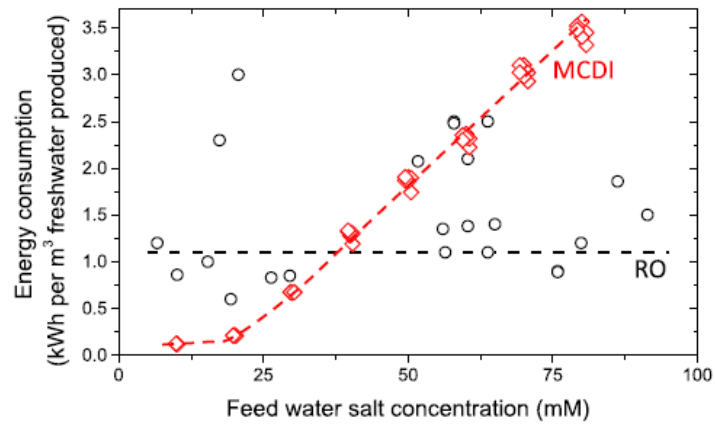
(b)

Figure 2-8. The SEM images of carbon electrode (a) coated with ion-exchange resin (Kim and Choi 2010a) and (b) fabricated with ion-exchange resin as a binder (Kim and Choi 2010a; Liu et al. 2014).

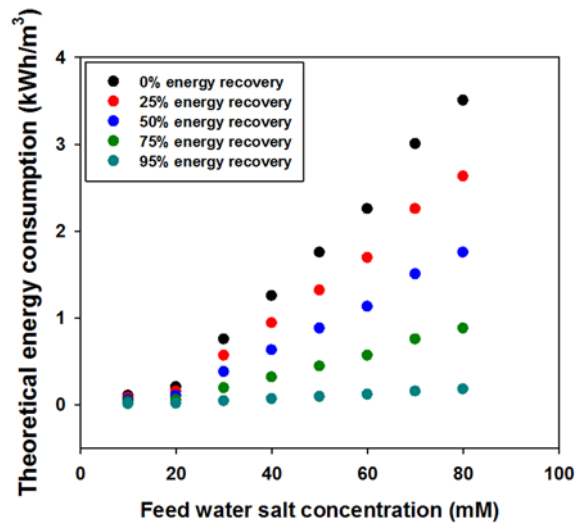
2.4. Energy recovery in CDI

Energy recovery in CDI is the energy-saving technique for storage or reuse of electrical energy generated by ion release from electrodes during the regeneration step. It was suggested based on similarity of the principle between CDI and capacitors. Due to the limitation of carbon electrode capacity, CDI is suitable desalination technology for low feed concentration such as brackish water. In other words, at high feed concentration, RO is superior process than CDI as shown in Figure 2-9a. The energy consumption of CDI is determined by cell voltage and charge capacity and is proportional to the concentration of feed water. To secure the competitiveness of CDI compared to the conventional process such as RO, the energy consumption of CDI should be below 1 kWh/m³ of energy consumption for RO aimed to seawater desalination and it is feasible on condition that 75% of consumed energy is recovered (Figure 2-9b) (Anderson et al. 2010; Shannon et al. 2008). If the brackish water would be targeted, it is expected that the efficiency and competitiveness of CDI is superior to RO process. Lately, the prediction of energy recovery ratio using CC operation was reported by Długolecki and van der Wal (Długolecki and van der Wal 2013) and conceptual energy recovery system using converter (electric device for power conversion) was proposed by Alkuran et al. and Pernia et al. (Alkuran et al. 2008; Pernia et al. 2012). The methodologies for energy recovery is classified into two categories; storage of recovered energy into supercapacitor and energy transfer

from primary CDI module to secondary CDI module (Figure 2-10). The former, firstly suggested by Shiue et al., is conducted by connection between CDI cell and supercapacitor through DC/DC converter and enables recovered energy to be utilized for various purposes (Shiue et al. 2003). The latter is conducted by connection of two CDI modules using alternating charge-discharge in parallel CDI modules and enables direct utilization of recovered energy for charging process. Considering that energy recovery is necessarily required for large-scale CDI process, the energy recovery with alternating charge-discharge in parallel CDI is suitable method rather than storage of recovered energy into supercapacitor because the cost and stacking volume for supercapacitors to deal with large-scale energy is very high.



(a)



(b)

Figure 2-9. (a) Comparison for energy consumption between CDI and RO, (b) theoretical energy consumption with different energy recovery ratio.

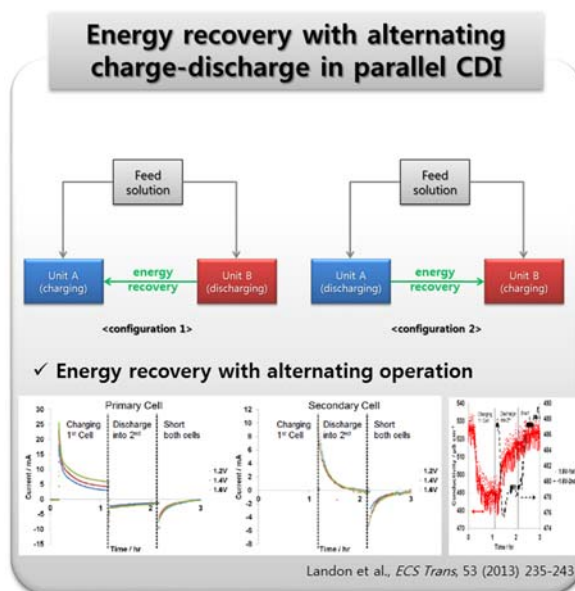
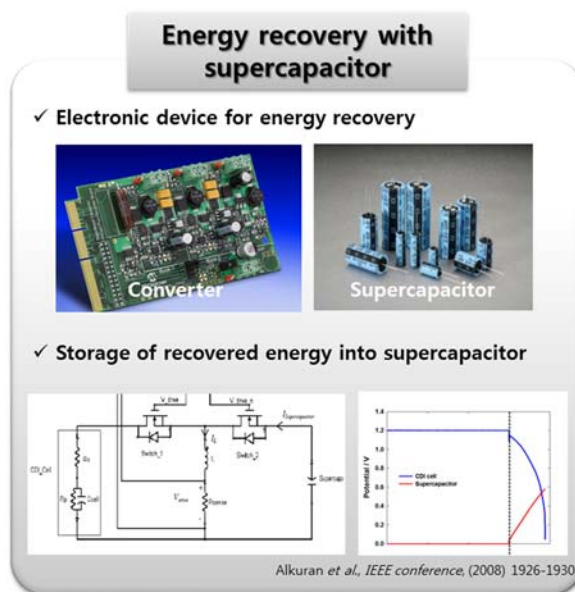


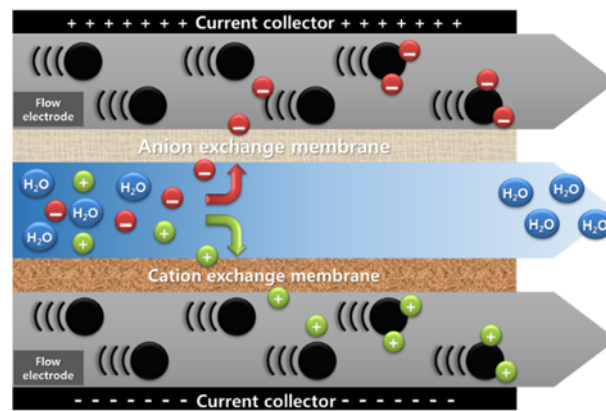
Figure 2-10. The methodologies for energy recovery in CDI process

2.5. State of the art CDI system

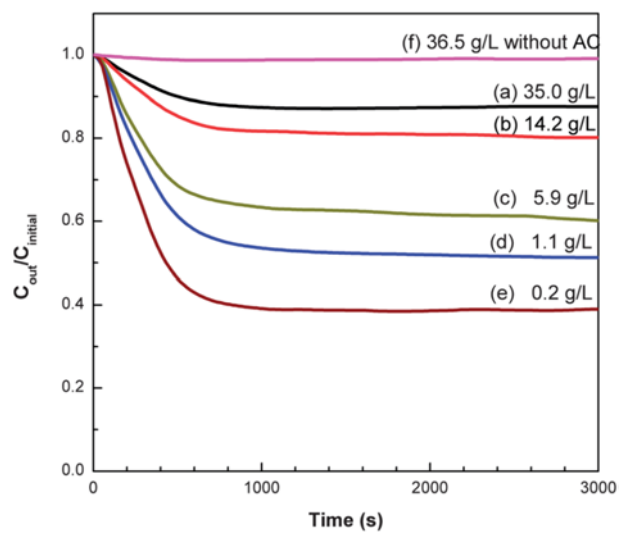
The enhancement of desalination performance and energy efficiency has been a perennial problem to many researchers in the CDI field. Numerous studies reporting the increasing performance and efficiency is established on modified electrode materials and operating system. In this chapter, some state of the art CDI system which innovatively enhance the performance and efficiency will be introduced; those are flow-CDI (FCDI), hybrid CDI (HCDI), inverted CDI (i-CDI).

Flow-CDI (FCDI), firstly reported by Kim et al. in Korea Institute of Energy Research, is advanced CDI process using slurry electrodes which are forms of activated carbon particles dispersed in electrolyte as shown in Figure 2-11 (HeeáCho et al. 2013). Compared to conventional immobilized carbon sheet electrodes, this novel process can provide infinite desalination capacity because flowable carbon particles holding salts are continuously replaced by new ones. Therefore, it is the most powerful advantage of FCDI that FCDI is applicable to desalination process for high-concentration saline water such as seawater desalination which conventional CDI cannot be applied. In addition, in case of treating positive flow electrodes (which adsorb anions) and negative electrodes (which adsorb cations) in same reservoir, it enables continuous production of desalinated water because electrodes are automatically regenerated by electro-neutrality. This means that a separated regeneration step is not required in FCDI

(Jeon et al. 2014).



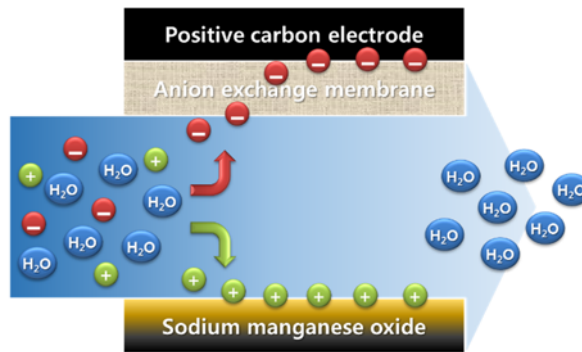
(a)



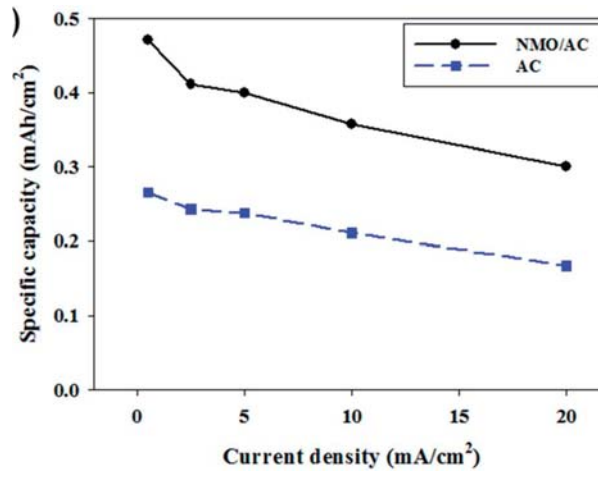
(b)

Figure 2-11. Flow-CDI (FCDI); (a) schematic and (b) variation in the NaCl concentration in the effluent stream (HeeáCho et al. 2013).

Hybrid-CDI (HCDI), firstly reported by Yoon et al. in Seoul National University, is desalination process with very high-capacity derived from sodium manganese oxide ($\text{Na}_4\text{Mn}_9\text{O}_{18}$)(Lee et al. 2014) as shown in Figure 2-12a. Sodium manganese oxide electrode, widely used as positive electrode materials, has very high-capacity compared to carbon electrode due to its faradaic intercalation of sodium ions. While general CDI process is operated with symmetrical system composed of two identical carbon electrodes, HCDI utilizes asymmetrical system composed of sodium manganese oxide and carbon electrode. This advanced system is beneficial to provide high desalination capacity more than two times that of general CDI (the most highest capacity numerous studies have ever been reported, see Figure 2-12b) (Suss et al. 2015), rapid desalination rate and high stability for long periods.



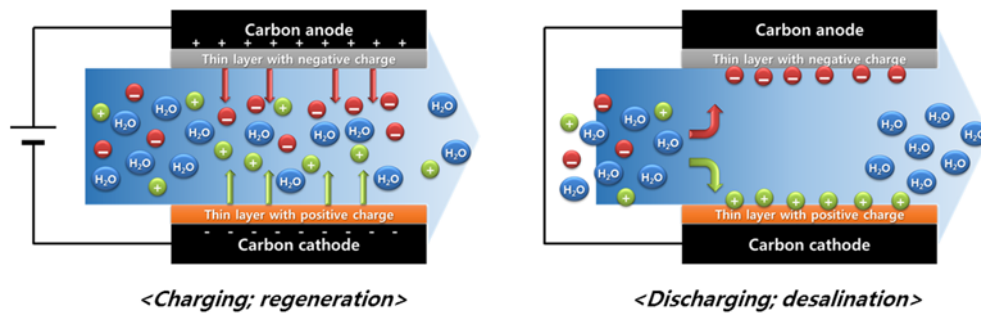
(a)



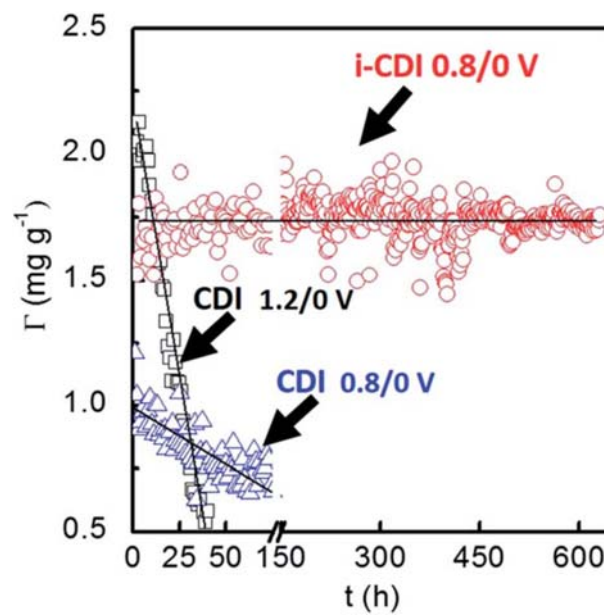
(b)

Figure 2-12. Hybrid CDI (HCDI); (a) schematic and (b) comparison of specific capacity (Lee et al. 2014).

Inverted CDI (i-CDI), firstly reported by James et al in Kentucky University, is highly stable desalination process for long-term operation using modified surface charge of electrodes. As shown in Figure 2-13a, the electrode regeneration by ion desorption is unusually conducted during the charging step and desalination is occurred during the discharging step, which resulted from the modified point of zero charge (PZC) in electrodes (Gao et al. 2014; Gao et al. 2015). The name “i-CDI” is originated by inversed sequences of desalination and regeneration in conventional CDI. Because the desalination (salts adsorption) is implemented during the discharging step without applying electrical energy, the energy efficiency is quite high and the carbon electrode oxidation, main cause of performance degradation in CDI, does not occur (Gao et al. 2014). It was reported that the performance degradation was not observed for long-term operation (600 hours) and this improved stability was superior to conventional CDI over 530% (Figure 2-13b).



(a)



(b)

Figure 2-13. Inverted CDI (i-CDI); (a) schematic and (b) enhanced stability by the i-CDI system (Gao et al. 2015).

3. Comparison of salt adsorption capacity and energy consumption between constant voltage and constant current operation in capacitive deionization

3.1. Introduction

Critical water shortages have come into the spotlight as a result of increasing water demands caused by worldwide industrialization and population growth (Jury and Vaux Jr 2007; Shannon et al. 2008). Many investigators have pursued technical solutions to address such shortages. A major strategic technical approach to water shortage is desalination because 98% of Earth's water resources are either salt or brackish (Anderson et al. 2010; Elimelech and Phillip 2011; Greenlee et al. 2009). Thus far, thermal distillation and membrane separation are the most common desalination processes. Although these processes can achieve high salt removal with excellent stability, they have several major disadvantages including high energy consumption, high maintenance costs, and equipment fouling problems. To overcome such problems, innovative desalination technologies are required.

Capacitive deionization (CDI) is an electrochemically controlled desalination technology which removes ions from salt water by electro-sorption via a two-

step, non-faradaic process occurring in the electrical double layer region. During the CDI process, ions in the feed water flowing through a spacer between the cathode and the anode are removed by electrostatic attraction, referred to as the charging (purification) step. Subsequently, when the applied electrical energy is stopped, the adsorbed ions are released from the electrodes, referred to as the discharging (regeneration) step. CDI is reported to have many environmental and energy consumption advantages over thermal distillation desalination and membrane separation desalination methods because CDI does not require chemical treatment to regenerate membranes nor high pressure for water recovery (Farmer et al. 1996; Gabelich et al. 2002; Li et al. 2010; Nadakatti et al. 2011; Xu et al. 2008)

Electrode properties and operating conditions are the two main factors affecting CDI performance. CDI-based desalination performance is widely reported to be affected by various physicochemical electrode properties such as materials, electrical conductivity, specific surface area, pore structure, and wettability (Farmer et al. 1996; Gabelich et al. 2002; Jung et al. 2007; Li et al. 2010; Lim et al. 2009; Nadakatti et al. 2011; Park et al. 2011; Porada et al. 2012; Wang et al. 2011; Welgemoed and Schutte 2005; Yoram 2008). In addition, CDI performance is also affected by operating conditions such as cell voltage, flow rate, concentration, and operational mode as reported in the previous studies (Porada et al. 2013b; Zhao et al. 2012; Zhao et al. 2013b). In particular, the type

of operational mode is important operating condition because it is directly related to electrical energy consumption or charge efficiency of CDI process. CDI operational modes generally consist of constant voltage (CV) and constant current (CC) modes. Compared to CC mode studies, reports on CV mode are more common in both the academic and commercial fields (Anderson et al. 2010; Welgemoed and Schutte 2005; Yoram 2008), presumably because there is difficulty in controlling voltage levels in CC mode. Several studies recently reported the operational technique and energy consumption of CC mode in membrane assisted CDI (MCDI) with emphasizing the strength of CC mode which can produce constant concentration in desalinated water, as shown in Figure 3-1 (Jande and Kim 2013; Porada et al. 2013b; van Limpt and van der Wal 2014; Zhao et al. 2012; Zhao et al. 2013a; Zhao et al. 2013b). However, no study was done on direct comparison of salt adsorption capacity and energy consumption between CV and CC mode in CDI. Therefore, this study intends to evaluate comparatively salt adsorption capacity and energy consumption in addition to charge efficiency of two operational modes (CV and CC mode) in CDI operation as identical electrical charge consumed or identical amount of ion removal are considered.

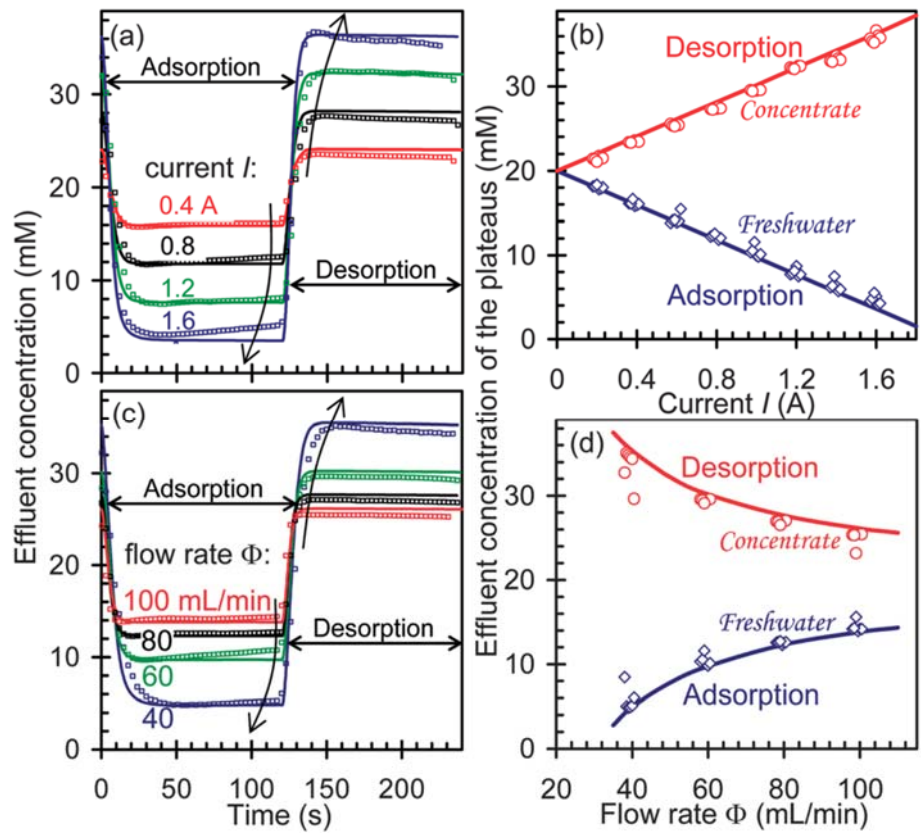


Figure 3-1. Control of the effluent concentration of freshwater and concentrate in MCDI-CC-RCD mode, using as control variable: (a) current, (c) water flow rate (Zhao et al. 2012).

3.2. Materials and Methods

Experimental deionization setup

Figure 3-2 shows a schematic of the flow mode CDI system employed in this study. The CDI unit cell comprised graphite current collectors, carbon sheet electrodes (thickness $\sim 300\ \mu\text{m}$, electrode weight $\sim 42.6\pm 2.1\ \text{mg}$), and a polymer spacer (nylon filter, thickness $\sim 180\ \mu\text{m}$). The carbon sheet electrodes were fabricated by compressing a mixture of 86 wt% activated carbon powder (MSP20, Kansai Coke and Chemicals, Amagasaki, Japan), 7 wt% carbon black (Super P, Timcal, Bodio, Switzerland), and 7 wt% polytetrafluoroethylene (PTFE, Sigma-Aldrich, St. Louis, MO, USA). The MSP20 carbon for electrode material was selected due to its high electrical conductivity and capacitance (Kim and Yoon 2013; Porada et al. 2013a). A feed solution of 10 mM NaCl was supplied to the CDI cell by using a peristaltic pump (Gilson, Middleton, WI, USA) at a flow rate of 10 mL/min. Electrical energy was applied to the CDI cell by using an automatic battery cycler (WBCS3000, WonaTech, Korea), which was also used to measure cell voltage and current. The CDI operation process comprises cyclic charging (purification) and discharging (regeneration) steps. During CV operation, 1.2 V (charging) and 0 V (discharging) were applied to the CDI module for 10 min each. A constant cell voltage of 1.2 V was used as an application of more than 1.2 V may cause undesirable reactions such as water splitting. In contrast, during CC charging period, various constant current

densities with a range of 1.5 to 3.5 mA/cm² (electrode area = 3.14 cm²) was applied to the CDI unit until cell voltage reached 1.2 V. During CC discharging step, the reversal current was applied until the cell voltage fell to zero. The conductivity of the effluent from the CDI unit cell was measured by using a conductivity meter (3573-10C, HORIBA, Kyoto, Japan). Conductivity measures were converted to actual concentration by using a calibration curve. Within that curve, a 10 mM NaCl solution corresponded to a 1.2 mS/cm solution conductivity. All experiments were conducted at 25°C and repeated three times for reproducibility.

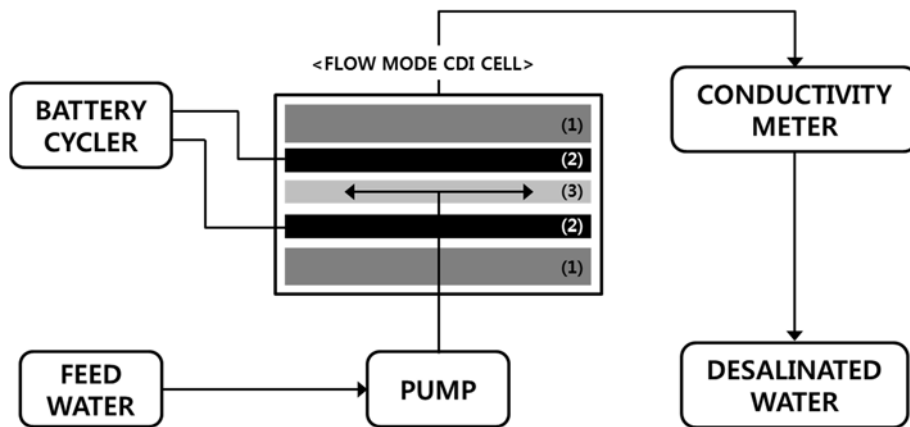


Figure 3-2. Schematic of flow mode capacitive deionization process used in this study. The capacitive deionization module comprised (1) current collectors (graphite), (2) electrodes (activated carbon sheet), and a (3) spacer (polymer).

Calculation of salt adsorption capacity, energy consumption, and charge efficiency

The salt adsorption capacity (mg/g) indicating the amount of salt removed was calculated by integrating salt concentration over time during the charging time, multiplying by flow rate and molecular weight of NaCl in the feed solution, and dividing by both electrode weight, that is:

$$\text{Salt adsorption capacity (mg/g)} = \frac{M_w \times \int (C_i - C_o) \Phi dt}{M_e} \quad (3-1)$$

where M_w is the molecular weight of NaCl (58.443 mg/mmol); C_i and C_o are the influent and effluent concentrations (mM), respectively, during charging; Φ is the flow rate (mL/min), and M_e is the total weight of both electrodes (g).

Energy consumption (kJ/mol) is presented as the ratio of the applied electrical energy to the removed amount of ions. The amount of applied electrical energy in CV (or CC) mode was obtained by integrating cell voltage (or current) over time during charging, and then multiplying by the current (or cell voltage) applied. Energy consumption is thus determined by:

$$\text{Energy consumption (kJ/mol)} = \frac{\int V_c I dt}{2 \times \int (C_i - C_o) \Phi dt} \quad (3-2)$$

, where V_c is cell voltage (V); I is current (A). The factor of 2 is applied to include both positive and negative ions in the salt solution.

Charge efficiency (faradaic efficiency) is the ratio of the removed amount of ions multiplied by Faraday's constant (F , C/mol) to the total charge transferred to the CDI cell, that is:

$$\text{Charge efficiency} = \frac{F \times \int (C_i - C_o) \Phi dt}{\int I dt} \quad (3-3)$$

Charging time (10 min) was established before the start of CV mode, but while in CC mode, charging time was dependent upon the duration required for cell voltage to increase to 1.2 V. Thus, results from the two operational modes with different charging time were adjusted to have the identical electrical charge consumed criterion needed to precisely compare the energy consumption and charge efficiency of the two operational modes. Additionally, analysis based on attaining identical amount of ion removal in the two operational modes was considered (Figure 3-3). For CV operation, 1.2 V was fixed to obtained large capacity with avoiding faradaic reaction such as water splitting. All experimental results are presented as if they were collected from third charging-discharging cycle which showed steady-state.

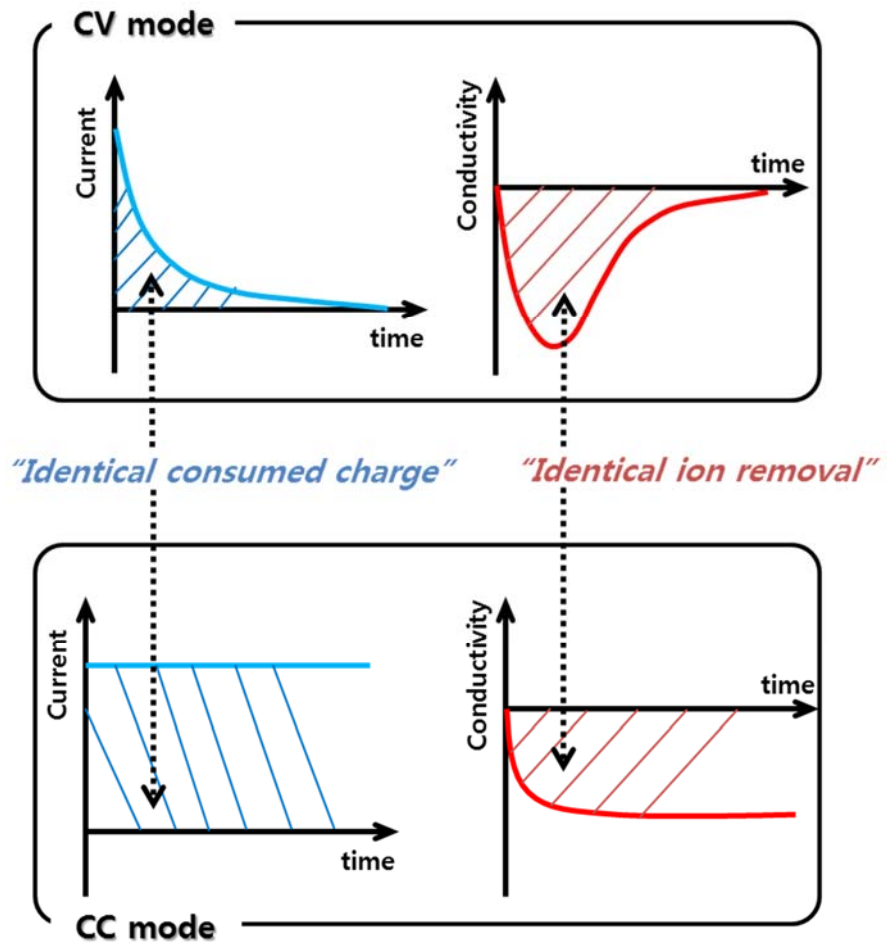


Figure 3-3. Two criteria for accurate comparison of CV and CC operation; identical consumed charge and ion removal during the desalination step.

3.3. Results and Discussion

Constant voltage and constant current modes in CDI operation

Figure 3-4 presents representative conductivity, current, and voltage results of CDI operation in CV and CC modes with 2.5 mA/cm^2 of current density. In CV mode, a constant voltage ($V_c = 1.2 \text{ V}$, Figure 3-4c) was applied for 600 s to the CDI unit. The associated conductivity and current profiles for one cycle are presented in Figure 3-4a and 3-4b, respectively. After application of a constant 1.2 V during 600 s of charging, the voltage was zero for 600 s of discharging (Figure 3-4c).

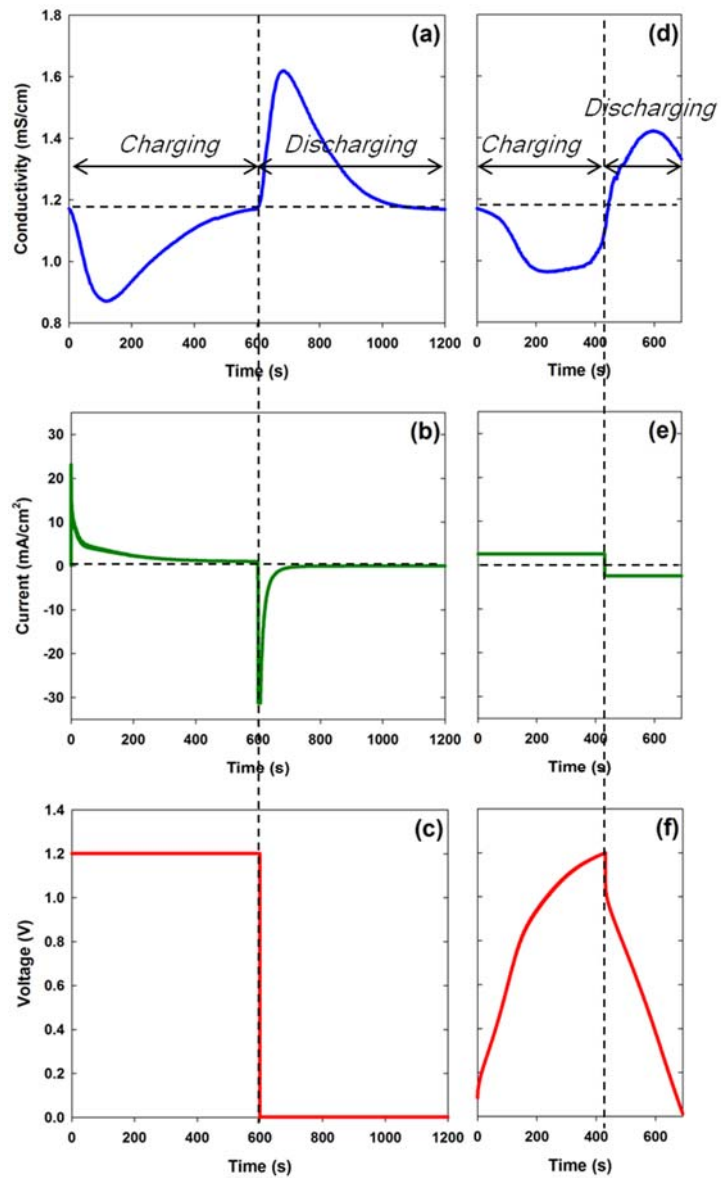


Figure 3-4. Comparison of constant voltage (CV) and constant current (CC) modes in capacitive deionization. Shown are conductivity (a), current (b), and cell voltage (c) graphs from CV mode. (cell voltage = 1.2 V, charging &

discharging time = 10 min respectively, flow rate = 10 mL/min) and conductivity (d), current (e), and cell voltage (f) from CC mode (current density = 2.5 mA/cm² for charging and -2.5 mA/cm² for discharging, flow rate = 10 mL/min).

During CV operation, as a result of ion adsorption to the electrode of the CDI cell, effluent conductivity rapidly decreased to a minimum (~ 0.9 mS/cm at ~ 150 s) from the initial conductivity (1.2 mS/cm; Figure 2a). Subsequently, effluent conductivity gradually increased to the initial conductivity as the ion adsorption capability of the electrode was gradually being exhausted during continuous ion adsorption. During discharging, a rapid increase in conductivity was observed, possibly as a result of the abrupt release of ions as they were desorbed from CDI cell's electrode. Afterwards, there was a gradual decrease in conductivity until the conductivity level of the influent solution was attained. The electrical current in charging step dramatically increased at initiation of charging and then gradually decreased to zero at the end of charging (Figure 3-4b). The current pattern during discharging was similar to that during charging step, but opposite in sign.

During CC mode, a constant current (2.5 mA/cm²) was applied until the CDI cell voltage reaches to 1.2V, whereas for discharging, a reversal current (-2.5 mA/cm²) was applied until the CDI cell voltage reaches to zero (Figure 3-4e). Corresponding conductivity and voltage profiles are displayed in Figure 3-4d & f, respectively. In CC mode, cell voltage gradually increased to the prescribed upper voltage limit (1.2 V) from zero during charging and then decreased to zero during discharging (Figure 3-4f). Note that an instantaneous rise in cell voltage from zero to 0.2 V occurred at the initiation of charging. Similarly, a 0.2 V drop

(1.2 V to 1.0 V) occurred at the beginning of discharging. This 0.2 V change is the result of an ohmic drop caused by the CDI cell's electrolyte resistance.

Two major differences were observed in the conductivity profiles (i.e., the ion removal profile) of CV and CC modes. First, in CV mode, the time to reach the minimum conductivity level was shorter than that in CC mode (~100 s for CV mode and ~200 s for CC mode). Second, in CC mode compared with CV mode, the low conductivity level in the desalinated stream was broadly maintained over a longer period (approximately 200 ~ 350 s). Those results indicate that CC mode may be advantageous as it can produce a more constant ion concentration in the desalinated stream (Zhao et al. 2012). These tendency of differences between CV and CC modes are identically observed in MCDI as shown in Figure 3-5

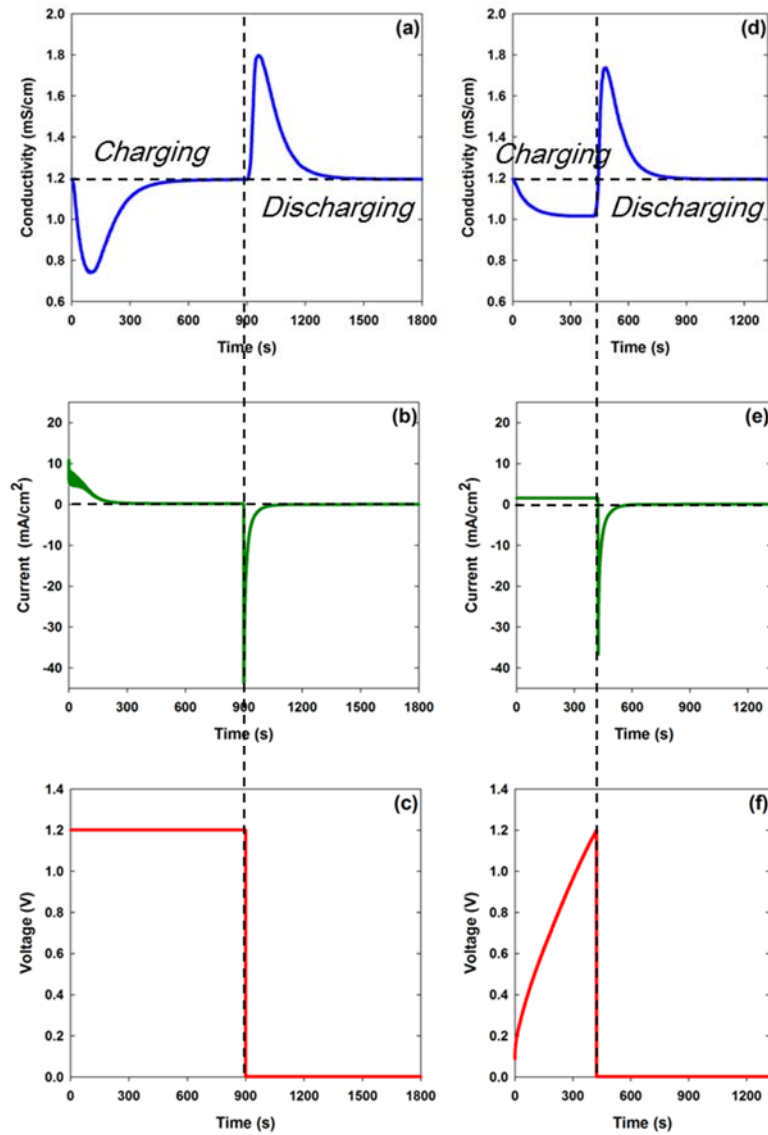


Figure 3-5. Comparison of constant voltage (CV) and constant current (CC) modes in membrane-assisted capacitive deionization. Shown are conductivity (a), current (b), and cell voltage (c) graphs from CV mode. (cell voltage = 1.2 V, charging & discharging time = 10 min respectively, flow rate = 10 mL/min) and

conductivity (d), current (e), and cell voltage (f) from CC mode (current density = 2.5 mA/cm² for charging and -2.5 mA/cm² for discharging, flow rate = 10 mL/min).

Salt adsorption capacity

Figure 3-6 presents the representative salt adsorption capacity from CV and CC modes with 2.5 mA/cm^2 of current density (Figure 3-4a & b, respectively). The salt adsorption capacity was derived by applying equation (1) to the effluent conductivity data obtained during the charging step. In CV mode (Figure 3-4a), the salt adsorption curve was convex and its primary differential value indicating the rate of change in salt adsorption capacity with time approached zero, which means the salt adsorption capacity without further increase. This behavior indicates that ion removal was fastest at the beginning of charging (after a short lag period) and then gradually slowed. In contrast, in CC mode (Figure 3-4b), there was a longer lag period than CV mode and the salt adsorption curve approached that of a straight line. The curves primary differential value remained steady, which indicates approximately constant ion removal rate during CC charging. Similar observations were made at the conditions of other current densities ($1.5 \text{ mA/cm}^2 \sim 3.5 \text{ mA/cm}^2$), refer to Figure 3-7. Figure 3-7 shows the salt adsorption capacity and salt adsorption rate of CV and CC modes with various constant current densities ($1.5 \sim 3.5 \text{ mA/cm}^2$). As shown in Figure 3-7, the salt adsorption capacity in CV and CC modes is fundamentally different. For example, during charging period, the salt adsorption capacity curve of CV mode is convex, while that of CC mode appeared to be linear after initial significant lag period. This difference is more vividly displayed by salt adsorption rate in

Figure 3-7b. In CV mode, the ion removal rate rapidly increased at the very beginning, and gradually decreased passing its maximum, and eventually became zero at the end of charging. On the other hand, in CC mode, that appeared to be steady for a considerable period of time after sluggish increasing at the beginning (1.5, 2.0, 2.5 mA/cm², Figure 3-7b). Note that the steady ion removals were not observed at the conditions of the higher current density (3.0, 3.5 mA/cm²). This is because the maximum allowable voltage (1.2V) was quickly reached before the region of steady ion removal rate.

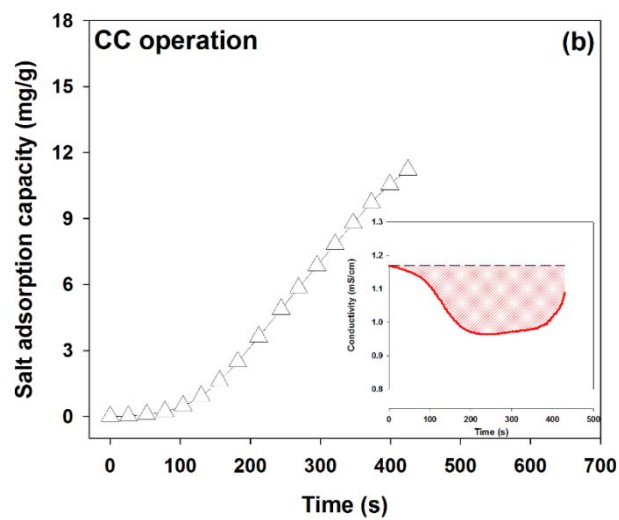
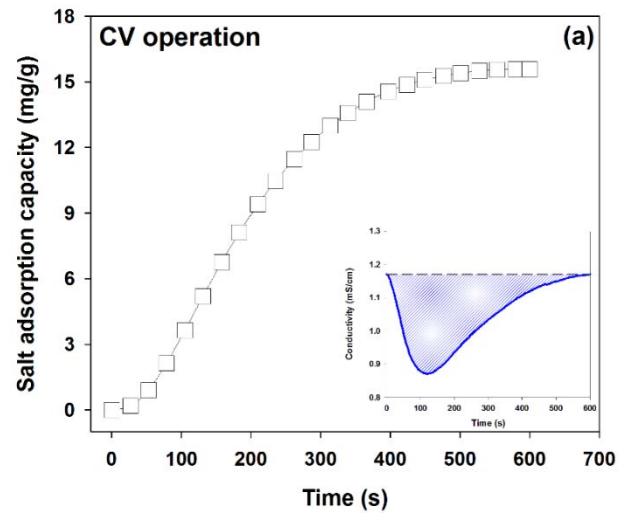


Figure 3-6. The representative salt adsorption capacity curve in (a) constant voltage (CV) and (b) constant current (CC) operation during charging step. The salt adsorption capacity from (a) constant voltage (CV) mode (cell voltage = 1.2 V, charging and discharging time = 10 min respectively, flow rate = 10 mL/min)

and (b) constant current (CC) mode (current density = 2.5 mA/cm^2 for charging and -2.5 mA/cm^2 for discharging, flow rate = 10 mL/min) during capacitive deionization. The inserted figure displays the effluent conductivity during charging time (from Figure 3-4a & d). The shaded areas in the inserts represent the salt adsorption capacity.

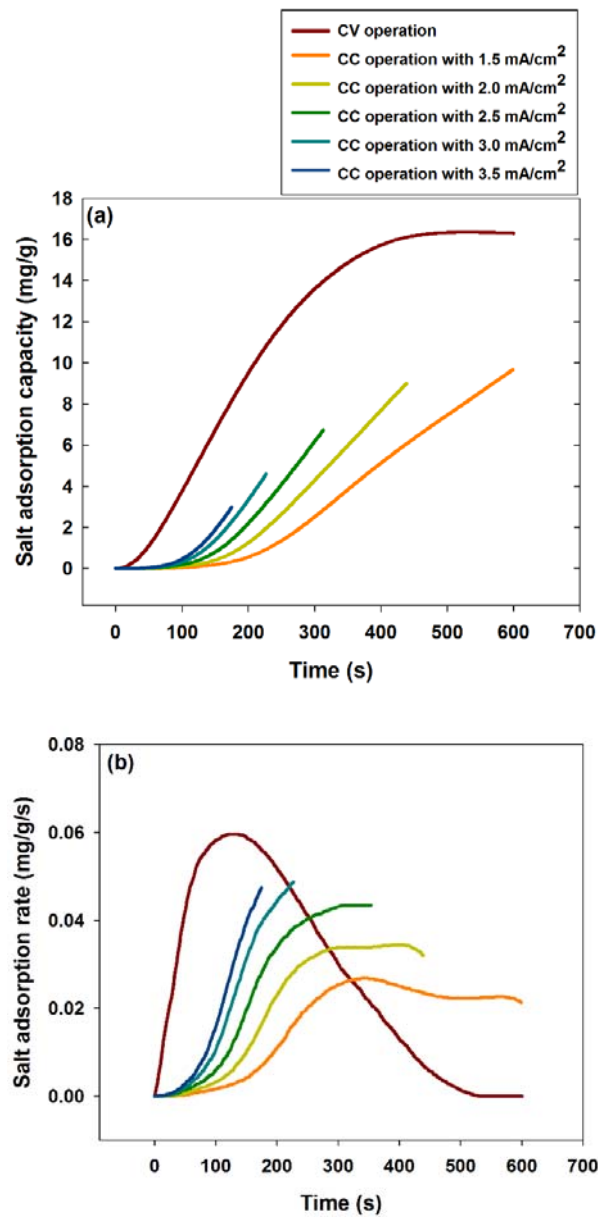


Figure 3-7. The salt adsorption capacity curve (a) and salt adsorption rate (b) of constant voltage (CV, 1.2V) and constant current (CC) operation with various constant current densities (1.5 ~ 3.5 mA/cm²).

The different ion adsorption characteristics in the two CDI operational modes are the result of differences in cell voltage between the two modes. For CV mode, large amounts of ions are rapidly adsorbed due to the strong initial electrostatic force ($V_c \sim 1.2$ V) applied at the beginning of the charging step. Subsequently, ion adsorption decreased gradually due to the gradual exhaustion of ion adsorption capacity of the electrodes. However, in CC mode, a fixed current level results in a gradual increase in cell voltage from zero to the limiting voltage (1.2 V; see Figure 3-4f). This constant current results in a linear increase in ion adsorption, following an initial lag time at the beginning of the charging step. The lag time in CC mode was induced by the low initial cell voltage. Application of voltage to the CDI electrodes simultaneously generates counter-ion adsorption and co-ion expulsion. The ratio of counter-ion adsorption to co-ion expulsion increases with an increase in cell voltage (Porada et al. 2013b). Therefore, the ion removal rate at the beginning of charging step in CC mode is slow because co-ion expulsion and counter-ion adsorption rates are equivalent, thus producing the initial lag time. With similar logic, the short lag time in CV mode is the result of high initial adsorption rate and a low initial expulsion rate.

Energy consumption and charge efficiency

Figure 3-8a shows the energy consumption and charge efficiency depending on charging current with typical CC operation. It was observed that with increasing charging current, energy consumption is increased and charge efficiency is decreased due to conduction loss. In addition, high charging current could not provide the sufficient charging time (Figure 3-8b) for desalination step and this caused the high energy consumption and low charge efficiency.

Figure 3-9 shows the energy consumption and charge efficiency in CV and CC modes under two comparison conditions: identical electrical charge consumed and identical amounts of ion removal. As shown in Figure 3-9, energy consumption in CC mode with various constant current densities was reduced by about 26 ~ 30% compared to CV mode at two criteria for comparison (Figure 3-8a & b). The lower energy consumption in CC mode is due to the lower overall cell voltage in CC mode than in CV mode, suggesting that CC mode is superior to CV mode in terms of energy consumption. In MCDI, this preferable energy consumption of CC mode was also observed as shown in Figure 3-10. On the other hand, the charge efficiencies of the two modes of operation were notably similar (Figure 3-9c & d). These charge efficiency are similar to those reported in the previous studies (Kim and Choi 2010b; Zhao et al. 2012). However, because our CDI process operated at a low voltage (<1.2 V) with no faradaic reaction, our charge efficiency is lower than expected. Current leakage due to

CDI cell design characteristics or to secondary reactions such as localized oxidation of the electrode surface (electrode degradation) and pH change, may have contributed to this lower than expected level of charge efficiency (Bouhadana et al. 2011). Compared to results of CDI, the charge efficiencies of MCDI as shown in Figure 3-10 was over 90% at high salt adsorption capacity and charge. This can be explained by the prevention of side effect in MCDI using ion exchange membrane.

Although the results indicate that CC mode is more energy-efficient than CV mode, CC mode is not absolutely favorable in all CDI processes because the CV operation can result in faster desalination than CC operation under a given operation time due to the use of a high cell voltage. That is., CV operation is advantageous in case of seeking for a high desalination rate (kinetic point of view). On the other hand, CC operation is more energy efficient than CV operation due to the use of low cell voltage. CC operation, in other words, is advantageous in case of seeking for low energy consumption (thermodynamic point of view). In these respect, we can achieve optimal salt adsorption capacity and energy consumption in a CDI facility by selecting or integrating appropriate CV and CC operations to meet the required CDI process.

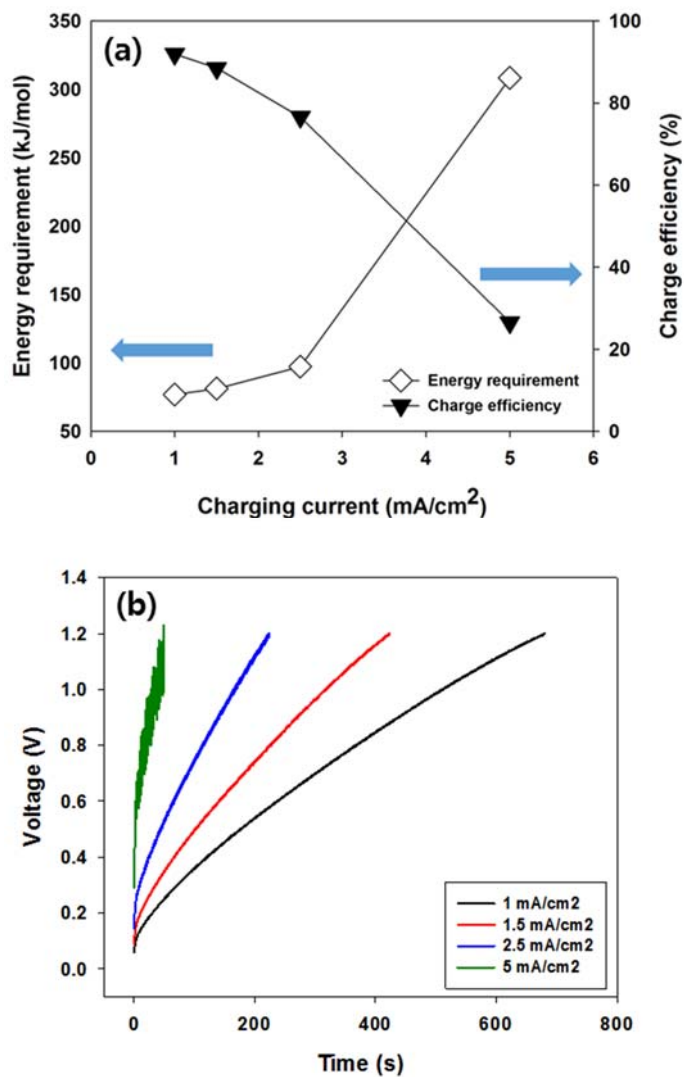


Figure 3-8. (a) Energy consumption and charge efficiency, (b) voltage profiles depending on charging currents (1, 1.5, 2.5, 5 mA/cm²) with CC operation in MCDI.

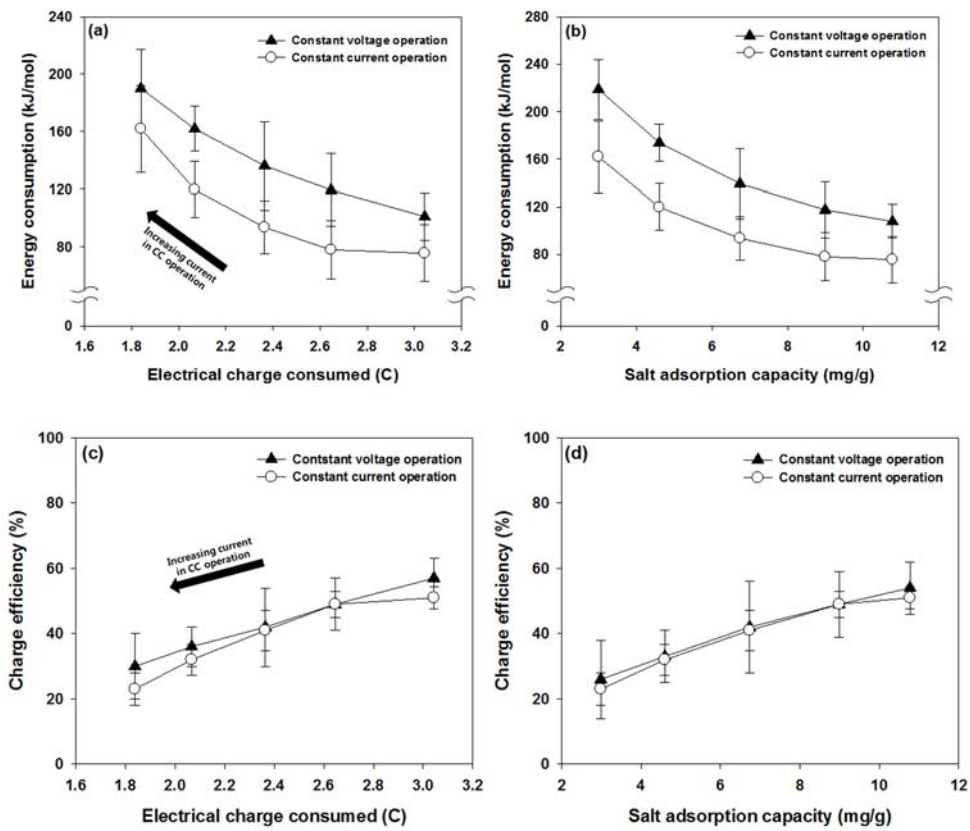


Figure 3-9. Comparison of energy consumption and charge efficiency in CDI constant voltage (CV) and constant current (CC) mode with various constant current densities (1.5, 2, 2.5, 3.0, 3.5 mA/cm²). Two criteria of identical electrical charge consumed (a and c) and identical amount of ion removal (b & d) were employed. The arrows indicate the increasing current in CC operation.

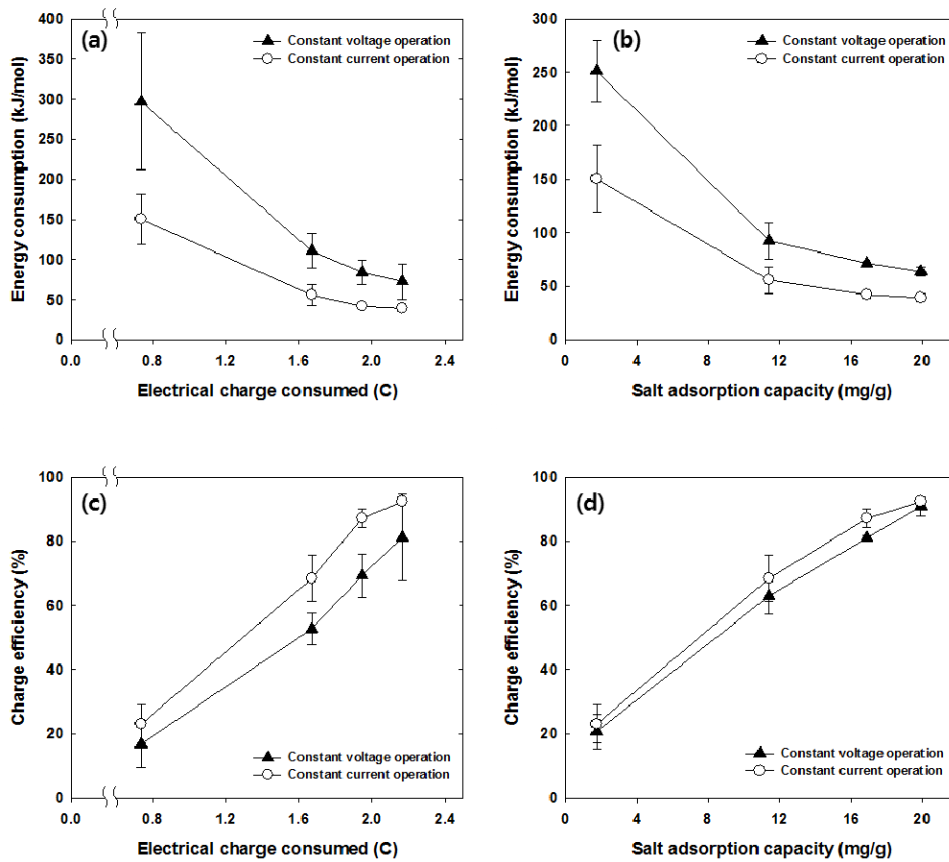


Figure 3-10. Comparison of energy consumption in MCDI constant voltage (CV) and constant current (CC) mode with various constant current densities (1, 1.5, 2.5, 5 mA/cm²). Two criteria of identical electrical charge consumed (a and c) and identical amount of ion removal (b & d) were employed. The arrows indicate the increasing current in CC operation.

Figure 3-11 shows desalination performance and energy consumptions of integrated CDI operation with CV and CC. To investigate integrated operation, desalination process was designed to operate with CC operation until cell voltage reached to 1.2 V, and followed by CV operation for 10 min. The concentration and voltage profiles (Figure 3-11a and 11b) reflected the characteristics of each operation (CC and CV) as discussed in Figure 3-5. In desalination performance (Figure 3-11c), the integrated operation with CV and CC showed similar salt adsorption capacity with single CV operation (~20 mg/g) and higher salt adsorption capacity than single CC operation (~12 mg/g). This suggests that integrated operation can compensate insufficient desalination capacity of single CC operation. Moreover, in Figure 3-11d, energy consumption of integrated operation was lower than single CV operation in spite of similar salt adsorption capacity, indicating good energy efficiency of integrated operation.

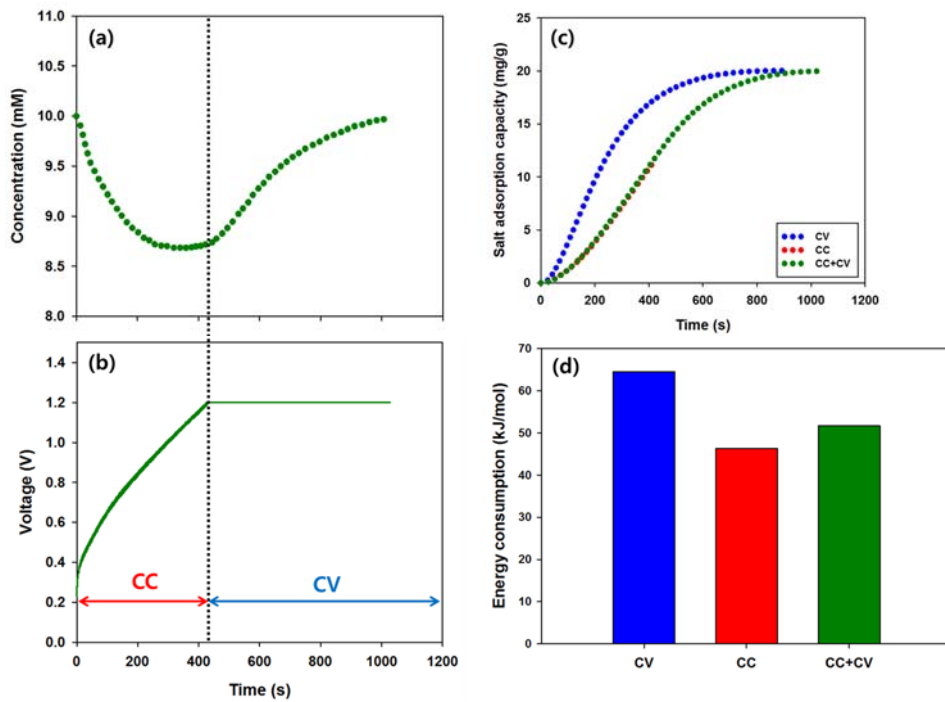


Figure 3-11. Integration of CV and CC operation. The (a) concentration, (b) voltage, (c) salt adsorption capacity profiles were obtained by integrated CDI operations with CC (1.5 mA/cm^2 to 1.2 V) and CV (1.2 V). The energy consumption (d) of integrated operation was compared to that of CV and CC operation, respectively.

3.4. Summary

The salt adsorption capacity and energy consumption in two operational modes (CV and CC) in a CDI desalination cell were compared on the bases of identical amount of ion removal and electrical charge consumed criteria. The higher overall cell voltage of CV mode results in faster salt adsorption under a given charging time than CC mode. Nevertheless, CC mode consumed approximately 26 ~ 30% less energy than that consumed in CV mode in both criteria, but there were similar charge efficiencies in CC and CV modes. Our results suggest that, in practice, optimal salt adsorption capacity and energy consumption in a CDI facility can be achieved by combining or selecting appropriate CV and CC modes.

4. Direct energy recovery system for capacitive deionization

4.1. Introduction

With greater water scarcity caused by worldwide industrialization and population growth, desalination has become a crucial strategy to address water scarcity; desalination involves the use of a water treatment technology that produces fresh water from sea or brackish water (Anderson et al. 2010; Elimelech and Phillip 2011; Greenlee et al. 2009; Jury and Vaux 2007; Shannon et al. 2008). Capacitive deionization (CDI) is the state-of-the-art desalination approach that is based on the use of the electrical double layer induced by a cell voltage difference between two electrodes (Farmer et al. 1997; Jia and Zou 2012; Oh et al. 2006; Ryoo and Seo 2003).

CDI has many advantages in terms of environmental aspects and energy efficiency because chemical treatment for regeneration is not required and a low electrical voltage is applied for the desalination process (Porada et al. 2013b; Suss et al. 2015; Welgemoed and Schutte 2005). Furthermore, the energy consumed during the desalination step can be partially recovered by ion release during the regeneration step due to the capacitive nature of CDI (Anderson et al. 2010; Demirer et al. 2013; García-Quismondo et al. 2013a; García-Quismondo

et al. 2013b; Zhao et al. 2013a). Recovered energy can be utilized to charge another CDI cell operating in a purification step or captured in an energy storage medium such as a supercapacitor for another use, which enhances the energy efficiency of CDI. Because the energy efficiency is an important parameter in today's desalination technology, the energy recovery in CDI is a substantial advantage versus other desalination technologies. In addition, the energy recovery system combined with CDI technology will facilitate its application to desalinate a high concentration brine such as seawater, which is not generally recommended because of the high energy consumption (Anderson et al. 2010).

Following the first study on the conceptual energy recovery in CDI reported in 2003 (Shiue et al. 2003), Długolecki and van der Wal estimated the potential of energy recovery in membrane-assisted CDI (MCDI) without the actual energy recovery by calculating the consumed and recoverable energy from the voltage profiles under constant current operation as shown in Figure 4-1 (Długolecki and van der Wal 2013). However, this approach has a limitation in that the energy from the charged MCDI cell was not actually recovered. Alternatively, Alkuran et al. and Pernía et al. introduced a buck-boost converter in the energy recovery system of the modeled CDI cell (composed of a resistor and a capacitor), and the extent of energy recovery was reported (Alkuran and Orabi 2008; Alkuran et al. 2008; Pernía et al. 2014; Pernía et al. 2012; Pernía et al. 2014). Figure 4-2 illustrates the proposed circuit of recovery system in CDI combined with a buck-

boost converter. A buck-boost converter is an electronic device used to control the energy transfer between the CDI cell and the supercapacitor. These studies had a limitation in that the modeled CDI cell cannot describe the actual desalination behavior of the CDI.

Therefore, this study intended to construct the direct energy recovery system in an actual MCDI cell with a buck-boost converter and to investigate the energy recovery ratio (recovered energy / consumed energy) under various operational conditions (Kang et al. 2014; Kim and Yoon 2013; Porada et al. 2013a; Zhao et al. 2012; Zhao et al. 2013b) (constant voltage (CV) charging with various voltages and times, constant current (CC) charging with various currents and concentrations of feed water, discharging with various reference currents of the buck-boost converter, and capacitances of the supercapacitor) to determine the influential parameters affecting energy recovery in the MCDI cell.

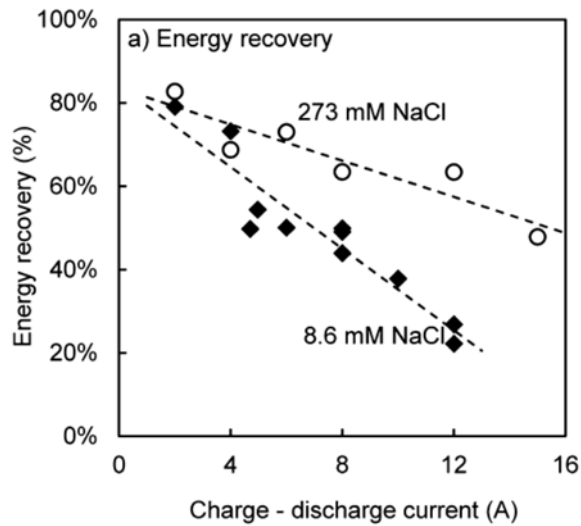
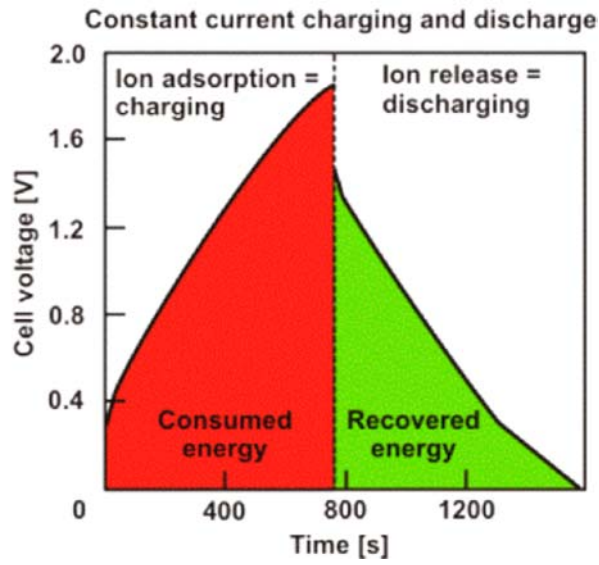


Figure 4-1. Prediction of energy recovery of CDI process using constant current charging and discharging. Energy recovery ratio can be calculated by the ratio of recovered energy during the discharging step to consumed energy during the charging step (Długolecki and van der Wal 2013).

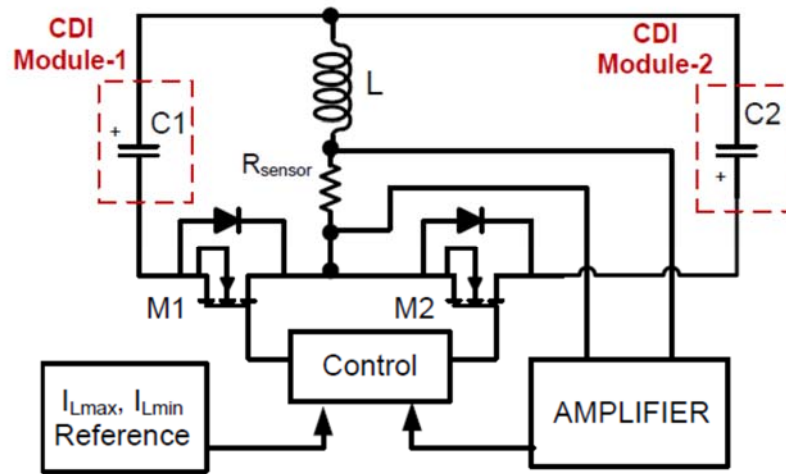


Figure 4-2. The schematic of proposed circuit of energy recovery system in CDI with a buck-boost converter (Pernia et al. 2014)

4.2. Materials and Methods

Electrode preparation

The carbon sheet electrodes for the CDI cell were fabricated from a mixture of activated carbon powder (MSP20, Kansai Coke and Chemicals, Amagasaki, Japan) (Kim and Yoon 2013; Porada et al. 2013a), carbon black (Super P, Timcal), and polytetrafluoroethylene (PTFE, Sigma-Aldrich, USA) with a weight ratio of 86:7:7. The mixture was kneaded with a few ml of ethanol for uniformity and then made into a sheet form using a roll press machine (electrode thickness of $\sim 300 \mu\text{m}$). The pressed mixture in sheet form was dried in a vacuum oven at $120 \text{ }^\circ\text{C}$ for 12 h and then cut for use for desalination and energy recovery processes after drying.

Construction of a real MCDI cell with a buck-boost converter

Figure 4-3 shows a schematic of the actual MCDI cell for energy recovery that is connected with a supercapacitor via a buck-boost converter. The MCDI cell is composed of a graphite current collector, anion- and cation-exchange membranes (Selemion, AGC ENGINEERING CO. LTD, Japan), carbon sheet electrodes (area $\sim 3 \text{ cm}^2$), and a polymer spacer (nylon sheet, thickness $\sim 200 \text{ }\mu\text{m}$). Note that the buck-boost converter is composed of an inductor and an electronic switch for controlling the energy transfer between the MCDI cell and the supercapacitor.

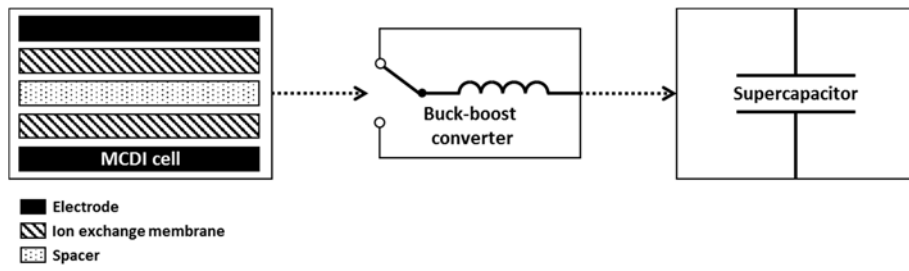


Figure 4-3. The schematic of an actual membrane capacitive deionization (MCDI) cell for energy recovery that is connected with a supercapacitor via a buck-boost converter. The MCDI cell is composed of electrodes, ion exchange membranes and a spacer. The electrical energy consumed during the desalination step is partially transferred to the supercapacitor.

MCDI operation with energy recovery is divided into the desalination (charging) step and the energy recovery (discharging) step. The desalination step in a real MCDI cell was performed in single-pass mode in this study (Porada et al. 2013b). A NaCl feed solution was supplied to the MCDI cell with a peristaltic pump at a flow rate of 2 mL/min. The conductivity of the effluent from the MCDI cell was measured using a flow-type conductivity meter (3573-10C, HORIBA, Japan) and then converted to the actual concentration. Two charging modes, CV and CC charging, were employed for desalination using a cycler (WBCS3000, WonaTech, Korea).

For CV charging, a constant voltage (0.3, 0.6, 0.9, and 1.2 V) was applied to the MCDI cell for the predetermined charging time (1, 3, 6, and 10 min) with a fixed concentration of NaCl (10 mM). For CC charging, constant current (1, 1.5, 2.5, and 4 mA/cm²) was applied until the cell voltage reached 1.2 V with several levels of NaCl concentration (5, 10, 50, and 100 mM). The voltage and current of the MCDI cell during the charging step were recorded by a cycler. Following the completion of charging, the discharging step was conducted to transfer energy from the MCDI cell to the supercapacitor using the buck-boost converter controlled by a digital signal processor (TMS320C28346, Texas Instrument, USA). Note that zero or reverse voltage are applied during the discharging step in a typical MCDI process without an energy recovery system.

Figure 4-4 shows the schematic for how the buck-boost converter is operated to deliver the energy stored in the CDI cell into the supercapacitor. The energy flow is dominated by the voltage difference between the input voltage (CDI cell) and the output voltage (supercapacitor). A buck-boost converter is required to construct an energy recovery system in the CDI process. Without a buck-boost converter, the energy transfer is terminated if the voltage is equal on both sides with remaining residual energy in the CDI cell. In addition, the energy transfer through the direct connection has the possibility to damage the cell by generating unexpected massive current flow. As shown in Figure 4-4a, the electrical current flows from the CDI cell to the inductor as the switch toward the CDI cell is closed (stage #1). Next, the CDI cell is discharged until the inductor current reaches the maximum value. As the switch toward the CDI cell is opened and the switch toward the supercapacitor is closed (stage #2), the current starts to charge the supercapacitor until the inductor current reaches zero. Figure 4-4b shows the specific current profiles of the CDI cell and the supercapacitor corresponding to stage #1 and stage #2. These numerous cyclic operations continue until the CDI cell is completely discharged. Please refer to a previous study for the details regarding the operation of the buck-boost converter (Pernía et al. 2012). The ratio of the duration of stage #1 over the entire duration in one cycle (stage #1 and stage #2) is presented as the converter duty (D), and the average current through the CDI cell is expressed as the reference current (I_{ref}), which is the operating parameter controlling the energy transfer rate during the discharging

step. The reference current and the capacitance of supercapacitor were adjusted over the values of 5, 25, 50, and 100 mA and 2.5, 5, 10, and 20 F, respectively.

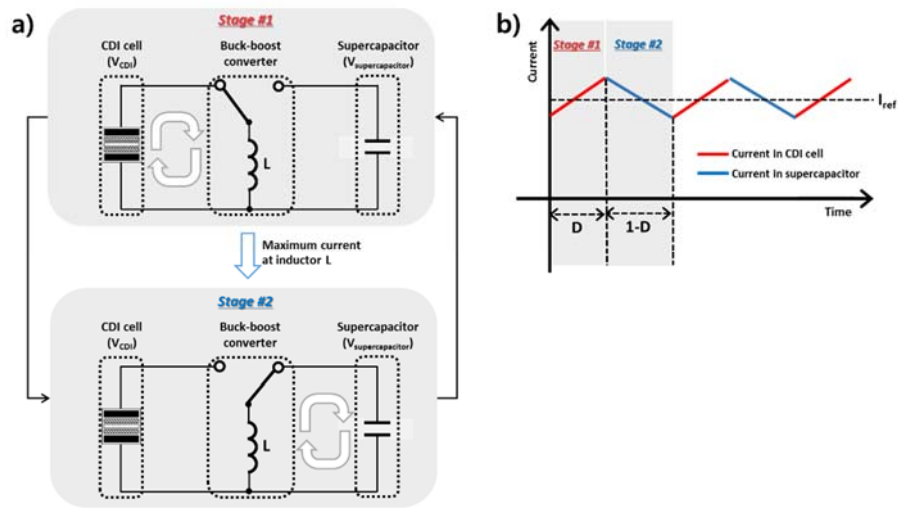


Figure 4-4. Schematic of the buck-boost converter operation during delivery of the energy stored in the CDI cell into the supercapacitor. The buck-boost converter is operated by a) an automatic switching depending on the current intensity at an inductor (L), and it generates b) specific current profiles in the CDI cell and the supercapacitor. The ratio of the duration of stage #1 over the whole duration in one cycle (stage #1 and stage #2) is presented as the converter duty (D), and the average current through the CDI cell is expressed as the reference current (I_{ref}).

Energy recovery ratio and salt adsorption capacity

The energy recovery ratio is defined as the amount of energy recovered in the supercapacitor during the discharging step divided by the consumed energy during the charging step. The consumed energy can be calculated by integrating the power of the MCDI cell over the charging time, and the recovered energy can be calculated as the square of the voltage increase of the supercapacitor multiplied by half of the capacitance, as expressed in Equation 4-1.

$$\text{Energy recovery ratio} = \frac{0.5 C_s \Delta V^2}{\int V_c I dt} \quad (4-1)$$

, where C_s is the capacitance of the supercapacitor (F); ΔV is the voltage increase (V) in the supercapacitor from 0 V; V_c is the cell voltage (V); I is the current (A). Figure 4-5 shows how the energy recovery ratio was obtained in this study.

In Equation 4-1, the current (I) in the denominator reflects the ion adsorption rate during the charging step, and the voltage increase in supercapacitor (ΔV) in the numerator reflects the amount of electrons delivered from the MCDI cell during the discharging step. This equation implies that the energy recovery ratio is closely related to the ion removal performance. Accordingly, the salt

adsorption capacity was investigated under various operational conditions affecting the energy recovery ratio. As expressed in Equation 4-2, the salt adsorption capacity (mg/g) was calculated by integrating the concentration difference over time, multiplied by the flow rate and molecular weight of NaCl over two electrode weights.

$$\text{Salt adsorption capacity (mg/g)} = \frac{M_w \int (C_i - C_o) \Phi dt}{M_e} \quad (4-2)$$

, where M_w is the molecular weight of NaCl (58.443 mg/mmol); C_i and C_o are the influent and effluent concentrations (mM), respectively, during charging; Φ is the flow rate (mL/min); and M_e is the total weight of both electrodes (g).

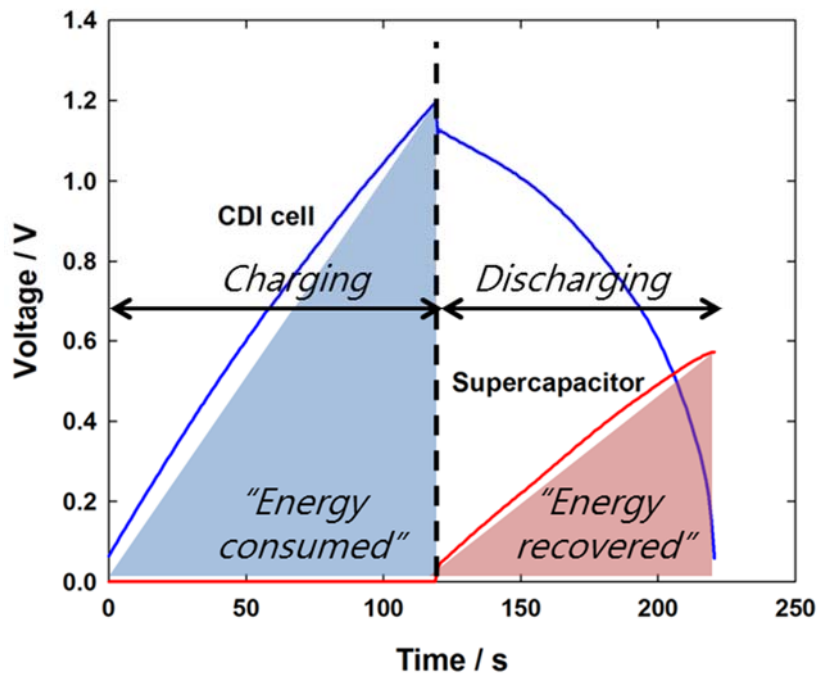


Figure 4-5. The calculation of energy recovery ratio. The energy recovery is obtained from the ratio of energy consumed for desalination (ion adsorption) to energy recovered (stored into the supercapacitor) by the buck-boost converter.

4.3. Results and Discussion

MCDI operation with energy recovery process

Figure 4-6 shows the representative voltage and conductivity profiles during the charging (desalination) and discharging (energy recovery) steps with two charging modes: CV (Figures 4-6a and b) and CC (Figures 4-6c and d) charging. Figure 3a shows the constant voltage (1.2 V) during the CV charging step, and its corresponding conductivity was rapidly decreased to a minimum and then gradually increased to the initial value (~ 1.2 mS/cm, Figure 4-6b), while Figure 4-6c shows the linear increase in voltage from zero to 1.2 V (a pre-set voltage) during the CC charging step, which is the capacitive characteristic of the MCDI cell (Zhao et al. 2012). The corresponding conductivity in CC charging was widely maintained with a constant value (Figure 4-6d). Note the instantaneous cell voltage increase of approximately 0.1 V at the beginning of charging, which indicates the ohmic resistance of the MCDI cell (Xu et al. 2007). This characteristic of conductivity according to charging modes is consistent with previous studies (Kang et al. 2014; Zhao et al. 2012).

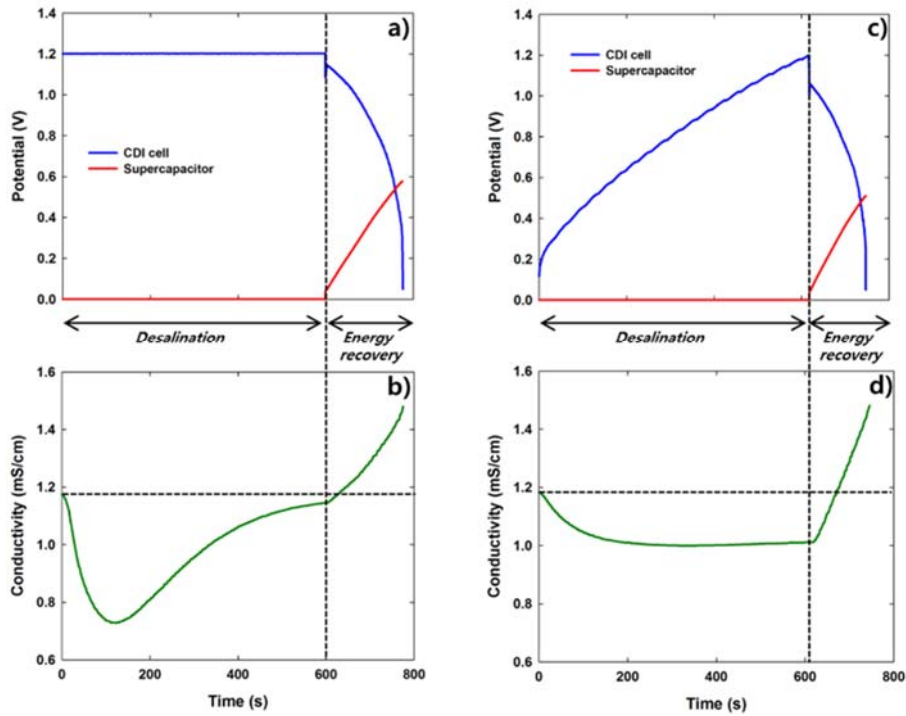


Figure 4-6. Representative voltage and conductivity profile in one cycle during MCDI operation with energy recovery. Shown are the potential (a) and conductivity (b) from constant voltage (CV) charging (1.2 V, 10 min, and 10 mM) and the potential (c) and conductivity (d) from constant current (CC) charging (1.5 mA/cm² and 10 mM). The energy recovery process was performed with a reference current of 5 mA of the buck-boost converter and capacitance of 5 F of the supercapacitor. The voltage profiles of the CDI cell and the supercapacitor are depicted as the blue solid line and red solid line, respectively.

During the discharging step, two important observations can be made in Figure 4-6. The first observation is that the voltage profile of the MCDI cell (expressed as V_{CDI} in Figure 4-4) decreases to zero (Figures 4-6a and c), regardless of CV or CC charging, indicating the energy release as a result of ion desorption from the electrodes. Simultaneously, the voltage increase in the supercapacitor (expressed as $V_{\text{supercapacitor}}$ in Figure 4-4) from zero indicates the actual energy transfer from the MCDI cell to the supercapacitor. The energy consumed during the charging step to desalt the feed water is released by ion desorption from the electrodes during the discharging step and is partially transferred into the supercapacitor via the buck-boost converter. The second observation is that the conductivity increases in an approximately linear manner during the discharging step (corresponding to the voltage decrease in the MCDI cell) as a result of desorption and release of ions from electrodes to the flow channel, as shown in Figures 4-6b and d. This linearly increasing conductivity profile during the discharging step is a distinctive phenomenon in the MCDI system with a buck-boost converter in contrast with that without a buck-boost converter (Zhao et al. 2012). This observation can be explained by the specific current profile with time applied to the MCDI cell, which is determined by multiplying the converter duty (D) by the reference current (I_{ref}) of the buck-boost converter. Figure 4-7 shows the actual current profile applied to the MCDI cell during the discharging step. In energy recovery process using buck-boost converter, actual current applied to the MCDI cell is determined by multiplying converter duty (D) with

reference current (I_{ref}) of the buck-boost converter, the relationship between input / output voltage (MCDI cell / supercapacitor voltage in this study) and converter duty is defined as follows:

$$\frac{V_{supercapacitor}}{V_{MCDI}} = \frac{D}{1 - D} \quad (4-3)$$

$$D = \frac{V_{supercapacitor}}{V_{supercapacitor} + V_{MCDI}} \quad (4-4)$$

, where V_{MCDI} is voltage in MCDI cell (V); $V_{supercapacitor}$ is voltage in supercapacitor (V); D is converter duty with dimensionless value varied from zero to unity. While buck-boost converter was operated by tuning the reference current, I_{ref} (A), actual current in the MCDI cell is applied with $I_{ref} \times D$ as shown in Figure 4-7. The linearly increasing current with time flows through the MCDI cell and causes a linearly increasing conductivity, which is characteristic of the MCDI system with a buck-boost converter.

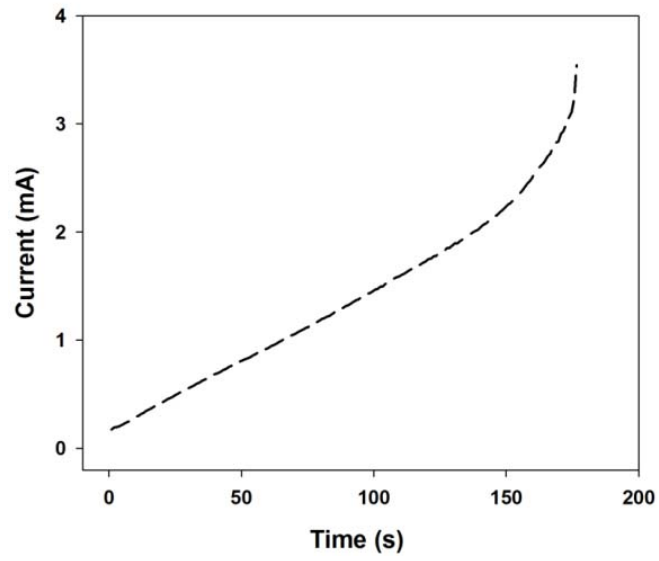
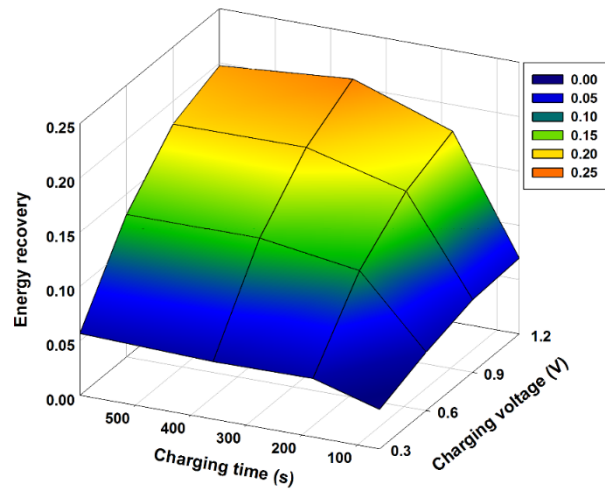


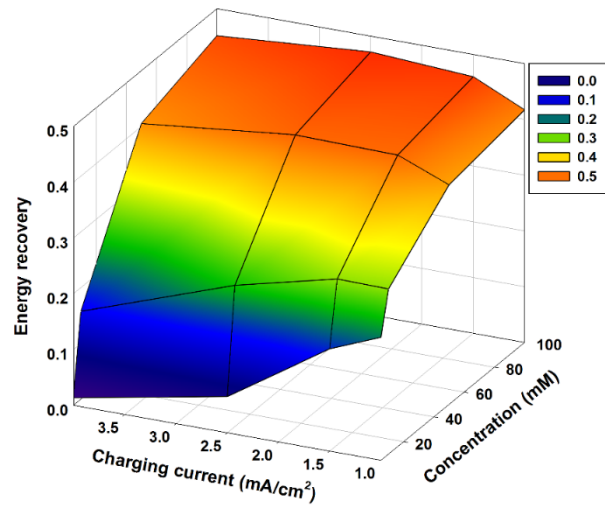
Figure 4-7. The actual current profile applied to the MCDI cell during the discharging step. The discharging current is obtained from the experimental data set of I_{ref} ($=5$ mA), V_{MCDI} , $V_{supercapcitor}$.

Energy recovery in MCDI with CV and CC charging

Figure 4-8 shows the energy recovery ratio (calculated by Equation 4-1) in MCDI operation as a function of the charging time and the voltage in CV mode (Figure 4-8a) and as a function of the charging current and the concentration in CC mode (Figure 4-8b). Note that a reference current of 5 mA of the buck-boost converter and a capacitance of 5 F of the supercapacitor were employed during the discharging step. As shown in Figure 4-8a, in CV charging mode, the higher energy recovery ratio was achieved with the longer charging time and higher voltage. The energy recovery ratio was approximately 0.2 at a charging voltage of 1.2 V and charging time of 10 min. The energy recovery ratio of 0.2 means that 20% out of the total energy consumed for desalting the feed water is recovered. The energy recovery ratio was approximately 0.036 (3.6%) at a charging voltage of 0.3 V and a charging time of 1 min. In CV charging mode, the change in the energy recovery ratio became more sensitive at the region of the longer charging time (0.06 ~ 0.20 of energy recovery ratio for 10 min vs. 0.06 ~ 0.07 of energy recovery ratio for 1 min with varying charging voltages) and the region of the higher charging voltages (0.07 ~ 0.20 of energy recovery ratio at 1.2 V vs. 0.04 ~ 0.06 of energy recovery ratio at 0.3 V with varying charging times).



(a)



(b)

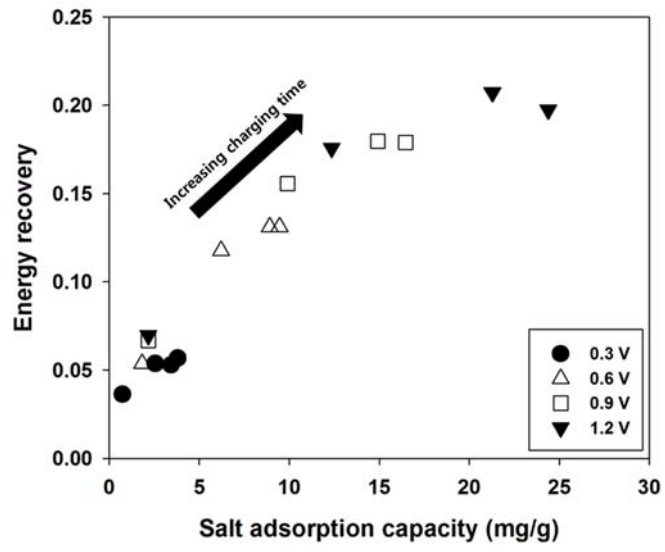
Figure 4-8. Three-dimensional representation of the energy recovery ratio in the MCDI with two charging modes. Constant voltage (CV) charging (a) was conducted with various charging voltages and times for a NaCl concentration of

10 mM. Similarly, constant current (CC) charging (b) was conducted with various charging currents and concentrations of feed water. The discharging step was performed with reference current of 5 mA of the buck-boost converter and capacitance of 5 F of the supercapacitor.

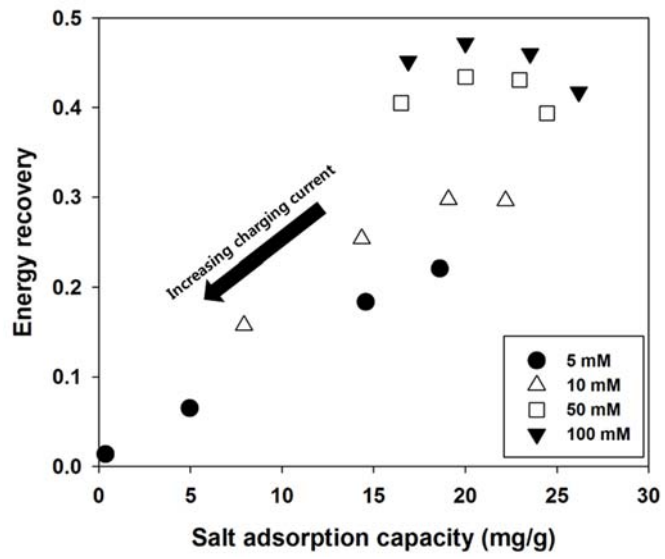
For CC charging, as shown in Figure 4-8b, the higher energy recovery ratio was achieved with the lower charging current and the higher concentration of the feed water. The change in the energy recovery ratio appears to be more sensitive to charging current at low concentration, (for the region of 1 ~ 4 mA/cm² of charging current, 0.01 ~ 0.22 of energy recovery ratio at 5 mM vs. 0.41 ~ 0.47 of energy recovery ratio at 100 mM), while it is similarly sensitive to the solution concentration at all conditions of charging currents.

Figure 4-9 shows the relationship between the energy recovery ratio and the salt adsorption capacity (calculated by Equation 4-2) at CV charging (a) and CC charging (b), with all of the experimental observations in this study considered. From Figure 4-9, two noticeable observations can be made. First, as shown in Figures 4-9a and b, a positive relationship can be found between the energy recovery ratio and the salt adsorption capacity, although it is not exactly linear. This observation indicates that the salt adsorption capacity can be one of the indicating parameters for evaluating the extent of the energy recovery ratio. This observation is further supported by the positive relationship between the salt adsorption capacity with charging time and charging voltage in CV mode and that between the salt adsorption capacity with the solution concentration and the reciprocal of charging current in CC mode (see Figure 4-10), which were similarly observed in the energy recovery ratio in Figure 4-8a and b. Figure 4-10S shows the salt adsorption capacity with CV and CC charging under various

operational condition. In CV charging, the salt adsorption capacity was increased with increasing charging time (Figure 4-10a) and increasing charging voltage (Figure 4-10b). In CC charging, the salt adsorption capacity was increased with decreasing charging current (Figure 4-10c) and increasing concentration of feed water (Figure 4-10d).



(a)



(b)

Figure 4-9. The relationship between the energy recovery ratio and the salt adsorption capacity in MCDI with two charging modes. Shown are the constant voltage (CV, 0.3 ~ 1.2 V at 10 mM) charging (a) and the constant current (CC, 1 ~ 4 mA/cm² at 5 ~ 100 mM) charging (b). The arrow indicates the direction of increasing charging time in CV mode and charging current in CC mode.

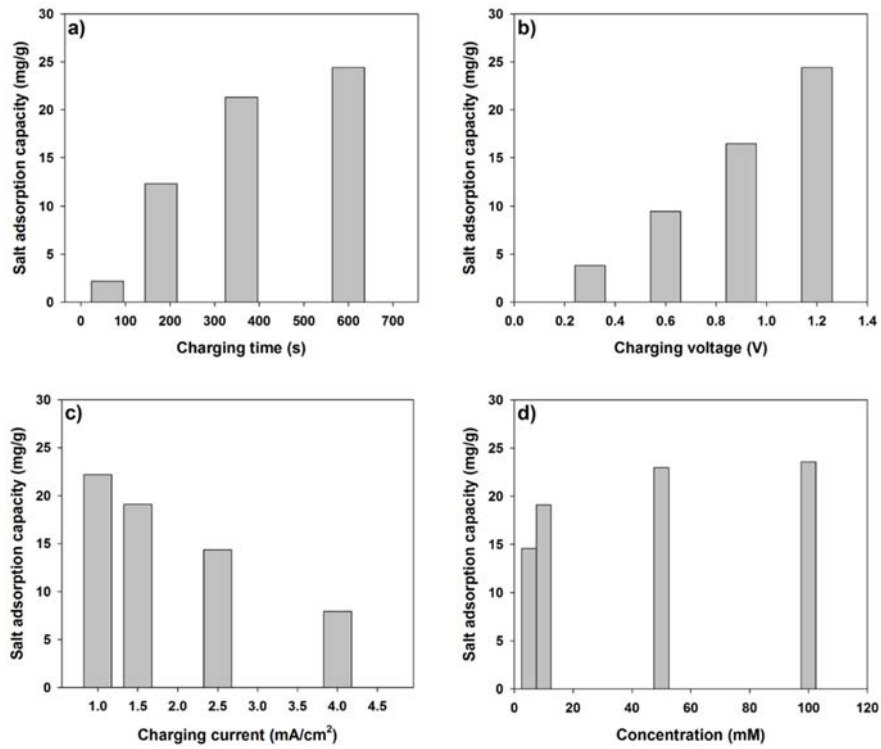
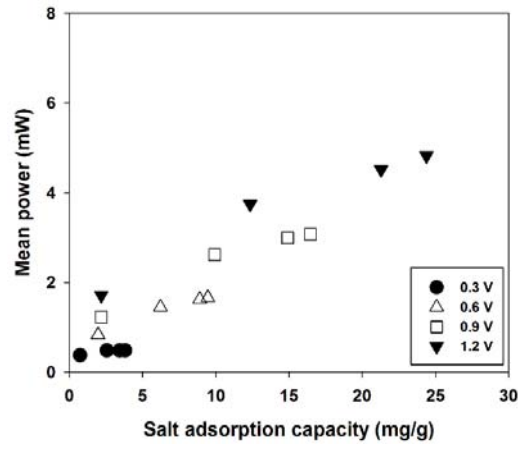


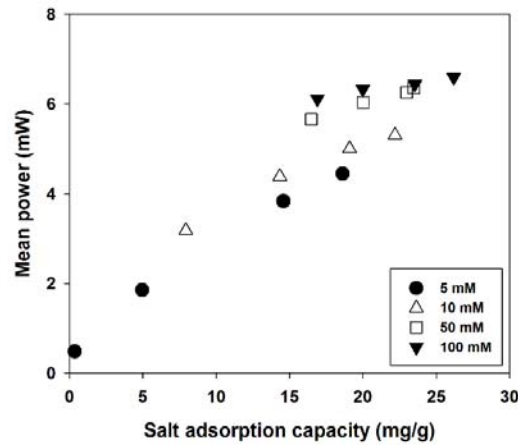
Figure 4-10. The salt adsorption capacity with CV charging as a function of a) charging time at 1.2 V and b) charging voltage for 10 min and with CC charging as a function of c) charging current at 10 mM and d) concentration of feed water at 1.5 mA/cm².

In this study, the energy recovery ratio is defined as the amount of energy recovered during the discharging step over the amount of energy consumed during the charging step (Equation 4-1). The salt adsorption capacity (indicating the ion removal performance during the charging step) is closely related to the amount of consumed energy because the ion removal performance is proportional to the amount of charge applied to the electrodes. This means that the amount of consumed energy is directly converted into the salt adsorption capacity under conditions of good charge efficiency. As a result, the positive relationship between the energy recovery ratio and the salt adsorption capacity indicates that the high salt adsorption capacity can also lead to an increase in the recovered energy under identical discharging conditions. In the mathematical expression of Equation 4-1, a larger increase in the numerator versus the increase in the denominator is required to realize the positive relationship between the energy recovery and the salt adsorption capacity, i.e., the state of a highly charged MCDI cell (which reflects the high salt adsorption capacity) is more favorable for energy transfer to the supercapacitor. This observation can be further explained by the power of the charged MCDI cell, which represents the energy transfer capability of the charged state as shown in Figure 4-11. The mean power of the charged MCDI cell can be obtained from the energy recovered in the supercapacitor divided by the discharging time. In Figure 4-11, a positive relationship was found between the mean power of the charged MCDI cell and the high salt adsorption capacity, providing an explanation for the

positive relationship between the energy recovery ratio and salt adsorption capacity.



(a)



(b)

Figure 4-11. The mean power of charged MCDI cell during the discharging step as a function of the salt adsorption capacity in case of a) CV charging and b) CC charging.

In Figure 4-9, in CC mode, it is interesting to observe that the sudden rise of the energy recovery ratio at high solution concentrations (50 ~ 100 mM) is off the linear relationship between the salt adsorption capacity and the energy recovery ratio. This phenomenon can be explained by solution resistance depicted in Figure 4-12 resulting from the concentration of feed water. The solution resistance was obtained from initial voltage increase divided by the charging current according to ohm's law ($V=iR$). In high concentration conditions exceeding 50 mM, the solution resistance was approximately $24 \Omega \cdot \text{cm}^2$, which is much less than $80 \Omega \cdot \text{cm}^2$ in low concentration conditions below 10 mM, thereby facilitating energy transfer from the charged MCDI cell to the supercapacitor.

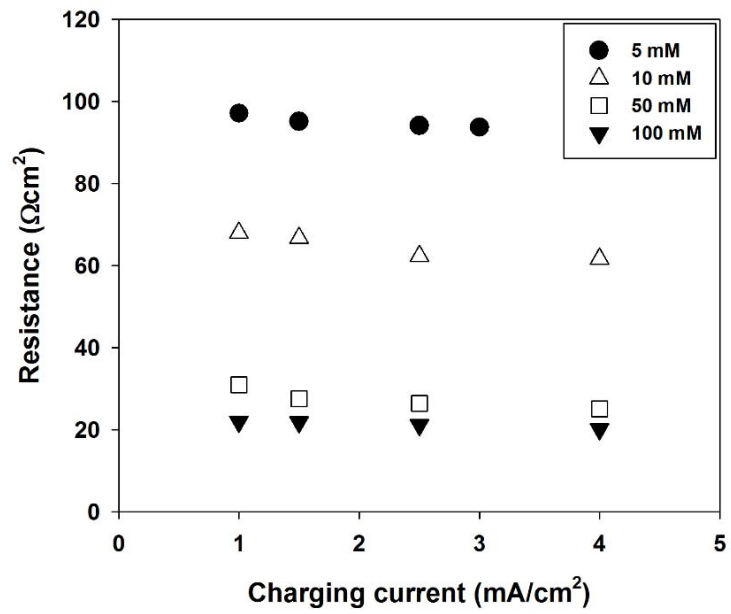


Figure 4-12. Solution resistance as a function of charging current with various concentration of feed water (5~100 mM).

In addition, the energy recovery in CC charging is much more favorable than CV charging. For example, the energy recovery at CC charging (Δ , Figure 4-9b) is approximately 0.3 at the solution concentration of 10 mM and salt adsorption capacity of approximately 20 mg/g, which is 50% higher compared to that at CV charging with 1.2 V at identical conditions (\blacktriangledown , Figure 4-9a); that is, the energy recovery ratio curve in CC charging was greater than that in CV charging with the salt adsorption capacity. This observation is consistent with the previous study that reported that CC charging consumed less energy to obtain the same salt adsorption capacity than CV charging due to the overall lower cell voltage (Kang et al. 2014). This lower energy consumption in CC charging indicates a high energy recovery ratio compared with CV charging for the same salt adsorption capacity.

Energy recovery with operational conditions in the buck-boost converter

Figure 4-13 shows the energy recovery ratio in the MCDI with the reference current of the buck-boost converter and the capacitance of the supercapacitor, i.e., the operational conditions of the buck-boost converter during the discharging step. Note that charging was made at the identical charging current (~ 1.5 mA/cm²) and concentration (~ 10 mM) to make the energy consumed during the charging step equal. As shown in Figure 4-13, a higher energy recovery ratio was achieved with a lower reference current and a higher capacitance of the supercapacitor. In addition, the energy recovery was more sensitively affected by the reference current rather than the capacitance of the supercapacitor. The effect of the reference current in the energy recovery ratio can be explained by the conduction loss, which indicates that the loss of electrical energy resulting from the current flow through the conductive materials is proportional to the square of the electric current (Mulligan et al. 2005). Accordingly, the lower reference current resulted in a higher energy recovery ratio due to lower conduction loss, indicating that a slow rate of energy transfer is favorable to attain a higher energy recovery ratio.

The capacitance of the supercapacitor did not appear to have a significant effect on the energy recovery ratio in comparison with the reference current, as shown in Figure 4-13. However, the capacitance of the supercapacitor plays an important role in determining the speed of energy recovery due to their voltage

rating (Alkuran et al. 2008). For example, with 5 mA of the reference current, the recovery time in the case of employing 2.5 F of the supercapacitor was 106 s, whereas that in the case of employing 20 F of the supercapacitor was 373 s. This result indicates that the low capacitance of the supercapacitor can contribute to faster energy recovery.

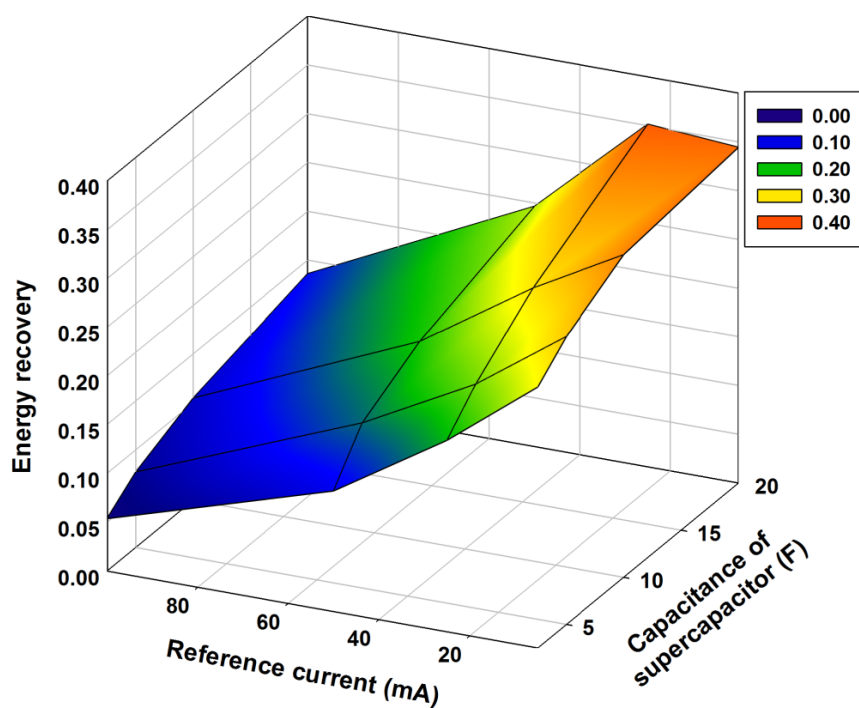


Figure 4-13. Three-dimensional representation of the energy recovery ratio with various reference currents of the buck-boost converter and capacitances of the supercapacitor. The charging step was performed with constant current operation at 1.5 mA/cm^2 and a NaCl concentration of 10 mM. The average salt adsorption capacity was 19 mg/g.

Energy loss during converter operation (energy recovery step)

Figure 4-14 shows the energy loss of converter during energy recovery step. To calculate the energy loss of converter, two energy storage medium (supercapacitor in this study) were connected through the converter and energy was transferred from supercapacitor#1 to supercapacitor#2 as shown in Figure 4-14a. The energy loss of converter was calculated from the ratio of energy released from supercapacitor#1 and energy stored into supercapacitor#2.

Figure 4-14a and 14b shows the energy loss of converter as a function of charging potentials and reference currents. It was observed that energy loss was increased with decreasing charging potentials and increasing reference current. The reference current is especially main factor to govern the energy loss of converter. The average energy loss was about 30 % as shown in Figure 4-14b and it was assumed that this energy loss resulted in low energy recovery ratio (20~30% in this study). In addition, energy loss in supercapacitor and leakage current of external circuit might be also reduce the energy recovery ratio. It is assumed that these energy loss in converter is mainly dominated by low-energy scale of CDI cell in this study. If the energy scale has increased, the efficiency of converter will approach over 99% and the energy recovery ratio will be increased as shown in Figure 4-15. In this respect, the optimization of converter is necessarily required to enhance energy recovery ratio.

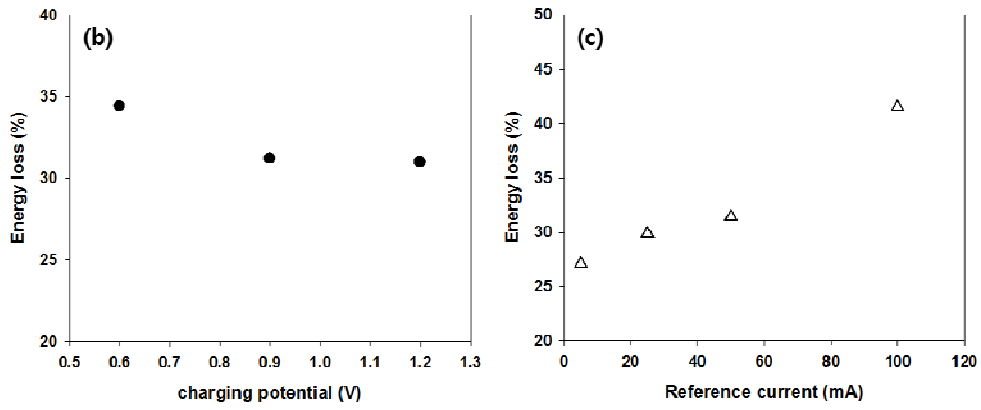
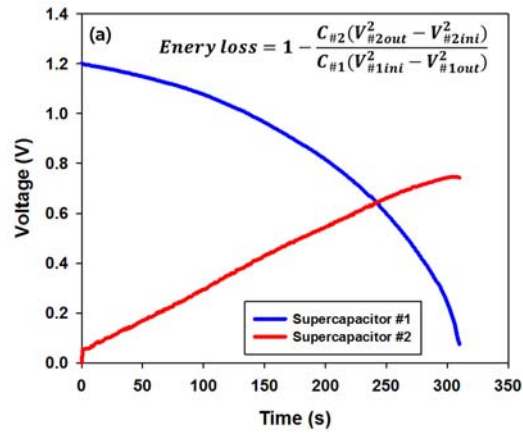


Figure 4-14. Calculation of energy loss during converter operation (energy recovery step). (a) voltage profiles of supercapacitor#1 (energy donor) and supercapacitor#2 (energy receptor), (b) energy loss of converter as a function of charging potentials and reference currents.

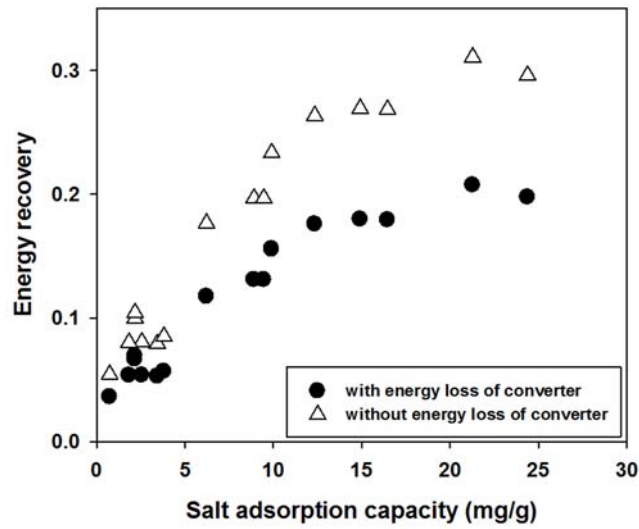


Figure 4-15. Comparison of energy recovery ratio with considering energy loss of converter (30% in this study) and without considering energy loss of converter. This data is based on the energy recovery ratio with CV charging depicted in Figure 4-9a.

4.4. Summary

This study reports the successful construction of an energy recovery system in an actual MCDI cell with a buck-boost converter; the buck-boost converter facilitated the delivery of the energy stored in the CDI cell into a supercapacitor. The energy recovery ratio was investigated under various operational conditions to determine the influential parameters affecting energy recovery in the MCDI cell. For charging conditions, the energy recovery was increased with the longer charging time and higher charging voltage in the case of CV mode and with the lower charging current and the higher concentration in the case of CC mode. From these results, the salt adsorption capacity was found to play an important role in the energy recovery and constant current charging was found to be more favourable for energy recovery than constant voltage charging. For discharging conditions with the buck-boost converter operation, the energy recovery was more sensitively affected by the reference current rather than the capacitance of the supercapacitor. The smaller reference current mainly resulted in a higher energy recovery ratio in contrast with the capacitance of the supercapacitor. In summary, to achieve the high energy recovery system, the development of an electrode with a high salt adsorption capacity and a cell design with low cell resistance will be required with a well-optimized buck-boost converter to facilitate a high energy recovery ratio.

5. Influential electrode properties on energy recovery performance in capacitive deionization

5.1. Introduction

With demands for efficient desalination technology against the industrialization and population growth (Jury and Vaux 2007; Shannon et al. 2008), many desalination technologies have been proposed to cope with this increasing requirements such as thermal distillation (Freshwater 1951), reverse osmosis (RO) (Greenlee et al. 2009), membrane distillation (MD) (Lawson and Lloyd 1997), electrodialysis (ED) (Strathmann 2010) and capacitive deionization (CDI) (Porada et al. 2013b). Among those, Capacitive deionization (CDI), an electrochemical desalination technology using electrical double layer on the electrode surface, has come into spotlight in terms of environment-friendly and low-energetic process (Anderson et al. 2010; Farmer et al. 1996; Welgemoed and Schutte 2005).

One of important strengths in CDI is an easily feasible energy recovery; partial energy consumed to operate the system can be recovered (Anderson et al. 2010). The principle of CDI is based on electrical double layer capacitor (EDLC), indicating that it is possible to harness some energy consumed for the desalination (where capacitor is charged) during the regeneration step (where

capacitor is discharged). The recovered energy can be either stored as electricity in electronic storage media (Alkuran and Orabi 2008; Alkuran et al. 2008; Pernía et al. 2014; Pernía et al. 2012) or directly utilized for the next purification step (Landon et al. 2013). The energy recovery technique enables the energy efficiency of CDI to be improved and the importance of energy recovery deserves attention in this regard.

In previous literature, Długolecki and van der Wal have reported energy recovery ratio under different currents and salt concentrations using constant current (CC) operation (Długolecki and van der Wal 2013). From the voltage profiles, the ratio of released energy during the discharging step to consumed energy during the charging step was defined as energy recovery ratio. This approach was also employed in other studies (Demirer et al. 2013; García-Quismondo et al. 2013a; Zhao et al. 2013a). However, so far, no study have been reported that provide the effect of electrode properties on energy recovery performance whereas the effect of operating conditions was exclusively reported. The approach to electrode properties on energy recovery performance must be inevitable because the carbon materials for CDI electrodes play an important role in desalination capacity and rate (Kim and Yoon 2013; Kim and Yoon 2015; Porada et al. 2013a; Suss et al. 2015; Yang et al. 2014)

Therefore, this study aimed to investigate the relationship between electrode properties and energy recovery performance by using various carbon materials

with different properties. To determine the effect on energy recovery performance, influential factors (electrode properties) were considered as capacity (salt adsorption capacity) and rate (salt adsorption rate).

5.2. Materials and Methods

Materials and electrode preparation

Six carbons were utilized as follows; MSP-20 (Kansai Coke and Chemicals) (Kang et al. 2012; Kim and Yoon 2013), P-60 (Kuraray), SX PLUS and S-51HF (Norit) (Kim and Yoon 2013), Metal-organic framework derived carbons, (MDC, Carbon Nanomaterials Design Laboratory in Seoul National University) (Yang et al. 2014), Carbon aerogel (CA, Enen). Among these carbons, MDC was fabricated by a template-free and solvent evaporation method during carbonizing a metal-organic framework while others were commercially purchased. Nitrogen adsorption/desorption measurement (at 77 K) was implemented using a Micromeritics ASAP2010 and specific surface area (SSA) was determined according to the Brunauer–Emmett–Teller (BET) equation. In addition, pore distributions were analyzed by Barrett-Joyner-Halenda (BJH) equation to investigate pore structure of various carbon powders.

The carbon sheet electrodes were fabricated from a mixture of activated carbon powder, carbon black (Super P, Timcal), and polytetrafluoroethylene (PTFE, Sigma-Aldrich, USA) with a weight ratio of 86:7:7. This mixture was kneaded with a few ml of ethanol for uniformity and then made into a sheet form using a roll press machine (electrode thickness of ~ 300 μm). The pressed dough in sheet form was dried in a vacuum oven at 120 °C for 12 h and then cut for use for

desalination and energy recovery processes after drying.

Electrochemical characterization

The electrochemical properties of carbon composite electrodes were investigated by using galvanostatic charge/discharge tests. An electrochemical cell was assembled with graphite current collectors (diameter~ 18 mm), cellulose nitrate filter (thickness~ 110 μm , Advanced Microdevices, India) as a spacer. Galvanostatic charge/discharge tests were implemented in a two-electrode system with 1 M of NaCl as an electrolyte using automatic battery cycler (WBCS3000, WonaTech, Korea). Voltage profiles were recorded with various current densities (0.5, 2.5, 5, 10, 20 mA/cm^2) in the potential range of 0.0 ~ 0.4 V. From voltage profiles, the specific capacitance was calculated as follows (Khomenko et al. 2005; Yang et al. 2014);

$$C = 2i\Delta t/m\Delta V \quad (5-1)$$

, where C is the specific capacitance (F/g); i is the current (A); Δt is the duration of charging step (s); ΔV is the potential difference (0.4 V in this study); m is the mass of an electrode (g).

To analyze the rate response characteristic of carbon materials, retention was obtained by the ratio of specific capacitance at current density of $x \text{ mA}/\text{cm}^2$ (C_x) to the specific capacitance at current density of $0.5 \text{ mA}/\text{cm}^2$ ($C_{0.5}$).

Deionization test and performance evaluation

For deionization test, The custom-made MCDI cell composed of a graphite current collector, anion- and cation-exchange membranes (Selemion, AGC ENGINEERING CO. LTD, Japan), carbon sheet electrodes (area $\sim 3 \text{ cm}^2$), and a polymer spacer (nylon sheet, thickness $\sim 200 \text{ }\mu\text{m}$) was utilized. The deionization test was performed under constant current operation (Kang et al. 2014; Zhao et al. 2012) with 10 mM of NaCl concentration and 2 ml/min of flow rate. The constant current density during the charging step was controlled by WBCS3000 and tuned in the range of $1 \sim 4 \text{ mA/cm}^2$ with cut-off voltage of 1.2 V. The discharging step was conducted by reverse current with opposite value to the charging step. The conductivity of effluents was measured by using a conductivity meter (3573-10C, HORIBA, Japan) and the measured conductivity were converted to actual concentration by a calibration curve. Within that curve, a 10 mM NaCl solution corresponded to a 1.2 mS/cm of solution conductivity.

The energy recovery performance using constant current charge and discharge was evaluated by the ratio of the amount of energy consumed during the charging step to the energy recovered during the discharging step as shown in Figure 5-1 (Długolecki and van der Wal 2013; García-Quismondo et al. 2013a; Zhao et al. 2013a). Note that energy recovery ratio in this chapter is different from that in chapter 4; the ratio of consumed energy during the charging step to the stored energy in the supercapacitor. The salt adsorption capacity and salt

adsorption rate was calculated to evaluate the desalination performance according to carbon materials. The salt adsorption capacity derived from the area below effluent conductivity during the charging step was calculated by the mass of removed NaCl divided by the mass of both electrodes (mg/g) (Kang et al. 2014; Kim and Yoon 2013). The average salt adsorption rate was calculated by dividing the salt adsorption capacity by the duration of charging step (mg/g/s) (Zhao et al. 2013b). In addition, the mean power was obtained by dividing the energy recovered during the discharging step by the duration of discharging step and the mass of electrodes (mW/g).

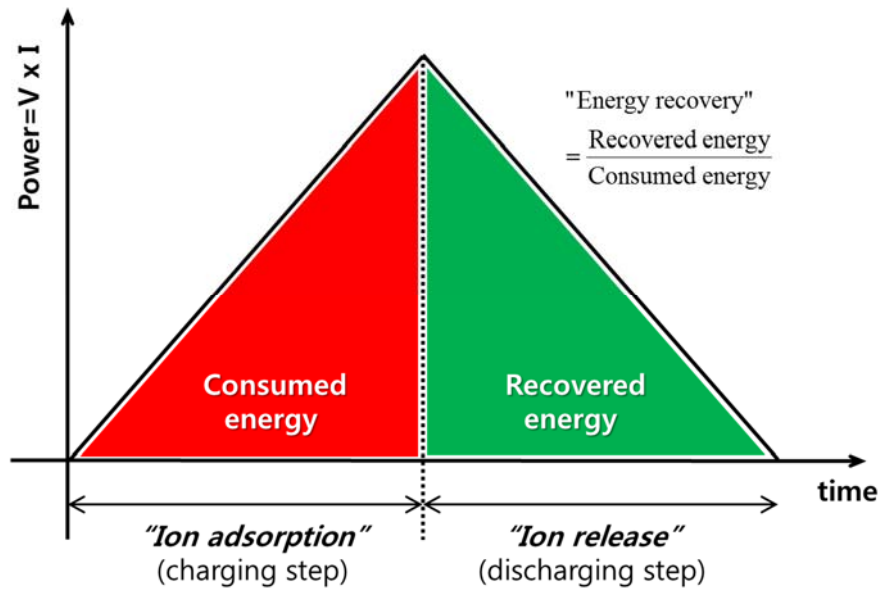


Figure 5-1. Definition of energy recovery ratio in CDI with constant current operation

5.3. Results and Discussion

Characterization of carbon composite electrode

The Physical properties of various carbon electrodes used in this study are presented in Table 5-1. The BET surface area ranged from 534 to 1578 m²/g, where MSP-20 and S-51HF respectively showed the lowest and highest area. The various BET surface area was closely connected with the development of micropore structures (< 2 nm) with considering that the micropore ratio in S-51HF was 0.65 and that of MSP-20 was 0.72. In table 5-1, one notable thing could be observed that MDC had quite high BET surface area (1537 m²/g) in spite of its low micropore ratio (0.31). To understand this trend, it is required to check the meso- (2 ~ 50 nm) and macropore (> 50 nm) distribution of carbon materials

Figure 5-2 shows the meso- and macropore distributions of carbon materials derived from BJH equation. Almost the whole pores of MSP-20 were developed with micro structure, which caused high BET surface area. However, in case of MDC, the pore sizes were distributed ranging from micro-, meso- and macro structures and small mesopores below 10 nm were especially developed. Although the micropore ratio was low, the development of low meso-structures lead to high BET surface area. This explanation could be confirmed by the pore distribution of CA. The relatively well-developed large meso- and macro-

structure resulted in low BET surface area as shown in table 5-1.

Table 5-1. Characterization of activated carbons

	MSP-20	P-60	SX PLUS	S-51HF	MDC	Aerogel
BET surface area (m ² /g)	1578	1062	673	434	1537	534
Micropore area (m ² /g) ^a	1133	740	434	132	479	118
Ratio ^b	0.72	0.70	0.65	0.30	0.31	0.22
Mesopore area (m ² /g) ^c	445	232	239	302	1058	416

^a calculated from *t*-plot analysis

^b Micropore area / BET surface area

^c BET surface area – micropore area

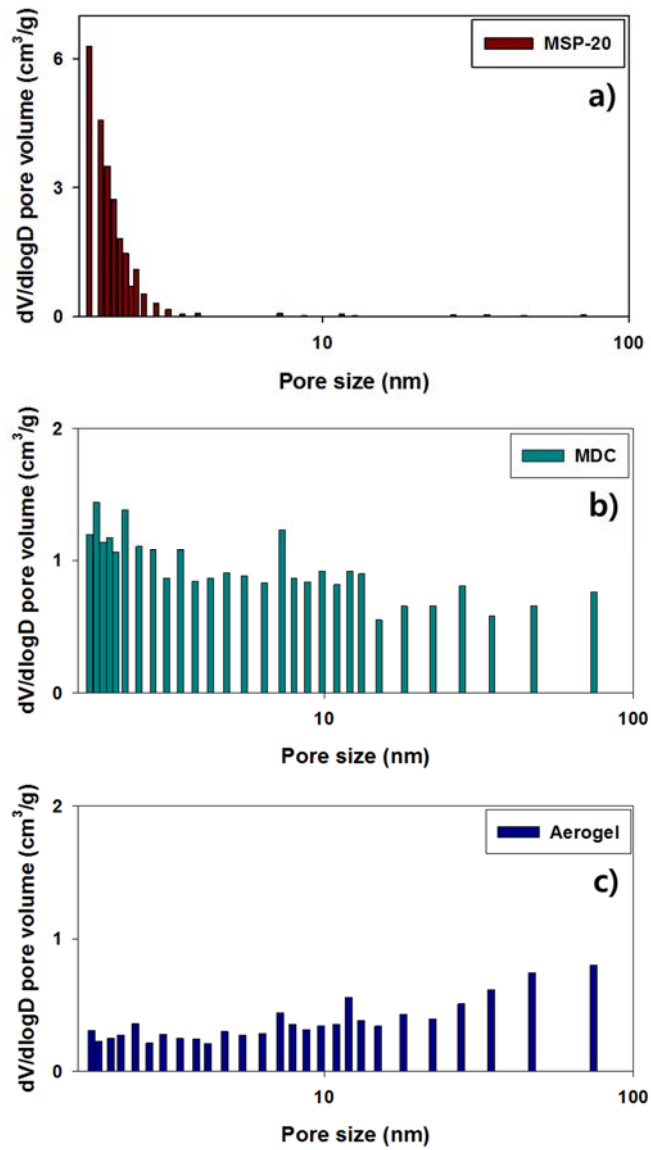


Figure 5-2. The meso- and macropore distributions of carbon materials derived from BJH equation; (a) MSP-20, (b) MDC, (c) CA.

Figure 5-3 ~ 5-8 respectively show the voltage profiles of MSP-20, P-60, SX PLUS, S-51HF, MDC, CA obtained from galvanostatic charge/discharge tests under different constant current densities. As shown in each voltage profile, typical capacitive behavior was observed at the lowest current density (0.5 mA/cm²) and the specific capacity was decreased with increasing current densities due to ohmic resistance (Bard and Faulkner 2001). This deformation of voltage profiles is related with the rate response characteristic of carbon materials, which means that the carbon material with fast rate response show little or no deformation of voltage profiles. Previous studies reported that rate response of carbon materials is influenced by their pore structure (Porada et al. 2013a; Yang et al. 2014). Considering the pore distributions in Figure 5-2, the rate responses were coincident with previous studies. For example, MDC and CA showed relative little deformation of voltage profiles because they mainly had not micropore but meso- and macropore compared to other materials with primary micropore structure.

In table 5-2, specific capacitances of carbon materials calculated from voltage profiles using equation 5-1 were presented. The specific capacitances were ranged from 120 to 38 F/g and the increase in specific capacitance corresponded to the increase of micropore shown in table 5-1. This is why the micropore is mainly available for ion adsorption site to motivate capacitance (Zhang and Zhao 2009). Figure 5-9 shows the retention obtained by the ratio of specific

capacitance at current density of $x \text{ mA/cm}^2$ (C_x) to the specific capacitance at current density of 0.5 mA/cm^2 ($C_{0.5}$). The retention of specific capacitance also indicates the rate response characteristic of materials like the deformation of voltage profiles in galvanostatic charge/discharge tests. As shown in Figure 5-9, MDC and aerogel had high retention of specific capacitance of 0.97 and 0.99, indicating that meso- and macropore structure is advantageous for excellent rate response. These results suggested that the ions in electrolyte could be rapidly transported into the pore structures of the electrode with the development of meso- and macropores (Yang et al. 2014).

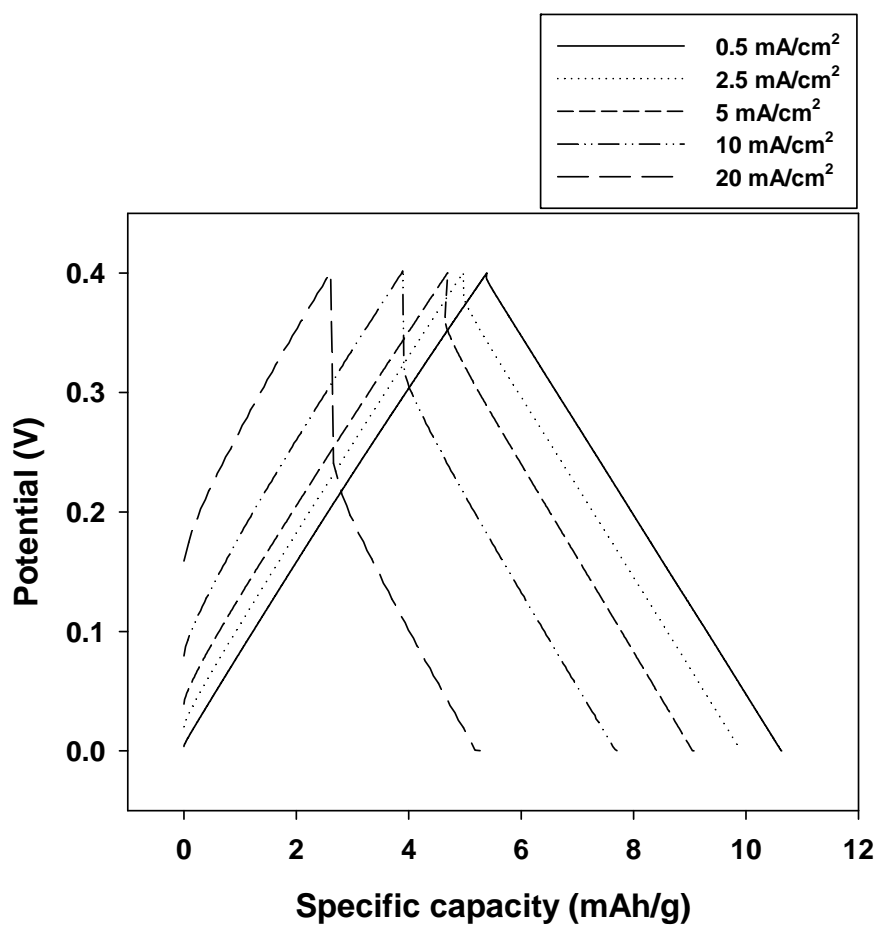


Figure 5-3. Galvanostatic charge/discharge voltage profiles of MSP-20

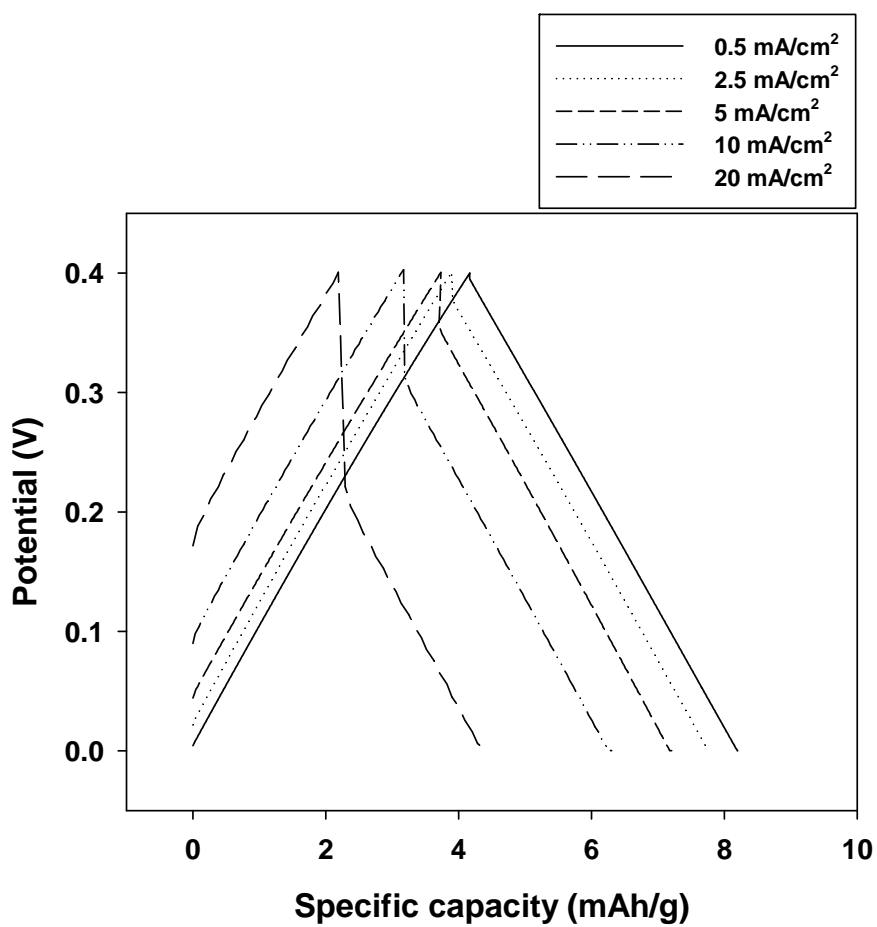


Figure 5-4. Galvanostatic charge/discharge voltage profiles of P-60

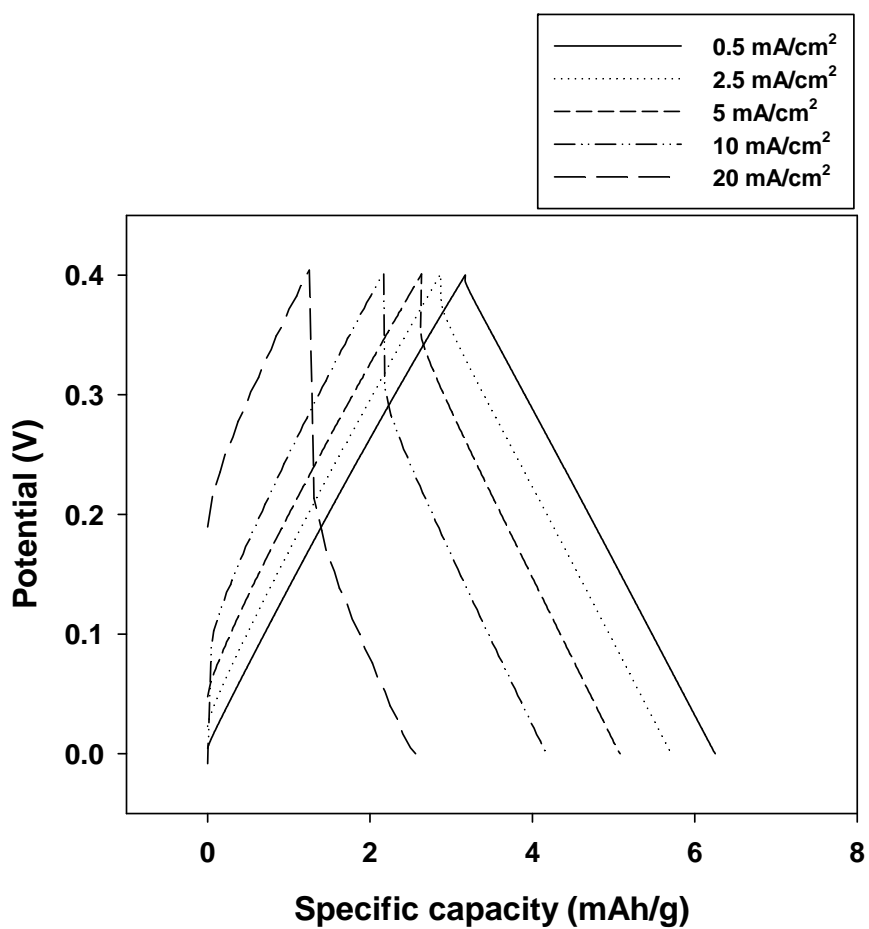


Figure 5-5. Galvanostatic charge/discharge voltage profiles of SX-PLUS

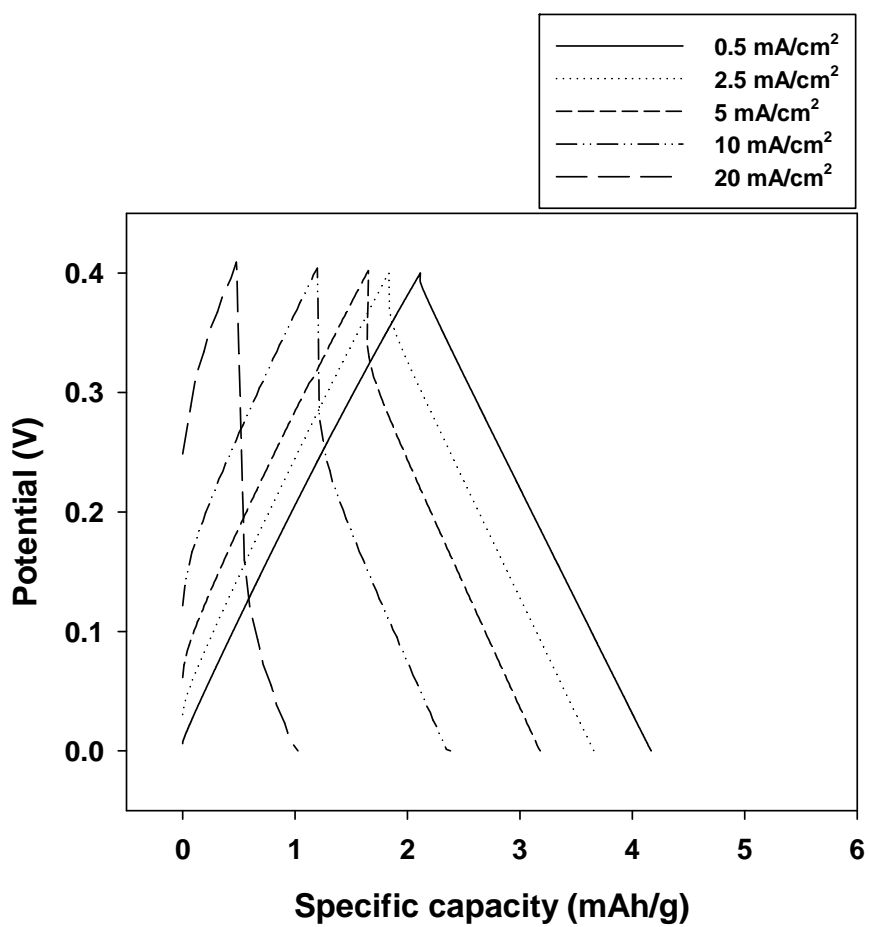


Figure 5-6. Galvanostatic charge/discharge voltage profiles of S-51HF

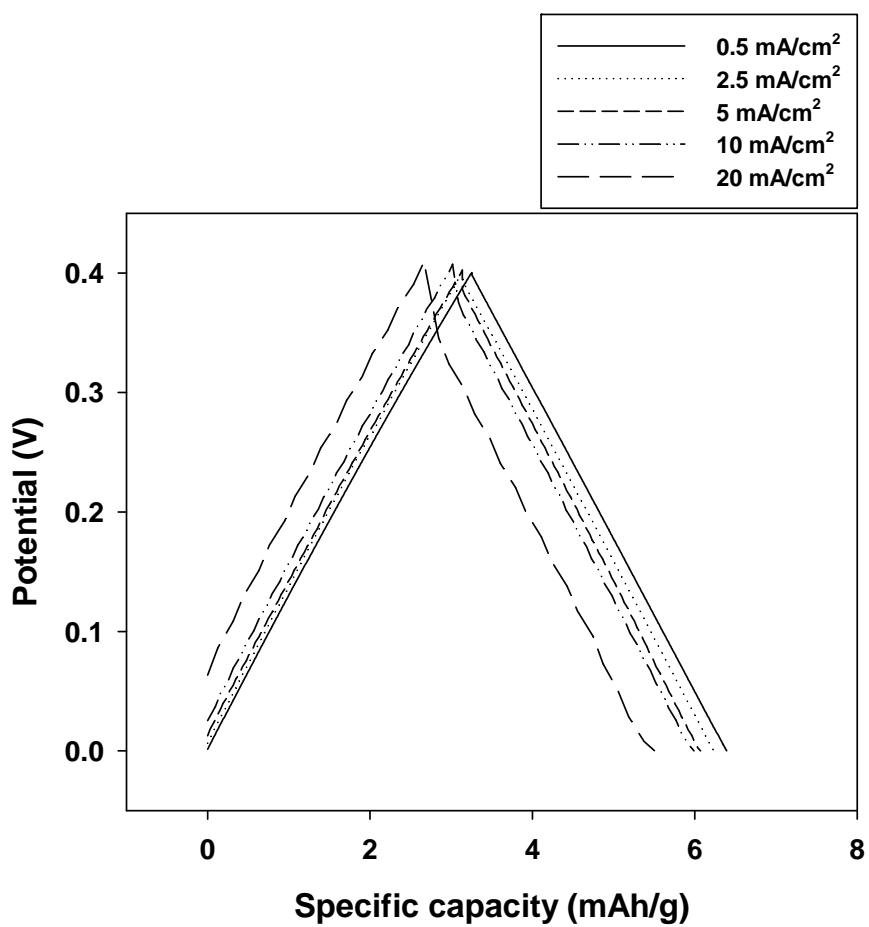


Figure 5-7. Galvanostatic charge/discharge voltage profiles of MDC

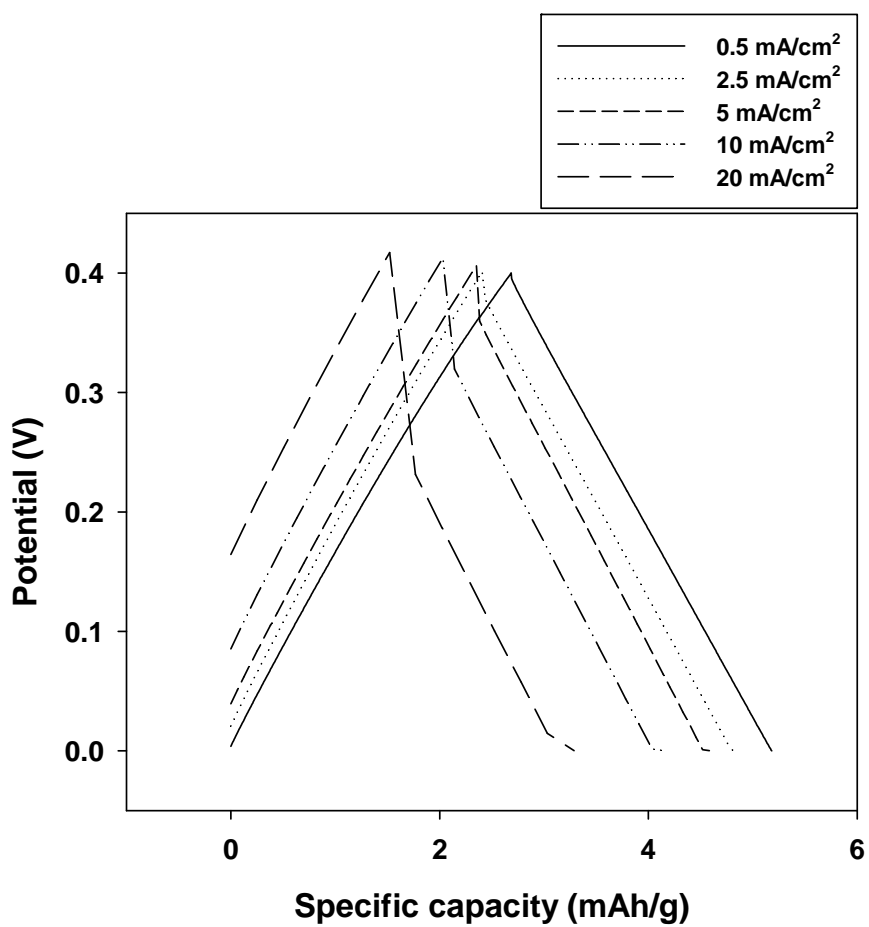


Figure 5-8. Galvanostatic charge/discharge voltage profiles of Carbon aerogel

Table 5-2. Specific capacitance of various carbon composite electrodes derived from galvanostatic charge/discharge voltage profile.

	MSP-20	P-60	SX PLUS	S-51HF	MDC	Aerogel
Capacitance (F/g)	120	73	56	38	57	46
Retention (%)	93	95	76	60	97	99

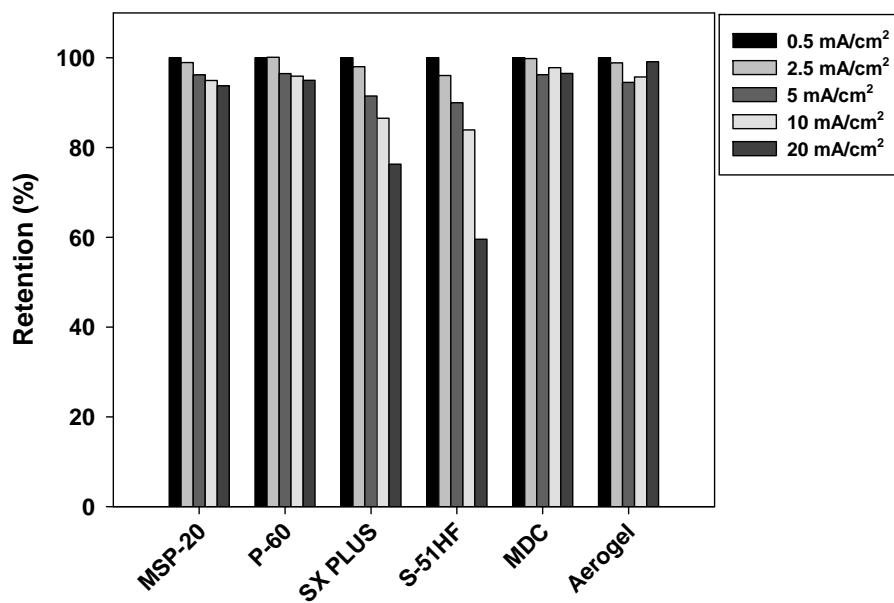


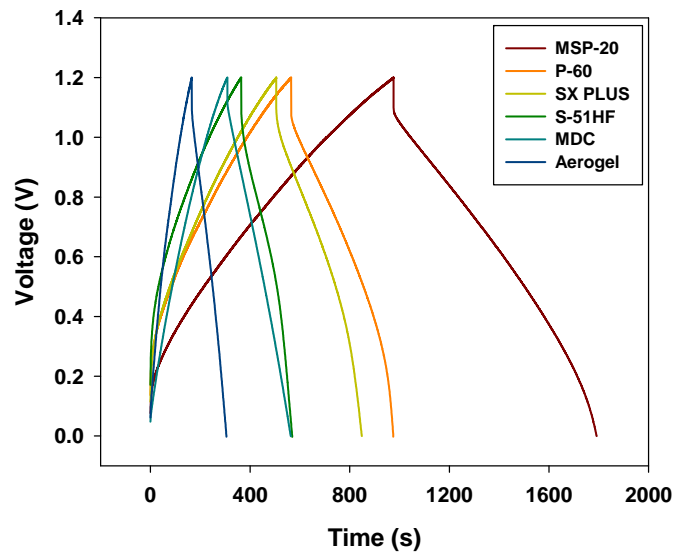
Figure 5-9. Retention of specific capacitance as a function of scan rate (0.5 mA/cm² ~ 20 mA/cm²) with various carbon composite electrodes.

Desalination performance with CC operation

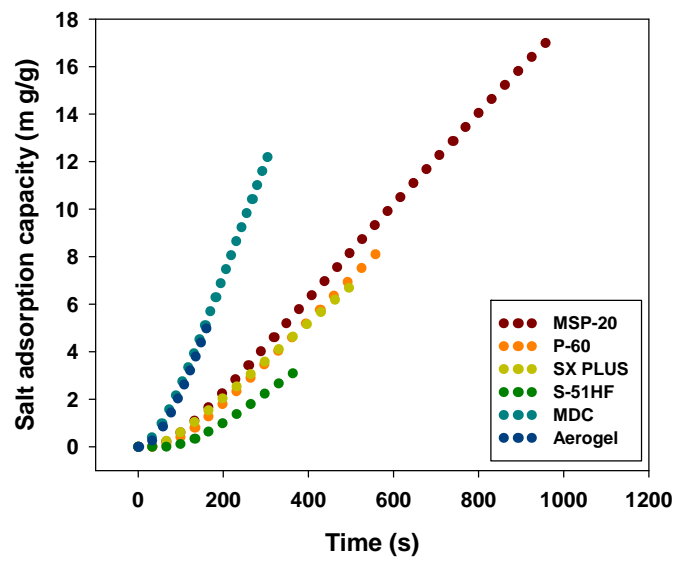
Figure 5-10 shows the representative voltage profiles and salt adsorption capacities of CC mode in MCDI operation. A constant current (1 mA/cm^2) is applied until the CDI cell voltage reaches to 1.2V, whereas for discharging step, a reverse current (-1 mA/cm^2) was applied until the CDI cell voltage reaches to zero. The linear increasing/decreasing voltage during the charging/discharging step, which is characteristic of CC operation (Jande and Kim 2013; Kang et al. 2014; Zhao et al. 2012). An instantaneous rise of cell voltage about 0.1 V occurred at the beginning of charging (also drop at the beginning of discharging) is the result of an ohmic drop caused by the MCDI cell's electrolyte resistance. As shown in Figure 5-10a, various voltage profiles according to carbon materials are observed due to their different capacity and rate response affecting on desalination performances.

In Figure 5-10b, salt adsorption capacities as a function of time are presented according to carbon materials. Note that these salt adsorption capacities are measured under not only equilibrium state but also dynamic state (Biesheuvel and Bazant 2010; Biesheuvel et al. 2009; Zhao et al. 2009). The highest and lowest salt adsorption capacity were 17 mg/g with MSP-20 and 3 mg/g with S-51HF, respectively. These value is directly related with specific capacitance presented in table 5-2 because the salt adsorption capacity can be converted to about 70% of electrode capacitance (Kim and Yoon 2013). However, the MDC

showed the second highest salt adsorption capacity (13 mg/g) in spite of low capacitance, which is due to low electrode density, i.e., low mass of electrodes. In addition, desalination rate capability is qualitatively analyzed by the slope of salt adsorption curve. From Figure 5-10b, the carbon materials can be intuitively split into two groups; MDC, CA with fast desalination rate capability and MSP-20, P-60, SX PLUS, S-51HF with slow desalination rate capability. This classification according to rate capability is due to the development of large meso- and macropores, which trend is partly confirmed by the results in Figure 5-9. In addition, note that these results were based on salt adsorption capacity per electrode weight (mg/g). If the salt adsorption capacity per electrode volume (mg/cm^3) is considered, electrodes with low density such as MDC and aerogel show poor desalination performance compared other materials (Figure 5-11). In large-scale CDI process, electrode volume is important due to module design and MDC might not be suitable for large-scale process in spite of its fast rate capability.



(a)



(b)

Figure 5-10. (a) The representative voltage profiles and (b) salt adsorption capacities (mg/g) of CC mode in MCDI operation with various carbon electrodes. (current density = 1 mA/cm² for charging and -1 mA/cm² for discharging, flow rate = 10 mL/min, NaCl concentration = 10 mM).

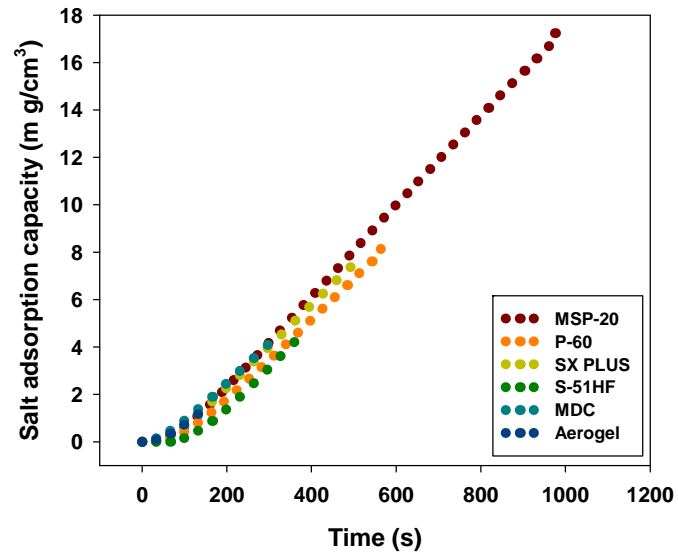


Figure 5-11. Salt adsorption capacities (mg/cm^3) of CC mode in MCDI operation with various carbon electrodes. (current density = $1 \text{ mA}/\text{cm}^2$ for charging and $-1 \text{ mA}/\text{cm}^2$ for discharging, flow rate = $10 \text{ mL}/\text{min}$, NaCl concentration = 10 mM).

Energy recovery performance depending on electrode properties

To analyze the energy recovery performance, energy consumed during the charging step and energy recovered during the discharging step was calculated from the voltage profile shown in Figure 5-10a and all the values of carbon materials are plotted in Figure 5-12.

Figure 5-12 shows the energy consumed during the charging step (E_c) and energy recovered during the discharging step (E_r) with various carbon materials under identical CDI operating conditions. As can be seen, it was observed E_c and E_r was increased with increasing salt adsorption capacity depicted in Figure 5-11b. MSP-20 showed the highest E_c and E_r with the highest salt adsorption capacity, whereas S-51HF showed the lowest E_c and E_r with the lowest salt adsorption capacity. The slope of depicted line in Figure 5-12 refers to proportional constant, indicating energy recovery ratio. For example, the line with proportional constant of unity means that all of the energy consumed during the charging step are perfectly recovered during the discharging step. Interestingly, the noticeable observation can be made in Figure 5-12; almost the whole data points of carbon materials are located between $E_r=0.5E_c$ and $E_r=0.75E_c$, indicating the energy recovery ratios of carbon materials ranged from 50% to 75%. This phenomenon can be explained by the high resistance of low electrolyte. The targeting concentration of CDI process with typical carbon sheet electrodes is low concentration due to the their limitation in adsorption site

(HeeáCho et al. 2013; Lee et al. 2014). However, this low concentration revealing high electrical resistance resulted in energy loss during the charging step. The previous study reported that the resistance over the MCDI cell is mainly dominated by the spacer which act as an flow channel of feed water with low concentration (Dykstra et al. 2016). The inserted table presents the calculated value of energy recovery ratio, showing that different energy recovery ratios according to carbon materials under the same operating conditions. To analyze this result, we investigated the relationship of energy recovery ratio, salt adsorption capacity and salt adsorption rate.

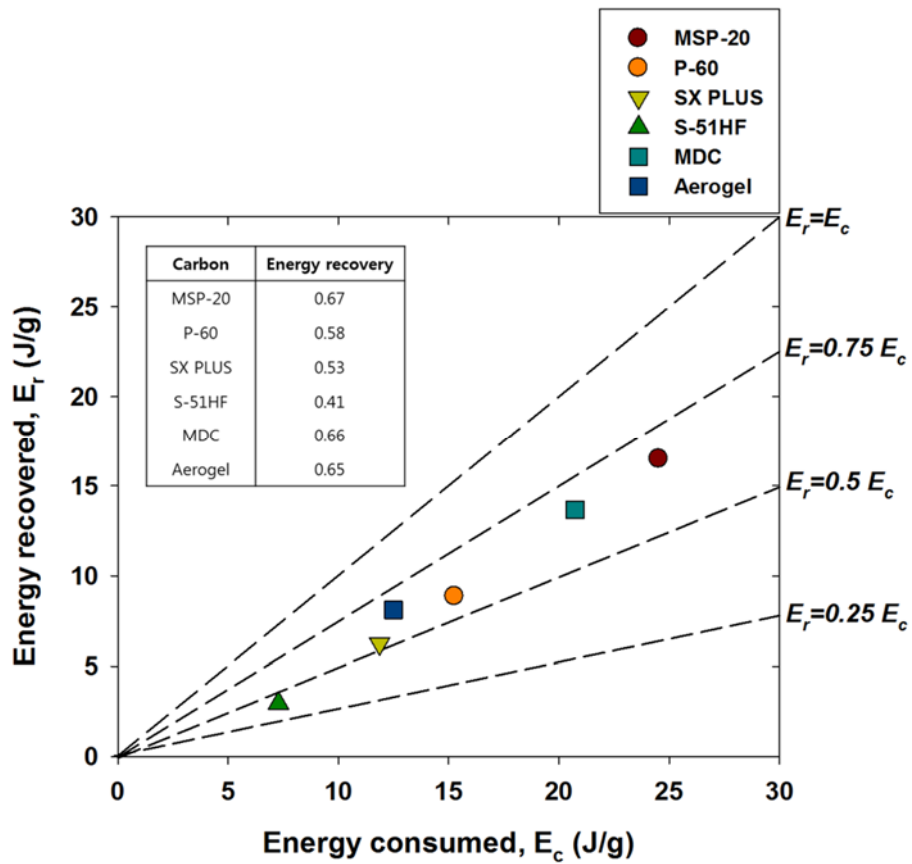


Figure 5-12. The energy consumed during the charging step (E_c) and energy recovered during the discharging step (E_r) with various carbon materials. Inserted table shows the energy recovery ratio calculated from E_r/E_c as presented in Figure 5-2. CC operation in desalination test was performed with 1/-1 mA/cm² of charging/discharging current density up to 1.2 V of cut-off voltage and 10 mM NaCl solution. The symbols are located between $E_r=0.5E_c$ and $E_r=0.75E_c$, indicating the energy recovery ratios of carbon materials ranged from 50% to 75%.

Figure 5-13 shows the correlation between the salt adsorption capacity and energy recovery ratio. As can be seen in Figure 5-13, we can infer the linear correlation between salt adsorption capacity and energy recovery ratio with data points of MSP-20, P-60, SX PLUS and S-51HF. This correlation unambiguously proves that the capacity of carbon electrode (which is excellent agreement with salt adsorption capacity) plays an important role in energy recovery performance. This result is strongly coincident with previous experimental results in part 4, especially Figure 4-9. In part 4, salt adsorption capacities were varied with operating conditions and it was suggested that a highly charged MCDI cell (which reflects the high salt adsorption capacity) is more favorable for energy recovery.

However, in Figure 5-13, it is required to take notice of exceptional data points with MDC and CA. These two carbon materials deviated from the correlation between salt adsorption capacity and energy recovery ratio; higher energy recovery ratios of MDC (0.66) and CA (0.65) compared to P-60 (0.58) and SX PLUS (0.53) in spite of similar salt adsorption capacities, respectively. This can be explained by fast rate response characteristics of MDC and CA which has the development of meso- and macropores.

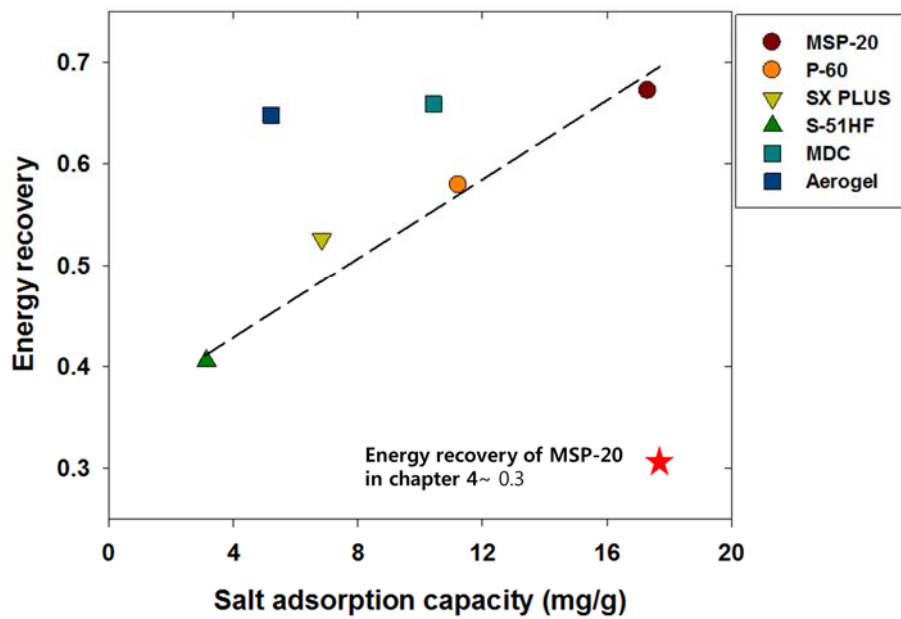


Figure 5-13. Correlation between the salt adsorption capacity and energy recovery ratio. Salt adsorption capacity was obtained from Figure 5-11b and regression line was plotted with MSP-20, P-60, SX PLUS and S-51HF. The red star indicates the energy recovery ratio of converter system in Figure 4-9.

Figure 5-14 shows the correlation between the average salt adsorption rate and mean power. As shown in Figure 5-14, the group with MDC and CA and the other group with MSP-20, P-60, SX PLUS and S-51HF are distinctively classified, which clearly explains the reason why MDC and CA showed high energy recovery ratio. Considering that the energy recovery (or energy extraction) of CDI is induced by the release of ions away from electrode pores, pore structures necessarily affect the energy recovery performance. High mean powers of MDC and CA caused by fast ion transport into/from electrode pores support the hypothesis because mean power strongly reflects energy recovery rate. This observation suggests that high salt adsorption rate, *i.e.*, fast rate response are also important electrode properties as an influential factor on energy recover performance as well as salt adsorption capacity.

After establishing the salt adsorption capacity and salt adsorption rate as influential factors on energy recovery performance, degradation of energy recovery ratio by varying charging current density was investigated. Figure 5-15 shows the normalized energy recovery as a function of different charging-discharging current density. It was observed that MDC with high salt adsorption capacity and rate showed the least degradation in energy recovery performance and our discussions are strongly underpinned by this result.

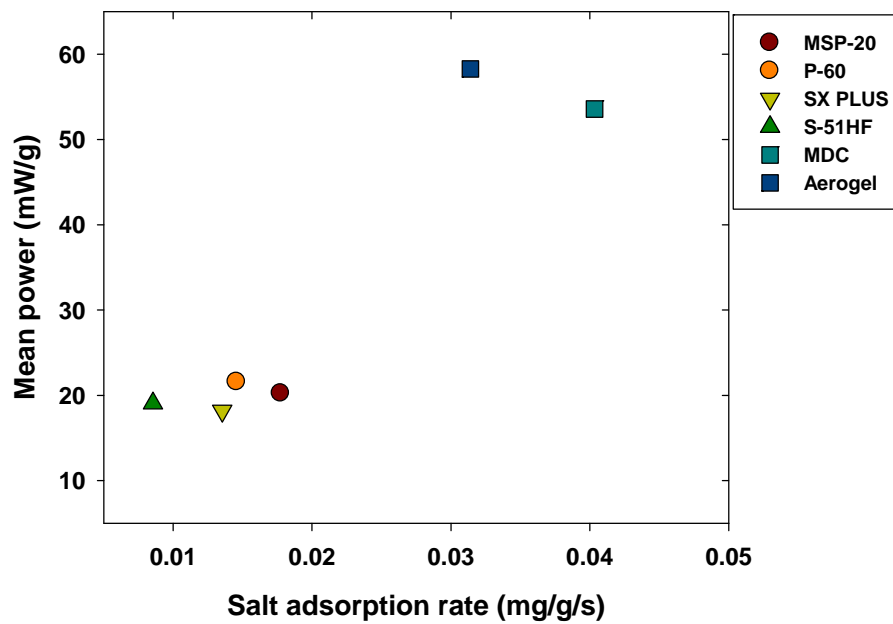


Figure 5-14. Correlation between the average salt adsorption rate and mean power. The average salt adsorption rate was calculated by dividing the salt adsorption capacity by the duration of charging step (mg/g/s) and mean power was obtained by dividing the energy recovered during the discharging step by the duration of discharging step and the mass of electrodes (mW/g).

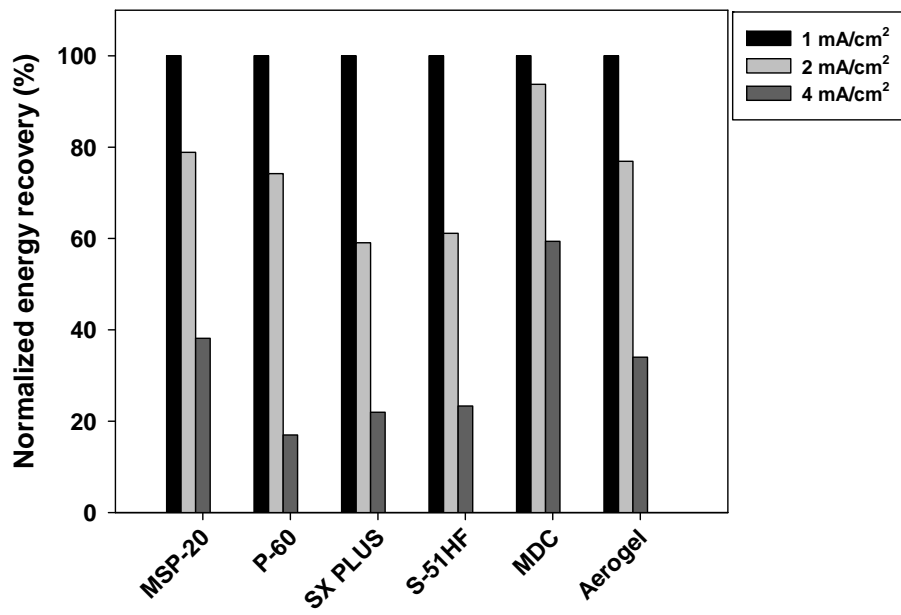


Figure 5-15. The normalized energy recovery as a function of different charging-discharging current density (± 1 , ± 2 , ± 4 mA/cm²). All of desalination test were identically performed with 1.2 V of Cut-off voltage and 10 mM NaCl solution.

5.4. Summary

In this study, energy recovery ratio in MCDI depending on electrode properties was investigated using constant current operation. Almost the whole carbon electrodes showed energy recovery ratios of 0.5 ~ 0.75 due to high electrical resistance of low electrolyte. In particular, we found out that not only salt adsorption capacity but also salt adsorption rate play an important role in energy recovery performance. Our findings were confirmed by the least degradation of energy recovery performance in case of using carbon electrode with excellent salt adsorption capacity and rate. We expect that this study can provide important considerations to design and fabricate carbon materials and electrodes which are applied energy recovery system in MCDI.

6. Conclusions

In this dissertation, design and analysis of CDI techniques for high energy efficiency and energy recovery was implemented by focusing on the evaluation of energy consumption according to operational modes and energy recovery system. In the first part, the salt adsorption capacity and energy consumption in two operational modes (CV and CC) in a CDI desalination cell were compared on the bases of identical amount of ion removal and electrical charge consumed criteria. The higher overall cell voltage of CV mode results in faster salt adsorption under a given charging time than CC mode. Nevertheless, CC mode consumed less energy than that consumed in CV mode in both criteria, but there were similar charge efficiencies in CC and CV modes. In the second part, the energy recovery system in an actual MCDI cell with a buck-boost converter was constructed and the energy recovery ratio was investigated under various operational conditions to determine the influential parameters affecting energy recovery in the MCDI cell. As major results, the salt adsorption capacity was found to play an important role in the energy recovery and constant current charging was found to be more favourable for energy recovery than constant voltage charging. In addition, for discharging conditions with the buck-boost converter operation, the energy recovery was more sensitively affected by the reference current rather than the capacitance of the supercapacitor. The smaller reference current mainly resulted in a higher energy recovery ratio in contrast

with the capacitance of the supercapacitor. We suggested that the development of an electrode with a high salt adsorption capacity and a cell design with low cell resistance will be required with a well-optimized buck-boost converter to facilitate a high energy recovery ratio. Lastly, energy recovery ratio in MCDI depending on electrode properties was investigated using constant current operation. Almost the whole carbon electrodes showed partial loss of energy recovery ratios due to high electrical resistance of low electrolyte. In particular, we found out that not only salt adsorption capacity but also salt adsorption rate play an important role in energy recovery performance. Our findings were confirmed by the least degradation of energy recovery performance in case of using carbon electrode with excellent salt adsorption capacity and rate. In conclusion, this dissertation focused on design and analysis of operating techniques, CC operation and energy recovery process with investigating energy efficiency and energy recovery according to operating condition. We expect that this dissertation will provide a comprehensive guide for the construction and operation of high energy-efficiency CDI process.

References

- Alkuran M, Orabi M. Utilization of a buck boost converter and the method of segmented capacitors in a CDI water purification system; 2008. IEEE. p 470-474.
- Alkuran M, Orabi M, Scheinberg N. Highly efficient Capacitive De-Ionization (CDI) water purification system using a buck-boost converter; 2008. IEEE. p 1926-1930.
- Anderson MA, Cudero AL, Palma J. 2010. Capacitive deionization as an electrochemical means of saving energy and delivering clean water. Comparison to present desalination practices: Will it compete? *Electrochimica Acta* 55(12):3845-3856.
- Avraham E, Bouhadana Y, Soffer A, Aurbach D. 2009. Limitation of charge efficiency in capacitive deionization I. on the behavior of single activated carbon. *Journal of the Electrochemical Society* 156(6):P95-P99.
- Avraham E, Noked M, Bouhadana Y, Soffer A, Aurbach D. 2010. Limitations of charge efficiency in capacitive deionization processes III: The behavior of surface oxidized activated carbon electrodes. *Electrochimica Acta* 56(1):441-447.
- Bard AJ, Faulkner LR. 2001. *Electrochemical methods: fundamentals and applications*, 2nd. Hoboken: Wiley and Sons.
- Biesheuvel P, Bazant M. 2010. Nonlinear dynamics of capacitive charging and

- desalination by porous electrodes. *Physical review E* 81(3):031502.
- Biesheuvel P, Van der Wal A. 2010. Membrane capacitive deionization. *Journal of Membrane Science* 346(2):256-262.
- Biesheuvel P, Van Limpt B, Van der Wal A. 2009. Dynamic adsorption/desorption process model for capacitive deionization. *The Journal of Physical Chemistry C* 113(14):5636-5640.
- Blair JW, Murphy GW. 1960. Electrochemical demineralization of water with porous electrodes of large surface area: University of Oklahoma.
- Bouhadana Y, Ben-Tzion M, Soffer A, Aurbach D. 2011. A control system for operating and investigating reactors: the demonstration of parasitic reactions in the water desalination by capacitive de-ionization. *Desalination* 268(1):253-261.
- Demirer ON, Naylor RM, Rios Perez CA, Wilkes E, Hidrovo C. 2013. Energetic performance optimization of a capacitive deionization system operating with transient cycles and brackish water. *Desalination* 314:130-138.
- Długolecki P, van der Wal A. 2013. Energy recovery in membrane capacitive deionization. *Environmental science & technology* 47(9):4904-4910.
- Dykstra J, Zhao R, Biesheuvel P, van der Wal A. 2016. Resistance identification and rational process design in Capacitive Deionization. *Water research* 88:358-370.
- Elimelech M, Phillip WA. 2011. The future of seawater desalination: energy, technology, and the environment. *Science* 333(6043):712-717.
- Evans S, Hamilton W. 1966. The mechanism of demineralization at carbon

electrodes. *Journal of The Electrochemical Society* 113(12):1314-1319.

Farmer JC, Bahowick SM, Harrar JE, Fix DV, Martinelli RE, Vu AK, Carroll KL. 1997. Electrosorption of chromium ions on carbon aerogel electrodes as a means of remediating ground water. *Energy & fuels* 11(2):337-347.

Farmer JC, Fix DV, Mack GV, Pekala RW, Poco JF. 1996. Capacitive deionization of NaCl and NaNO₃ solutions with carbon aerogel electrodes. *Journal of the Electrochemical Society* 143(1):159-169.

Freshwater D. 1951. Thermal economy in distillation. *Trans. Inst. Chem. Eng* 29:149-160.

Gabelich CJ, Tran TD, Suffet IM. 2002. Electrosorption of inorganic salts from aqueous solution using carbon aerogels. *Environmental science & technology* 36(13):3010-3019.

Gao X, Omosebi A, Landon J, Liu K. 2014. Dependence of the capacitive deionization performance on potential of zero charge shifting of carbon xerogel electrodes during long-term operation. *Journal of The Electrochemical Society* 161(12):E159-E166.

Gao X, Omosebi A, Landon J, Liu K. 2015. Surface charge enhanced carbon electrodes for stable and efficient capacitive deionization using inverted adsorption–desorption behavior. *Energy & Environmental Science* 8(3):897-909.

García-Quismondo E, Gómez R, Vaquero F, Cudero AL, Palma J, Anderson M. 2013a. New testing procedures of a capacitive deionization reactor. *Physical Chemistry Chemical Physics* 15(20):7648-7656.

- García-Quismondo E, Santos C, Lado J, Palma Js, Anderson MA. 2013b. Optimizing the energy efficiency of capacitive deionization reactors working under real-world conditions. *Environmental science & technology* 47(20):11866-11872.
- Greenlee LF, Lawler DF, Freeman BD, Marrot B, Moulin P. 2009. Reverse osmosis desalination: water sources, technology, and today's challenges. *Water research* 43(9):2317-2348.
- HeeáCho C, HeeáHan M, KookáKim D. 2013. Desalination via a new membrane capacitive deionization process utilizing flow-electrodes. *Energy & Environmental Science* 6(5):1471-1475.
- Jande Y, Kim W. 2013. Desalination using capacitive deionization at constant current. *Desalination* 329:29-34.
- Jeon S-i, Yeo J-g, Yang S, Choi J, Kim DK. 2014. Ion storage and energy recovery of a flow-electrode capacitive deionization process. *Journal of Materials Chemistry A* 2(18):6378-6383.
- Jia B, Zou L. 2012. Graphene nanosheets reduced by a multi-step process as high-performance electrode material for capacitive deionisation. *Carbon* 50(6):2315-2321.
- Johnson A, Newman J. 1971. Desalting by means of porous carbon electrodes. *Journal of the Electrochemical Society* 118(3):510-517.
- Jung H-H, Hwang S-W, Hyun S-H, Lee K-H, Kim G-T. 2007. Capacitive deionization characteristics of nanostructured carbon aerogel electrodes

synthesized via ambient drying. *Desalination* 216(1):377-385.

Jury WA, Vaux HJ. 2007. The emerging global water crisis: managing scarcity and conflict between water users. *Advances in Agronomy* 95:1-76.

Jury WA, Vaux Jr HJ. 2007. The emerging global water crisis: managing scarcity and conflict between water users. *Advances in Agronomy* 95:1-76.

Kang J, Kim T, Jo K, Yoon J. 2014. Comparison of salt adsorption capacity and energy consumption between constant current and constant voltage operation in capacitive deionization. *Desalination* 352:52-57.

Kang J, Kim T, Tak Y, Lee J-H, Yoon J. 2012. Cyclic voltammetry for monitoring bacterial attachment and biofilm formation. *Journal of Industrial and Engineering Chemistry* 18(2):800-807.

Khomenko V, Frackowiak E, Beguin F. 2005. Determination of the specific capacitance of conducting polymer/nanotubes composite electrodes using different cell configurations. *Electrochimica Acta* 50(12):2499-2506.

Kim J-S, Choi J-H. 2010a. Fabrication and characterization of a carbon electrode coated with cation-exchange polymer for the membrane capacitive deionization applications. *Journal of membrane science* 355(1):85-90.

Kim T, Yoon J. 2013. Relationship between capacitance of activated carbon composite electrodes measured at a low electrolyte concentration and their desalination performance in capacitive deionization. *Journal of Electroanalytical Chemistry* 704:169-174.

Kim T, Yoon J. 2015. CDI ragone plot as a functional tool to evaluate

desalination performance in capacitive deionization. *RSC Advances* 5(2):1456-1461.

Kim Y-J, Choi J-H. 2010b. Enhanced desalination efficiency in capacitive deionization with an ion-selective membrane. *Separation and Purification Technology* 71(1):70-75.

Kim Y-J, Choi J-H. 2010c. Improvement of desalination efficiency in capacitive deionization using a carbon electrode coated with an ion-exchange polymer. *Water research* 44(3):990-996.

Landon J, Gao X, Neathery JK, Liu K. 2013. Energy Recovery in Parallel Capacitive Deionization Operations. *ECS Transactions* 53(30):235-243.

Lawson KW, Lloyd DR. 1997. Membrane distillation. *Journal of membrane Science* 124(1):1-25.

Lee J-B, Park K-K, Eum H-M, Lee C-W. 2006. Desalination of a thermal power plant wastewater by membrane capacitive deionization. *Desalination* 196(1):125-134.

Lee J-B, Park K-K, Yoon S-W, Park P-Y, Park K-I, Lee C-W. 2009. Desalination performance of a carbon-based composite electrode. *Desalination* 237(1):155-161.

Lee J, Kim S, Kim C, Yoon J. 2014. Hybrid capacitive deionization to enhance the desalination performance of capacitive techniques. *Energy & Environmental Science* 7(11):3683-3689.

Li H, Zou L, Pan L, Sun Z. 2010. Novel graphene-like electrodes for capacitive

- deionization. *Environmental science & technology* 44(22):8692-8697.
- Lim J-A, Park N-S, Park J-S, Choi J-H. 2009. Fabrication and characterization of a porous carbon electrode for desalination of brackish water. *Desalination* 238(1):37-42.
- Liu Y, Pan L, Xu X, Lu T, Sun Z, Chua DH. 2014. Enhanced desalination efficiency in modified membrane capacitive deionization by introducing ion-exchange polymers in carbon nanotubes electrodes. *Electrochimica Acta* 130:619-624.
- Mulligan MD, Broach B, Lee TH. 2005. A constant-frequency method for improving light-load efficiency in synchronous buck converters. *Power Electronics Letters, IEEE* 3(1):24-29.
- Murphy G, Caudle D. 1967. Mathematical theory of electrochemical demineralization in flowing systems. *Electrochimica Acta* 12(12):1655-1664.
- Nadakatti S, Tendulkar M, Kadam M. 2011. Use of mesoporous conductive carbon black to enhance performance of activated carbon electrodes in capacitive deionization technology. *Desalination* 268(1):182-188.
- Oh H-J, Lee J-H, Ahn H-J, Jeong Y, Kim Y-J, Chi C-S. 2006. Nanoporous activated carbon cloth for capacitive deionization of aqueous solution. *Thin Solid Films* 515(1):220-225.
- Park B-H, Kim Y-J, Park J-S, Choi J. 2011. Capacitive deionization using a carbon electrode prepared with water-soluble poly (vinyl alcohol) binder. *Journal of Industrial and Engineering Chemistry* 17(4):717-722.

- Pernía AM, J Alvarez-González F, Díaz J, Villegas PJ, Nuño F. 2014. Optimum peak current hysteresis control for energy recovering converter in CDI desalination. *Energies* 7(6):3823-3839.
- Pernía AM, Normiella JG, Martín-Ramos JA, Díaz J, Martínez JA. 2012. Up-Down Converter for Energy Recovery in a CDI Desalination System. *Power Electronics, IEEE Transactions on* 27(7):3257-3265.
- Pernia A, Alvarez-Gonzalez FJ, Prieto M, Villegas P, Nuno F. 2014. New control strategy of an up-down converter for energy recovery in a CDI desalination System.
- Porada S, Borchardt L, Oschatz M, Bryjak M, Atchison J, Keesman K, Kaskel S, Biesheuvel P, Presser V. 2013a. Direct prediction of the desalination performance of porous carbon electrodes for capacitive deionization. *Energy & Environmental Science* 6(12):3700-3712.
- Porada S, Weinstein L, Dash R, Van Der Wal A, Bryjak M, Gogotsi Y, Biesheuvel P. 2012. Water desalination using capacitive deionization with microporous carbon electrodes. *ACS applied materials & interfaces* 4(3):1194-1199.
- Porada S, Zhao R, Van Der Wal A, Presser V, Biesheuvel P. 2013b. Review on the science and technology of water desalination by capacitive deionization. *Progress in Materials Science* 58(8):1388-1442.
- Ryoo M-W, Seo G. 2003. Improvement in capacitive deionization function of activated carbon cloth by titania modification. *Water Research* 37(7):1527-1534.

Shannon MA, Bohn PW, Elimelech M, Georgiadis JG, Mariñas BJ, Mayes AM. 2008. Science and technology for water purification in the coming decades. *Nature* 452(7185):301-310.

Shiue L-R, Sun A, Shiue C-C, Hsieh F-C, Hsieh Y-H, Jou J-J. 2003. Deionizers with energy recovery. Google Patents.

Soffer A, Folman M. 1972. The electrical double layer of high surface porous carbon electrode. *Journal of Electroanalytical Chemistry and Interfacial Electrochemistry* 38(1):25-43.

Strathmann H. 2010. Electrodialysis, a mature technology with a multitude of new applications. *Desalination* 264(3):268-288.

Suss M, Porada S, Sun X, Biesheuvel P, Yoon J, Presser V. 2015. Water desalination via capacitive deionization: what is it and what can we expect from it? *Energy & Environmental Science*.

Suss ME, Baumann TF, Bourcier WL, Spadaccini CM, Rose KA, Santiago JG, Stadermann M. 2012. Capacitive desalination with flow-through electrodes. *Energy & Environmental Science* 5(11):9511-9519.

Tsouris C, Mayes R, Kiggans J, Sharma K, Yiacoumi S, DePaoli D, Dai S. 2011. Mesoporous carbon for capacitive deionization of saline water. *Environmental science & technology* 45(23):10243-10249.

van Limpt B, van der Wal A. 2014. Water and chemical savings in cooling towers by using membrane capacitive deionization. *Desalination*.

Wang G, Dong Q, Ling Z, Pan C, Yu C, Qiu J. 2012. Hierarchical activated

carbon nanofiber webs with tuned structure fabricated by electrospinning for capacitive deionization. *Journal of Materials Chemistry* 22(41):21819-21823.

Wang L, Wang M, Huang Z-H, Cui T, Gui X, Kang F, Wang K, Wu D. 2011. Capacitive deionization of NaCl solutions using carbon nanotube sponge electrodes. *Journal of Materials Chemistry* 21(45):18295-18299.

Welgemoed T, Schutte C. 2005. Capacitive deionization technology™: an alternative desalination solution. *Desalination* 183(1):327-340.

Xu B, Wu F, Chen S, Zhang C, Cao G, Yang Y. 2007. Activated carbon fiber cloths as electrodes for high performance electric double layer capacitors. *Electrochimica Acta* 52(13):4595-4598.

Xu P, Drewes JE, Heil D, Wang G. 2008. Treatment of brackish produced water using carbon aerogel-based capacitive deionization technology. *Water research* 42(10):2605-2617.

Yang SJ, Kim T, Lee K, Kim YS, Yoon J, Park CR. 2014. Solvent evaporation mediated preparation of hierarchically porous metal organic framework-derived carbon with controllable and accessible large-scale porosity. *Carbon* 71:294-302.

Yoram O. 2008. Capacitive deionization (CDI) for desalination and water treatment-past, present and future. *Desalination* 228:10-29.

Zhang D, Shi L, Fang J, Dai K, Li X. 2006. Preparation and desalination performance of multiwall carbon nanotubes. *Materials Chemistry and Physics* 97(2):415-419.

Zhang LL, Zhao X. 2009. Carbon-based materials as supercapacitor electrodes.

Chemical Society Reviews 38(9):2520-2531.

Zhao R, Biesheuvel P, Miedema H, Bruning H, Van der Wal A. 2009. Charge efficiency: a functional tool to probe the double-layer structure inside of porous electrodes and application in the modeling of capacitive deionization. *The Journal of Physical Chemistry Letters* 1(1):205-210.

Zhao R, Biesheuvel P, Van der Wal A. 2012. Energy consumption and constant current operation in membrane capacitive deionization. *Energy & Environmental Science* 5(11):9520-9527.

Zhao R, Porada S, Biesheuvel P, Van der Wal A. 2013a. Energy consumption in membrane capacitive deionization for different water recoveries and flow rates, and comparison with reverse osmosis. *Desalination* 330:35-41.

Zhao R, Satpradit O, Rijnaarts H, Biesheuvel P, van der Wal A. 2013b. Optimization of salt adsorption rate in membrane capacitive deionization. *Water research* 47(5):1941-1952.

Zou L, Li L, Song H, Morris G. 2008. Using mesoporous carbon electrodes for brackish water desalination. *Water research* 42(8):2340-2348.

손덕영, 최윤호, 박대욱, 정충효. 2010. 수치모사를 이용한 CDI Unit Cell 내부의 유로성능 평가. *한국전산유체공학회지* 15(1):31-36.

이주영, 서석준, 박정우, 문승현. 2010. 축전식 탈염 시스템을 위한 셀 구조에 관한 연구. *Korean Chem. Eng. Res.(화학공학)* 48(6):791-794.

국문초록

축전식 탈염 (Capacitive Deionization, CDI) 기술은 전극표면에 형성되는 전기이중층을 이용하여 수내 이온을 제거하는 담수화 기술로서 역삼투막법과 증류법과 같은 기존 담수화 공정에 비하여 친환경적이고 낮은 에너지를 이용하는 새로운 담수화 기술로서 각광받고 있다. CDI 공정은 정전류 운전과 에너지 회수와 같은 운전 기술에 의해 공정 및 에너지 효율이 결정되므로 이러한 운전기술에 대한 적절한 설계 및 분석이 요구된다. 따라서 본 논문에서는 고 에너지 효율 및 에너지 회수를 위한 CDI의 운전기술의 설계 및 분석을 위해 전기인가방식에 따른 에너지 효율을 분석하고 운전조건과 전극 특성에 따른 에너지 회수 성능을 조사하고자 하였다. 우선 정전류 운전과 정전위 운전의 탈염 용량과 에너지 소비량을 인가 전하와 탈염량이 동일한 조건에서 비교 분석한 결과 탈염 용량 측면에서 평균 인가 전위가 높은 정전위 운전이 더 높은 탈염용량을 나타내는 반면, 정전류 운전은 약 26 ~ 30% 낮은 에너지 소비량을 나타내는 것을 확인하였다. 다음으로, 실제 에너지 회수 시스템을 구현하기 위해 전력 변환 장치인 buck-boost 컨버터를 MCDI와 결합한 회수 시스템을 구축하였으며 이를 이용하여 슈퍼캐패시터에 회수에너지를 저장하였다. 또한 CDI셀의 탈염용량이 에너지 회수율에

매우 중요한 영향을 미친다는 것을 알 수 있었으며 정전류 운전에서 높은 에너지 회수율을 달성됨을 밝혔다. 마지막으로, 에너지 회수 성능에 영향을 미치는 전극 특성을 조사하고자 다양한 기공구조를 가지는 재료를 이용해 전극을 제조하고 에너지 회수 성능을 평가한 결과, 일반적인 CDI공정에서 50 ~ 75%의 에너지 회수율이 나타남과 전극의 탈염용량과 탈염속도 특성이 에너지 회수 성능에 미치는 영향을 규명하였다. 결론적으로, 본 논문에서는 운전 방식에 따른 에너지 소비량을 비교하고 소비된 에너지를 회수하는 시스템 및 운전조건을 조사함으로써 고 에너지 효율 및 에너지 회수를 위한 CDI 운전기술의 설계 및 분석이 이루어졌다. 이러한 결과를 통하여 에너지 회수 시스템의 구축 및 운전에 요구되는 종합적인 지식을 제공할 수 있을 것으로 기대된다.

주요어: 담수화, 축전식 탈염기술, 에너지 효율성, 정전류 운전, 에너지 회수, 전극 특성

학 번: 2010-30802